POTENTIAL SHIFTING OF CLIMATE ZONES AND ASSOCIATED HYDROLOGICAL IMPACTS UNDER CHANGING CLIMATE CONDITIONS IN SRI LANKA

Chamal Jayaminda

228089M

Degree of Master of Science

Department of Civil Engineering

University of Moratuwa

Sri Lanka

February 2024

POTENTIAL SHIFTING OF CLIMATE ZONES AND ASSOCIATED HYDROLOGICAL IMPACTS UNDER CHANGING CLIMATE CONDITIONS IN SRI LANKA

Kulanda Arachchige Chamal Jayaminda

228089M

Thesis submitted in partial fulfilment of the requirements for the degree of Master of Science in Civil Engineering

Department of Civil Engineering

University of Moratuwa

Sri Lanka

February 2024

DECLARATION

I declare that this is my own work and this thesis does not incorporate without acknowledgement any material previously submitted for a Degree or Diploma in any other University or institute of higher learning and to the best of knowledge and belief it does not contain any material previously published or written by another person except where the acknowledgement is made in text.

Also I hereby grant to University of Moratuwa the non-exclusive right to reproduce and distribute my thesis, in whole or in part in print, electronic or other medium. I retain the right to use this content in whole or part in future works (Such as articles or books)

Signatire: Date: 2024-02-14

The above candidate has carried out research for the Master's thesis under my supervision.

Name of the Supervisor: Dr. H.G.L.N. Gunawardhana

Signature of the Supervisor: Date: 2024-02-14

ACKNOWLEDGMENT

I extend my heartfelt gratitude to the free education system of Sri Lanka, which has been instrumental in shaping my academic journey. I am profoundly thankful to all the dedicated teachers and lecturers who have imparted their knowledge to me until now.

I would like to express my sincere appreciation to the Meteorology Department for providing valuable data, and a special thank to Dr. Panduka Neluwala for his insightful comments and guidance during the progress review evaluations.

A special mention goes to my research supervisor, Dr. H.G.L.N. Gunawardhana, whose unwavering support has been crucial to the success of this research. His patience, motivation, and guidance have played a pivotal role, and without his dedicated supervision, this thesis would not have been possible.

I am grateful to Professor R.L.H.L Rajapakse, the Centre Chairman, for his essential assistance in achieving success in the program. His kindness, guidance, and consistent encouragement, provided amidst a busy schedule, are deeply appreciated.

I extend my thanks to Late Shri Madanjeet Singh, the Founder of SAF-Madanjeet Singh Scholarship Scheme, the South Asia Foundation (SAF), and the University of Moratuwa for enabling me to pursue a Master's Degree in Civil Engineering. My gratitude also goes to Mr. Wajira Kumarasinghe, Mr. Samantha Ranaweera, Mrs. K. A. V. Kalanika, Ms. L. J. N. Silva, and all UMCSAWM staff for their support and encouragement throughout my studies at the University of Moratuwa.

Finally, I would like to express my profound gratitude to my parents and friends for their unfailing support and continuous encouragement throughout this research journey.

Potential Shifting of Climate Zones and Associated Hydrological Impacts under Changing Climate Conditions in Sri Lanka

ABSTRACT

Climate change plays a significant role in decision-making related to water resources management. Understanding the future climate of Sri Lanka is crucial for the development of adaptation and mitigation strategies. This study investigated the potential shifting of climate zones in Sri Lanka under changing climate conditions using the Köppen-Geiger Climate Classification system and identified the associated hydrological impacts. The research utilized observed daily precipitation data from 27 meteorological stations. Predictive mean matching (PMM) and normal imputation method (Norm) were employed using the Multiple Imputation by Chained Equations (MICE) algorithm to impute missing data. The performances of 15 Global Climate Models (GCMs) from Coupled Model Intercomparison Project Phase 6 (CMIP6) were evaluated using the Evaluation Based on Distance from Average Solution (EDAS) method. In distributing station data into higher spatial resolution, a linear regression analysis was conducted to develop a relationship between observed station data points with corresponding Climate Hazards Group InfraRed Precipitation with Station data (CHIRPs) grid cells. The calculated gradient values (m) were then utilized to distribute historical and future projection data from GCMs to each CHIRPs cell (0.05˚ resolution). Furthermore, a distributed hydrological model was used with a 0.05˚×0.05˚ grid cell resolution for calculating water balance and identifying hydrological impacts of future climate change on basin hydrology.

The results depicted varied performance among the CMIP6 models in simulating the monsoon climate of Sri Lanka. The MPI-ESM1-2-HR, CNRM-CM6-1-HR, and CNRM-ESM2-1 models were identified as the top performers in simulating monsoon rainfall patterns in both the wet and intermediate zones, while the CNRM-ESM2-1, CNRM-CM6-1-HR and MRI-ESM2-0 models emerged as the top GCMs for the dry zone. The CNRM-CM6-1-HR and CNRM-ESM2-1 models were the best-performing models among the selected GCMs, with the high-resolution version of CNRM-CM6-1-HR being well-suited for small countries like Sri Lanka. When the Mean-Based method and the Quantile Mapping (QM) method were compared for bias correction performances, the QM method demonstrated strong relationships between observed data and model projections. The results of the Köppen-Geiger Climate Classification indicated that future climate zone influenced by climate change, particularly in the South-West region and the highland areas of Sri Lanka. Highland climates will be the most affected in all projection scenarios, with Cfb and Cwb climate zones projected to disappear under the SSP5-8.5 long-term (TL, 2070-2100) scenario. The outcomes of these changes in basin level indicated that, in the near-term (TN, 2020-2050) period, basins in the eastern side of the island will experience decreased runoff while the west will show an increase. Analyzing the Wet zone under SSP1-2.6 showed a 10% TN increase in runoff, rising to 15% in TL. Under SSP5-8.5, the runoff increase is more significant at 27% (TN) and 38% (TL) levels. In the Dry zone under SSP1-2.6, the TN projections result a 10% increase in runoff, escalating to 35% in the TL period. The findings of this study highlight that the potential climate shifts associated with global warming scenarios vary across distinct regional climate zones in Sri Lanka. This underscores the necessity for region-specific adaptation strategies to effectively mitigate the multifaceted impacts on water resources.

Keywords: Climate Change, Data Imputation, Distributed Hydrological Model, Köppen-Geiger Climate Classification

Table of Content

LIST OF FIGURES

LIST OF TABLES

List of Abbreviations

ACCESS	- Australian Community Climate and Earth-System Simulator
Af	- Tropical Rainforest Climate
AIM/CGE	- Asia-Pacific Integrated Model with Computable General Equilibrium
Am	- Tropical Monsoon Climate
AMIP	- Atmospheric Model Inter-comparison Project
ARCCSS	- Australian Research Council Centre of Excellence for Climate System Science
ASTER GDEM	- Advanced Spaceborne Thermal Emission and Reflection Radiometer Global Digital Elevation Model
Aw	- Tropical Savanna
BCC	- Beijing Climate Center
CAMS	- Chinese Academy of Meteorological Sciences
CAS	- Chinese Academy of Sciences
CDF	- Empirical CumulativeDensity Function
CERFACS	- Centre Européen de Recherche et de Formation Avancée en Calcul Scientifique (European Centre for Research and Advanced Training in Scientific Computation)
CESM	- Community Earth System Model
Cfb	- Subtropical Highland Climate without a Dry Season
CHIRPs	- Climate Hazards Group InfraRed Precipitation with Station
CMA	- China Meteorological Administration
CMCC	- Centro Euro-Mediterraneo sui Cambiamenti Climatici (Euro-Mediterranean Center on Climate Change)
CMIP	- Coupled Model Intercomparison Project
CNRM	- Centre National de Recherches Météorologiques (National Center for Meteorological Research)
Csb	- Warm-Wummer Mediterranean Climate
CSIRO	- Commonwealth Scientific and Industrial Research Organisation

Cwb	- Subtropical Highland Climate with a Dry Season
DEM	- Digital Elevation Model
ECDF	- Empirical Cumulative Distribution Function
EDAS	- Evaluation Based on Distance from Average Solution
ERA	- European Reanalysis
ESGF	- Earth System Grid Federation
ESM	- Earth System Model
ET	- Evaporation
FGOALS	- Flexible Global Ocean-Atmosphere-Land System
FIM	- First Inter Monsoon
GCM	- Global Climate Model
GFDL	- Geophysical Fluid Dynamics Laboratory
GHG	- Green Hosue Gas
GLOBIOM	- Global Biosphere Management Model
GPCC	- Global Precipitation Climatology Centre
GPCP	- Global Precipitation Climatology Project
HR	- High Resolution
IIASA	- International Institute for Applied Systems Analysis
INM	- Institute of Numerical Mathematics
IPCC	- Intergovernmental Panel on Climate Change
MAE	- Mean Absolute Error
MAgPIE	- Model of Agricultural Production and its Impact on the Environment
MAP	- Mean Annual Precipitation
MAT	- Mean Annual Temperature
MESSAGE	- Model for Energy Supply Strategy Alternatives and their General Environmental Impacts
MICE	- Multiple Imputation by Chained Equations
MPI-M	- Max Planck Institute for Meteorology

MRI	- Meteorological Research Institute
NCAR	- National Center for Atmospheric Research
NDA	- Negative Distance from the Average Solution
NEM	- North East Monsoon
NIES	- National Institute for Environmental Studies
NOAA	- National Oceanic and Atmospheric Administration
Norm	- Normal Imputation Method
NRMC	- Natural Resources Management Centre
PBIAS	- Percentage Bias
PBL	- Planetary Boundary Layer
PDA	- Positive Distance from the Average Solution
P_{dry}	- precipitation of the driest month
PERSIANN	- Precipitation Estimation from Remotely Sensed Information using Artificial Neural Networks
PMM	- Predictive Mean Matching Method
P_{sdry}	- precipitation of the driest month in summer
P_{swet}	- precipitation of the wettest month in summer
P_{wdry}	- precipitation of the driest month
P_{wwet}	- precipitation of the wettest month in winter
QM	- Quantile Mapping
R	- Correlation Coefficient
RCM	- Regional Climate Model
RCP	- Representative Concentration Pathways
REMIND	- Regionalized Model of Investments and Development
RMSE	- Root Mean Square Error
RRI	- Rainfall-Runoff-Inundation
SIC	- Sea Ice Concentrations
SIM	- Second Inter Monsoon
SS	- Taylors Skill Score

SSP	- Shared Socioeconomic Pathways
SST	- Sea Surface Temperatures
SWAT	- Soil and Water Assessment Tool
SWM	- South West Monsoon
TB	- Historical Period
T_{cold}	- Temperature of the Coldest Month
T_{hot}	- Temperature of the Hottest Month
TL	- Long-Term Period
T_{mon10}	- Number of Months Where the Temperature is Above 10
TN	- Near Term Period
TRMM	- Tropical Rainfall Measuring Mission
WaPOR	- Water Productivity Open-access portal
WMO	- World Meteorological Organization
μ	- Mean
σ	- Standard Deviation

1. INTRODUCTION

1.1 General

Climate change is a global phenomenon that affects the economic, social, and environmental well-being across every region of the earth. The South Asian region has been identified by the Intergovernmental Panel on Climate Change as being particularly subject to the effects of climate change (IPCC, 2022). These impacts include increased global surface temperature, intensified land monsoon precipitation regime, rising sea levels, declining water resources, and increased food insecurity (IPCC, 2022). As a result, the public, scientists, and lawmakers have all given climate change great attention in recent years (Abbass et al., 2022).

A climate zone is a defined geographical area characterized by specific temperature patterns, precipitation, and weather conditions (Kim et al., 2022; Mondal et al., 2021; Roshan et al., 2022). Climate zoning is essential for identifying and categorizing diverse regions according to climate, enabling well-informed decisions for hydrology, ecology, and water resource management. Previous research has demonstrated a direct correlation between climate change and alternation of climate zones, both at global and regional scales (Buksha et al., 2021; Kim et al., 2022; Malone, 2023).

Climate change affects the balance of sensitive hydrological processes, including precipitation, evaporation, runoff, and groundwater recharge (Epting et al., 2021; Mensah et al., 2022). These changes can have complex implications for water resources, particularly in regions with shifting climate zones. Therefore, understanding the relationship between climate change, climate zone shifting, and subsequent hydrological impacts is essential to uncovering the challenges communities and ecosystems face in the effect of a changing climate. Furthermore, the projections of potential meteorological and hydrological changes allow policymakers to implement adaptation and mitigation measurements that serve the greater good of their constituents (Visweshwaran et al., 2022).

1.2 Background

Climate change, driven primarily by anthropogenic factors, has emerged as one of this generation's most pressing global challenges. Given the inevitability of climate change affecting planet Earth, it is evident that the consequences of these changes will have a substantial impact at regional and local levels (Jacob et al., 2020; Santos et al., 2020). One of the most noticeable effects of climate change is the shifting of climate zones. As global temperatures rise, various regions experience changes in their climatic patterns. This shift often involves the migration of climate zones towards higher latitudes or altitudes, leading to altered weather patterns, precipitation distribution, and temperature regimes (Cui et al., 2021). In parallel with climate zone shifts, the hydrology of these zones also changes. When precipitation and temperature patterns alter in a specific region, its hydrology deviates significantly, particularly in

mountainous areas. Mountainous regions experience climate zone shifts before low-altitude regions are affected (Mahlstein et al., 2013). Mountain ranges are the source of hydrological systems. Alterations within these regions will not only affect the water balance within their respective basins but will also have repercussions on trans-basin and transboundary water management. Subcequent hydrological changes will directly affect aquatic ecosystems, biodiversity, water supply for irrigation, water management systems, hydropower generation and finally, displacement and migration of both people and other living species (Siddha & Sahu, 2022; Upadhyay, 2020; Sadoff & Muller, 2009; Dudgeon, 2000).

The South Asia region, home to over 1.8 billion people and encompassing countries like India, Pakistan, Bangladesh, Nepal, Bhutan, and Sri Lanka, is particularly vulnerable to the effects of climate change. By the end of the 21st century, the annual average temperature across South Asia is projected to rise by 1.2°C, 2.1°C, and 4.3°C under the Shared Socioeconomic Pathways (SSPs) known as SSP1-2.6, SSP2-4.5, and SSP5-8.5, respectively (Almazroui et al., 2020). Sri Lanka is no exception to these global and regional trends, as its unique geographical location in the Indian Ocean renders it vulnerable to such changes. Given the critical role of climate change in sustaining life, ecosystems, and economic activities, understanding the climate zone shifting and hydrological consequences in Sri Lanka is paramount.

1.3 The Significance of Studying Climate-Induced Changes in Sri Lanka

Developing countries, such as Sri Lanka, are particularly susceptible to the adverse effects of climate change. These countries encounter considerable challenges in managing natural systems closely connected with regulating biodiversity services and natural resource management (Khaniya et al., 2021). Sri Lanka is exposed to a wide range of changes related to climate, including land and sea surface temperature change, shifts in rainfall frequency and distribution, increased extreme weather events, and sea level rise with consequent impacts directly affecting agriculture, forestry, and water resources (Eriyagama et al., 2010). Furthermore, due to climate change, there has been a notable increase in the intensity and frequency of extreme weather events in recent decades (Tabari, 2020). These weather events have contributed to heightened natural disasters, such as floods, droughts, cyclones, and landslides (Naveendrakumar et al., 2018; Cho, 2020). Several studies provide evidence suggesting that the hydrology at the basin level in Sri Lanka will change due to climate change. Imbulana et al. (2018) demonstrated the impact of climate change in the Mahaweli River Basin by projecting extreme precipitation events and changes in the monsoon climate of Sri Lanka using global climate models under different emission scenarios. Chathuranika et al. (2022) showed that the future annual streamflow would rise by 59.3% and 65.8% under two Representative Concentration Pathways (RCPs) known as RCP4.5 and RCP8.5, respectively, in the Nilwala River Basin.

The changes in temperature and precipitation play a crucial role in shaping the climate zones and hydrological cycles, which, in turn, significantly influence the course of climate change. Therefore, it is crucial to use state-of-the-art climate projections particularly applicable to the monsoon climate in Sri Lanka to anticipate the future effects. Global Climate Model (GCM) is the most widely used technique in simulating the global climate system and projecting future climate under various emission scenarios (Cai et al., 2018). The GCMs are commonly employed to assess the responses occurring on global or regional scales in a particular area or a limited geographical zone (Salimian et al., 2021).

1.4 Problem Statement

Sri Lanka is an island nation with a diverse range of climates, which are vulnerable to the influences of climate change. Recent studies have projected significant changes in temperature and precipitation patterns in Sri Lanka over the decades, likely to result in shifting the existing climate zones. However, the potential hydrological impacts of such shifting are not yet fully understood. The hydrological impacts of climate change include changes in river flow, groundwater recharge, and water availability, which are vital for the country's economy and survival.

The climate in Sri Lanka experiances significant spatial and temporal variations. Therefore, to develop reliable climate change scenarios in Sri Lanka, GCMs must accurately represent seasonal climate variations across the country. Yet, there haven't been any comprehensive studies that thoroughly evaluate a fitting GCM specifically for the monsoon climate in Sri Lanka. Moreover, identifying the spatial variation of Sri Lanka's climatology requires high-resolution data sets. The limitted availability of spatially distributed data across Sri Lanka poses a significant challenge for hydrological and climate change studies.

1.5 Aim of the Study

This research aims to identify the potential shifting of climate zones in Sri Lanka according to the Köppen climate classification system and assess the associated hydrological impacts.

1.6 Specific Objectives

- To identify the climate zones of Sri Lanka according to the Köppen climate classification
- To project potential changes in temperature and rainfall regimes in the future in Sri Lanka
- To estimate the shifting of climate zones according to the projected climate variables in Sri Lanka.
- To develop a hydrological model to simulate the impacts of climate shifting on dry and wet zones hydrology

2. LITERATURE REVIEW

2.1 General

This literature review reviewed studies relevant to observed climate change over the globe, observed climate trends, climate variations and impacts, and different climate zone classification methods. For future climate change predictions, the review covered GCMs, climate change projections, reliability of the climate models, selection and validations of the climate model, and bias correction methods. The referred studies also included satellite weather data and its usage for climate studies, hydrological modelling studies in Sri Lanka, and distributed hydrological model calibration and validation.

2.2 Climate Change and Global Impact

The Earth's atmosphere includes gases that entrap heat from the Sun, called greenhouse gases, which support keeping the Earth warm. According to the World Meteorological Organization (WMO), the primary greenhouse gases naturally occurring in the atmosphere are carbon dioxide (CO_2), methane (CH_4), and nitrous oxide (N_2O), which cause the greenhouse effect. Natural processes such as decomposition, volcanic eruptions, and Earth's crust shifts release greenhouse gases, influencing climate over time (Gahlawat & Lakra, 2020). This natural greenhouse effect keeps the Earth's average surface temperature at 15˚C by maintaining the radiative balance of the Earth and the atmosphere (Maji et al., 2022). In recent years, anthropogenic activities such as fossil fuel burning and some agricultural and industrial processes have led to the escalations of the concentrations of other greenhouse gases such as nitrous oxide, methane, hydrofluorocarbons (HFCs), perfluorocarbons (PFCs), and sulfur hexafluoride (SF6). For this reason, the atmospheric temperature has continously increased in last decades due to human activities in addition to natural causes. Figure 2-1 highlights the alarming rise in global net greenhouse gas emissions over the past three decades, underlining the urgent need for action to combat global warming in the coming years.

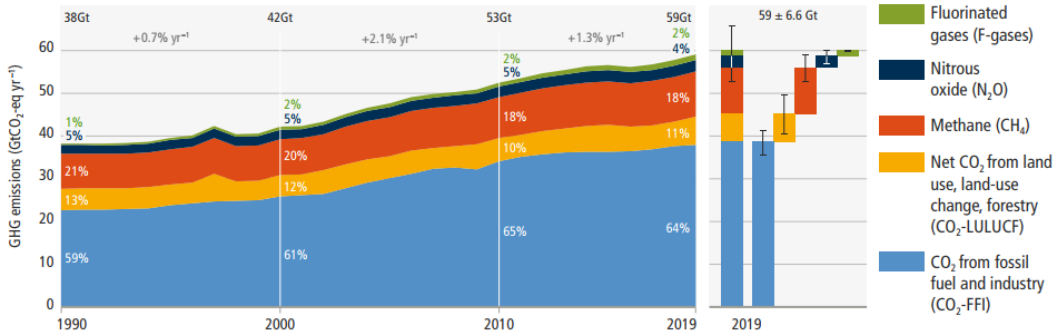

Figure 2-1: Global net emissions of greenhouse gases from anthropogenic activities, 1990–2019 (IPCC, 2022)

2.2.1 Observed Trend of Climate

Over the past 65 years, the world has witnessed an unprecedented transformation of its climate, which will continue into the twenty-first century, resulting in unprecedented impacts.

Global warming, a key driver of this transformation, has left an indelible mark on our planet, and the observed and projected climate changes of the era have affected the complex interplay of atmospheric variables beyond temperature rise and precipitation trends such as pressure and humidity (Abbass et al., 2022).

Atmospheric pressure, humidity levels, and other climate parameters contribute to this complex transformation, creating a more holistic understanding of the shifting dynamics of the climate.

Temperature is a pivotal factor in the climate change phenomena. In 2021, the global surface temperature rose by 1.12°C compared to the average from 1880-1920 (Figure 2-2), as Hansen et al. (2022) reported. Figure 2 reveals a notable temperature increase after 1970, attributed to industrialization. Over the past four decades, there has been a significant trend, with temperatures rising by 0.18°C per decade. These findings underscore the profound impact of human activities on our planet's climate.

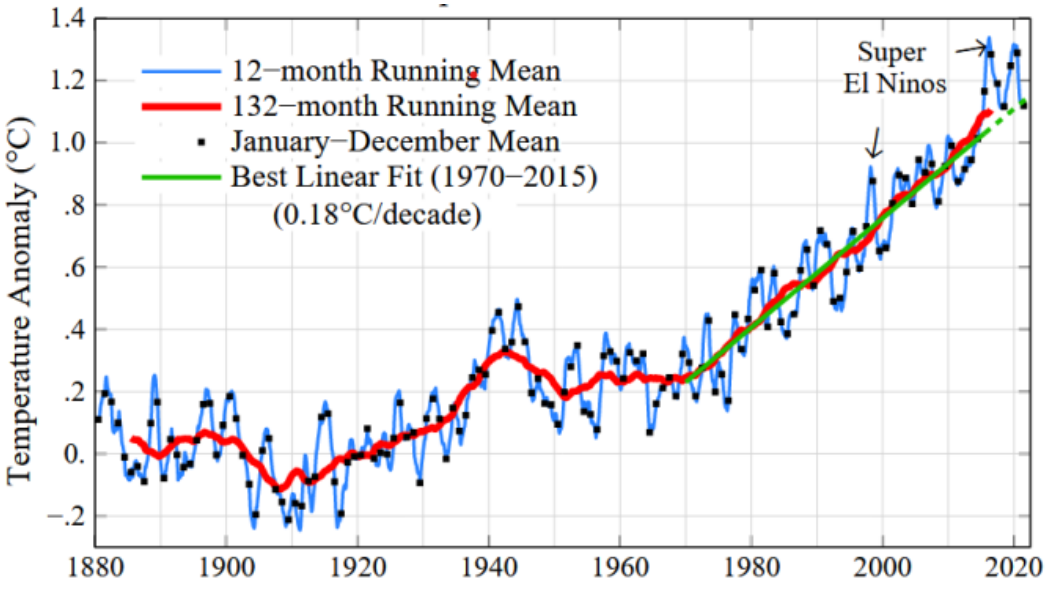

Figure 2-2: Temperature anomaly relative to 1880-1920 (Hansen et al., 2022)

Global warming has caused an increase in atmospheric moisture content, causing precipitation events to become more frequent (Tabari, 2020). Climate change, driven by global warming, is responsible for altering global precipitation patterns (Raihan, 2023). Observational data and climate models consistently indicate that precipitation patterns are shifting, with many regions experiencing alterations in the timing and distribution of rainfall (Dore, 2005). These changes have profound implications for

ecosystems, agriculture, and human societies, requiring adaptive strategies to mitigate their impacts.

2.2.2 Future Climate Change

Future climate change is primarily driven by anthropogenic factors, particularly the increase in greenhouse gas emissions. Projections from climate models and scientific assessments suggest that if emissions continue to rise at current rates, global temperatures will increase by 1.5°C to 4.5°C by the end of the 21st century (IPCC, 2022). Figure 2-3 illustrates the anticipated temperature changes under various greenhouse gas emission scenarios by the end of the 21st century. Global climate change will become a critical issue in the future as natural resources, including water resources, decrease due to the effects of climate change, and the global population is expected to surge by over 30% by 2050 (Mikhaylov et al., 2020).

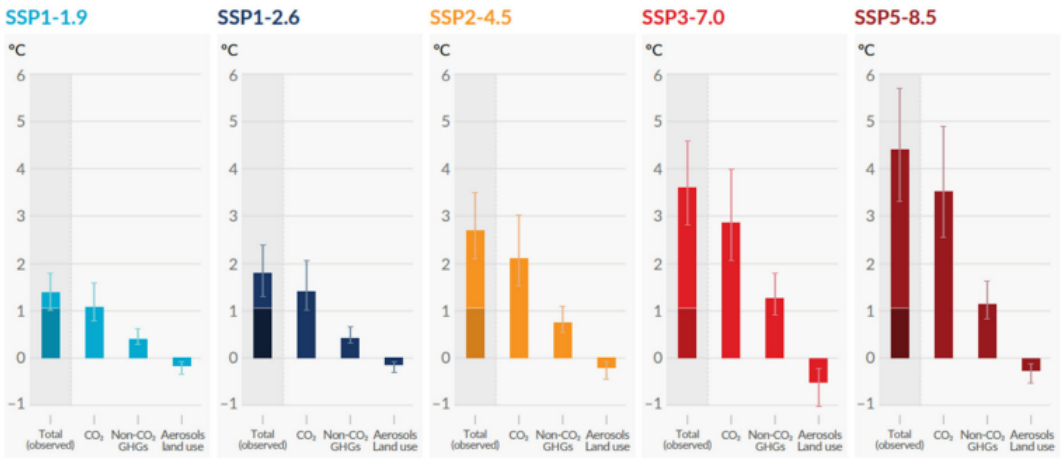

Figure 2-3: Changes in global surface temperature with greenhouse gas emission scenarios for the period 2081 - 2100 compared to the period 1850 – 1900 (IPCC, 2021).

South Asia, a region characterized by its diverse topography, including the Himalayas and the Indian subcontinent, is particularly vulnerable to future climate change impacts. Projections indicate that South Asia may experience higher-than-average temperature increases and changes in precipitation patterns, potentially increasing by 4-25% in the long term (Krishnan et al., 2019). The region is also at risk of glacial retreat in the Himalayas, which could affect the hydrological system in the major river basins from these mountains. The results reveal that the total area of glaciers is retreating at a rate of 12 myr^{-1} due to the impact of climate change in the Himalayas area (Kaushik et al., 2020). The hydrological cycle of the South Asian region, as a near-equatorial area, is exceptionally vulnerable to changes in rainfall patterns, rising temperatures, and glacial retreat.

2.2.3 Extensive Global Ramifications of Climate Change

Climate change has led to many of the most prominent impacts, including rising global temperatures, increased frequency and severity of extreme weather events, and changing precipitation patterns (Dore, 2005; Mondal et al., 2021). The increased

incidence of extreme weather events, such as hurricanes, droughts, and wildfires, can have catastrophic consequences for human societies and ecosystems. This change has far-reaching consequences, including melting polar ice sheets and glaciers, which contribute to rising sea levels threatening coastal communities and ecosystems (Kumar et al., 2021).

Climate zones, which define geographic regions with temperature and precipitation patterns, are not immune to the effects of climate change. As temperatures rise, climate zones shift to higher latitudes and altitudes, and this movement has extreme consequences in polar and mountainous regions (Cui et al., 2021). It can lead to the displacement and extinction of plant and animal species adapted to specific climate zones, disrupting ecosystems and biodiversity (Elsen et al., 2022). Furthermore, these shifts can impact agriculture and food security as traditional crop regions may become less suitable for cultivation. Changes in climate zones can also exacerbate water scarcity as precipitation patterns shift, affecting the availability of freshwater resources and exacerbating conflicts over water access in regions already facing water stress.

Climate change profoundly impacts the hydrological cycle, affecting the distribution and availability of water resources (Yang et al., 2021). Rising temperatures increase evaporation rates, altering the balance between surface water and atmospheric moisture. This phenomenon can result in more intense and variable precipitation patterns, contributing to droughts and floods in different regions. Changes in the hydrological cycle can disrupt ecosystems, threaten water supplies, and exacerbate conflicts over access to water resources, especially in arid and semi-arid regions (Stringer et al., 2021).

Climate variations driven by climate change have a profound global impact, affecting climate zones, the hydrological cycle, and numerous ecosystems and human societies. As climate change continues, understanding and mitigating its consequences remains a critical challenge for the global community, with far-reaching implications for future generations.

2.3 Climate Zone Classification

Climate zone classification is a fundamental aspect of climate science, serving as the basis for understanding and characterizing the diverse climatic conditions on Earth. Climate zones are geographical regions that share similar patterns of temperature, precipitation, and other climatic variables (Kim et al., 2022; Mondal et al., 2021). These zones are defined based on long-term weather data, allowing scientists to systematically categorize and study the Earth's diverse climates. Climate zones provide a framework for understanding regional differences in climate and help researchers predict and interpret climatic changes.

Factors such as latitude, topography, proximity to oceans, and atmospheric circulation patterns drive climate zones. Latitude plays a crucial role in determining temperature patterns, with regions closer to the equator generally experiencing warmer climates

and those closer to the poles experiencing colder climates. The presence of oceans and large bodies of water moderates temperature extremes, leading to more moderate climates near coastlines. Topography, such as mountain ranges, can influence local climate patterns, creating rain shadows and temperature gradients (Laignel et al., 2023; Cui et al., 2021).

Climate zones are paramount for various fields, including agriculture, ecology, urban planning, and climate modelling. They help determine the suitability of an area for specific crops and ecosystems, guide decisions on building design and infrastructure, and assist in the development of climate change adaptation strategies. Understanding climate zones is essential for predicting climate change's potential impacts, as temperature and precipitation changes can have far-reaching consequences for ecosystems and human societies (Demuzere et al., 2019; Masson et al., 2020).

Several widely recognized climate zone classifications are commonly used in climate studies. The most notable classifications are the Köppen climate classification system, Thornthwaite climate classification, Trewartha climate classification, Bergeron climate classification, and Koppen-Geiger climate classification, shown in Table 2-1. Each system has unique characteristics and methodologies for categorizing climates, making them valuable tools for researchers in different contexts.

Table 2-1: Summary of climate zones classification systems

Classification System	Summary	Reference
Köppen Climate Classification	Developed by climatologist Wladimir Köppen, this system is one of the most widely recognized and used climate classification systems. It categorizes climates based on temperature and precipitation patterns. The major Köppen climate types include tropical (A), arid (B), temperate (C), polar (E), and highland (H) climates, with further subdivisions based on seasonal variations and temperature regimes.	(Köppen,1931)
Trewartha Climate Classification	This system, developed by American geographer Glenn Thomas Trewartha, modifies the Köppen system and divides the world into five main climate types: tropical, dry, temperate, polar, and polar tundra. It incorporates additional factors such as humidity and vegetation and provides a more detailed classification of climate regions.	(Trewartha & Horn ,1980)

Classification System	Summary	Reference
Thornthwaite Climate Classification	The Thornthwaite Climate Classification is a system that categorises climate types based on moisture availability and temperature. Developed by climatologist C.W. Thornthwaite, it divides climates into five main categories: arid, semi-arid, temperate, subarctic, and tropical. This classification helps in understanding and studying regional climate patterns.	(Thornthwaite ,1948)
Bergeron Climate Classification	The Bergeron Climate Classification is a system used to categorize climates based on temperature and precipitation patterns. This classification was developed by climatologist and meteorologist Emile Bergeron. This classification scheme divides climates into five primary types: tropical, arid, temperate, cold, and polar, providing a framework for understanding and comparing various climate regions worldwide.	(Bergeron Jr ,1928)
Koppen-Geiger Climate Classification	The Köppen-Geiger Climate Classification, developed by Wladimir Köppen and modified by Rudolf Geiger, categorizes the world's climates based on temperature and precipitation patterns. It uses letters and symbols to represent climate types, such as tropical (A), arid (B), temperate (C), polar (E), and more. This system aids in understanding and comparing global climate diversity.	(Köppen,1936)

The Köppen Climate Classification is a widely used classification developed by Russian-German climatologist Wladimir Köppen in 1931 to classify climates based on temperature and precipitation patterns (Peel et al., 2007). The global vegetation map of Grisebach inspires the Köppen Classification published in 1866 and Köppen's background in plant sciences (Wilcock, 1968). Wladimir Köppen and Rudolf Geiger developed the Geiger Climate Classification System, first published in 1936, based on five major climate types and several subtypes defined based on temperature and precipitation patterns.

Table 2-2: Description of Köppen- Geiger Climate Symbols and Defining Criteria (Peel et al., 2007)

1st	2nd	3rd	Description	Criterion
A			Tropical	$T_{cold} \geq 18$
	f		- Rainforest	$P_{dry} \geq 60$
	m		- Monsoon	Not (Af) & $P_{dry} \geq 100 - MAP/25$
	w		- Savannah	Not (Af) & $P_{dry} < 100 - MAP/25$
B			Arid	$MAP < 10 \times P_{threshold}$
	w		- Desert	$MAP < 5 \times P_{threshold}$
	s		- Steppe	$MAP \geq 5 \times P_{threshold}$
		H	- Hot	MAT ≥ 18
		K	- Cold	MAT < 18
C			Temperature	$T_{hot} > 10$ & $0 < T_{cold} < 18$
	s		- Dry Summer	$P_{sdry} < 40$ & $P_{sdry} < P_{wwet}/3$
	w		- Dry Winter	$P_{wdry} < P_{swet}/10$
	f		- Without dry season	Not (Cs) or (Cw)
		a	- Hot Summer	$T_{hot} \geq 22$
		b	- Warm Summer	Not (a) & $T_{mon10} \geq 4$
		c	- Cold Summer	Not (a or b) & $1 \leq T_{mon10} < 4$
D			Cold	$T_{hot} > 10$ & $T_{cold} \leq 0$
	s		- Dry Summer	$P_{sdry} < 40$ & $P_{sdry} < P_{wwet}/3$
	w		- Dry Winter	$P_{wdry} < P_{swet}/10$
	f		- Without dry season	Not (Ds) or (Dw)
		a	- Hot Summer	$T_{hot} \geq 22$
		b	- Warm Summer	Not (a) & $T_{mon10} \geq 4$
		c	- Cold Summer	Not (a, b, or d)
		d	- Very Cold Winter	Not (a or b) & $T_{cold} < -38$
E			Polar	$T_{hot} < 10$
	T		- Tundra	$T_{hot} > 0$
	F		- Frost	$T_{hot} \leq 0$

2.4 Meteorological Data Gap Filling

Observed meteorological data are the core of climate change and hydrological analysis (Costa et al., 2021). A network of meteorological or climate observations consists of an array of weather stations strategically positioned across specific geographic regions.

The primary objective is ascertaining those designated areas' meteorological and climatological parameters. Each station collects data on various factors, including air temperature, atmospheric pressure, wind speed and direction, relative humidity, rainfall, evaporation and solar radiation. Subsequently, this gathered information is transmitted to a central database within the network for processing and storage. Nevertheless, unforeseen circumstances may render manual weather stations ineffective over time, leading to their temporary closure, permanent shutdown, operational malfunction, or precarious functionality (Costa et al., 2021). In these situations, it is required to fill that gaps using adequate techniques to get a continuous time series of data.

Analyzing climate zone shifting and its hydrological impacts in Sri Lanka requires long and comprehensive time series data. However, acquiring continuous datasets for Sri Lanka proves challenging due to irregular data collection. Specifically, some weather stations, mainly manual stations in the north and east provinces, remained inoperable during the Civil War. This lack of continuous data makes it difficult to understand and predict climate change and climate zone shifting and impacts Sri Lanka's hydrological systems.

To overcome these data limitations, researchers have employed various strategies, including data gap-filling techniques, spatial interpolation methods, and the integration of satellite-based data (Table 2-3). These approaches help mitigate the impact of missing data points and provide a more complete picture of Sri Lanka's climate and hydrology.

Table 2-3: Summary of existing missing data imputation methods

Method	Summary	Reference
Linear Regression	The gap-filling through linear regression involves utilizing data acquired from a consistently operating station during the gap period. When confronted with missing observations in dataset Y at a specific station, the historical series is reconstructed by incorporating observations from another dataset X sourced from a neighbouring station with similar characteristics. The estimation method involves applying a regression equation tailored based on the concurrently observed values at the two stations.	(Fagandini et al., 2023)

Method	Summary	Reference
Spatial Interpolation	This method employs two primary techniques: Inverse Distance Weighting (IDW) and Kriging. IDW assigns weights to neighbouring stations based on their proximity to the location with missing data. The weighted average of these values is then used to estimate the missing value. Kriging, on the other hand, is a geostatistical interpolation technique that considers the spatial correlation structure of the data to predict missing values. It utilizes a variogram, a statistical measure of spatial correlation, to determine the weights assigned to neighbouring stations. While IDW is more straightforward and computationally efficient, Kriging offers more accurate estimates, particularly in areas with complex spatial patterns.	(Addi et al., 2022)
Machine Learning Techniques	Neural networks have emerged as a powerful tool for addressing missing data in meteorological datasets. By trining the connections between various meteorological parameters, neural networks can effectively predict missing values based on the relationships learned during training. The methodology proposed intends to create a precipitation time series using observed data from nearby stations. The outcomes have been contrasted with those of a Multiple Linear Regression model, serving as a foundation for enhancements to conventional practices.	(Papailiou et al., 2022)
The Multiple Imputation by Chained Equations	MICE is a multiple imputation technique that iteratively imputes missing values in a multivariate dataset. It works by repeatedly imputing each missing value while considering all other variables in the dataset. This process ensures that the imputed values are consistent with the overall distribution of the data.	(Buuren & Oudshoorn, 2011)

2.4.1 The Multiple Imputation by Chained Equations

The Multiple Imputation by Chained Equations (MICE) algorithm is a multiple imputation method (Rubin, 1996) developed by Buuren & Oudshoorn (2011), which

imputes missing values by producing multiple complete data sets in which missing values are substituted with probable values based on information available in the observed data. The MICE algorithm is implemented by writing an S-PLUS function (Mazumdar et al., 1999). To handle incomplete variables, the user can select a set of predictors for imputation. This feature is advantageous for imputing substantial collections of data series encompassing numerous variables. This method helps estimate climatological parameters through imputation, using a comprehensive collection of input data sets, therefore has a more extensive variety of applications in climatological parameter gap filling (de Carvalho et al., 2017; Turrado et al., 2014; Wesonga, 2015). The following section discusses two methods in MICE commonly used to fill the gaps in data series.

- Predictive Mean Matching Method (PMM)

The predictive mean matching (PMM) method involves using the mean of a set of similar observations to attribute the value of a missing observation. This method assumes that the missing value is likely to be similar to the mean of a set of similar observations (Vink et al., 2014).

- Normal Imputation Method (Norm)

The normal imputation method is a method (Norm) of imputing missing data in a dataset. It involves replacing the missing value with the mean or median of the entire dataset or with a randomly generated value from a normal distribution. This method is based on the assumption that the missing value is likely to be similar to the mean of the entire dataset (Lee & Carlin, 2010).

2.4.2 Data Imputation Performance Evaluation

In data imputation, assessing the quality and reliability of imputed data is paramount to ensure the robustness of subsequent analyses and modelling. Performance evaluation metrics are essential for quantifying how well-imputed data align with the missing values. This section discusses the significance of performance evaluation metrics. It introduces the use of Percentage Root Mean Square Error (RMSE) and Mean Absolute Error (MAE) as two critical metrics for evaluating data imputation performance (Turrado et al., 2014).

$$RMSE = \sum_{i=1}^{n} \sqrt{\frac{1}{n}\left(\hat{G}_i - G_i\right)^2} \quad \text{----------(1)}$$

$$RMSE(\%) = \frac{RMSE}{\frac{1}{n}\sum_{i=1}^{n} G_i} \times 100\% \quad \text{----------(2)}$$

$$MAE = \frac{1}{n}\sum_{i=1}^{n}\left|\hat{G}_i - G_i\right| \quad \text{----------(3)}$$

$$MAE(\%) = \frac{MAE}{\frac{1}{n}\sum_{i=1}^{n} G_i} \times 100\% \quad \text{----------(4)}$$

where G_i and $\hat{G}_i$ are the measurements and the model-estimated values of precipitation, respectively, and *n* is the number of data points of the validation set. The evaluation was conducted on three timescales: daily, 10-day, and monthly (Costa et al., 2021).

2.5 Global Climate Models

The Global Climate Model (GCM) has become the predominant tool for future climate change studies, facilitating climate projections under various emission scenarios (Cai et al., 2018). Over the past few decades, GCMs have significantly improved, leading to more precise simulations of climate and its changes. The establishment of the Coupled Model Intercomparison Project (CMIP) aimed to investigate and compare the climate simulations produced by GCMs (Meehl et al., 2000).

The most advanced GCM was developed under the sixth phase of the IPCC, providing insights into past climate mechanisms and enabling the projection of future climate scenarios. Compared to previous model intercomparison projects, CMIP6 projections can simulate various monsoon characteristics (Gusain et al., 2020).

2.5.1 Reliability of the Global Climate Models

The GCMs have several notable strengths. They provide a comprehensive framework for simulating the Earth's climate system, incorporating complex interactions among the atmosphere, oceans, land surface, and cryosphere (Mohandas, 2022). The GCMs have successfully reproduced historical climate variability and trends, demonstrating their ability to capture essential climate processes. They are instrumental in understanding the physical principles that govern the climate system and are crucial for climate predictions and projections. Moreover, GCMs offer the advantage of assessing the impacts of various climate forcings, including greenhouse gas emissions, volcanic eruptions, and solar variability, allowing researchers to quantify their contributions to observed climate changes (Maher et al., 2021).

Despite their strengths, global climate models also have limitations and face challenges. One primary challenge is the complexity of the climate system, as it involves countless interacting components and processes. The GCMs require simplifications and parameterizations to make computations feasible, leading to uncertainties in model outputs (Wang et al., 2020). Additionally, the spatial and temporal resolutions of GCMs may not adequately capture small-scale climate phenomena and rapid changes (Kendon et al., 2021).

2.5.2 GCMs Used in Past Studies in South Asia

When selecting climate models for this study, several key factors were considered, including previous research on monsoon climate and spatial resolution. Table 4 provides an overview of the selected climate models based on these criteria. All the models listed in Table 2-4 have been extensively studied within the South Asia domain and possess a spatial resolution of less than 2.0˚. By considering these factors, the

chosen models are expected to provide relevant and accurate predictions about the monsoon climate domain of the study region.

Table 2-4: Details of the CMIP6 GCMs Assessed in this Study

SN	Source ID	Institution ID	Country	Nominal Resolution	Variant label
1	ACCESS-CM2	CSIRO-ARCCSS	Australia	1.2˚ × 1.8˚	r1i1p1f1
2	ACCESS-ESM1-5	CSIRO	Australia	1.2˚ × 1.8˚	r1i1p1f1
3	BCC-CSM2-MR	BCC	China	1.1˚ × 1.1˚	r1i1p1f1
4	CAMS-CSM1-0	CAMS	China	1.1˚ × 1.1˚	r1i1p1f1
5	CESM2	NCAR	USA	0.9˚ × 1.3˚	r1i1p1f1
6	CMCC-CM2-SR5	CMCC	Italy	1.0˚ × 1.0˚	r1i1p1f1
7	CMCC-ESM2	CMCC	Italy	1.0˚ × 1.0˚	r1i1p1f1
8	CNRM_CM6-1-HR	CNRM-CERFACS	France	0.5˚ × 0.5˚	r1i1p1f2
9	CNRM-ESM2-1	CNRM-CERFACS	France	1.4˚ × 1.4˚	r1i1p1f2
10	GFDL-ESM4	NOAA-GFDL	USA	1.3˚ × 1.0˚	r1i1p1f1
11	FGOALS-f3-L	CAS	China	1.3˚ × 1.0˚	r1i1p1f1
12	INM-CM4-8	INM	Russia	1.5˚ × 2.0˚	r1i1p1f1
13	INM-CM5-0	INM	Russia	1.5˚ × 2.0˚	r1i1p1f1
14	MPI-ESM1-2-HR	MPI-M	Germany	0.9˚ × 0.9˚	r1i1p1f1
15	MRI-ESM2-0	MRI	Japan	1.1˚ × 2.1˚	r1i1p1f1

2.5.3 Selection of an appropriate GCM for monsoon climate in Sri Lanka

Selecting an appropriate GCM is a critical step in climate research and prediction. The GCMs are complex computer simulations that attempt to represent the Earth's climate system and its dynamics. These models incorporate a wide range of physical, chemical, and biological processes to simulate the behaviour of the Earth's atmosphere, oceans, land surfaces, and ice sheets. However, no single GCM can accurately capture all aspects of global climate, and the choice of model can significantly affect the outcomes of climate simulations and predictions (Jose & Dwarakish, 2020).

Like many other South Asian regions, Sri Lanka experiences a distinct monsoon climate characterized by seasonal shifts in wind patterns and precipitation (Naveendrakumar et al., 2019). Accurate modelling of monsoon behaviour is vital for predicting rainfall patterns, agricultural planning, and disaster management in the country. However, not all GCMs are equally adept at representing monsoon systems, and some may struggle to simulate the fine-scale processes that drive the monsoon.

- Global Climate Model selection based on Evaluation Based on Distance from Average Solution (EDAS) -
  To select the best-performing GCM, a methodology based on the distance from the average solution is employed. The distance method to the average solution, known as EDAS, was introduced by Ghorabaee et al. (2015), which enables the effective processing of decision information during multi-criteria decision analysis and therefore has a wider variety of applications (Chen, 2023; Phan & Nguyen, 2022). The fundamental concept of EDAS is to assess the available alternatives using positive and negative distances regarding the average answer derived from the decision matrix (Mishra et al., 2022).

2.5.4 Coupled Model Intercomparison Project Phase 6

The CMIP was established to investigate and contrast climate simulations using coupled GCMs, which incorporate ocean, atmosphere, cryosphere, and land components (Meehl et al., 2000). The CMIP provides a framework for comparing and evaluating climate models through standardized experiments. The CMIP Phase 6 (CMIP6) represents the latest iteration of this project and has helped improve our understanding of climate change and its potential impacts. The CMIP6 (Coupled Model Intercomparison Project Phase 6) primarily aims to address several key research questions related to the Earth's system response to external forces. These questions include understanding the origins and implications of systematic model biases and assessing future climate change in the face of internal climate variability, climate predictability, and scenario uncertainties (Eyring et al., 2016).

The core experiments include the Historical Simulation for understanding past climate and future projections up to 2100 by exploring emission scenarios. Historical projections are based on observations and various forcing data, and they are:

- Emissions of short-lived species and long-lived greenhouse gases (GHGs)
- GHG concentrations
- Global gridded land-use forcing data sets
- Solar forcing
- Stratospheric aerosol data set (volcanoes)
- Atmospheric Model Inter-comparison Project (AMIP) sea surface temperatures (SSTs) and sea ice concentrations (SICs)
- For simulations with prescribed aerosols, a new approach to prescribing aerosols in terms of optical properties and the fractional change in cloud droplet effective radius to provide a more consistent representation of aerosol forcing
- For models without ozone chemistry, time-varying gridded ozone concentrations and nitrogen deposition

Enabling model groups to employ diverse forcing data sets can enhance the representation of uncertainty (Eyring et al., 2016).

2.5.5 Shared Socioeconomic Pathways (SSPs)

Scenarios play a crucial role in climate change research and assessment as they facilitate our comprehension of the long-term implications of anthropogenic activities. Additionally, they allow researchers to investigate various potential futures within the framework of intrinsic uncertainties that lie ahead.

The development of SSPs consisted of population, urbanization and Gross Domestic Product (GDP) as main socioeconomic scenario drivers (essential SSP elements). One of the critical contributions offered by the SSPs lies in their incorporation of socioeconomic development alongside climate change mitigation and adaptation. The SSPs give helpful information about the challenges and opportunities of meeting climate goals by showing different paths for population growth, economic growth, and energy systems.

Table 2-5: Overview of Shared Socioeconomic Pathways

SSP	Description	Marker Team	Reference
SSP1-2.6	Sustainability	IMAGE (PBL)	Van Vuuren et al. (2017)
SSP2-4.5	Middle of the Road	MESSEGE-GLOBIOM (IIASA)	Fricko et al. (2017)
SSP3-7.0	Regional Rivalry	AIM/CGE (NIES)	Fujimori et al. (2017)
SSP5-8.5	Fossil-fueled Development	REMIND-MAgPIE (PIK)	Kriegler et al. (2016)

2.6 Methods of Bias Correction

Climate models are imperfect and may not always accurately represent the complex interactions between different climate system components. This can lead to errors in the projections, mainly when predicting regional or local climate conditions. To address these issues, bias correction methods are used to improve the fitting of climate model simulations to observations in the control period (Worku et al., 2020). Biased climate model simulations may lead to incorrect assessments of climate impacts, hinder the reliability of long-term projections, and limit the usefulness of model results for decision-making in various sectors. These methods aim to adjust the model output to match more closely with the observed data while preserving the overall patterns and trends in the model.

2.6.1 Empirical Statistical Bias Correction

Empirical Statistical Bias Correction is a data-driven method to rectify systematic errors in global climate models. It involves developing statistical relationships between model-simulated and observed data, allowing for fine-scale adjustments. This approach improves the accuracy and reliability of climate model outputs, enhancing their utility for climate change research and impact assessments. Table 2-6 provides the equation for the empirical statistical bias corrected method.

Table 2-6: Empirical statistical bias correction methods

Method	Transformation for Precipitation	Transformation for Temperature	Reference
Mean Based Method	$X'_o = X'_M \times \frac{\mu_o}{\mu_M}$	$X'_o = X'_M + \mu_o - \mu_M$	(Schmidli et al., 2006)
Variance Based Method	$X'_o = \frac{(X'_M - \mu_M)}{\sigma_M} \times \sigma_O + \mu_O$	Same as Precipitation	(Hawkins et al., 2013)

Subscript '*O*' represents observation, and '*M*' represents the modelled variable; with or without the apostrophe, it represents the future and calibration period, respectively.

2.6.2 Quantile Mapping Bias Correction

Quantile mapping is a widely used bias correction method in climate research. This approach aligns the cumulative distribution functions of model-simulated data with observed data, correcting biases in distribution percentiles. By preserving the statistical characteristics of the climate signal while minimizing biases, quantile mapping improves the accuracy and reliability of climate model outputs for various applications (Ayugi et al., 2020). Table 2-7 provides the equation for the quantile mapping method.

Table 2-7: Quantile mapping bias correction methods

Method	Transformation for Precipitation	Transformation for Temperature	Reference
Quantile Mapping	$X'_o = F'_O[F_M(X'_M)]$	Same as precipitation	(Wood et al., 2004)
Quantile Correcting	$X'_o = X'_M \times \frac{F'_O[F_M(X'_M)]}{F'_M[F_M(X'_M)]}$	$X'_o = X'_M + F'_O[F_{M'}(X'_M)] - F_O^{-1}[F_{M'}(X'_M)]$	(Mpelasoka & Chiew, 2009)
Transfer Function	$X'_o = a \times X_M^b$	$X'_o = a \times X'_M + b$	(Prudhomme et al., 2002)

Subscript '*O*' represents observation, and '*M*' represents the modelled variable; with or without the apostrophe represents future and calibration period, respectively; *F* and F^{-1} represent empirical cumulative distribution function (ECDF) and reverse ECDF, respectively.

2.7 Methods of Developing Gridded Meteorological Data Sets

Gridded meteorological data sets are crucial tools in climate research and hydrological modelling. They provide spatially continuous and temporally consistent information about weather and climate variables, which is invaluable for various applications (Blankenau et al., 2020).

Gridded datasets are crucial as they enable interpolating meteorological observations, offering estimates of weather and climate variables in locations lacking direct

measurements (Blankenau et al., 2020). These datasets are essential inputs for various environmental models, including climate and hydrological models. Table 2-8 discusses the existing methods for developing gridded datasets.

Table 2-8: Summary of gridded dataset development methods

Method	Summary	Reference
Kriging method of interpolation	Kriging is a geostatistical interpolation method used to estimate values at unsampled locations based on the spatial autocorrelation of observed data. It involves characterising spatial property variations through variograms and aims to minimize the estimation errors associated with predicting variations.	(Oliver & Webster, 1990)
Ensemble Kalman Filter	Ensemble Kalman Filter integrates observed data with model simulations to create gridded meteorological data sets. These methods are particularly suitable for real-time applications, where near-real-time observations are incorporated into the analysis.	(Houtekamer & Mitchell, 1998, 2001)

2.7.1 Satellite Weather Data

Traditional methods of rainfall measurement, such as rain gauges, are limited in their spatial and temporal coverage. Rain gauges are often sparsely distributed, making obtaining more accurate and dispersed rainfall estimates difficult. Satellite rainfall data is a valuable tool that offers comprehensive global rainfall coverage, with the advantage of high temporal and spatial resolutions. Climate change studies high spatial resolution data for reliable mitigation measurements. This makes satellite rainfall data ideal for drought monitoring, flood forecasting, and water resource management (Dumont et al., 2022; Hinge et al., 2022; Lemma et al., 2022).

Table 2-9: Key features of satellite rainfall data sources

Product	Spatial Resolution	Temporal Resolution	Temporal Domain
GPCC	2.5˚	Monthly	1951 - 2000
GPCP	0.5˚,1.0˚,2.5˚	Daily, Monthly	1979 - 2004
PERSIANN	0.25˚	6-Hours, Daily	1983 - present
TRMM	0.25˚	3-Hours, Daily	1998 - present
ERA-Interim	0.75˚	6-Hours	1950 - present
ERA5	0.25˚	Hourly	1979 - present
CHIRPs	0.05˚	Daily, Monthly, Pentad, Decadal, Annual	1981 - present

Spatial resolution was the most critical factor when validating the database selection for a small island like Sri Lanka. Considering its spatial resolution, temporal resolution, and data availability period, the Climate Hazards Group InfraRed Precipitation with Station (CHIRPs) dataset is the most suitable for high-resolution climatological studies.

2.7.2 The CHIRPs Dataset

The CHIRPS dataset is a global, high-resolution rainfall dataset produced by the University of California, Berkeley Climate Hazards Group. The dataset is created by combining satellite rainfall estimates with ground-based observations. The development of the CHIRPS dataset involved the collaboration of the U.S. Geological Survey, the Climate Hazards Group at the University of California in Santa Barbara, the Climate Prediction Center and the National Climatic Data Center (Marulanda et al., 2022). The CHIRPS satellite observation employs two thermal infrared satellites to collect data from observation archives. This data is obtained by measuring the duration of cold clouds (Funk et al., 2015). The calibration process of CHIRPs involves using the Tropical Rainfall Measuring Mission (TRMM) and in situ precipitation observations (Funk et al., 2015). The CHIRPS dataset was previously used in Sri Lanka by Alahacoon and Edirisinghe (2021) to study historical rainfall and analyse trends.

2.8 Hydrological Modelling

Hydrological Modelling is a process used to understand natural ecological systems, and this understanding is employed to improve decision-making in water resource planning, policymaking, irrigation practices, and the identification of flood-prone areas and groundwater improvement. Comprehensive hydrological parameters are inputted into the mathematical or systematic process, and these models perform complex hydrological processes, providing results in the form of hydrological components, such as runoff (Pandi et al., 2021).

The earliest attempt at hydrological modelling can be traced back to the 18th century when Mulvany (1851) introduced the method to compute peak discharge by calculating the concentration time. Fundamental theories that used hydrological modelling were developed until the 1960s and the 1960s witnessed the initiation of the computer revolution. The computational power of computers enabled the development of a new hydrological subfield called numerical hydrology (Singh, 2018). With the power of computers, it became possible to simulate the entire hydrological system with the development of the Stanford Watershed Model (Crawford & Linsley, 1966). Since then, two and three-dimensional modelling has become possible (Bear, 1979), and the simulation of water flow, sediment, and pollutant transport has been undertaken (Bear & Verruijt, 1987). Operational techniques, such as reservoir management, were developed, introducing techniques to calibrate hydrological models (Beven, 2001).

Moreover, computers have facilitated the creation of accessible software and tools for user convenience in tasks such as acquiring, storing, retrieving, processing and distributing data (Croley, 1980). The development of remote sensing tools facilitates the development of geographical information systems (GIS) to analyse large quantities of vector and raster data (Maidment, 2005). After computer revolution, artificial intelligence made huge impact on hydrological modelling. Early 21st century witnessed the new nural network models such as fuzzy logic, genetic programming, and wavelet models and these new methods made significant impact in hydrological model development (Kumar et al., 2005; Sen, 2009; Tayfur, 2014).

2.8.1 Objectives of Hydrological Modelling

Hydrological modelling plays a vital role in understanding hydrological processes within a watershed, encompassing phenomena such as precipitation, runoff, infiltration, and evaporation. Finally, it can explain the water balance in the given study area. With these results, primary objectives of hydrological modelling can be achieved, such as water resource management, a comprehensive assessment of water availability, demand prediction, and strategic allocation for agricultural, industrial, and domestic purposes. Moreover, hydrological models perform a critical role in disaster management, such as flood and drought predictions, by identifying vulnerable areas and formulating preventive measures.

Beyond the above primary objectives, hydrological models address broader challenges, including climate change impact assessment on water resources. Additionally, hydrological models aid in environmental impact assessments, evaluating anthropogenic activities on water quality. With these capabilities, hydrological models can be used as decision-making tools and simulate diverse scenarios, providing valuable insights for informed decision-making and policy development in water-related issues and disaster preparedness.

2.8.2 Types of Hydrological Models

Hydrological models address spatial scale, complexity, and purpose, enabling researchers to choose models that best suit their specific objectives and data availability. Hydrological models can be classified based on model structure, spatial distribution, stochasticity, and spatial-temporal application (Wheater, 2002). The following table 2-10 discusses different types of hydrological models.

Table 2-10: Summary of different types of hydrological models

Type	Summary	Reference
Lumped Model	The lumped model is a hydrological model representing a catchment as a single unit, considering average values of variables over the entire catchment area. Typically, a lumped model is formulated using differential or empirical algebraic equations, neglecting consideration for spatial variations in processes, inputs, boundary conditions, and geometric characteristics within the system.	(Beven, 2001)
Distributed Model	Distributed models produce spatially distributed predictions by representing local averages by discretising the catchment into numerous elements or grid squares. The equations for the state variables related to each element are then solved to capture the spatial variability within the modelled system.	(Beven, 2001)
Semi-distributed Model	A semi-distributed hydrological acts as a balance model between lumped and fully distributed models. These models split the basin into several smaller subbasins, and spatial parameter variation is partially permitted.	(Orellana et al., 2008)

2.8.3 Distributed Hydrological Model

There are different types of distributed hydrological models. The Rainfall-Runoff-Inundation (RRI) model is a popular distributed hydrological model that serves as a comprehensive framework in hydrological science and is used for rainfall, runoff, and inundation processes. This model uses meteorological, geographical, and hydraulic factors to simulate the dynamic cascade of events from precipitation to flooding, offering a holistic perspective on watershed behaviour. At its core, the RRI model delineates how rainfall infiltrates the soil, transforms into runoff, and subsequently contributes to inundation, encapsulating the entire hydrological cycle. However, RRI models simplify the complex physical processes involved in rainfall, runoff, and inundation. These simplifications may not capture all relevant details, leading to potential inaccuracies in modelling certain hydrological phenomena.

The Soil and Water Assessment Tool (SWAT) model is a prominent and widely used watershed-scale distributed hydrological model employed to simulate and assess the intricate interactions of soil, water, and land management practices. SWAT facilitates comprehensive analyses of hydrological processes by integrating meteorological, topographical, and land use data. It employs a basin-scale approach, allowing researchers and water resource managers to evaluate the impact of various land management strategies, climate scenarios, and land use changes on water availability and quality. However, SWAT requires substantial data for accurate simulations, including detailed information on topography, soils, land use, and meteorology.

In this study, the simulation of natural water balance was conducted using the distributed hydrological runoff model created by Kashiwa & Kazama (2010) within the framework outlined by Kazama (2004). The model was modified to estimate the distributed water balance in Sri Lanka. This distributed hydrological model process combines layers with precipitation, evaporation, surface runoff, groundwater flow and water balance. The methodology used for flow estimation included direct and ground flow in the model. Because of that, this model can provide a comprehensive idea of the water balance.

The selection of this model for the study was based on its requirement for less data compared to RRI and SWAT models. Additionally, software-based models such as RRI and SWAT are challenging to reshape for specific objectives, whereas program-based models can be improved to achieve user needs.

2.8.4 Calibration of Hydrological Model

Model calibration involves the selection of suitable values for model parameters to simulate the hydrological behavior of a study area accurately (Moore & Doherty, 2005; Wagener et al., 2004). Most models include two types of parameters: physical parameters and process parameters (Singh, 1995). Physical parameters reflect measurable properties of the catchment, such as the catchment area and surface slope. On the other hand, process parameters represent characteristics that are not easily

measured, such as the average depth of water storage capacity and the coefficient of nonlinearity controlling discharge rates from component stores (Singh, 1995). The calibration process of the model can be done manually or automated. The following table 2-11 summaries the different methods available in the model calibration.

Table 2-11: Summary of different methods of hydrological model calibration

Method	Summary	Reference
Manual Calibration	Model calibration involves manually adjusting parameter values until the model output closely matches observed data, requiring familiarity with the model and study catchments. It's a trial-and-error process with no clear endpoint, leading to variability in results. This method is time-consuming, and formal uncertainty analysis is a disadvantage.	(Wheater, 2002; Sorooshian and Gupta, 1995)
Automatic Calibration	Computer-based methods for automatic calibration of hydrological models aim to expedite the calibration process and enhance objectivity by eliminating subjective manual human judgment. While these methods offer increased objectivity and reduced dependency on model-specific expertise, they have not replaced manual methods entirely due to challenges in constructing objective functions and optimization algorithms. Automatic calibration is often most successful when used alongside manual procedures.	(Boyle et al., 2000; Sorooshian and Gupta, 1995)
Objective Functions	An objective function quantifies the disparity between model-simulated and observed catchment outputs. Standard objective functions include Weighted Least Squares (WLS), incorporating weight parameters for specific hydrograph characteristics. The Nash-Sutcliffe Efficiency (NSE) criterion is widely used. Still, the Kling and Gupta Efficiency (KGE) has emerged to address NSE limitations, exhibiting better performance in capturing variability, peaks, and means of flows. Maximum Likelihood-based functions by Sorooshian and Dracup rigorously address autocorrelation and heteroscedasticity in streamflow data errors but are less favoured in hydrology due to justifiability concerns.	(Schaefli and Gupta, 2007; Gupta et al., 2009; Pechlivanidis et al., 2010a; Sorooshian and Dracup, 1980; Beven, 2001)

3. DATA AND METHODOLOGY

3.1 General

This section outlines the methodology to fulfill the research aim and specific objectives. Figure 4 illustrates the flowchart detailing the methodology. It is essential to select suitable methods to gap-fill the missing meteorological data to maintain a continuous time series of data to accomplish the main and specific research objectives. Accordingly, the Multiple Imputation by Chained Equations (MICE) method was selected based on simplicity and handling extensive data range with an advanced mathematical model.

To select the most suitable global climate model (GCM) for capturing the monsoon signal of Sri Lanka, the Evaluation Based on Distance from Average Solution (EDAS) method was chosen based on a comprehensive literature review. The EDAS method is a multi-criteria decision analysis approach that relies on an evaluation based on the distance to the average solution. Using the EDAS method, the best-performing models were ranked for each climate zone in Sri Lanka.

Achieving the primary objectives of this study necessitates the development of a high-resolution meteorological dataset to identify the spatial variation of climatology. This goal was achieved by establishing a relationship between the observed data series and the CHIRPs satellite data series. This methodology generated a high-resolution 0.05˚ precipitation data series encompassing the entire island of Sri Lanka. In parallel, temperature data series were integrated into each cell using the Thiessen polygon method, assuming uniform temperature distribution within each polygon. This approach made it possible to develop a high-resolution meteorological data series, facilitating the identification of spatial variation of climate zones according to the Koppen-Geiger Climate Classification for Sri Lanka climatology. This section provides comprehensive overview of the data and methods used for the study.

Regarding model selection for hydrological applications, the literature review examined various hydrological models and their applications, identifying the different hydrological models previously used and the purposes for utilizing these models to assess water balance. This study utilized Kashiwa et al. (2010) distributed hydrological runoff model within the framework of Kazama et al. (2004) for simulating runoff and calculating water balance.

3.2 Methodology Flow Chart

The methodology adopted in the present study is illustrated in Figure 3-1 below.

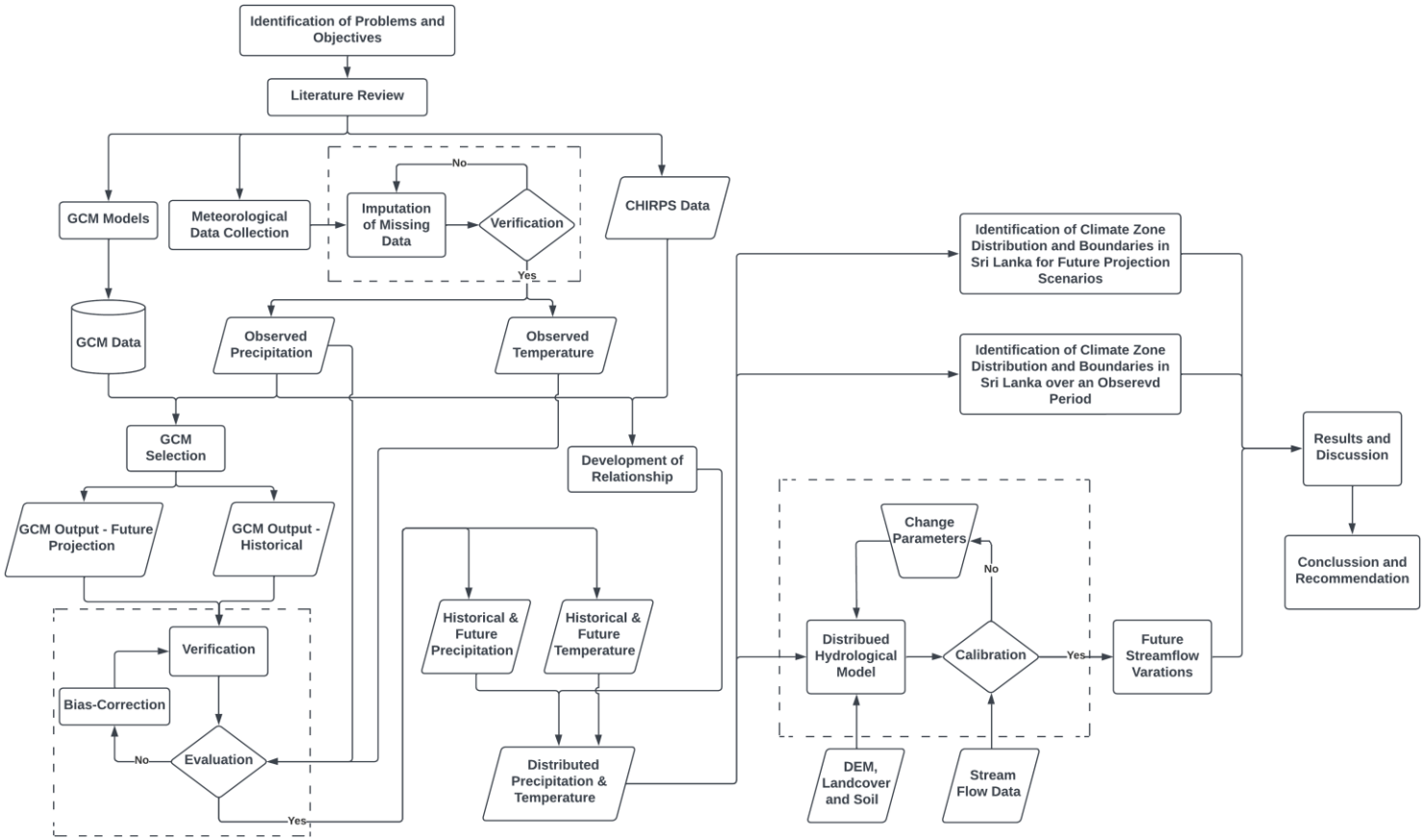

Figure 3-1: Methodology flowchart

3.3 Study Area

The study focuses on Sri Lanka, a tropical island nation located in the Indian Ocean off the southern coast of India. The geographic location of Sri Lanka falls between the latitudes 5°55′ and 9°51′ north and longitudes 79°41′ and 81°53′ east, covering an area of 65,610 km^2. Sri Lanka is a small island nation susceptible to extreme weather events such as floods, landslides, and droughts. Consequently, According to the IPCC, Sri Lanka falls into the category of vulnerable small island nations that are under threat from the impacts of climate change.

The climate of Sri Lanka is characterized by a tropical monsoon climate, which is further divided into two major monsoon rainfall seasons and two discernible inter-monsoon rainfall seasons (Esham & Garforth, 2013). The distinct monsoon seasons experienced in Sri Lanka are the Northeast Monsoon (NEM) from December to February and the Southwest Monsoon (SWM) from May to September. Additionally, two inter-monsoon periods of rainfall are observed, namely the First Inter-Monsoon (FIM), lasting from March to April and the Second Inter-Monsoon (SIM), occurring between October and November. The topography of Sri Lanka is diverse, with elevations ranging from sea level to 2,505 m. This topographical variation results in slight variations in air temperature throughout the island and changes in rainfall patterns. Furthermore, based on topography, precipitation patterns and soil type, the island is divided into three principal climatic zones: wet, intermediate, and dry (Panabokke, 1996).

3.4 Data Collection

Observed daily precipitation and temperature data spanning a period of 40 years (1975-2014) was obtained from 27 meteorological stations (Table 3-1) from the Department of Meteorology, Sri Lanka (Figure 3-2). The data is assumed to be missing completely at random.

The current study selected a collection of fifteen CMIP6 global climate models (GCMs) to assess their performance in simulating the monsoon climate of Sri Lanka for precipitation (Table 2-4), where data was obtained from the Earth System Grid Federation (ESGF) portal. Model performances were assessed over the 1975–2014 period. The model selection study was based on the analysis of monthly precipitation values, which have been derived from the above daily data set with missing data imputed.

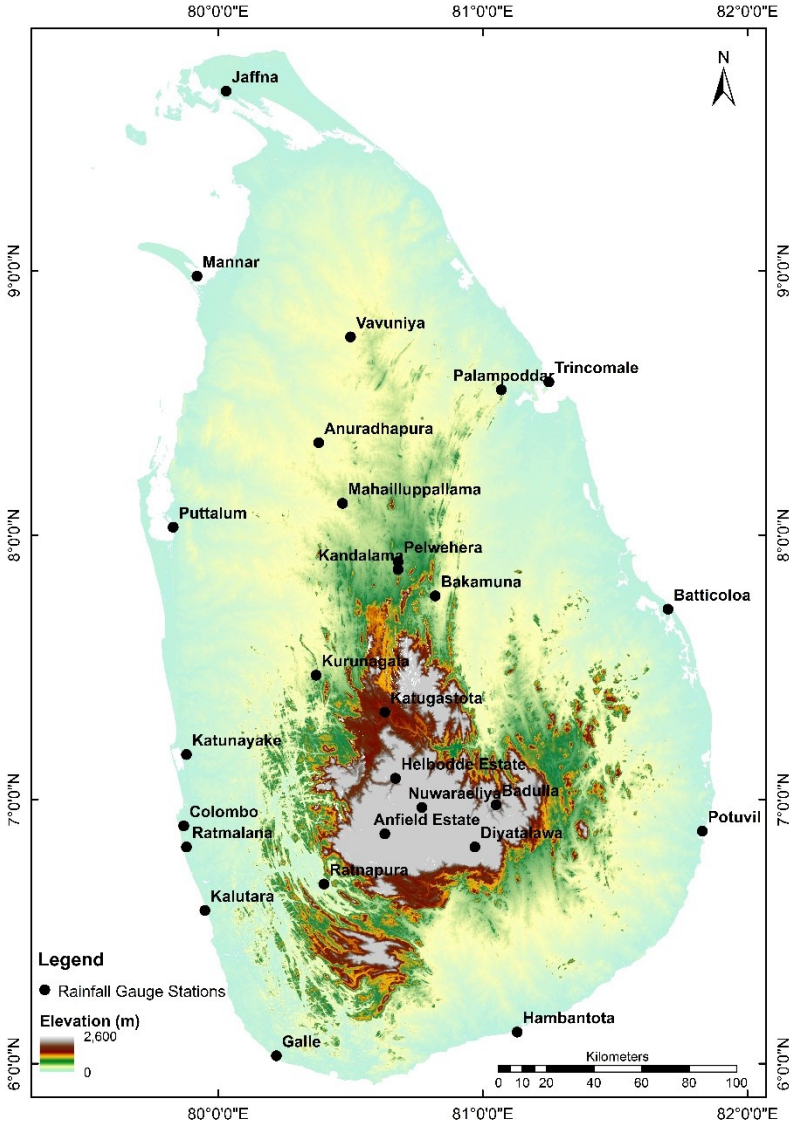

Figure 3-2: Selected Gauging Stations

Table 3-1: Coordinates of Meteorological Stations

Gauging Station	Coordinates		Precipitation	Temperature
	Latitude	Longitude		
Anfield Estate	N 6° 52' 12"	E 80° 37' 48"	✓	
Anuradhapura	N 8° 21' 00"	E 80° 22' 48"	✓	✓
Bakamuna	N 7° 46' 12"	E 80° 49' 12"	✓	
Badulla	N 6° 58' 48"	E 81° 03' 00"	✓	✓
Batticoloa	N 7° 43' 12"	E 81° 42' 00"	✓	✓
Colombo	N 6° 54' 00"	E 79° 52' 12"	✓	✓

Gauging Station	Coordinates		Precipitation	Temperature	Gauging Station
	Latitude	Longitude			
Diyatalawa	N 6° 49' 12"	E 80° 58' 12"	✓	✓	
Galle	N 6° 01' 48"	E 80° 13' 12"	✓	✓	
Hambantota	N 6° 07' 12"	E 81° 07' 48"	✓	✓	
Helbodde Estate	N 7° 04' 48"	E 80° 40' 12"	✓		
Jaffna	N 9° 40' 48"	E 80° 01' 48"	✓		
Kalutara	N 6° 34' 48"	E 79° 57' 00"	✓		
Kandalama	N 7° 52' 12"	E 80° 40' 48"	✓		
Katugastota	N 7° 19' 48"	E 80° 37' 48"	✓	✓	
Katunayake	N 7° 10' 12"	E 79° 52' 48"	✓	✓	
Kurunagala	N 7° 28' 12"	E 80° 22' 12"	✓	✓	
Mahailluppallama	N 8° 07' 12"	E 80° 28' 12"	✓	✓	
Mannar	N 8° 58' 48"	E 79° 55' 12"	✓	✓	
Nuwaraeliya	N 6° 58' 12"	E 80° 46' 12"	✓	✓	
Palampoddar	N 8° 33' 00"	E 81° 04' 12"	✓		
Pelwehera	N 7° 54' 00"	E 80° 40' 48"	✓		
Potuvil	N 6° 52' 48"	E 81° 49' 48"	✓		
Puttalam	N 8° 01' 48"	E 79° 49' 48"	✓	✓	
Ratmalana	N 6° 49' 12"	E 79° 52' 48"	✓	✓	
Ratnapura	N 6° 40' 48"	E 80° 24' 00"	✓	✓	
Trincomale	N 8° 34' 48"	E 81° 15' 00"	✓	✓	
Vavuniya	N 8° 45' 00"	E 80° 30' 00"	✓	✓	

3.5 Data Source and Resolution

The primary data types used in this study were precipitation, temperature and streamflow data. Data sources spatial and temporal resolution of the data set are shown in Table 3-2.

Table 3-2: Data Sources and Availability

Data Type	Temporal Resolution	Spatial Resolution	Data Period	Data Source
Observed Precipitation	Daily	Station	1975 – 2014	Department of Meteorology
Observed Temperature	Daily	Station	1975 – 2014	Department of Meteorology
GCM Precipitation and Temperature	Monthly	Vary (Table-4)	1975 – 2014 2015 - 2100	ESGF Portal
Satellite Precipitation	Monthly	0.05˚	1981 - 2014	USGS Portal
Streamflow	Monthly	Station	1999 - 2014	Hydrological Annual, Irrigation Department

3.6 Data Checking and Missing Data Imputation

The MICE algorithm was used to replace the missing data in records. To run the MICE algorithm, 27 stations were selected for this study, and an additional four stations were also used to impute missing data (Table 3-3). These stations were divided into eight separate groups (Table 3-4). This separation was done using a single mass curve (Figure 3-3) and the station's location.

Table 3-3: Additional Data Stations

Station	Coordinates		Period
	Latitude	Longitude	
Laxapana	N 6° 54' 00"	E 80° 31' 12"	1983 - 2014
Nawalapitiya	N 7° 04' 12"	E 80° 31' 48"	1983 - 2014
Peradeniya Botanical Garden	N 7° 16' 01"	E 80° 35' 60"	1989 – 2014
Thanamalwila	N 6° 28' 00"	E 81° 07' 45"	2000 - 2014

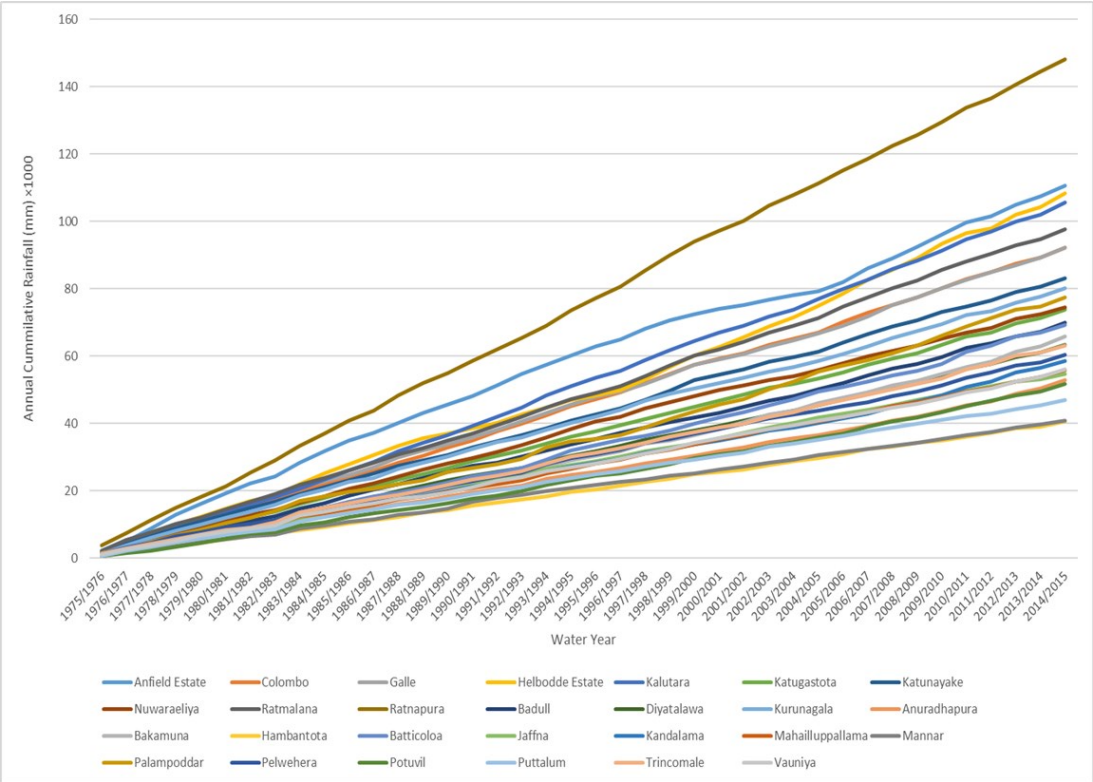

Figure 3-3: Single-mass curve

Table 3-4: Data Imputation Groups

Group	Stations
Wet Zone - 1	Katunayake, Colombo, Ratmalana
Wet Zone - 2	Kalutara, Ratnapura, Galle, Anfield Estate, Laxapana
North	Jaffna, Mannar, Vavuniya, Puttalam
North Central	Anuradhapura, Mahailluppallama, Kandalama, Pelwehera, Bakamuna
South	Hambantota, Pottuvil, Thanamalwila
East	Trincomalee, Batticoloa, Palampoddar
Central - 1	Kurunagala, Katugastota, Peradeniya Botanical Garden
Central - 2	Nuwaraeliya, Badulla, Diyatalawa, Helbodde, Nawalapitiya

3.7 Imputing Missing Daily Meteorological Data

The MICE algorithm is an imputation method (Buuren & Oudshoorn, 2011) which imputes missing values by producing multiple complete data sets in which missing values are substituted with probable values based on information available in the observed data. When multiple imputations are generated, the statistical uncertainty of the imputations decreases. The MICE algorithm is implemented by writing an S-PLUS function. To handle incomplete variables, the user can select a set of predictors for imputation. This feature is advantageous for imputing substantial collections of data series encompassing numerous variables. Figure 3-4 illustrates the three primary stages of multiple imputations: imputation, analysis, and clustering. The algorithm organizes the outcomes of each stage into distinct categories known as mids, mira, and mipo, which are elucidated in detail below.

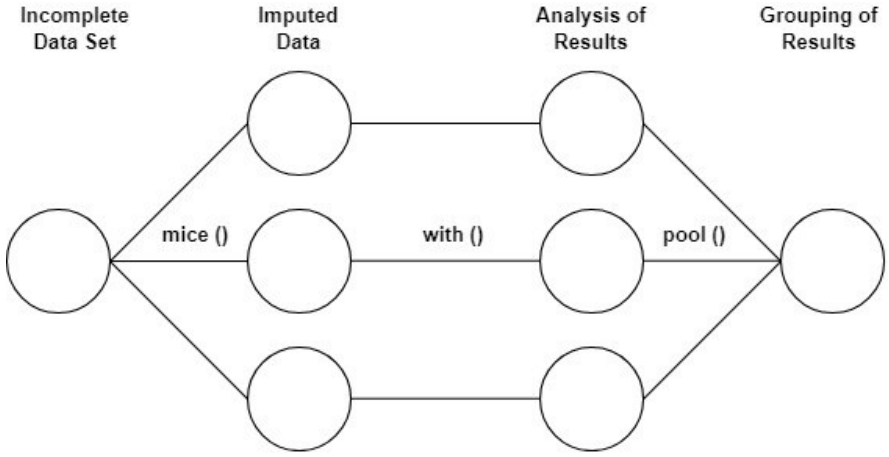

Figure 3-4: Main steps in multiple imputation

The MICE package in Rstudio version 2022.12.0 + 353 (RStudio Team, 2020) was used to impute the missing values in the collected meteorological data.

The following parameters were used in the imputation process:

- 'm': the number of imputed data sets to be created is five
- 'method': the imputation methods to be used are "PMM" (predictive mean matching) and "Norm" (normal imputation)
- 'maxit': the maximum number of iterations to use for the imputation process is 50
- 'seed': the seed for the random number generator used in the imputation process is 500

This would create five imputed data sets using the predictive mean matching method, with a maximum of 50 iterations and a seed value 500. This study employed the

"PMM" and "Norm" methods to compare their performance in imputing the missing values.

Root Mean Square Error (RMSE) assigns greater importance to substantial estimation errors than smaller ones, making it a crucial metric for model validation. Additionally, Mean Absolute Error (MAE) is a valuable supplement to the scatter plot of measured versus modelled data, particularly near the 1-to-1 line (Perez et al., 2013).

After imputing missing data using the MICE algorithm, the consistency of the rainfall data was checked by using the double mass curve analysis for each imputation group divided in the MICE method. The double mass curve indicated the homogeneity of annual rainfall. The double-mass curve theory relies on the principle that a graph depicting the cumulative value of one quantity against the cumulative value of another during the same period will exhibit a straight line when the data is proportional. In this context, the line's slope serves as the proportionality constant between the quantities.

3.8 Evaluation Based on Distance from Average Solution

The first step involved in the EDAS method is the selection of relevant performance criteria to derive a decision matrix (X).

$$X = [X_{ij}]_{n\times m} = \begin{bmatrix} X_{11} X_{12} \dots X_{1m} \\ X_{21} X_{22} \cdots X_{2m} \\ \dots \quad \dots \quad \dots \quad \dots \\ X_{n1} X_{n2} \cdots X_{nm} \end{bmatrix} \text{----------(5)}$$

Where n represents alternatives and m represents criteria. x_{ij} also indicates the status of the i^{th} alternatives considering the j^{th} criteria.

The approach of Rupp et al. (2013) was applied to generate the decision matrix to evaluate the effectiveness of GCMs and rank them based on performance indicators. Not all performance criterion measurements have equal value in indicating outcomes, which is notable in the literature. Specifically, specific metrics indicate a positive connection between performance and their corresponding numerical values, whereas others indicate an inverse correlation. Therefore, after calculating the performance metrics, those numerical values were normalized according to Rupp et al. (2013).

$$X_{ij}^{*} = \frac{X_{ij} - X_j^{worst}}{X_j^{best} - X_j^{best}} \text{----------(6)}$$

Where X_{ij}^{*} is the normalised performance of the i^{th} GCM on the j^{th} performance criterion.

The present study employs five primary statistical metrics to evaluate the performance of climate models, such as the correlation coefficient (R), skill score (Taylor, 2001), root-mean-square error ($RMSE$), mean absolute error (MAE), and percentage bias ($PBIAS$). The mathematical formulation for the indices above is given below. S_i and O_i denote the i$^{\text{th}}$ simulated and observed values, respectively. $\overline{S_i}$ and $\overline{O_i}$ refer to the

mean of simulated and observed values, and n represents the total number of observations.

$$R = \frac{\sum_{i=1}^{n}(S_i-\overline{S_i})(O_i-\overline{O_i})}{\sqrt{\sum_{i=1}^{n}(S_i-\overline{S_i})^2-\sum_{i=1}^{n}(O_i-\overline{O_i})^2}} \quad \text{----------(7)}$$

$$SS = \frac{4(1+R)^4}{(\sigma_n+\frac{1}{\sigma_n})^2(1+R)^4} \quad \text{----------(8)}$$

$$RMSE = \sqrt{\frac{\sum_{i=1}^{n}(O_i-S_i)^2}{n}} \quad \text{----------(9)}$$

$$MAE = \frac{\sum_{i=1}^{n}|O_i-S_i|}{n} \quad \text{----------(10)}$$

$$PBIAS = \frac{\sum_{i=1}^{n}(O_i-S_i)}{\sum_{i=1}^{n}O_i} \times 100 \quad \text{----------(11)}$$

In order to evaluate the best performance, a determination must be based on a set of specific performance criteria. Thus, to include all the performance criteria, the average solution matrix (AV) was determined as follows:

$$AV = \left[AV_j\right]_{1\times m} \quad \text{----------(12)}$$

where,

$$AV_j = \frac{\sum_{i=1}^{n}X_{ij}^{*}}{n} \quad \text{----------(13)}$$

The EDAS method's core concept is the performance evaluation by measuring distance from the average solution. The distances from the average value are calculated using the following equations, and the PDA (positive distance from the average solution) and NDA (negative distance from the average solution) matrices are formulated.

$$SP_i = \sum_{j=1}^{n}PDA_{ij} \quad \text{----------(14)}$$

$$SN_i = \sum_{j=1}^{n}NDA_{ij} \quad \text{----------(15)}$$

$$NSP_i = \frac{SP_i}{max_i(SP_i)} \quad \text{----------(16)}$$

$$NSN_i = \frac{SN_i}{max_i(SN_i)} \quad \text{----------(17)}$$

The best performance model selected based on the final score of each GCM (AS_i). The GCM that has the highest AS_i Value is the one that should be chosen above the other alternatives.

$$AS_i = \frac{1}{2}(NSP_i + NSN_i) \quad \text{----------(18)}$$

where,

$0 \leq AS_i \leq 1.$

The main objective of this research is to identify a climate model capable of accurately displaying the monsoon precipitation pattern signal for Sri Lanka. Although a small island, the varied topography of Sri Lanka results in distinct rainfall patterns throughout its various regions. As a result, the model performance was assessed using the methodology mentioned above through a climate zone-wise evaluation.

To analyse model performance for each climate zone, average values for both observed and model precipitation values were first calculated for each climate zone. These derived average values were then utilized throughout the EDAS method to rank the GCMs for each climate zone.

3.9 Development of a High-Resolution Meteorological Dataset

Data scarcity is one of the significant issues in climatology studies. While observations remain the most dependable meteorological data, their effectiveness is limited in offering comprehensive insights into the spatial distribution of rainfall in many regions (Dewan et al., 2019). To overcome this issue and develop a high-resolution dataset, this study used a novel method involving the development of a high-resolution dataset with satellite data and observed data. Satellite data provide a high-resolution dataset in the spatial and temporal domains. However, observed data stations provide data series for only a particular location. A high-resolution meteorological dataset can be developed in the spatial domain by developing a method to match and scatter observed data using satellite data.

3.9.1 CHIRPs Data Bias Correction

Satellite precipitation data are imperfect when compared to in-situ observed station data. Hence, correcting the bias present in the satellite precipitation data is necessary. This study used CHIRPs data to develop the relationship between observational data and create a high-resolution dataset. As a first step, CHIRPs data cells were identified for each observation station. According to the 27 observed stations, Sri Lanka was divided into 27 polygons using the ArcGIS Thiessen Polygon geoprocessing tool (Figure 8). Then, each CHIRPs cell corresponding to each observed station was identified. A mean-based method was employed for the bias correction of CHIRPs data, where average values were obtained for each polygon's CHIRPs cells. Bias factors for 12 months were then calculated for each polygon. These factors were used to correct the precipitation time series for each CHIRPs grid. A bias-corrected CHIRPs dataset for the entire island of Sri Lanka can be obtained by performing the above methodology.

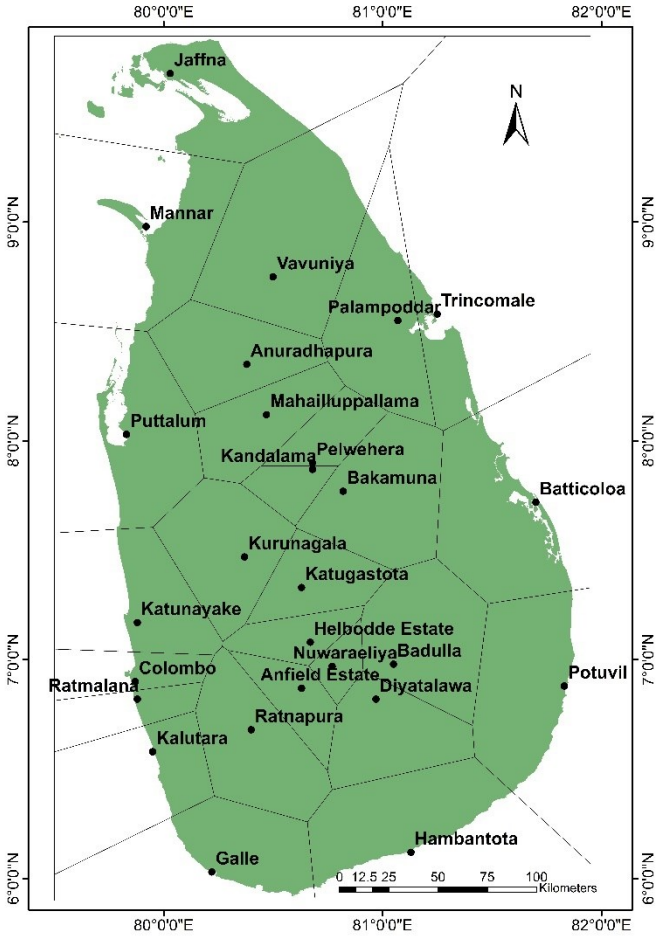

Figure 3-5: Precipitation Thiessen Polygons

3.9.2 Development of Relationship between CHIRPs and Observe Data

The CHIRPs precipitation data, accumulated monthly from 1981 to 2014, were utilized, while observed data were collected from 1975 to 2014. Since CHIRPs data is available only from 1981 onwards, satellite data from 1981 to 2014 was employed to establish the relationship between bias-corrected CHIRPs and the observed stations. Linear regression analysis was employed using equation 19 to develop this relationship between observed station data points with corresponding CHIRPs grid cells.

$$Y_{chirps} = mX_{Observed} \text{ ----------(19)}$$

The independent variable in this analysis is the observed data values ($X_{Observed}$), while the dependent variable is the CHIRPs data values (Y_{chirps}), and using the above equation, the gradient value (m) was calculated for each month of the year. This involved adding the values of particular CHIRPs grids corresponding to each station for each month to the relationship and calculating the gradient value. These calculated gradient values were then employed to distribute historical and future projection data from GCMs to each CHIRPs cell. By adopting this approach, a high-resolution dataset with 2,418 pixels was generated for Sri Lanka. This method offers the advantage of

developing accurate and high-resolution maps, overcoming the limitations of using only 27 stations.

3.9.3 Distribution of Temperature Data for CHIRPs Grid Cells

In this study, the Köppen-Geiger climate classification system is employed, relying on characterizing seasonal precipitation patterns and temperature levels. Following the distribution of precipitation data to CHIRPs cells to create the Köppen-Geiger Climate Map, it becomes imperative to similarly distribute temperature station data to these same cells. However, there is a lack of temperature satellite data with a resolution of 0.05˚ for developing a relationship for temperature, such as in Section 3.9.2. Factors such as latitude, altitude, proximity to the sea, and oceanic currents affect temperature variations in the atmosphere (Noor et al., 2020).

When considering the spatial distribution of temperature in Sri Lanka, the mean annual temperature ranges from 27°C in the Coastal Lowlands to 16°C in Nuwara Eliya (at an elevation of 1,900 AMSL) in the Central Highlands (Meegahakotuwa & Nianthi, 2018).

Based on observational data, no significant temperature variations exist in the Coastal Lowlands areas, as Meegahakotuwa & Nianthi (2018) indicated. However, the Central Highland regions exhibit noticeable temperature variations. To address this issue, dense station data were collected from the highland areas during the data collection process, totalling 18 stations. Subsequently, Sri Lanka was divided into 18 Thiessen polygons (Figure 9) to distribute the CHIRPs cells, assuming that each polygon experiences the same temperature variation as the corresponding observed station.

Historical and future data from the observed stations were distributed to each CHIRPs cell accordingly. This process enables the development of a climate dataset consisting of 2,418 pixels, facilitating the creation of a high-resolution Köppen-Geiger climate classification map.

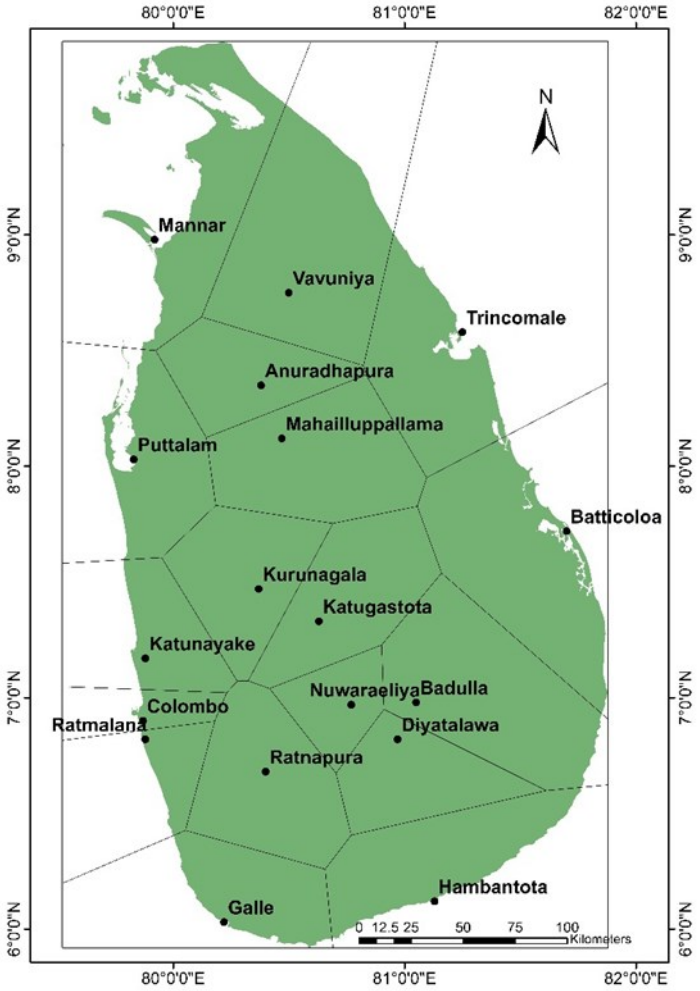

Figure 3-6: Temperature Thiessen Polygons

3.10 Distributed Hydrological Model

A distributed hydrological model is used as a 0.05˚×0.05˚ grid cell for calculating water balance and identifying a hydrological impact with future climate predictions. This hydrological model was primarily developed using the FORTRAN language in the Visual Studio source-code editor. The model considers subsurface and surface water tanks for calculating the water balance. The kinematic wave method has been employed to calculate direct runoff using this hydrological model, and base flow is calculated using the storage function method. The basic conceptual model is shown in Figure 10. The governing equations for both methods are as follows;

Kinematic Wave Equation-

$$\frac{\partial A}{\partial t} + \frac{\partial Q}{\partial x} = (R - R_{in} - ET)B \quad \text{----------(20)}$$

Here, 'A' refers to the cross-sectional area of the flow (m²), 't' represents time (s), 'Q' denotes the surface flow rate (m³/s), 'x' is the spatial distance along the flow path (m), 'R' stands for precipitation per unit time (m/s), 'R_{in}' is the penetration rate per unit time

(m/s), '*ET*' represents evaporation per unit time (m/s), and '*B*' denotes the grid width of the distributed model cell. This equation represents the conservation of mass for open-channel flow. It assumes the ignored rapid variations in flow and complex hydraulic phenomena, such as irrigation and reservoir control operations, in the calculations.

Manning's equation relates the flow velocity (*V*) to the hydraulic radius (*R*), the channel slope (*S*), and Manning's roughness coefficient (*n*).

$$V = \frac{1}{n} R^{2/3} S^{1/2} \quad \text{---------- (21)}$$

The discharge (*Q*) can be expressed as the product of the cross-sectional area (*A*) and the velocity (*V*):

$$Q = A.V \quad \text{---------- (22)}$$

$$A = B.h \quad \text{---------- (23)}$$

$$Q = (B.h)\left(\frac{1}{n} R^{2/3} S^{1/2}\right) \quad \text{---------- (24)}$$

The hydraulic radius (*R*) in terms of the cross-sectional area (*A*) and wetted perimeter (*P*):

$$R = \frac{A}{P} \quad \text{---------- (25)}$$

Assuming a rectangular channel, the wetted perimeter (*P*) is the sum of the bottom width (*B*) and twice the water depth (*h*):

$$P = B + 2h \quad \text{----------(26)}$$

$$Q = (B.h)\left(\frac{1}{n}\left(\frac{A}{B+2h}\right)^{2/3} S^{1/2}\right) \quad \text{----------(27)}$$

$$Q = \frac{1}{n} B h^{5/3} S^{1/2} \quad \text{----------(28)}$$

Here, '*h*' is water depth in a cell (*m*), '*S*' is the gradient flow and '*n*' is the Mannings roughness coefficient.

The term 'R_{in}' is represented by water depth infiltration into a subsurface to water depth '*h*'; that value can be calculated using the following equation.

$$R_{in} = k_a \times h \quad \text{----------(29)}$$

The constant '*ka*' is taken as 0.008 in this distributed hydrological model.

Evaporation (*ET*) is a crucial input in hydrological models, playing a key role in the water balance equation as a primary source of water exiting the system. The evaporation rate is directly influenced by temperature, and in this study, the daily average temperature was employed for this purpose. Consequently, the simplified Penman formula was used to calculate ET based on the mean temperature (Linacre, 1977).

$$ET = \frac{700T_m/(100-A)+15(T-T_d)}{(80-T)}$$ ----------(30)

$T_m = T+0.006h$, h is elevation, and T is daily mean temperature. A is latitude in degrees, and T_d is the mean dew point. However, according to the Penman,

$$(T - T_d) = 0.0023h + 0.37T + 0.53R + 0.35R_{ann} - 10.9$$ ----------(31)

Here, 'R' denotes the mean daily temperature range, while 'R_{ann}' represents the difference between the mean temperatures of the warmest and coldest months. Consequently, estimating the evaporation rate becomes straightforward, relying on elevation, latitude, and the daily maximum and minimum temperatures.

Storage Function Method-

$$\frac{ds}{\partial t} = R_{in} - q$$ ---------- (32)

$$S = kq^p$$ ----------(33)

Here, 'S' denotes the apparent height retention in meters (m), 'q' represents the high base flow discharge in meters per second (m/s), and 'k' and 'p' are the model constants.

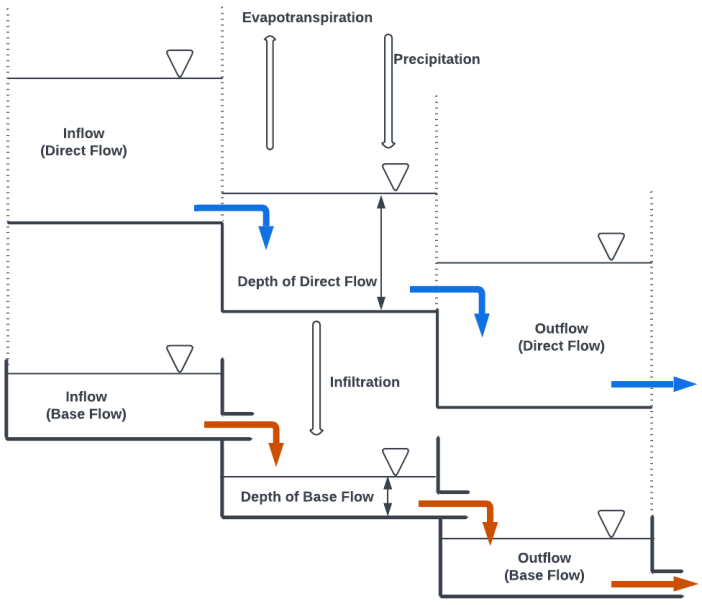

Figure 3-7: Conceptual Model

In addition to precipitation and temperature data, digital elevation data, land-use cover, and soil maps are required as inputs for this distributed model. Details of the datasets collected for this purpose are provided in Table 3-5.

Table 3-5: Additional data used in the distributed hydrological model

Dataset	Source
Digital Elevation Model	ASTER GDEM
Land use cover	WaPOR
Soil Map	NRMC

3.10.1 Methodology Flowchart for the Hydrological Model

The methodology of the distributed hydrological model in the present study is illustrated using Figure 3-8 below.

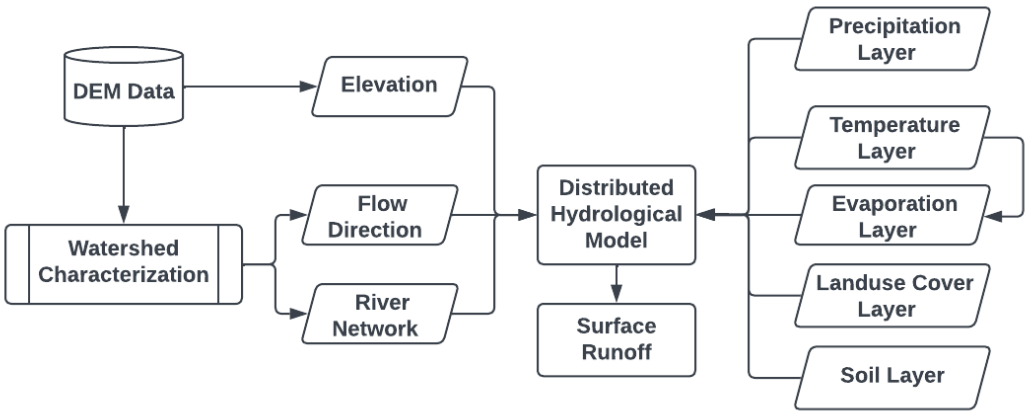

Figure 3-8: Methodology flowchart of the distributed hydrological model

4. RESULTS AND DISCUSSION

4.1 Imputation of Missing Data

In this study, missing precipitation and temperature data were gap-filled using the MICE algorithm. Gap-filling missing precipitation and temperature data is most significant to climatology studies because it facilitates continuous analysis in the temporal domain. Subsequently, MICE performance was compared with the Sri Lanka monsoon climate to identify how this algorithm performs in gap filling with the wet zone and dry zone precipitation patterns.

4.1.1 Comparison of MICE Data Imputation Methods

This study examined imputation results between the Wet Zone-1 and North groups (refer to Table 3-4). Figures 4-1 & 4-2 show a Stripplot of results between Predictive Mean Matching (PMM) and Noramal Imputation (Norm) methods for the Wet Zone-1 group. The findings revealed that the Norm method successfully imputed data across various data series while avoiding extreme events as imputed values. In contrast, the PMM method focused on imputing data near the mean of the dataset as the number of imputations increased.

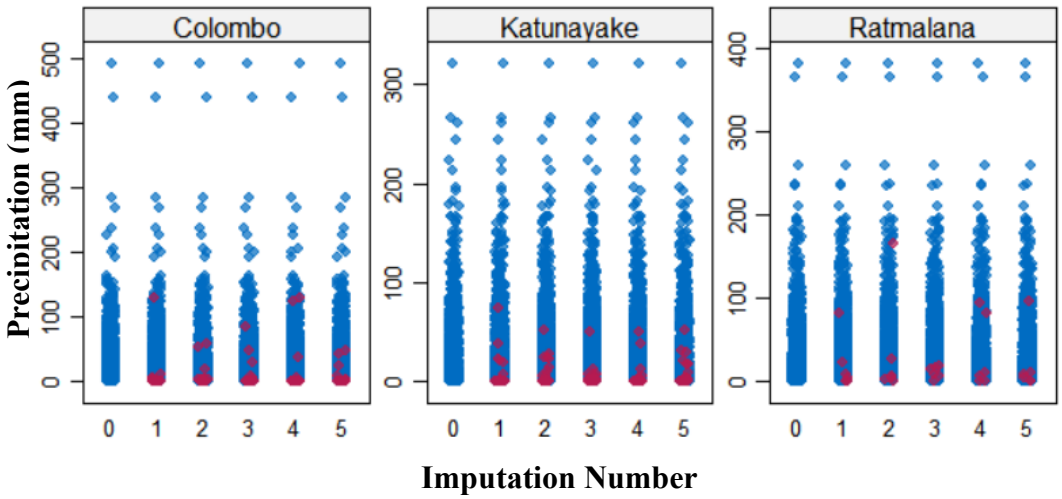

Figure 4-1: Strip plot of three stations in the original data and the five imputed data sets (PMM method) – [Blue- Original data, Red- Imputed data]

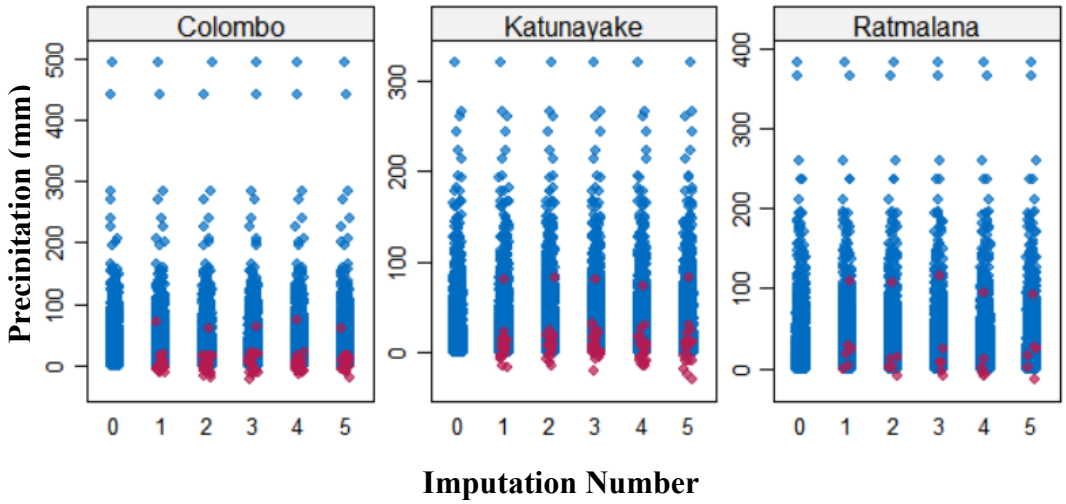

Figure 4-2: Strip plot of three stations in the original data and the five imputed data sets (Norm method) – [Blue- Original data, Red- Imputed data]

Two performance evaluation methods were used for both the wet and dry zones to determine the optimal imputation method.

Tables 4-1 and 4-2 display the RMSE and MAE values acquired through the leave-one-out cross-validation method using the MICE algorithm. The analysis involved two groups of meteorological stations, one in the wet zone and one in the dry zone. Error calculations were done over five years with no missing data, omitting one year of data from each station during the calculations. Using the MICE package, the missing year precipitations were then generated, and the performance of each method was evaluated.

Table 4-1: RMSE and MAE obtained for the wet zone

Station	**RMSE (%)**					
	Daily		**10 – Days**		**Monthly**	
	PMM	Norm	PMM	Norm	PMM	Norm
Colombo	105.29	84.05	37.42	47.18	25.78	42.08
Katunayake	118.18	119.79	41.18	64.4	36.53	58.96
Ratmalana	92.02	84.48	32.60	46.62	17.94	41.14
	MAE (%)					
Colombo	21.97	26.14	12.28	17.56	8.62	15.86
Katunayake	20.81	34.99	10.22	24.36	10.49	22.27
Ratmalana	19.75	26.41	10.24	17.15	6.37	15.74

Table 4-2: RMSE and MAE obtained for the dry zone

Station	RMSE (%)					
	Daily		10 - Days		Monthly	
	PMM	Norm	PMM	Norm	PMM	Norm
Jaffna	130.16	148.40	48.74	109.11	22.26	99.84
Mannar	138.55	164.71	52.81	136.45	32.88	126.34
Vavuniya	158.75	133.61	60.17	101.62	37.69	93.85
Puttalam	124.31	136.76	45.38	106.65	28.4	98.69
	MAE (%)					
Jaffna	17.4	45.21	10.29	32.01	5.41	30.99
Mannar	17.27	51.06	11.07	39.51	8.3	38.35
Vavuniya	22.73	41.74	11.21	29.36	7.74	28.66
Puttalam	16.76	41.99	9.93	31.45	5.69	29.64

The error percentage decreases as the time scale increases from one day to one month for both the PMM and Norm methods. In the wet zone evaluation, the PMM method demonstrated superior performance at the monthly scale, with RMSE percentages below 40% for Colombo, Katunayake, and Ratnapura, respectively. In contrast, the Norm method exhibited RMSE percentages ranging from 40% to 60% for the exact locations. Similarly, in the dry zone evaluation, the Norm method showed higher RMSE percentages than the PMM method, with increments of 77.5%, 93.4%, 56.2%, and 70.3% for Jaffna, Mannar, Vavuniya, and Puttalam, respectively.

Furthermore, the MAE percentages followed a similar trend to the RMSE percentages, with the Norm method displaying higher error percentages than the PMM method in wet and dry zone evaluations.

4.1.2 Double Mass Curve

A double mass curve was generated by plotting the cumulative precipitation of the chosen rainfall station against the average cumulative precipitation of other selected rainfall stations within the sub-basin. A fixed ratio in the graph indicates a consistent relationship between the rainfall variables, and any deviations from a straight line may signal changes in data collection methods or alterations in the rainfall station.

No notable inconsistencies were observed in the rainfall data, as evidenced by the straight-line nature of the plotted graphs for all stations. Figure 14 illustrates the double mass curve specifically for the wetzone-1 group (refer to Table 4-3), while additional graphs can be found in appendix B.

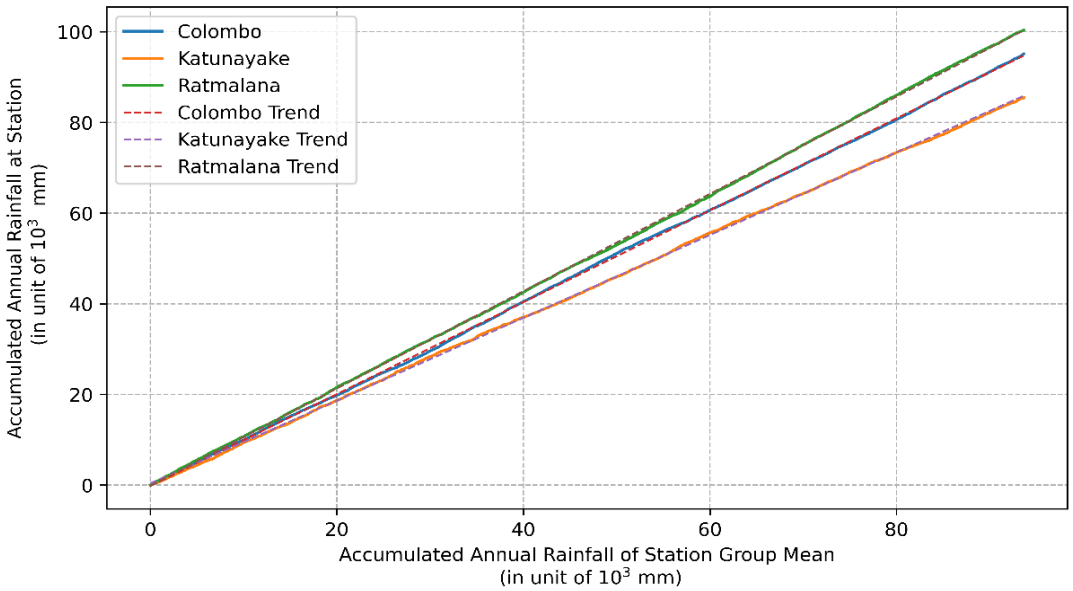

Figure 4-3: Double mass curve for wet zone-1 group

4.2 Global Climate Model Selection

4.2.1 Objective Functions Performance over the Historical Period

The performance of global climate models in Sri Lanka's various climate zones was assessed by first summarizing precipitation values for each zone. To accomplish this, the mean precipitation values were calculated for each climate zone for models, and the observed dataset, and the observed and modelled values were then evaluated based on this dataset. The following tables illustrate each model's performance outcomes with the objective function across the different climate zones.

Table 4-3: Values of performance indicators in the wet zone

Model	R	PBIAS(%)	MAE	RMSE	SS
ACCESS-CM2	0.14	-36.06	126.86	161.07	0.33
ACCESS-ESM1-5	0.18	-45.23	128.01	162.93	0.36
BCC-CSM2-MR	0.27	10.71	148.56	211.01	0.35
CAMS-CSM1-0	0.40	-56.08	123.47	154.14	0.67
CESM2	0.18	-3.23	143.91	184.52	0.32
CMCC-CM2-SR5	0.19	3.20	107.41	138.83	0.39
CMCC-ESM2	0.21	7.39	108.47	144.18	0.42
CNRM_CM6-1-HR	0.40	8.56	89.59	119.31	0.74
CNRM-ESM2-1	0.37	-3.33	100.54	128.74	0.68
GFDL-ESM4	0.27	-18.24	114.91	145.96	0.49
FGOALS-f3-L	0.23	7.59	130.93	171.14	0.40
INM-CM4-8	0.17	23.17	131.87	179.53	0.33
INM-CM5-0	0.20	-3.74	109.14	144.23	0.40
MPI-ESM1-2-HR	0.51	-40.73	106.49	134.07	0.99
MRI-ESM2-0	0.40	-27.16	114.03	144.22	0.72

Table 4-4: Values of performance indicators in the intermediate zone

Model	R	PBIAS(%)	MAE	RMSE	SS
ACCESS-CM2	0.09	-27.41	106.32	136.43	0.24
ACCESS-ESM1-5	0.14	-29.97	110.75	140.93	0.29
BCC-CSM2-MR	0.04	35.51	165.77	233.97	0.14
CAMS-CSM1-0	0.21	-47.40	104.81	136.61	0.34
CESM2	0.05	20.39	147.00	190.41	0.18
CMCC-CM2-SR5	0.27	28.92	105.16	135.44	0.45
CMCC-ESM2	0.28	35.41	110.22	145.25	0.46
CNRM_CM6-1-HR	0.46	47.40	102.61	127.16	0.80
CNRM-ESM2-1	0.41	-26.55	88.14	117.21	0.69
GFDL-ESM4	0.02	3.64	122.49	153.89	0.19
FGOALS-f3-L	0.11	54.79	158.23	205.99	0.21
INM-CM4-8	0.32	54.91	129.04	172.32	0.47
INM-CM5-0	0.19	19.15	110.65	142.02	0.35
MPI-ESM1-2-HR	0.55	-65.97	103.49	132.06	0.82
MRI-ESM2-0	0.31	-17.78	104.38	135.91	0.51

Table 4-5: Values of performance indicators in dry zone

Model	R	PBIAS(%)	MAE	RMSE	SS
ACCESS-CM2	0.43	-41.64	85.50	118.12	0.52
ACCESS-ESM1-5	0.39	-35.36	86.36	120.72	0.50
BCC-CSM2-MR	0.11	41.20	156.23	213.47	0.08
CAMS-CSM1-0	0.17	-41.36	97.08	133.62	0.22
CESM2	0.11	27.06	134.12	174.91	0.21
CMCC-CM2-SR5	0.48	46.93	101.42	130.02	0.69
CMCC-ESM2	0.50	51.22	104.18	135.80	0.72
CNRM_CM6-1-HR	0.62	-19.89	64.63	95.62	0.96
CNRM-ESM2-1	0.54	-4.17	77.39	112.28	0.81
GFDL-ESM4	0.29	-18.92	90.92	122.13	0.37
FGOALS-f3-L	0.26	26.23	115.35	152.90	0.37
INM-CM4-8	0.49	78.05	124.56	161.91	0.68
INM-CM5-0	0.33	29.34	101.59	133.67	0.45
MPI-ESM1-2-HR	0.47	-52.74	81.71	119.52	0.51
MRI-ESM2-0	0.47	-34.95	79.96	115.87	0.66

The performance metrics, including the correlation coefficient (R), skill score (SS), root-mean-square error (RMSE), mean absolute error (MAE), and percentage bias (PBIAS), were computed to assess the performance of each GCM in different climate zones. The results revealed varying performances across the climate zones. In the wet zone, the R values ranged from 0.14 to 0.51, in the intermediate zone from 0.05 to 0.55, and the dry zone from 0.11 to 0.62. In the dry zone, the uncorrected GCM projections exhibited a stronger relationship with the observed meteorological data

than the wet and intermediate zones. However, when the results from PBIAS, MAE, and RMSE are considered, the wet zone displayed significantly higher values than the observed data, highlighting the necessity for bias correction before conducting further analysis. Nevertheless, the primary objective of this model selection procedure is to gauge the ability of each GCM to capture the monsoon rainfall patterns. For this purpose, the uncorrected model projection data can be utilized.

Performance metrics indicate a positive connection between performance and their corresponding numerical values, whereas others indicate an inverse correlation. Therefore, after calculating the performance metrics, those numerical values were normalized according to Rupp et al. (2013), and normalised values for each model in each climate zone are shown in Figure 4-4.

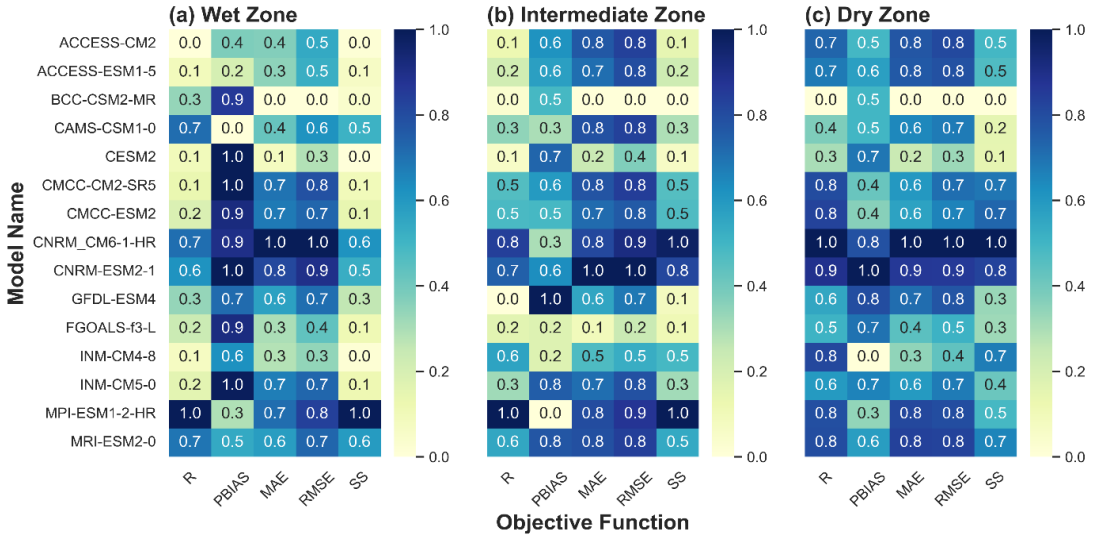

Figure 4-4: Normalised decision matrix values

4.2.2 GCM Selection based on Evaluation Based on Distance from Average Solution (EDAS)

Upon the computation of the NSP_i, NSN_i, and AS_i values for each climate zone, the models were ranked for each zone. This ranking process allowed the identification of the most favourable models for their performance in the various climate zones. The ranking procedure involved thoroughly examining and evaluating each model's NSP_i, NSN_i, and AS_i values to the corresponding values of other models. By ranking the models in this manner, it became possible to determine which models were the most adept at accounting for the specific climatic conditions of each zone. The following tables illustrate the ranks of each model across the different climate zones.

Table 4-6: Calculated values of NSPi, NSNi, ASi and Rank assigned for each GCM in the wet zone

Model	NSPi	NSNi	ASi	RANK
ACCESS-CM2	0.00	0.11	0.05	14
ACCESS-ESM1-5	0.00	0.14	0.07	11
BCC-CSM2-MR	0.05	0.06	0.05	13
CAMS-CSM1-0	0.36	0.63	0.49	6
CESM2	0.09	0.00	0.04	15
CMCC-CM2-SR5	0.22	0.59	0.41	9
CMCC-ESM2	0.17	0.69	0.43	7
CNRM_CM6-1-HR	0.80	1.00	0.90	2
CNRM-ESM2-1	0.61	1.00	0.81	3
GFDL-ESM4	0.06	0.96	0.51	5
FGOALS-f3-L	0.06	0.48	0.27	10
INM-CM4-8	0.00	0.13	0.06	12
INM-CM5-0	0.18	0.64	0.41	8
MPI-ESM1-2-HR	1.00	0.81	0.91	1
MRI-ESM2-0	0.47	0.93	0.70	4

Table 4-7: Calculated values of NSPi, NSNi, ASi and Rank assigned for each GCM in the intermediate zone

Model	NSPi	NSNi	ASi	RANK
ACCESS-CM2	0.00	0.11	0.05	14
ACCESS-ESM1-5	0.00	0.14	0.07	11
BCC-CSM2-MR	0.05	0.06	0.05	13
CAMS-CSM1-0	0.36	0.63	0.49	6
CESM2	0.09	0.00	0.04	15
CMCC-CM2-SR5	0.22	0.59	0.41	9
CMCC-ESM2	0.17	0.69	0.43	7
CNRM_CM6-1-HR	0.80	1.00	0.90	2
CNRM-ESM2-1	0.61	1.00	0.81	3
GFDL-ESM4	0.06	0.96	0.51	5
FGOALS-f3-L	0.06	0.48	0.27	10
INM-CM4-8	0.00	0.13	0.06	12
INM-CM5-0	0.18	0.64	0.41	8
MPI-ESM1-2-HR	1.00	0.81	0.91	1
MRI-ESM2-0	0.47	0.93	0.70	4

Table 4-8: Calculated values of NSPi, NSNi, ASi and Rank assigned for each GCM in dry zone

Model	NSPi	NSNi	ASi	RANK
ACCESS-CM2	0.20	0.97	0.58	4
ACCESS-ESM1-5	0.17	0.99	0.58	6
BCC-CSM2-MR	0.00	0.00	0.00	15
CAMS-CSM1-0	0.03	0.70	0.37	13
CESM2	0.07	0.43	0.25	14
CMCC-CM2-SR5	0.23	0.93	0.58	5
CMCC-ESM2	0.24	0.90	0.57	8
CNRM_CM6-1-HR	1.00	1.00	1.00	1
CNRM-ESM2-1	0.81	1.00	0.91	2
GFDL-ESM4	0.25	0.88	0.56	9
FGOALS-f3-L	0.08	0.75	0.41	11
INM-CM4-8	0.20	0.57	0.39	12
INM-CM5-0	0.07	0.94	0.50	10
MPI-ESM1-2-HR	0.25	0.90	0.58	7
MRI-ESM2-0	0.39	1.00	0.69	3

The approach employed in this methodology involved normalising all objective function performance values by their respective best and worst values. The resultant normalised values were bound between 1 and 0. Subsequently, these normalised values were utilised to evaluate the models. This normalisation process enabled the effective comparison of performance values and facilitated determining optimal outcomes.

In the wet zone, MPI-ESM1-2-HR, CNRM-CM6-1-HR, and CNRM-ESM2-1 demonstrated the highest Asi values of 0.91, 0.90, and 0.81, respectively. Conversely, BCC-CSM2-MR, ACCESS-CM2, and CESM2 displayed the lowest Asi values of 0.05, 0.05, and 0.04, respectively.

Within the intermediate zone, CNRM-ESM2-1, CNRM-CM6-1-HR, and MPI-ESM1-2-HR exhibited the highest Asi values of 0.95, 0.89, and 0.87, respectively. In contrast, CESM2, FGOALS-f3-L, and BCC-CSM2-MR demonstrated the lowest Asi values of 0.21, 0.06, and 0.00, respectively.

For the dry zone, CNRM-CM6-1-HR, CNRM-ESM2-1, and MRI-ESM2-0 attained the highest Asi values of 1.00, 0.91, and 0.69, respectively. Conversely, CAMS-CSM1-0, CESM2, and BCC-CSM2-MR exhibited the lowest Asi values of 0.37, 0.25, and 0.00, respectively.

Selecting the most appropriate GCM based on statistical criteria is crucial for accurately evaluating the impacts of various factors. Overall, CNRM-CM6-1-HR and CNRM-ESM2-1 have the best performance among the selected GCMs. Among these two, CNRM-CM6-1-HR models have 0.5˚×0.5˚ high resolution. Hence, considering the study area, that model is more suitable for small islands like Sri Lanka.

These findings contribute to a better understanding of GCM performance in different climate zones and aid in making informed decisions for future climate projections.

4.2.3 Comparison of Measured and Modelled Data by Climate Zones

Figure 4-5 illustrates the performance of the selected top-performed two models in each climate zone of Sri Lanka. Upon analyzing the results, it became evident that the selected models exhibited strong performance in both the dry and wet zones. However, the modelled values differed from the observed values in the intermediate zone. This variation can be attributed to the gradual fluctuations in climate conditions characteristic of the intermediate zone. Despite this variation, it is notable that the two selected models maintained a strong relationship with the observed values in all three climate zones.

In both the dry and wet zones, the mean values of the modelled data sets and observed data sets changed in tandem. However, the ability of the models to capture extreme events differed between the dry and wet zones. Specifically, the results indicate that only the CNRM-ESM2-1 model could accurately capture extreme events in the dry zone. The ability to capture extreme events is of particular importance in extreme data analysis, as it is essential for accurately projecting and preparing for the potential impacts of climate change. These findings highlight the need for continued refinement and improvement of climate models, particularly their ability to capture extreme events.

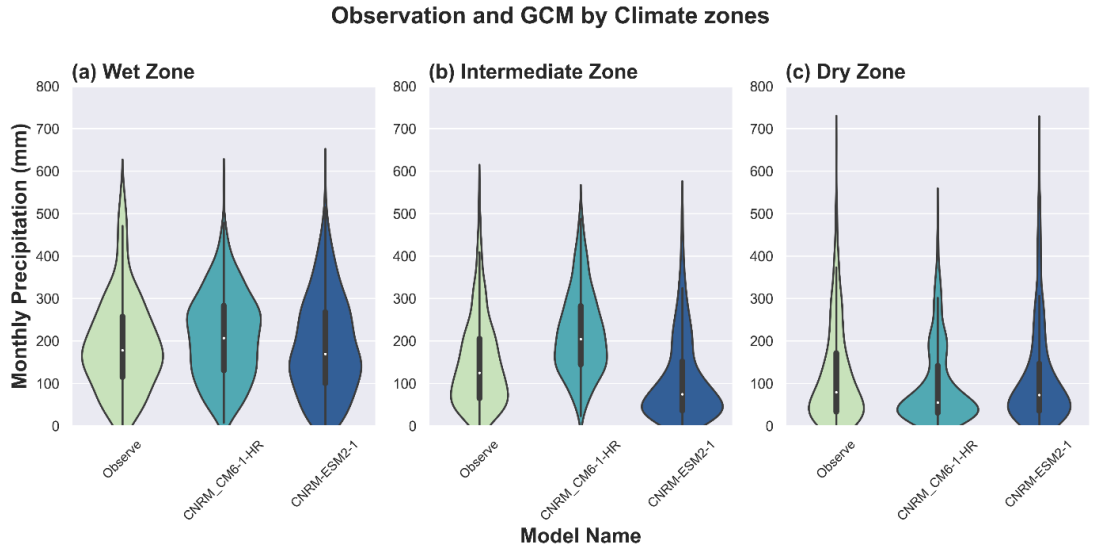

Figure 4-5: Monthly precipitation value distribution over the climate zones

4.2.4 Comparison of Measured and Modelled Monthly Precipitation

Comparing model data to observed data is challenging before bias correction. To overcome this obstacle, normalized monthly precipitations were calculated for each month using the following equation for both models and observed data.

$$Normalised\ Precipitation = \frac{Monthly\ Precipitation\ (mm)}{Yearly\ Cummulative\ Precipitation\ (mm)} \text{----------(34)}$$

The images below depict the monthly variation of normalized precipitation for the selected climate models compared to the observed monthly data. These bar graphs illustrate the sample stations from the wet zone (Kalutara) and the dry zone (Batticaloa), and other graphs are presented in appendix C. Upon analyzing these results, it becomes evident that both models exhibit a strong relationship with the observed data in the dry zone. Conversely, in the wet zone, the two models display varying degrees of correlation with the observed data across different months. However, it is essential to note these results before bias correction. Further optimization of the results can be achieved through this technique.

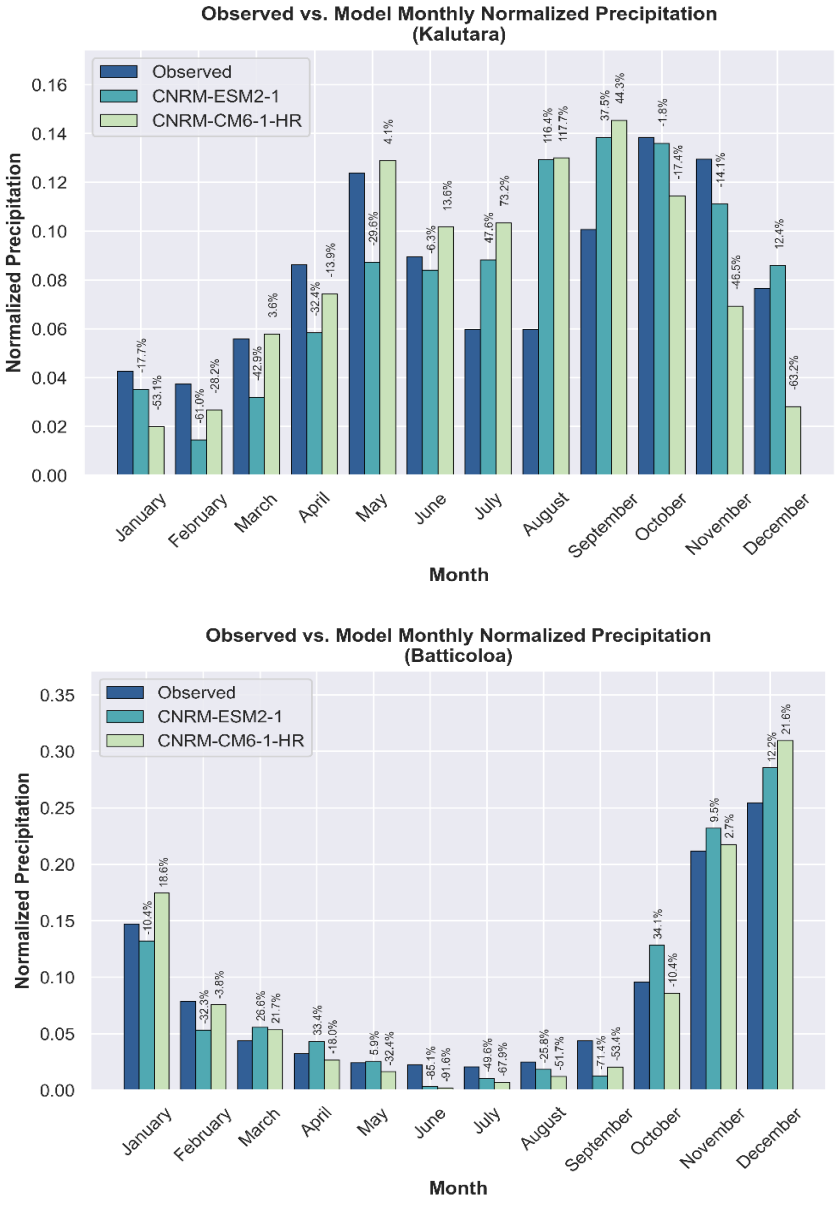

Figure 4-6: Observed vs model normalise monthly precipitation

The images above depict the monthly variation of normalized precipitation for the selected climate models compared to the observed monthly data. Upon analyzing these results, it becomes evident that both models exhibit a strong relationship with the observed data in the dry zone. Conversely, in the wet zone, the two models display varying degrees of correlation with the observed data across different months. It is important to note, however, that these results are before performing bias correction, and as such, further optimization of the results can be achieved through this technique.

4.2.5 Comparison of Measured and Modelled Precipitation with Seasonal Variation

Given that Sri Lanka is a country with a monsoon climate, it is imperative that any climate model used to analyze climate change in this context can accurately capture the monsoon signal. To understand this, Figure 4-7 presents two sample station datasets from the wet and dry zones, displaying seasonal variations in precipitation. Other graphs are presented in Appendix D. Upon analysing these box plots, it is evident that the selected models can effectively capture the monsoon precipitation patterns in both the wet and dry zones. Consequently, these models may be considered reasonably reliable for use in modelling the monsoon climate of Sri Lanka.

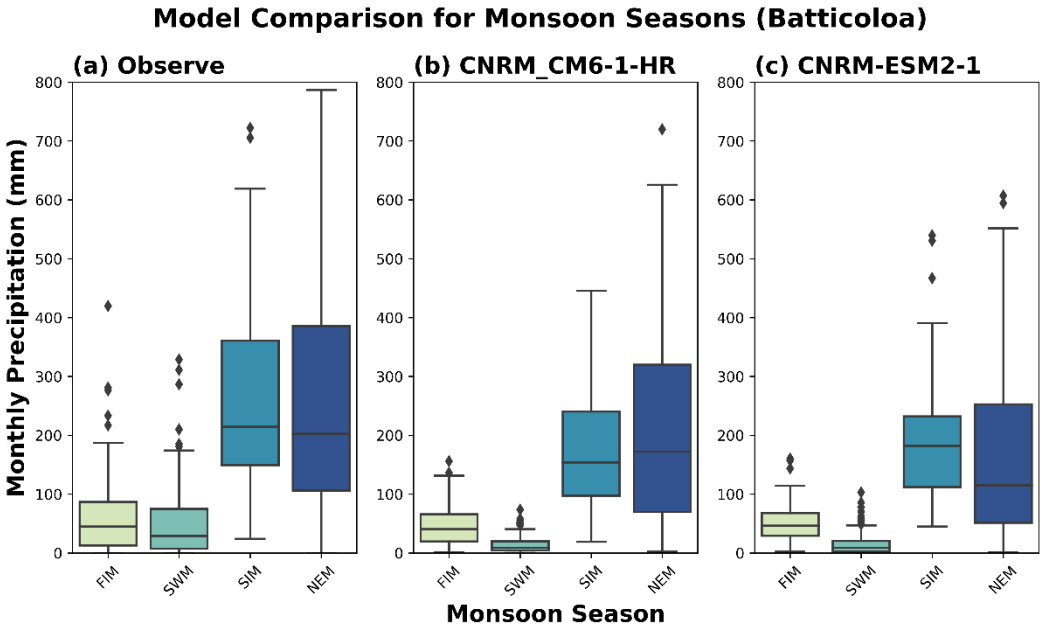

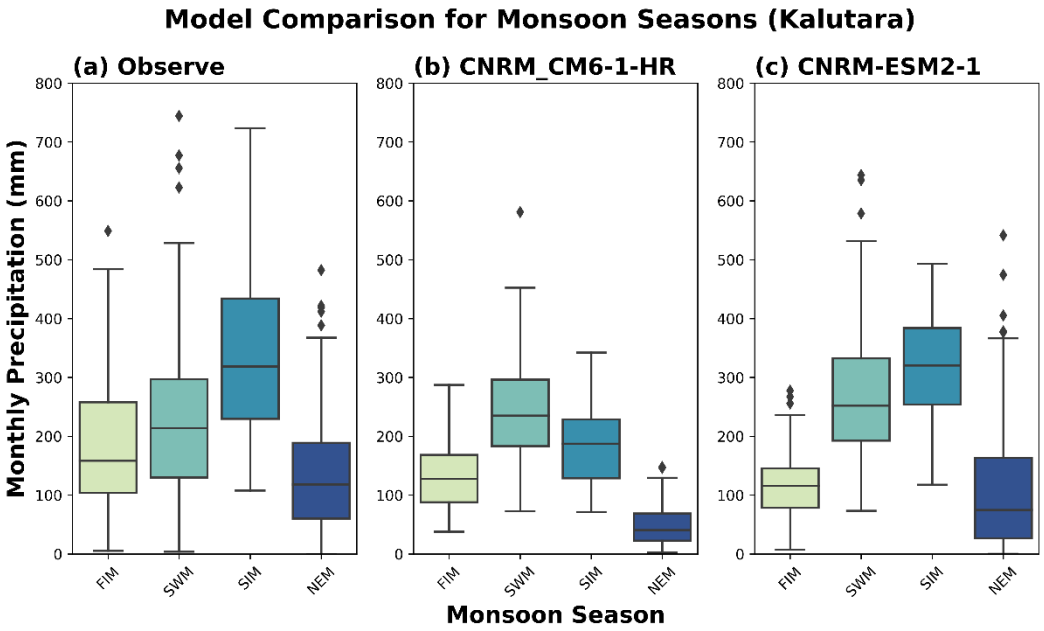

Figure 4-7: Box plot of observed vs model seasonal variation

4.3 Bias Correction of GCM Data

4.3.1 Mean Based Method

As discussed in Section 4.2.4, even the best-performing General Circulation Models (GCMs) exhibit significant bias between projected and observed data. Before additional analysis, bias correction was performed using the mean-based method. Bias factors were computed using the monthly mean values of both observed and projected historical data. These bias factors were subsequently applied to historical and future datasets to obtain mean-based bias-corrected values.

Figure 4-8 presents a scatter plot illustrating the comparison between observed and uncorrected model historical precipitation data and precipitation bias-corrected data obtained using the mean-based method. In this approach, data correction is conducted on an individual data value basis, with bias correction factors calculated using monthly mean values.

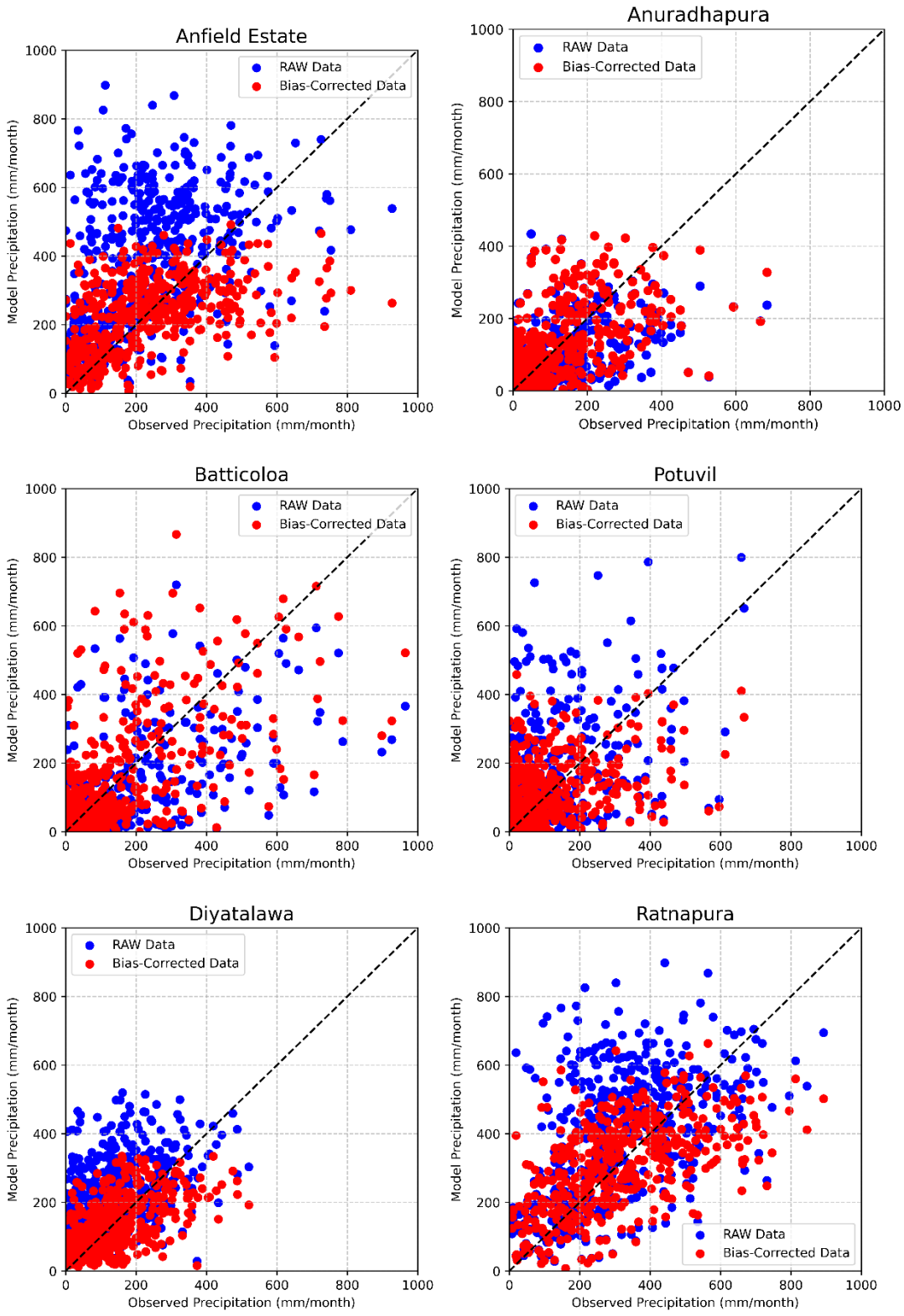

Figure 4-8: Scattered plots between observed data vs uncorrected and corrected GCM data for the Mean-Based method

Notably, in regions with high precipitation, such as Diyatalawa and Ratnapura, the scattered data points exhibit a good relationship between the bias-corrected model data and observed data. However, in dry zone stations, discrepancies arise, with the CNRM-CM6-1-HR model occasionally projecting higher precipitation than the observed data. The model sometimes predicts lower precipitation despite the observed data indicating higher values.

Figure 4-9 presents the empirical cumulative density function (CDF) graphs, offering a comparative analysis of observed data, uncorrected historical model data, and bias-corrected historical model data for precipitation. Examining the CDF curves reveals a discernible difference in the probability distribution between the bias-corrected precipitation data series and the observed data series.

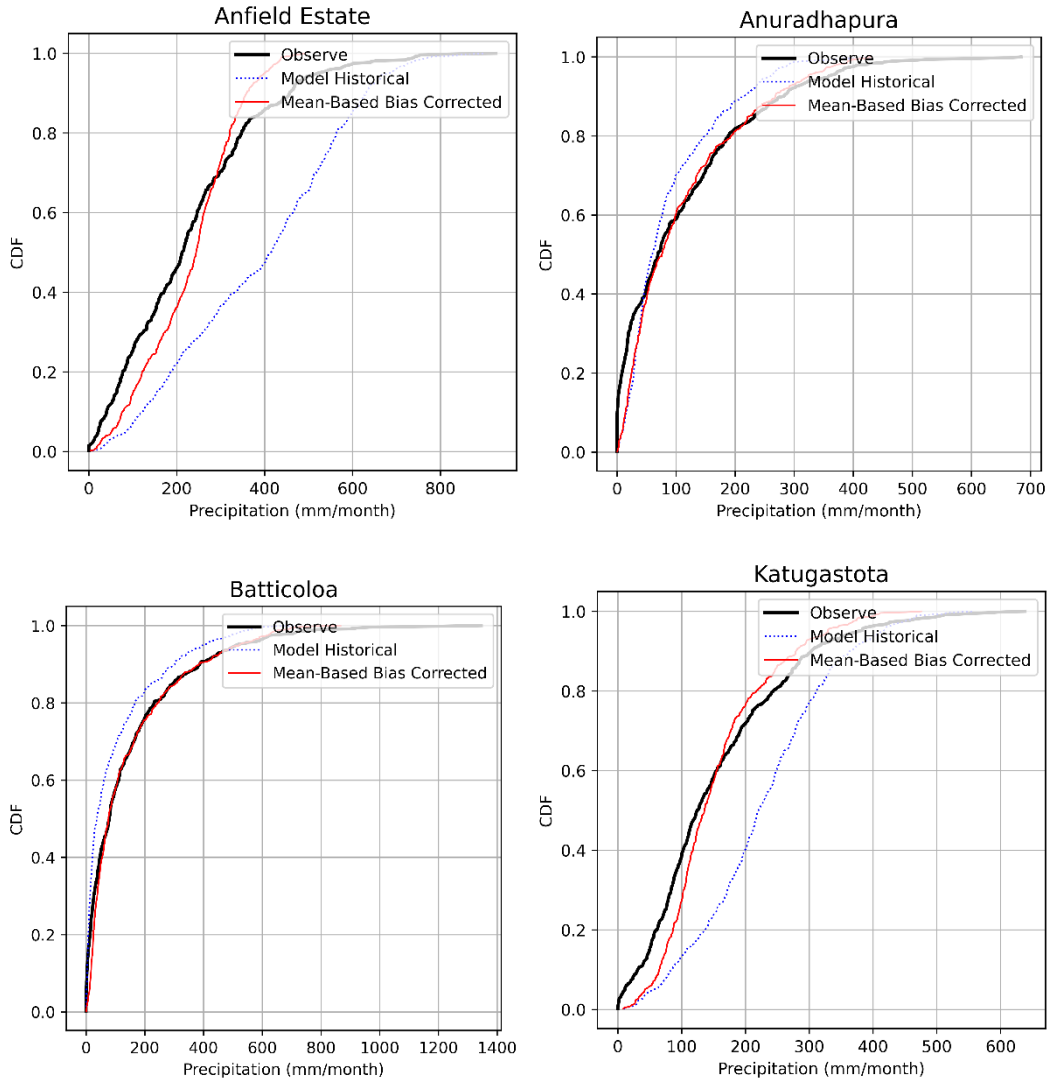

Figure 4-9: CDF curves between observed vs mean-based corrected model precipitation data

Specifically, in the context of the mean-based method, the bias-corrected data demonstrates elevated CDF values in the mid-range of precipitation data when

contrasted with the observed data series. This discrepancy is particularly pronounced in regions characterized by high precipitation, where the bias-corrected CDF curves exhibit substantial deviations from the observed CDF curves. On the contrary, in arid areas featuring scenarios of low precipitation, the CDF curves portray relatively consistent patterns across the various data series.

4.3.2 Empirical Quantile Mapping Method

Quantile mapping represents the latest advancement in bias-correction approaches and has gained popularity as the most widely used method in climate science studies due to its advanced statistical methodology (Thrasher et al., 2012). This method effectively addresses biases across the entire distribution of climate datasets. Recent research indicates that Quantile mapping outperforms more straightforward methods for bias correction for temperature and precipitation (Azmat et al., 2018; Worku et al., 2019).

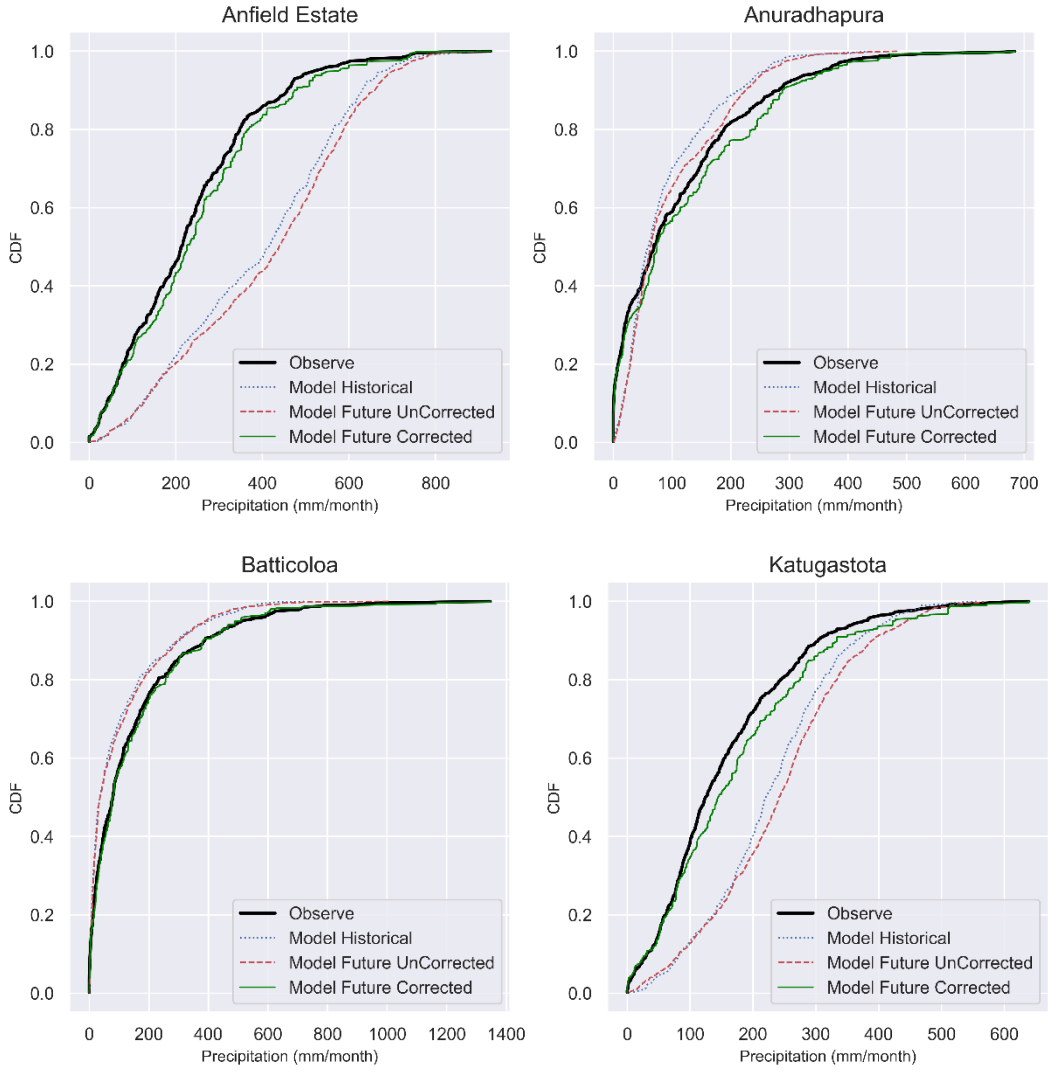

Figure 4-10: CDF Curves between Observed vs Bias Corrected Precipitation Data Using the Quantile Mapping Method

Figure 4-10 demonstrates the Cumulative Density Function (CDF) plots derived using the Quantile Mapping (QM) method for bias correction of precipitation data. This method adjusts the entire probability distribution of the baseline data series to align with the observed data series. Applied to future data series, this bias difference results in a reasonably accurate bias-corrected dataset suitable for future predictions. The figure clearly illustrates the effectiveness of the data series adjustment achieved through QM. The mean-based method exhibits significant differences in CDF values for high precipitation data stations. In contrast, the QM method closely resembles the observed series, highlighting its effectiveness in adjusting precipitation bias correction.

Figure 4-11 showcases the Cumulative Density Function (CDF) plots, encompassing observed, model, and QM-corrected data for temperature. A noteworthy observation emerges when comparing the precipitation data with the temperature data in the climate model; the CDF plots of temperature data demonstrate relatively lower prediction ability. Nevertheless, applying the QM method offers a promising solution, enabling the acquisition of a reliable and improved temperature dataset critical for robust future scenario predictions. This enhancement in temperature data accuracy paves the way for more informed and dependable climate projections, crucial for informed decision-making and policy formulation.

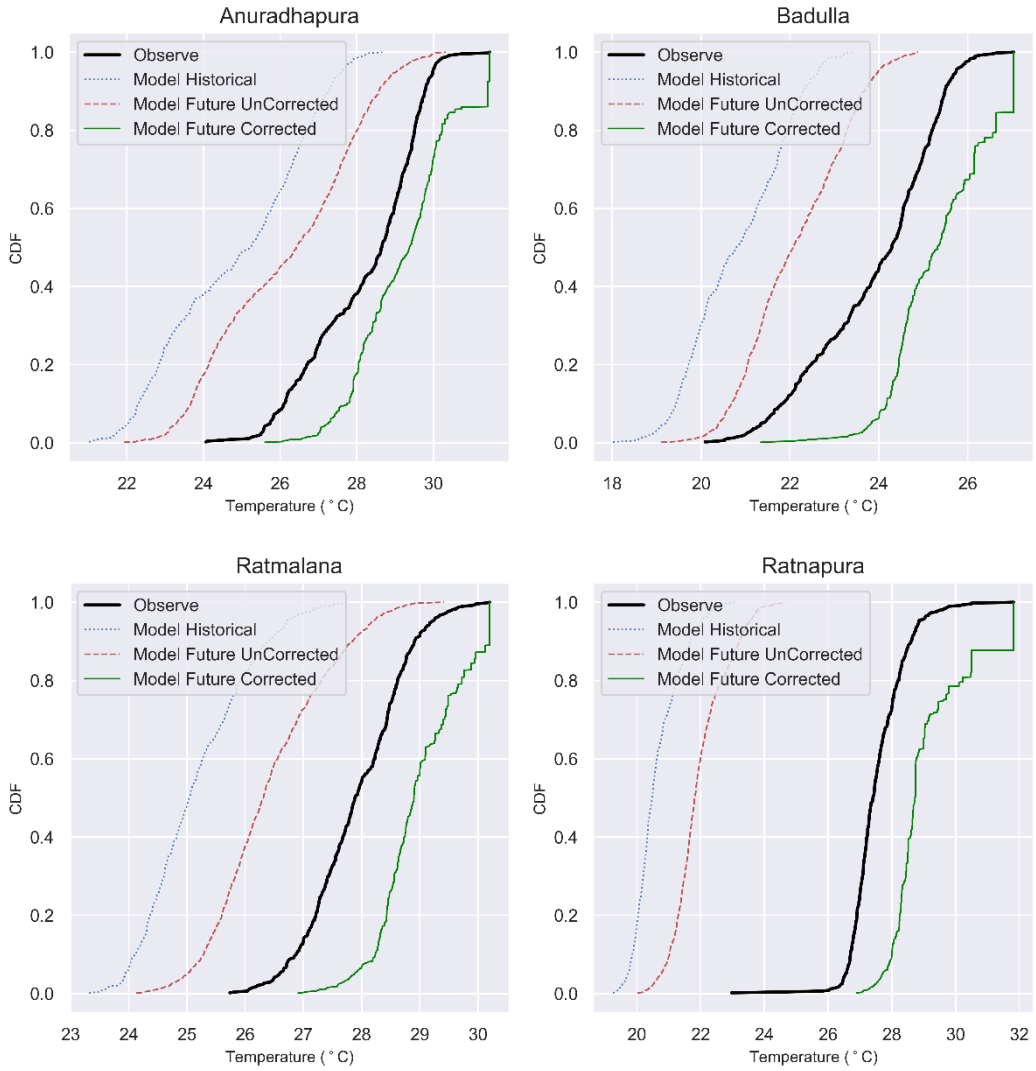

Figure 4-11: CDF curves between observed vs Quantile Mapping Method corrected model temperature data

The effectiveness of the data series adjustment achieved through QM is vividly depicted in the figures. In contrast, the mean-based method reveals significant differences in CDF values for high precipitation stations. Notably, the QM method closely resembles the observed series, highlighting its effectiveness in precipitation bias correction.

4.3.3 Relationship between CHIRPs and Observe Data

This study's main challenge is creating a high-resolution climate dataset covering Sri Lanka. To address this, the study employed a linear regression technique to establish a relationship between CHIRP cell data and the corresponding observational dataset. Figure 4-12 illustrates the gradient values derived from the CHIRPs dataset in conjunction with respective observed data stations. Sri Lanka was divided into 27 polygons, each corresponding to an observed data station. Gradient

Values were then calculated for the CHIRPS cells within each polygon and their respective observed data series.

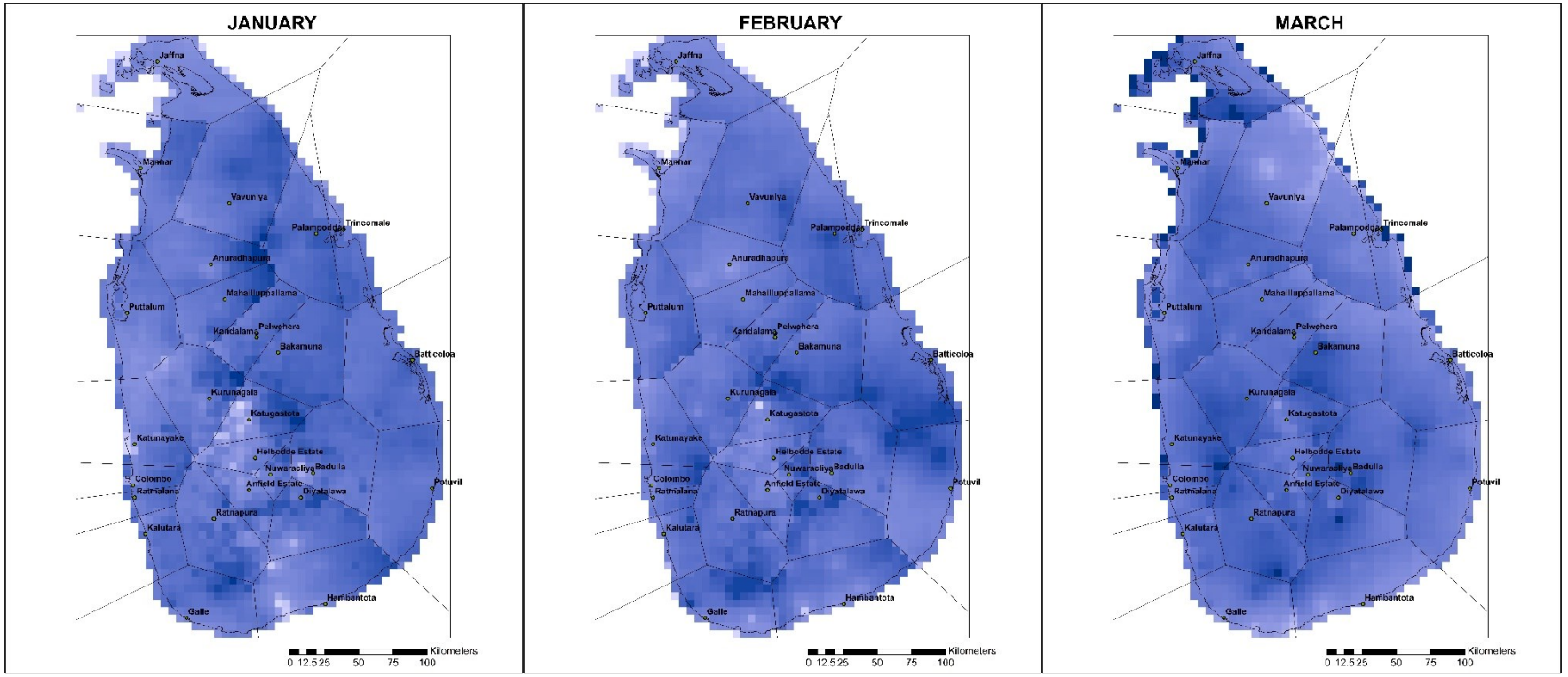

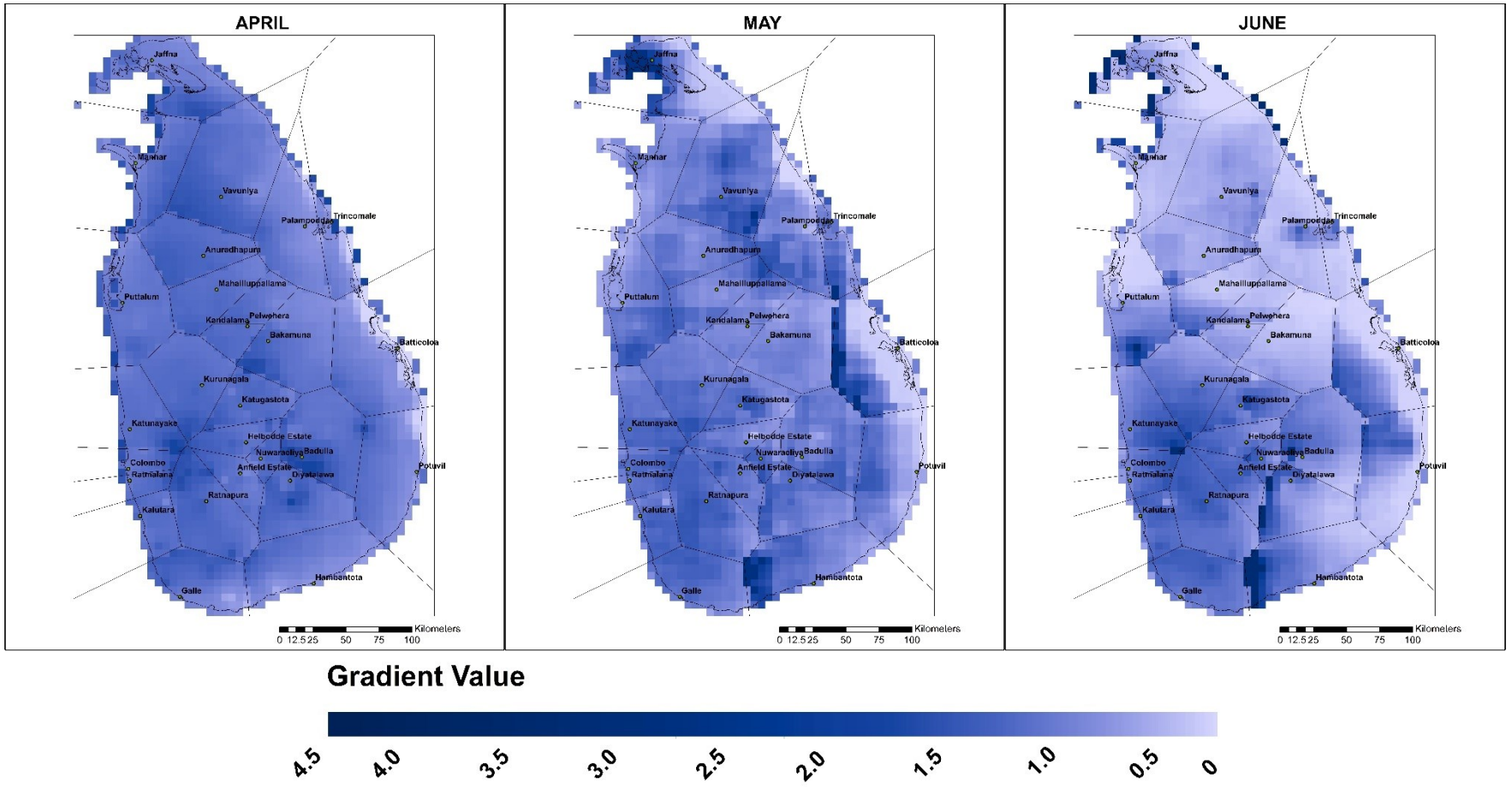
APRIL
MAY
JUNE
Jaffna
Mannar
Vavuniya
Trincomale
Palampoddai
Anuradhapura
Mahailluppallama
Puttalum
Kandalama
Pelwehera
Bakamuna
Batticoloa
Kurunagala
Katugastota
Katunayake
Helbodde Estate
Nuwaraeliya
Badulla
Colombo
Ratmalana
Anfield Estate
Diyatalawa
Potuvil
Ratnapura
Kalutara
Hambantota
Galle
Kilometers
0 12.5 25 50 75 100
Gradient Value
4.5
4.0
3.5
3.0
2.5
2.0
1.5
1.0
0.5
0

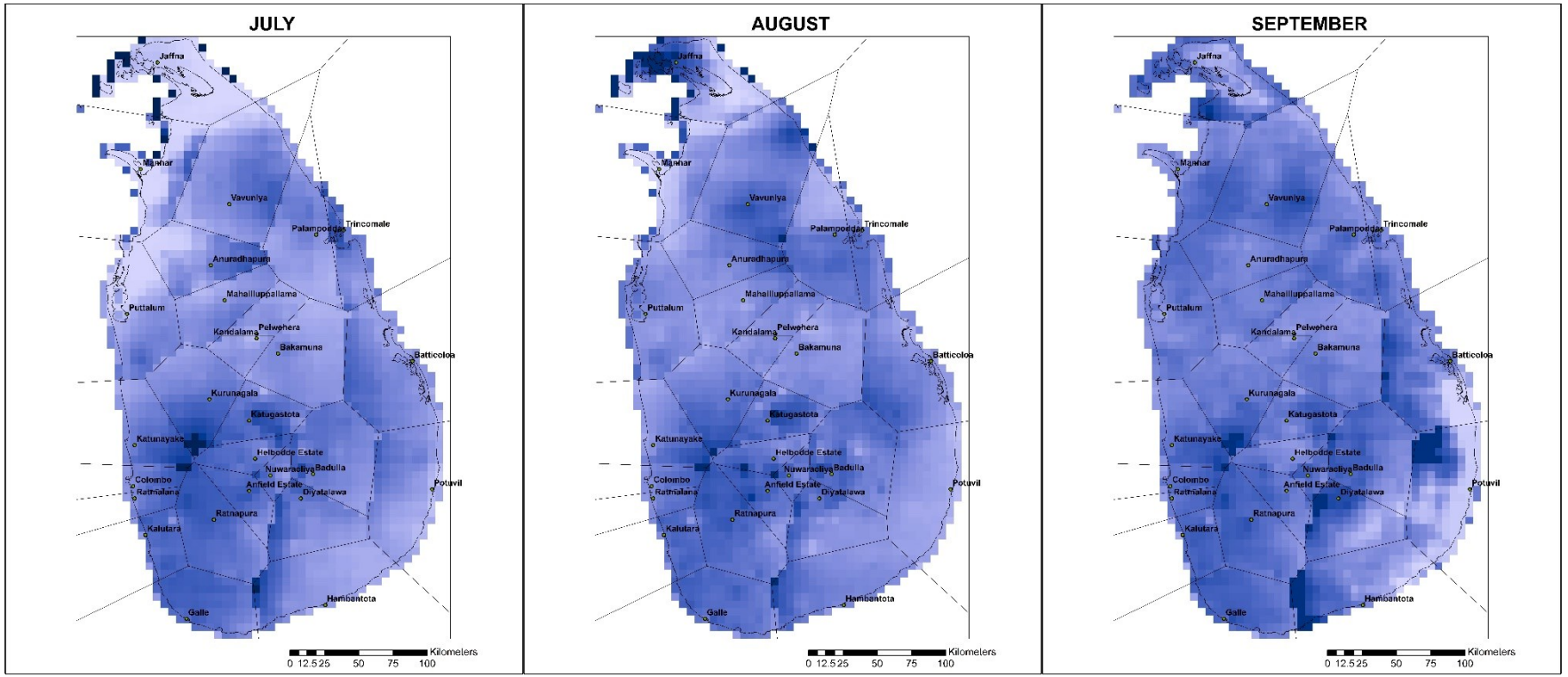
JULY
AUGUST
SEPTEMBER
Jaffna
Mannar
Vavuniya
Trincomale
Palampoddai
Anuradhapura
Mahailluppallama
Puttalum
Kandalama
Pelwehera
Bakamuna
Batticoloa
Kurunagala
Katugastota
Katunayake
Helboode Estate
Nuwaraeliya
Badulla
Colombo
Ratmalana
Anfield Estate
Diyatalawa
Potuvil
Ratnapura
Kalutara
Hambantota
Galle
Kilometers
0 12.5 25 50 75 100
Gradient Value
4.5
4.0
3.5
3.0
2.5
2.0
1.5
1.0
0.5
0

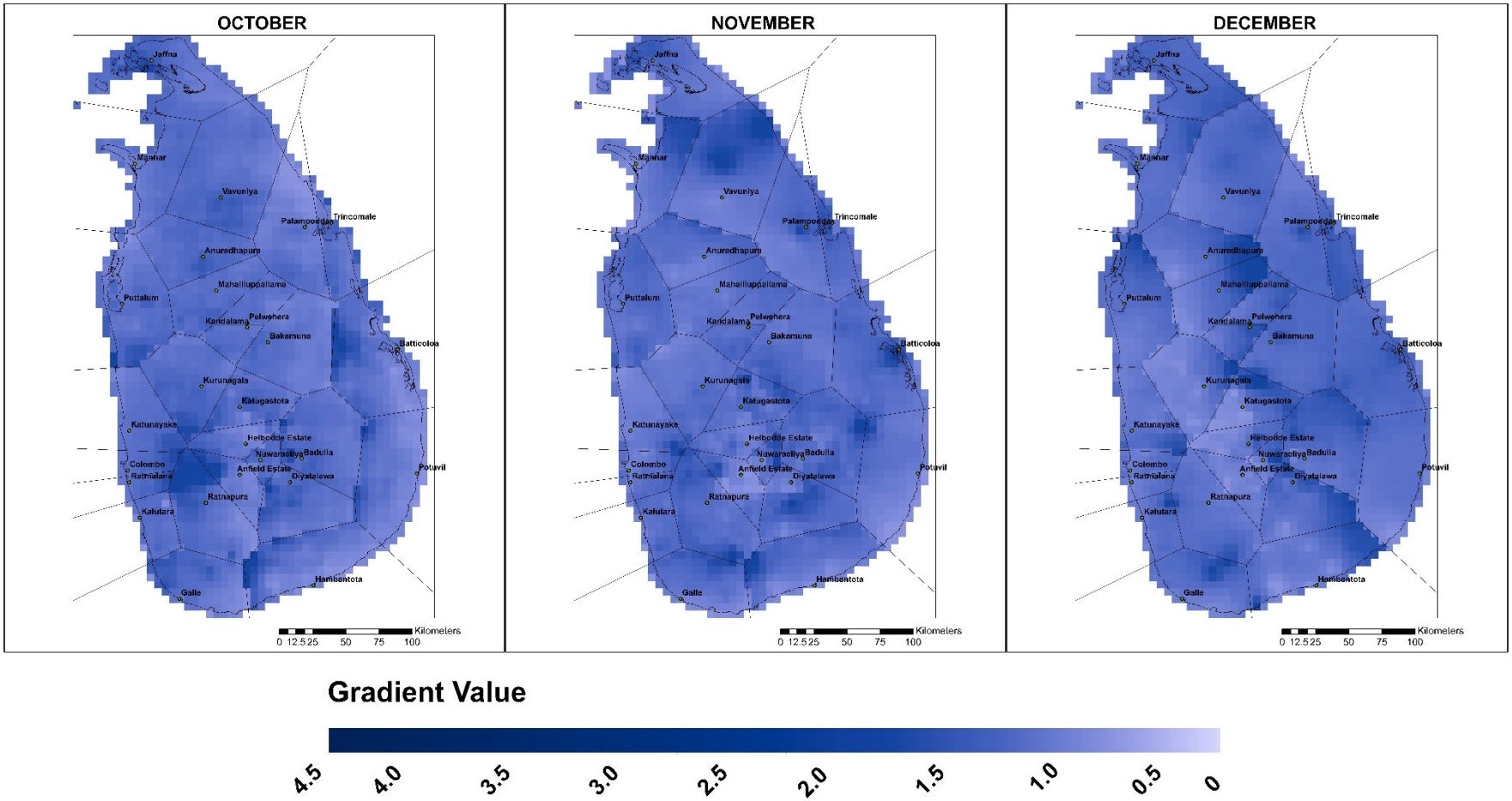

Figure 4-12: The gradient values derived from the CHIRPs dataset with respective observed data stations

This approach allows us to understand precipitation variation spatially for each month in each polygon and how precipitation is distributed across the area. Particularly during monsoon seasons, the distribution of precipitation is crucial for further studies. In the Northeast monsoon period, the highest rainfall occurs in the North, Eastern slopes of the hill country, and the Eastern slopes of the Knuckles range. The maps above clearly demonstrate nearly identical gradient values in the island's Northeast region from December to February, indicating similar precipitation levels.

In the first inter-monsoon season (March to April), there are low gradient values from the Eastern coast to the southwest coast for the observed stations. This is associated with the low precipitation experienced during this period, resulting in a weak relationship between the stations and cells in those areas. However, the hill areas' western coast and western slopes display a high precipitation relationship between the stations and cells.

During the southwest monsoon season (May to September), rainfall varies significantly, ranging from approximately 100 mm to over 3000 mm, and exhibits significant spatial variance. The analysis reveals considerable gradient variation in the maps from May to September due to diverse rainfall patterns. The second inter-monsoon period (October to November) exhibits a more evenly balanced rainfall distribution across Sri Lanka. This period is commonly influenced by weather systems such as depressions and cyclones in the Bay of Bengal, leading to varying gradient values in response to extreme weather events. However, compared to the southwest monsoon period, this distribution demonstrates a pattern consistent with the polygons, indicating a direct variation of gradient values with cell values during this period.

4.4 Köppen-Geiger Climate Classification

In this study, the Köppen-Geiger climate scheme (Peel et al., 2007) was employed to categorize the climate of Sri Lanka into tropical (A), arid (B), temperate (C), boreal (D), and highland (E) climate types. However, owing to the influence of the South Asian monsoon climate, Sri Lanka mainly exhibits tropical (A) and temperate (C) climate types. The climatic classification was based on mean monthly temperature and precipitation at each grid point, and the number of specific grid cells estimated the percentage of each climate type. Figure 4-13 shows the climate zone distribution in the historical period (1975-2014) and the four future projection scenarios (2015 - 2100).

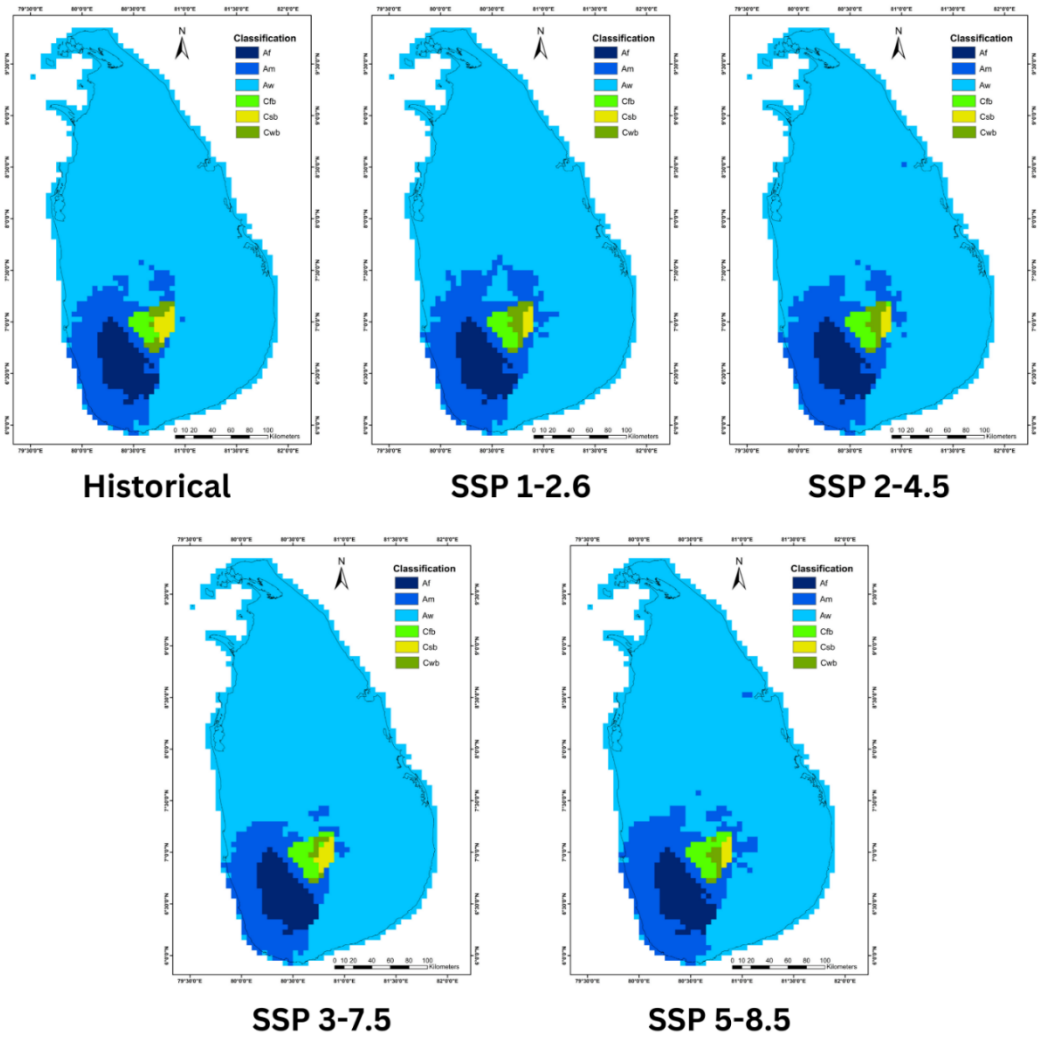

Figure 4-13: Köppen-Geiger zone distribution for the historical period (1975-2014) and future projections (2015-2100)

According to Figure 4-14, Sri Lanka is primarily covered by a Tropical savanna (Aw) climate with high precipitation in the rainy season, and temperature is hot all around the year. These areas mainly face dry and wet seasons throughout the year. The southwest part of the island is classified mainly tropical monsoon climate (Am), which experiences heavy rain during the year but also has a relatively short dry season due to the shifting direction of trade winds from land to sea and vice versa. Around 5% of the southwest low elevation area is covered with the tropical rainforest climate with rain and hot temperatures all year round. According to the classification map, the Rathnapura area, along with the Sinharaja rainforest area, is categorized as a tropical rainforest climate (Af). The southwest monsoon primarily influences this region but receives substantial yearly precipitation. Consequently, it exhibits the typical characteristics of an Af climate, including high rainfall year-round and consistently warm (but not excessively hot) temperatures throughout the year.

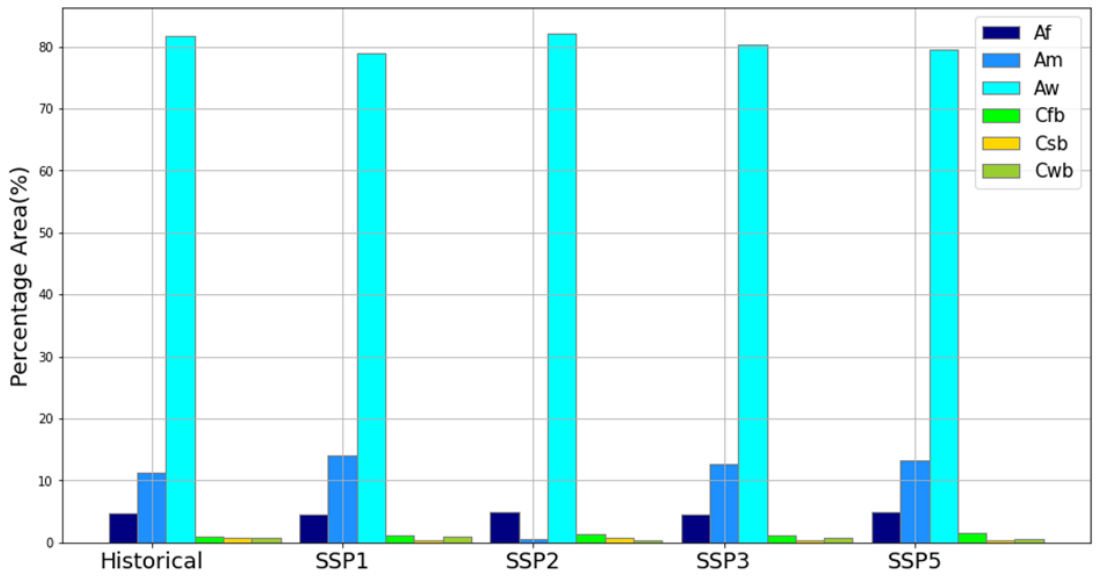

Figure 4-14: Köppen-Geiger climate scheme percentage area values for the historical period (1975-2014) and future projections (2015-2100)

This analysis particularly reveals the presence of a warm-summer Mediterranean climate (Csb) and a Subtropical highland climate without a dry season (Cfb), as well as with a dry winter (Cwb) in high-elevation regions. The Csb climate is characterized by low rainfall in summer (April - September) and substantial rainfall in winter (October–March), with temperatures transitioning from cool to warm throughout the year. The maps presented illustrate the prevalence of the Csb climate zone on the eastern slopes of the hill country, predominantly influenced by the Northeast monsoon (December-February) and second-inter monsoon (October-November).

Areas designated as Cfb climate zones experience moderate to high precipitation and consistently exhibit warm to cool temperatures throughout the year. The Cfb climate zone in Sri Lanka is in the western hill area, typically receiving precipitation throughout the year. The Cwb climate zone is primarily defined by high precipitation in summer and low precipitation in winter, surrounding the highland areas in Sri Lanka. This pattern is attributed to the greater influence of the southwest monsoon compared to the northeast monsoon in these regions.

4.5 Köppen-Geiger Climate Classification Comparison with Traditional Climate Classifications

4.5.1 Rainfall zones classification

Sri Lanka mainly devided in to three major climate zones based on the annual precipitation named ‘wet’, íntermediate’and ‘dry’ zones. The wet zone experiences significant rainfall throughout the year, averaging over 2,500 mm annually, mainly from the south-west monsoons from April to June. Conversely, the dry zone receives less rainfall, averaging below 1,750 mm per year, primarily during the north-east

monsoons from October to January, with a noticeable dry season from May to September. The intermediate zone falls between these extremes, with an annual rainfall ranging from 1,750 to 2,500 mm and a shorter, less pronounced dry season.

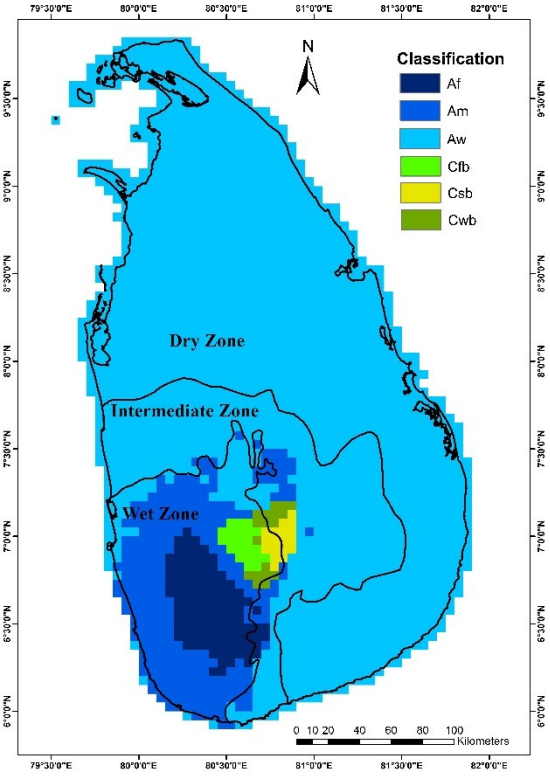

Figure 4-15: Köppen-Geiger climate zone classification comparison with the wet,driand intermediate zone classificatiofor historical (1975-2014)

The Köppen-Geiger climate classification identifies six major classes within Sri Lanka. In comparison to traditional classifications, the entire dry zone is categorized as a tropical savannah (Aw) climate, characterized by temperatures higher than 18°C and a driest month precipitation ranging from 0mm to 39mm, falling below the threshold of (100 - mean annual precipitation/25), which ranges from 20 to 80. The tropical savannah classification also encompasses areas within the intermediate zone. The maximum and minimum annual precipitation within tropical savannah areas range from 1995mm to 502mm, confirming that they receive less than 2500mm of annual precipitation, thus categorizing them as intermediate and dry zones.

The majority of the tropical rainforest (Af) climate class is situated in the wet zone region, with a driest month precipitation ranging from 61mm to 126mm, surpassing 60mm. These Af class cells received a maximum annual precipitation of up to 4520mm. Additionally, emaining most parts of the wet zone are classified under the tropical monsoon climate classification (Am), with a driest month precipitation ranging from 18mm to 60mm, exceeding the value of (100 - mean annual

precipitation/25), which ranges from -22 to 39, and with an annual precipitation range of 1925mm to 3041mm.

Three complex climate zones a warm-summer Mediterranean climate (Csb), a dry winter (Cwb), and a Subtropical highland climate without a dry season (Cfb) are situated within both the wet and intermediate zones. These zones are characterized by a hottest month temperature of 17.3°C or higher, a coolest month temperature above 0°C but below 18°C, and they fully lie within the wet zone.

4.6 Spatial Changes of Shifting Climate Types

Figure 4-15 presents the spatial and temporal characteristics of major climate types relative to historical (TB/1975–2014) in Sri Lanka from 2020 to 2050 (Near Term/TN) and 2070 to 2100 (Long Term/TL). A notable spatial feature is the disappearance of the Csb and Cwb climate zones, predominantly replaced by the Am climate zone. When compared to TB, spatial shifts were detected in the Highland areas of Sri Lanka, particularly in the Southwest and Southeast Mountains.

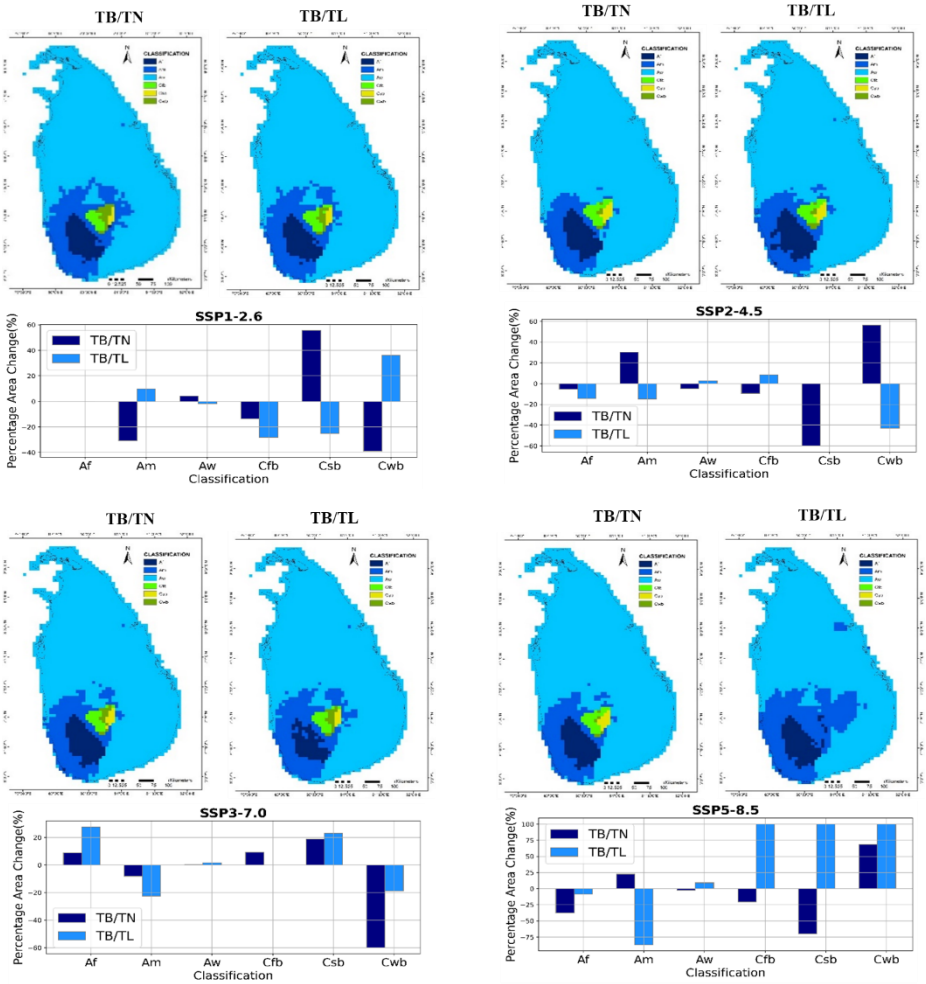

Figure 4-16: Köppen-Geiger zone distribution for near-term (2020-2050) and long-term (2070-2100) Periods

Regarding temporal changes, the percentage of area occupied by Af, Am, and Aw climate types fluctuates less during the future scenarios than TB. However, the percentage of area change for Cfb, Csb, and Cwb shows significant variations, ranging from -14% (TB/TN) to -28% (TB/TL), 56% (TB/TN) to -25% (TB/TL), and -39% (TB/TN) to 36% (TB/TL), respectively, in the SSP1-2.6 scenario. In the SSP5-8.5 scenario, the changes for Cfb, Csb, and Cwb range from -201% (TB/TN) to 100% (TB/TL), -70% (TB/TN) to 100% (TB/TL), and 68% (TB/TN) to 100% (TB/TL), respectively. These observations provide valuable insights into the potential climate changes and their spatial distribution in Sri Lanka under different future scenarios—the most notable observation in the disappearance of highland climate zones in the TL period.

In each scenario, identifying the changing areas is most important to future climate policy and strategy planning. Figure 4-16 shows the spatial changing areas in TN and TL due to climate change compared to TB.

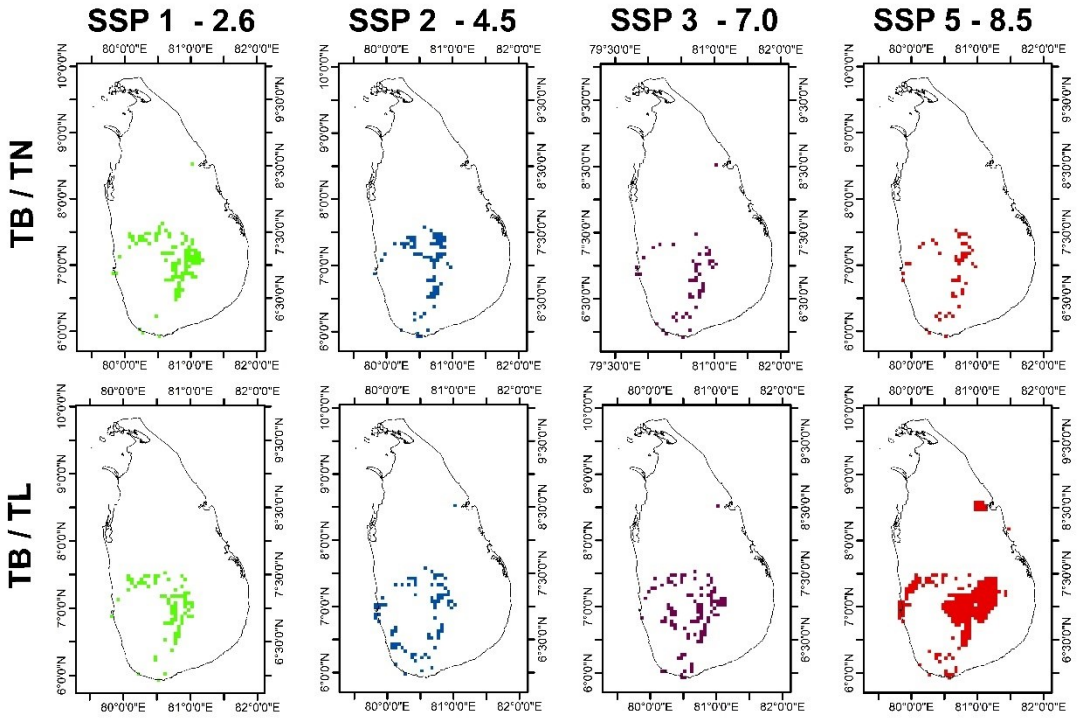

Figure 4-17: The spatial changing areas in TN (2020-2050) and TL (2070-2100) due to climate change compared to TB (1975-2014).

The study results show distinct spatial shifts are observed during the TN and TL periods. In the TN period, the shifts are primarily concentrated within elevated highland regions, while in the TL period, spatial shifts are more broadly distributed, encompassing both highland and southwest regions. Both periods exhibit significant climate zone shifts in the highland areas, constituting the central heart of Sri Lanka's hydrological system.

These observed changes carry profound implications for the hydrological system. As the focal point of these shifts, the highland areas play a crucial role in the water balance of Sri Lanka's hydrology. As these spatial shifts persist, they are expected to impact the hydrological system directly. Section 4.6 of this study focuses on a comprehensive analysis of the changes in hydrology resulting from these climate zone shifts.

4.6.1 Temporal Changes of Shifting Climate Types

Seasonal variation changes with the climate change scenarios will be discussed in this subsection. The following illustration shows the monthly mean precipitation and temperature variation in historical and two future (SSP1 & 5) projection scenarios.

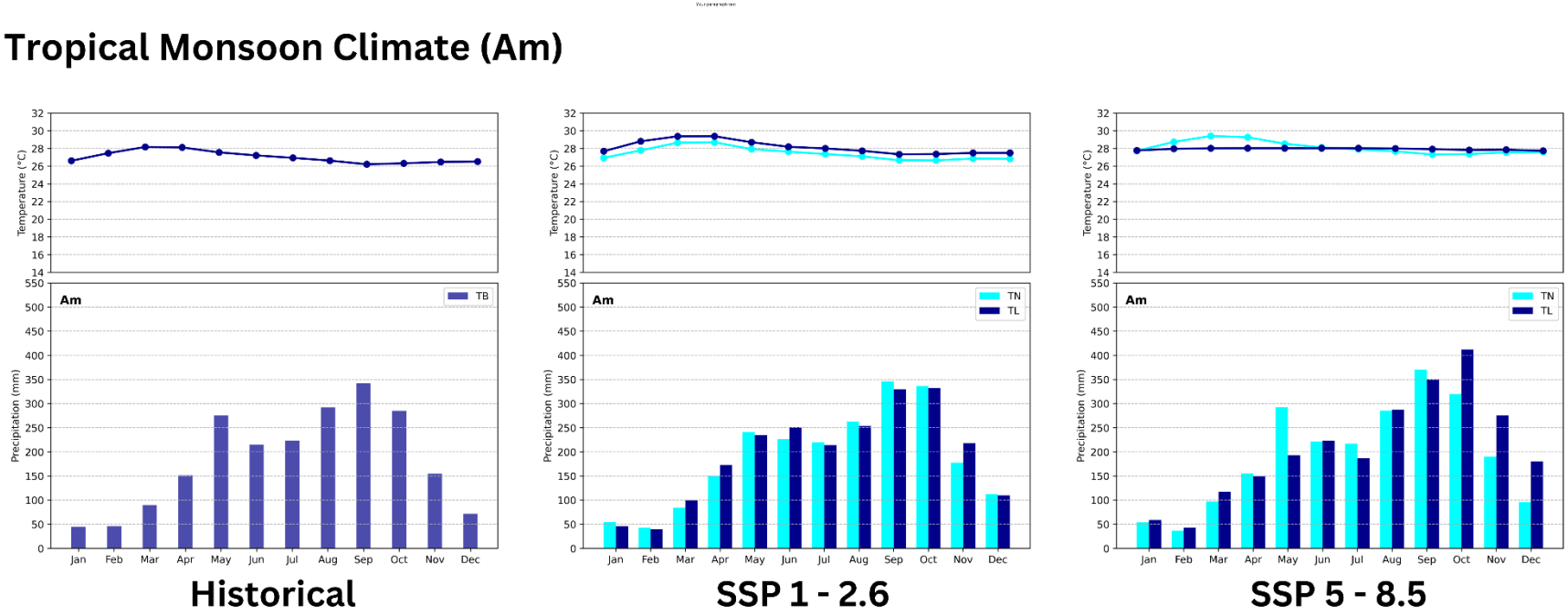

Tropical Rainforest Climate (Af)

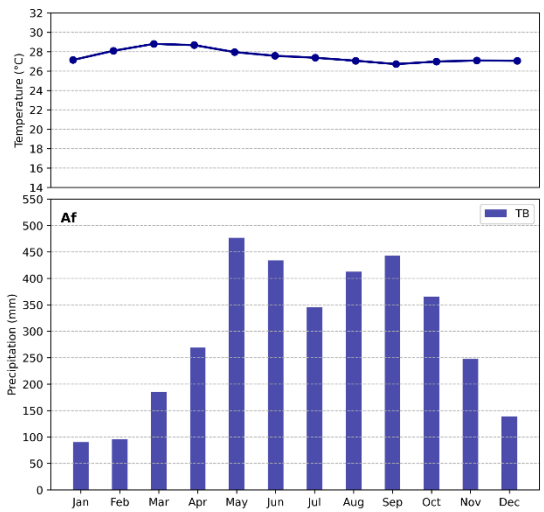

Historical

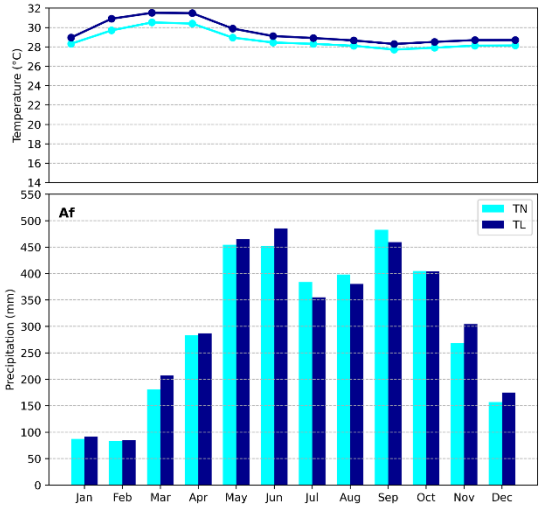

SSP 1 - 2.6

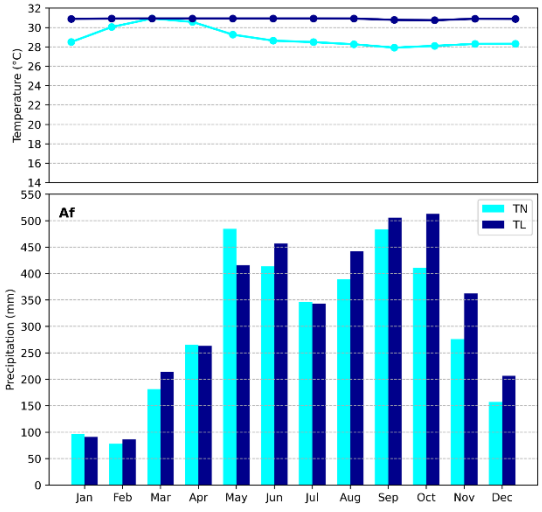

SSP 5 - 8.5

Subtropical Highland Climate with Dry Season (Cwb)

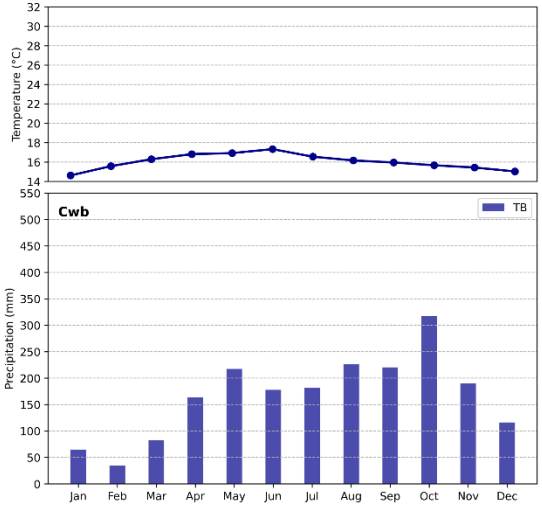

Historical

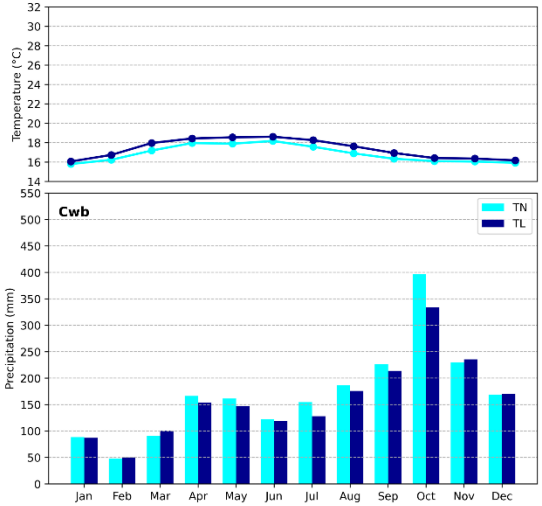

SSP 1 - 2.6

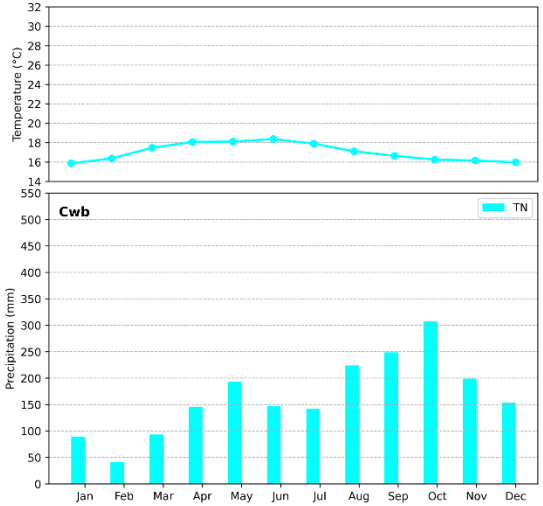

SSP 5 - 8.5

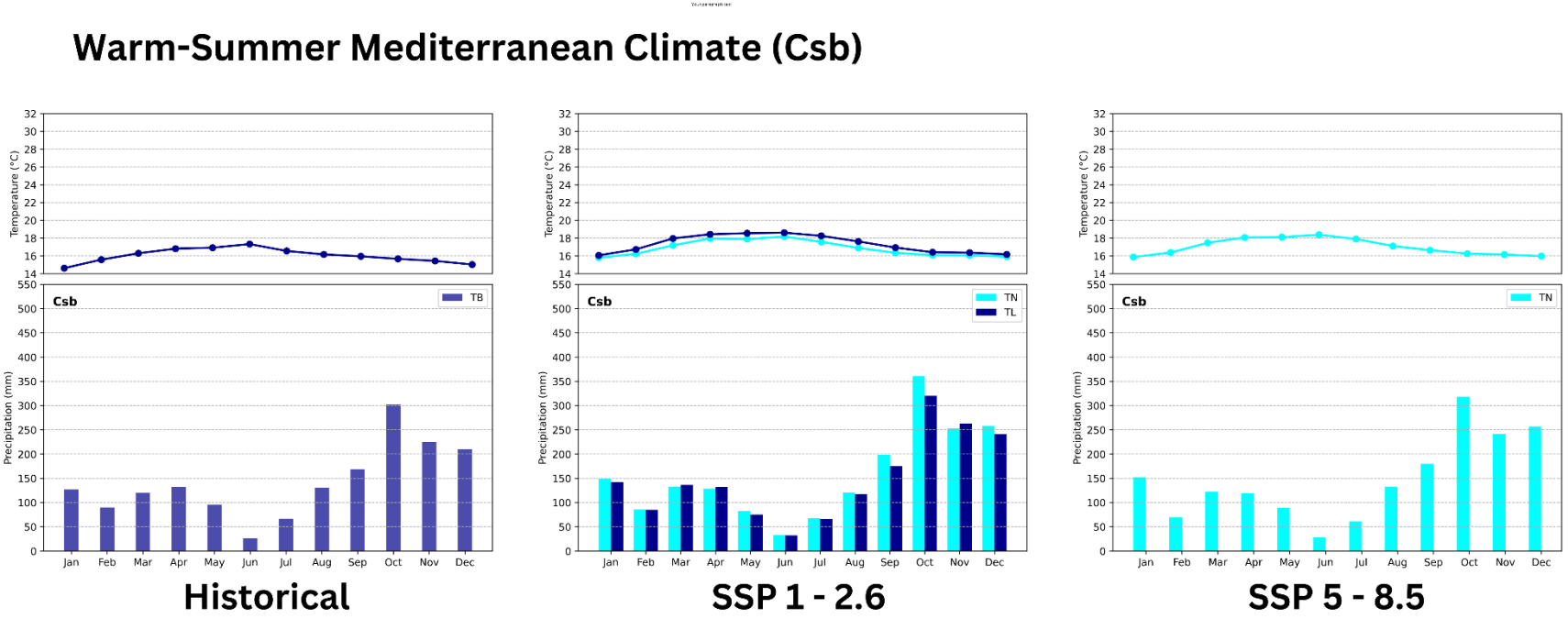

Figure 4-18: Temporal changes in mean precipitation and temperature with shifting climate for the historical period (1975-2014) and future projections (2015-2100)

The results generated from this study highlight a noteworthy trend in monsoon rainfall patterns, indicating their relative stability across different scenarios. However, a closer examination of the data reveals a discernible shift when comparing the TN and TL periods.

In the TL period, there is a notable increase in both precipitation and temperature magnitudes when compared with the TN period. This escalation suggests a substantive alteration in the climatic conditions over the long term. The observed rise in precipitation and temperature significantly affects the region's hydrological dynamics and broader climate resilience. Understanding these temporal changes is crucial for anticipating and adapting to evolving climate patterns, particularly as they are likely to affect the balance of precipitation and temperature that sustains the hydrological system. The subsequent sections of this study present a more detailed analysis of these trends, exploring the potential repercussions on water resources, ecosystems, and the overall resilience of the region's hydrological framework.

4.7 Hydrological Model

4.7.1 Model Calibration

The distributed hydrological model was built to assess the hydrological impact of climate change. This model was specifically designed to calculate the water balance in grid cells. For the calibration of the hydrological model, two basins from the wet zone and two basins from the dry zone were selected. The Kalu River Basin and Kelani River Basin were chosen from the wet zone, while the Kirindi Oya and Maduru Oya River Basins were selected from the dry zone.

The model parameters from the calibrated distributed model are represented in Tables 4-9 and 4-10. The calibration process utilized data from the years 2000 to 2005. The model comprises five layers: Digital Elevation Model (DEM), Precipitation Layer, Evaporation Layer, Landuse Cover Layer, and Soil Layer. Figure 4-18 displays land cover and soil maps for Sri Lanka, providing visual representation and context for the calibration process.

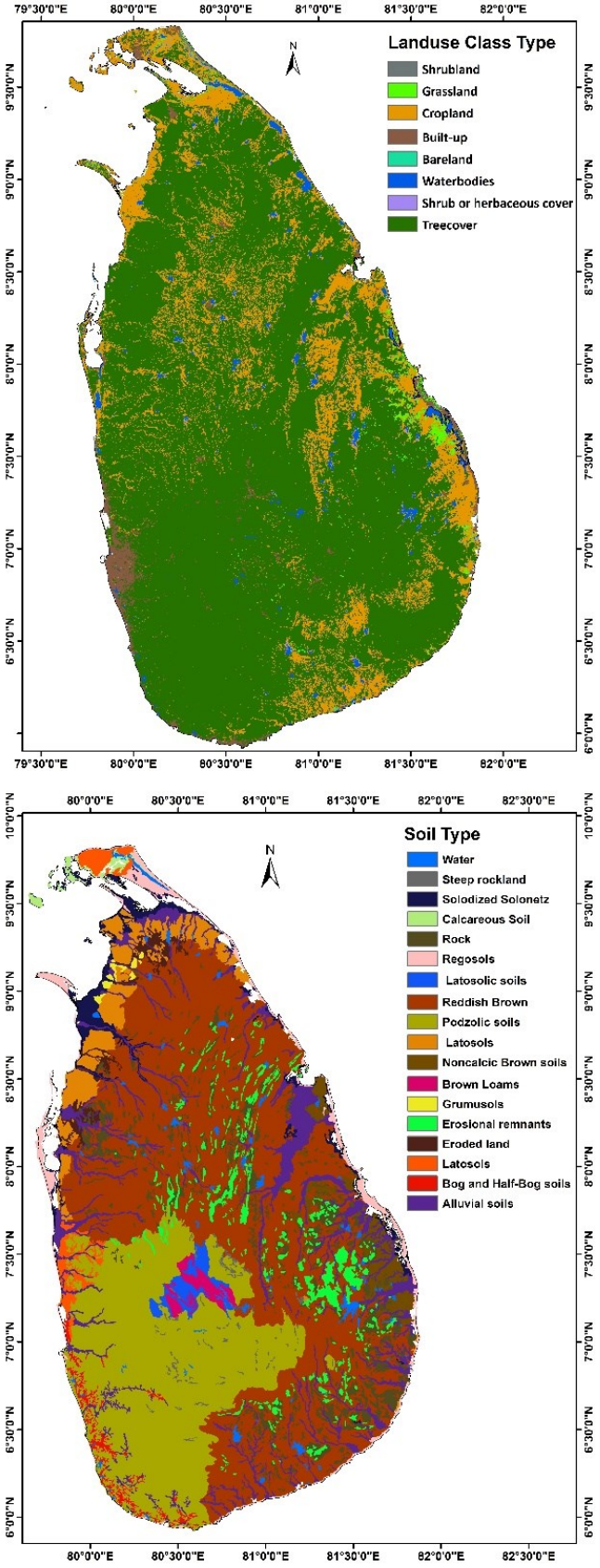

Figure 4-19: Landuse cover (2014) and soil map of Sri Lanka

Table 4-9: Calibrated manning roughness coefficients

Landuse Class Type	Manning Roughness Coefficient
Shrubland	0.052
Grassland	0.035
Cropland	0.03
Built-up	0.01
Bareland	0.03
Waterbodies	0.01
Herbaceous Cover	0.045
Tree Cover	0.25

Table 4-10: Calibrated infiltration coefficient

Soil Type	Infiltration Coefficient (mm/h)
Calcareous Soil	8.40
Regosols	7.20
Latosolic	12.40
Reddish Brown Soil	14.20
Podzolic Soil	19.40
Noncalcic Brown Soil	14.10
Loams	15.00
Grumusols	20.04
Erosional Remnants	8.10
Eroded Land	7.40
Bog and Half-Bog Soils	2.54
Alluvial Soil	22.00

4.7.2 Changes in Annual Runoff

Anthropogenic activities have been identified as significant contributors to future runoff changes, particularly in the context of climate change (Liu et al., 2022). Climate change plays a crucial role in influencing runoff patterns, and this study employs a distributed hydrological model to comprehensively understand the hydrological impact on water balances in Sri Lanka.

The hydrological model was calibrated using a baseline period sample dataset. Subsequently, future scenarios were simulated using the SSP1-2.6 and SSP5-8.5 scenarios for 2020 to 2100. The analysis was conducted for two distinct time frames: Near-term (TN/2020-2050) and Long-term (TL/2070-2100) to assess the impact on hydrology with climate zone shifts. Figure 4-19 illustrates the ensemble mean runoff percentage changes compared to the baseline period (TB/1975-2014) for the 45 river basins.

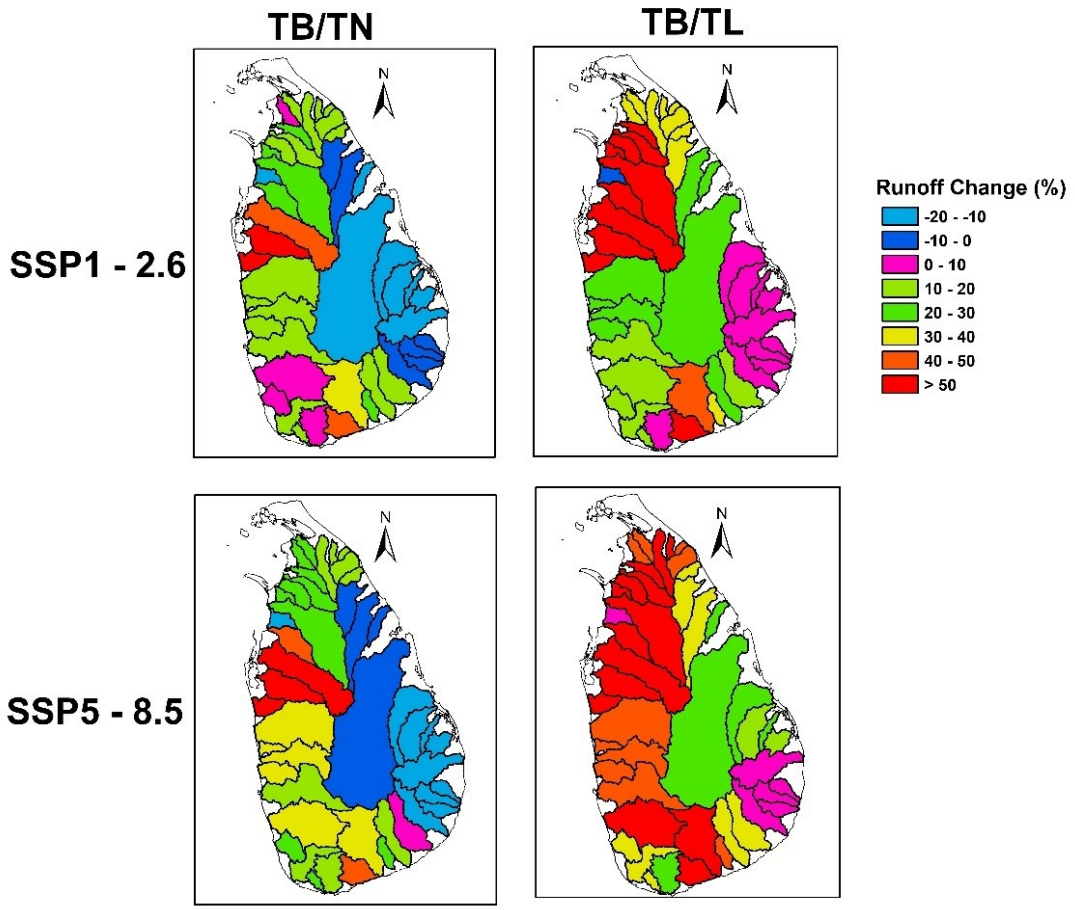

Figure 4-20: Projected mean runoff change percentage in TN (2020-2050) and TL (2070-2100) compared to TB (1975-2014) period

In Figure 4-19, the runoff changes are visually represented, depicting both increments and decrements during the TN and TL periods. Specifically, in the TN period, basins located on the island's eastern side exhibit a runoff decrement, while basins along the western coast show a runoff increment. However, in the TL period, all basins across the island demonstrated an increase in runoff with the impact of climate change.

Focusing on the Wet zone under the SSP1-2.6 scenario, comparing TN and TL periods with the baseline (TB) period reveals noteworthy changes. In the TN period, the average runoff change is 10%, while in the TL period, it increases to 15%. In contrast,

under the SSP5-8.5 scenario, the average runoff change in the Wet zone is more substantial, with 27% during TN and a higher increment of 38% during TL.

Examining the Dry zone under the SSP1-2.6 scenario, the TN period shows an average runoff change of 10%, which rises to 35% during the TL period. These findings highlight the varying impacts of climate change on runoff changes across different climate zones and scenarios, providing valuable insights for understanding the hydrological dynamics in Sri Lanka.

5. CONCLUSION

The research study aimed at assessing climate zone shifting attributed to future climate change in Sri Lanka according to Köppen-Geiger Climate Classification. First, the study evaluated the performances of the Multiple Imputation by Chained Equations (MICE) package and General Circulation Models (GCMs) in the context of the monsoon climate in Sri Lanka. The MICE package was assessed in wet and dry zones using RMSE and MAE percentages. Accordingly, the PMM method exhibited consistently lower error percentages than the Norm method across all time scales. As the time scale increased, both methods demonstrated a decrease in percentage errors, with smaller errors observed in monthly scales compared to daily scales. These findings suggest that MICE imputation data is more suitable for high-temporal scale analyses. According to the wet zone and dry zone RMSE and MAE, it can be concluded that the predictive mean matching method performs better than the normal imputation method for the monsoon climate in Sri Lanka.

Furthermore, fifteen GCMs were evaluated for their performance in simulating monsoon precipitation in Sri Lanka. The models were ranked based on their results compared to data from 27 meteorological stations using the EDAS method. The MPI-ESM1-2-HR, CNRM-CM6-1-HR, and CNRM-ESM2-1 were identified as the top performers in simulating precipitation in both the wet and intermediate zones. These findings will be valuable for future climate change studies, enabling the selection of well-performing models in different climate zones. CNRM-ESM2-1, CNRM-CM6-1-HR, and MRI-ESM2-0 emerged as the top three models in the dry zone. Notably, the MRI-ESM2-0 model did not perform strongly in the wet zone. The CNRM-CM6-1-HR and CNRM-ESM2-1 have the best performance among the selected GCMs. Two CNRM models are available, one of which features a high resolution of 0.5˚×0.5˚. Therefore, the abovementioned model appears to be better suited for a study area such as Sri Lanka.

The performance of the selected two GCMs through the EDAS method showed strong results across all seasons. It is worth noting that both climate models exhibit a strong ability to capture the monsoon signal throughout the year, indicating their effectiveness in simulating the precipitation patterns of Sri Lanka. The successful representation of the monsoon signal by these models is important for climate change studies, as it provides a solid foundation for projecting future climate scenarios and assessing potential impacts.

Precipitation and temperature data from the CNRM-CM6-1-HR model were used for further analysis. The Mean-Based and Quantile Mapping methods were used for the bias correction. A comparison of the CDFs showed better results in the Quantile Mapping method than in the Mean-Based method. The Quantile Mapping method

showed better relationships between observed data and the model prediction data in precipitation and temperature datasets.

Developing a high-resolution precipitation and temperature data dataset divided the Sri Lankan land area into different zones according to the Köppen-Geiger Climate Classification. A similar analysis was performed using future projections of precipitation and temperature. According to these results, climate zone shifting mostly affects the island's South-West region and the highland areas. Notably, Highland climates are the most affected in all the prediction scenarios. According to the SSP5-8.5 scenario, in the TL, the Cfb and Cwb climate zones will disappear. The findings further illustrated that the potential climate shifts associated with global warming scenarios vary across different regional climate zones.

The hydrological model aimed at stimulating the effects of climate shifts on hydrology within dry and wet zones. According to the model results, during the TN period, the eastern basins undergo a decrease in runoff, in contrast to the observed increase along the western coast. On the other hand, runoff is expected to increase across all basins during the TL in different magnitudes. When the results from different scenarios are considered, the Wet zone exhibits substantial runoff changes, with the SSP5-8.5 scenario demonstrating a more pronounced effect. Notably, the Dry zone experiences a significant surge in runoff during the TL period under the SSP1-2.6 scenario. These findings offer valuable insights into the complex interplay between climate change and runoff dynamics in Sri Lanka, emphasizing the need for region-specific adaptation strategies to mitigate the multifaceted impacts on water resources.

REFERENCE LIST

Abbass, K., Qasim, M. Z., Song, H., Murshed, M., Mahmood, H., & Younis, I. (2022). A review of the global climate change impacts, adaptation, and sustainable mitigation measures. *Environmental Science and Pollution Research*, *29* (28), 42539–42559. https://doi.org/10.1007/s11356-022-19718-6

Addi, M., Gyasi-Agyei, Y., Obuobie, E., & Amekudzi, L. K. (2022). Evaluation of imputation techniques for infilling missing daily rainfall records on river basins in Ghana. *Hydrological Sciences Journal*, *67*(4), 613–627.

Almazroui, M., Saeed, S., Saeed, F., Islam, M. N., & Ismail, M. (2020). Projections of Precipitation and Temperature over the South Asian Countries in CMIP6. *Earth Systems and Environment*, *4*(2), 297–320. https://doi.org/10.1007/s41748-020-00157-7

Ayugi, B., Tan, G., Ruoyun, N., Babaousmail, H., Ojara, M., Wido, H., Mumo, L., Ngoma, N. H., Nooni, I. K., & Ongoma, V. (2020). Quantile mapping bias correction on rossby centre regional climate models for precipitation analysis over Kenya, East Africa. *Water*, *12*(3), 801.

Azmat, M., Qamar, M. U., Huggel, C., & Hussain, E. (2018). Future climate and cryosphere impacts on the hydrology of a scarcely gauged catchment on the Jhelum river basin, Northern Pakistan. *Science of the Total Environment*, *639*, 961–976.

Bear, J. (1979). *Hydraulics of groundwater*. Courier Corporation.

Bear, J., & Verruijt, A. (1987). *Modeling groundwater flow and pollution* (Vol. 2). Springer Science & Business Media.

Bergeron Jr, T. C. (1928). Collation in the Civil Law. *Loy. LJ*, *9*.

Beven*, K. (2001). How far can we go in distributed hydrological modelling? *Hydrology and Earth System Sciences*, *5*(1), 1–12.

Beven, K. J. (2001). Rainfall-runoff modelling: The primer. *Hydrological Sciences Journal*, *46*(6), 1002–1002.

Blankenau, P. A., Kilic, A., & Allen, R. (2020). An evaluation of gridded weather data sets for the purpose of estimating reference evapotranspiration in the United States. *Agricultural Water Management*, *242*, 106376.

Buksha, I. F., Pyvovar, T. S., Buksha, M. I., Pasternak, V. P., & Buksha, T. I. (2021). MODELLING AND FORECASTING THE IMPACT OF CLIMATE CHANGE ON FORESTS OF UKRAINE FOR 21ST CENTURY TIME HORIZON. *Forestry Ideas*, *27*(2), 470–482.

Buuren, S. van, & Groothuis-Oudshoorn, K. (2011). **mice**: Multivariate Imputation by Chained Equations in *R*. *Journal of Statistical Software*, *45*(3). https://doi.org/10.18637/jss.v045.i03

Cai, L., Alexeev, V. A., Walsh, J. E., & Bhatt, U. S. (2018). Patterns, Impacts, and Future Projections of Summer Variability in the Arctic from CMIP5 Models. *Journal of Climate*, *31*(24), 9815–9833. https://doi.org/10.1175/JCLI-D-18-0119.1

Chathuranika, I. M., Gunathilake, M. B., Azamathulla, H. Md., & Rathnayake, U. (2022). Evaluation of Future Streamflow in the Upper Part of the Nilwala River Basin (Sri Lanka) under Climate Change. *Hydrology*, *9*(3), 48. https://doi.org/10.3390/hydrology9030048

Chen, T.-Y. (2023). A circular intuitionistic fuzzy evaluation method based on distances from the average solution to support multiple criteria intelligent decisions involving uncertainty. *Engineering Applications of Artificial Intelligence*, *117*, 105499. https://doi.org/10.1016/j.engappai.2022.105499

Cho, H. (2020). Climate change risk assessment for Kurunegala, Sri Lanka: Water and heat waves. *Climate*, *8*(12), 140.

Costa, R. L., Barros Gomes, H., Cavalcante Pinto, D. D., da Rocha Júnior, R. L., dos Santos Silva, F. D., Barros Gomes, H., Lemos da Silva, M. C., & Luís Herdies, D. (2021). Gap Filling and Quality Control Applied to Meteorological Variables Measured in the Northeast Region of Brazil. *Atmosphere*, *12*(10), 1278. https://doi.org/10.3390/atmos12101278

Crawford, N. H., & Linsley, R. K. (1966). *Digital Simulation in Hydrology'Stanford Watershed Model 4* (39, p. 210) [Technical Report]. Stanford University, Palo Alto.

Croley II, T. E. (1980). Gamma synthetic hydrographs. *Journal of Hydrology*, *47*(1–2), 41–52.

Cui, D., Liang, S., & Wang, D. (2021). Observed and projected changes in global climate zones based on Köppen climate classification. *Wiley Interdisciplinary Reviews: Climate Change*, *12*(3), e701.

de Carvalho, J. R. P., Almeida Monteiro, J. E. B., Nakai, A. M., & Assad, E. D. (2017). Model for Multiple Imputation to Estimate Daily Rainfall Data and Filling of Faults. *Revista Brasileira de Meteorologia*, *32*(4), 575–583. https://doi.org/10.1590/0102-7786324006

Demuzere, M., Bechtel, B., Middel, A., & Mills, G. (2019). Mapping Europe into local climate zones. *PloS One*, *14*(4), e0214474.

Dewan, A., Hu, K., Kamruzzaman, M., & Uddin, M. R. (2019). Evaluating the spatiotemporal pattern of concentration, aggressiveness and seasonality of precipitation over Bangladesh with time–series Tropical Rainfall Measuring Mission data. In *Extreme Hydroclimatic Events and Multivariate Hazards in a Changing Environment* (pp. 191–219). Elsevier.

Dore, M. H. (2005). Climate change and changes in global precipitation patterns: What do we know? *Environment International*, *31*(8), 1167–1181.

Dudgeon, D. (2000). Large-scale hydrological changes in tropical Asia: Prospects for riverine biodiversity: The construction of large dams will have an impact on the biodiversity of tropical Asian rivers and their associated wetlands. *BioScience*, *50*(9), 793–806.

Dumont, M., Saadi, M., Oudin, L., Lachassagne, P., Nugraha, B., Fadillah, A., Bonjour, J.-L., Muhammad, A., Dörfliger, N., & Plagnes, V. (2022). Assessing rainfall global products reliability for water resource management in a tropical volcanic mountainous catchment. *Journal of Hydrology: Regional Studies*, *40*, 101037.

Elsen, P. R., Saxon, E. C., Simmons, B. A., Ward, M., Williams, B. A., Grantham, H. S., Kark, S., Levin, N., Perez-Hammerle, K.-V., & Reside, A. E. (2022). Accelerated shifts in terrestrial life zones under rapid climate change. *Global Change Biology*, *28*(3), 918–935.

Epting, J., Michel, A., Affolter, A., & Huggenberger, P. (2021). Climate change effects on groundwater recharge and temperatures in Swiss alluvial aquifers. *Journal of Hydrology X*, *11*, 100071.

Eriyagama, N., Smakhtin, V., Chandrapala, L., & Fernando, K. (2010). *Impacts of climate change on water resources and agriculture in Sri Lanka: A review and preliminary vulnerability mapping.*

Esham, M., & Garforth, C. (2013). Climate change and agricultural adaptation in Sri Lanka: A review. *Climate and Development*, *5*(1), 66–76. https://doi.org/10.1080/17565529.2012.762333

Eyring, V., Bony, S., Meehl, G. A., Senior, C. A., Stevens, B., Stouffer, R. J., & Taylor, K. E. (2016). Overview of the Coupled Model Intercomparison Project Phase 6 (CMIP6) experimental design and organization. *Geoscientific Model Development*, *9*(5), 1937–1958. https://doi.org/10.5194/gmd-9-1937-2016

Fagandini, C., Todaro, V., Tanda, M. G., Pereira, J. L., Azevedo, L., & Zanini, A. (2023). Missing Rainfall Daily Data: A Comparison Among Gap-Filling Approaches. *Mathematical Geosciences*. https://doi.org/10.1007/s11004-023-10078-6

Gahlawat, I. N., & Lakra, P. (2020). Global Climate change and its effects. *Integrated Journal of Social Sciences*, *7*(1), 14–23.

Gusain, A., Ghosh, S., & Karmakar, S. (2020). Added value of CMIP6 over CMIP5 models in simulating Indian summer monsoon rainfall. *Atmospheric Research*, *232*, 104680. https://doi.org/10.1016/j.atmosres.2019.104680

Hansen, J., Sato, M., & Ruedy, R. (2022). Global temperature in 2021. *Diponível Em Http://Www. Columbia. Edu/~ Jeh1/Mailings/2022/Temperature2021. 13January2022. Pdf. Acesso Em*, *1*(02).

Hawkins, E., Osborne, T. M., Ho, C. K., & Challinor, A. J. (2013). Calibration and bias correction of climate projections for crop modelling: An idealised case study

over Europe. *Agricultural and Forest Meteorology*, *170*, 19–31. https://doi.org/10.1016/j.agrformet.2012.04.007

Hinge, G., Hamouda, M. A., Long, D., & Mohamed, M. M. (2022). Hydrologic utility of satellite precipitation products in flood prediction: A meta-data analysis and lessons learnt. *Journal of Hydrology*, *612*, 128103.

Houtekamer, P. L., & Mitchell, H. L. (1998). Data assimilation using an ensemble Kalman filter technique. *Monthly Weather Review*, *126*(3), 796–811.

Houtekamer, P. L., & Mitchell, H. L. (2001). A sequential ensemble Kalman filter for atmospheric data assimilation. *Monthly Weather Review*, *129*(1), 123–137.

Imbulana, N., Gunawardana, S., Shrestha, S., & Datta, A. (2018). Projections of Extreme Precipitation Events under Climate Change Scenarios in Mahaweli River Basin of Sri Lanka. *Current Science*, *114*(07), 1495. https://doi.org/10.18520/cs/v114/i07/1495-1509

IPCC. (2022). Summary for Policymakers. In P. R. Shukla, J. Skea, R. Slade, A. A. Khourdajie, R. van Diemen, D. McCollum, M. Pathak, S. Some, P. Vyas, R. Fradera, M. Belkacemi, A. Hasija, G. Lisboa, S. Luz, & J. Malley (Eds.), *Climate Change 2022: Mitigation of Climate Change. Contribution of Working Group III to the Sixth Assessment Report of the Intergovernmental Panel on Climate Change*. Cambridge University Press. https://doi.org/10.1017/9781009157926.001

Jacob, D., Teichmann, C., Sobolowski, S., Katragkou, E., Anders, I., Belda, M., Benestad, R., Boberg, F., Buonomo, E., & Cardoso, R. M. (2020). Regional climate downscaling over Europe: Perspectives from the EURO-CORDEX community. *Regional Environmental Change*, *20*, 1–20.

Jose, D. M., & Dwarakish, G. S. (2020). Uncertainties in predicting impacts of climate change on hydrology in basin scale: A review. *Arabian Journal of Geosciences*, *13*(19), 1037.

Kashiwa, S., & Kazama, S. (2010). Flood analysis Modeling of snow melting and Estimation. *Proceedings of the Rivers Technology*, *16*.

Kaushik, S., Dharpure, J. K., Joshi, P. K., Ramanathan, A., & Singh, T. (2020). Climate change drives glacier retreat in Bhaga basin located in Himachal Pradesh, India. *Geocarto International*, *35*(11), 1179–1198. https://doi.org/10.1080/10106049.2018.1557260

Kazama, S. (2004). Uncertainty of morphological data for rainfall-runoff simulation. *Proceedings of the International Conference on Sustainable Water Resources Management in the Changing Environment of the Monsoon Region 1*, 400–406.

Kendon, E. J., Prein, A. F., Senior, C. A., & Stirling, A. (2021). Challenges and outlook for convection-permitting climate modelling. *Philosophical Transactions of the Royal Society A*, *379*(2195), 20190547.

Keshavarz Ghorabaee, M., Zavadskas, E. K., Olfat, L., & Turskis, Z. (2015). Multi-Criteria Inventory Classification Using a New Method of Evaluation Based on Distance from Average Solution (EDAS). *Informatica*, *26*(3), 435–451. https://doi.org/10.15388/Informatica.2015.57

Khaniya, B., Gunathilake, M. B., & Rathnayake, U. (2021). Ecosystem-Based Adaptation for the Impact of Climate Change and Variation in the Water Management Sector of Sri Lanka. *Mathematical Problems in Engineering*, *2021*, 1–10. https://doi.org/10.1155/2021/8821329

Kim, S.-K., Shin, J., An, S.-I., Kim, H.-J., Im, N., Xie, S.-P., Kug, J.-S., & Yeh, S.-W. (2022). Widespread irreversible changes in surface temperature and precipitation in response to CO2 forcing. *Nature Climate Change*, *12*(9), 834–840.

Köppen, W. (1936). Das System der Klimaten. *Geographische Zeitschrift*, *42*(3), 243–284. https://doi.org/10.1002/1525-139X(193604)18:3<243::AID-ANGEO193604031>3.0.CO;2-8

Köppen, W. P. (1931). *Grundriss der klimakunde*. W. de Gruyter.

Krishnan, R., Shrestha, A. B., Ren, G., Rajbhandari, R., Saeed, S., Sanjay, J., Syed, M. A., Vellore, R., Xu, Y., & You, Q. (2019). Unravelling climate change in the Hindu Kush Himalaya: Rapid warming in the mountains and increasing extremes. *The Hindu Kush Himalaya Assessment: Mountains, Climate Change, Sustainability and People*, 57–97.

Kumar, A., Nagar, S., & Anand, S. (2021). Climate change and existential threats. In *Global Climate Change* (pp. 1–31). Elsevier. https://doi.org/10.1016/B978-0-12-822928-6.00005-8

Kumar, P., Folk, M., Markus, M., & Alameda, J. C. (2005). *Hydroinformatics: Data integrative approaches in computation, analysis, and modeling*. CRC Press.

Laignel, B., Vignudelli, S., Almar, R., Becker, M., Bentamy, A., Benveniste, J., Birol, F., Frappart, F., Idier, D., & Salameh, E. (2023). Observation of the coastal areas, estuaries and deltas from space. *Surveys in Geophysics*, 1–48.

Lemma, E., Upadhyaya, S., & Ramsankaran, R. (2022). Meteorological drought monitoring across the main river basins of Ethiopia using satellite rainfall product. *Environmental Systems Research*, *11*(1), 1–15.

Linacre, E. T. (1977). A simple formula for estimating evaporation rates in various climates, using temperature data alone. *Agricultural Meteorology*, *18*(6), 409–424. https://doi.org/10.1016/0002-1571(77)90007-3

Liu, Y., Yu, K., Zhao, Y., & Bao, J. (2022). Impacts of Climatic Variation and Human Activity on Runoff in Western China. *Sustainability*, *14*(2), 942. https://doi.org/10.3390/su14020942

Maher, N., Milinski, S., & Ludwig, R. (2021). Large ensemble climate model simulations: Introduction, overview, and future prospects for utilising multiple types of large ensemble. *Earth System Dynamics*, *12*(2), 401–418.

Mahlstein, I., Daniel, J. S., & Solomon, S. (2013). Pace of shifts in climate regions increases with global temperature. *Nature Climate Change*, *3*(8), 739–743. https://doi.org/10.1038/nclimate1876

Maidment, D. R. (2005). A data model for hydrologic observations. *Presentation at the CUAHSI Hydrologic Information Systems Symposium, University of Texas at Austin*.

Maji, S., Ahmed, S., & Ghosh, S. (2022). Source Apportionment of Greenhouse Gases in the Atmosphere. In S. Sonwani & P. Saxena (Eds.), *Greenhouse Gases: Sources, Sinks and Mitigation* (pp. 9–37). Springer Nature Singapore. https://doi.org/10.1007/978-981-16-4482-5_2

Malone, A. G. O. (2023). Quantifying Who Will Be Affected by Shifting Climate Zones. *Geographies*, *3*(3), 477–498. https://doi.org/10.3390/geographies3030025

Masson, V., Lemonsu, A., Hidalgo, J., & Voogt, J. (2020). Urban climates and climate change. *Annual Review of Environment and Resources*, *45*, 411–444.

Mazumdar, S., Begley, A. E., Houck, P. R., Yang, Y., Reynolds, C. F., & Kupfer, D. J. (1999). Residual analysis in random regressions using SAS and S-PLUS. *Computer Methods and Programs in Biomedicine*, *58*(3), 281–282. https://doi.org/10.1016/S0169-2607(98)00091-1

Meegahakotuwa, U. S., & Nianthi, K. (2018). *Spatial and Temporal Variation of Temperature Trends in Last Century of Sri Lanka*.

Meehl, G. A., Boer, G. J., Covey, C., Latif, M., & Stouffer, R. J. (2000). The Coupled Model Intercomparison Project (CMIP). *Bulletin of the American Meteorological Society*, *81*(2), 313–318. https://doi.org/10.1175/1520-0477(2000)081<0313:TCMIPC>2.3.CO;2

Mensah, J. K., Ofosu, E. A., Yidana, S. M., Akpoti, K., & Kabo-bah, A. T. (2022). Integrated modeling of hydrological processes and groundwater recharge based on land use land cover, and climate changes: A systematic review. *Environmental Advances*, *8*, 100224.

Mikhaylov, A., Moiseev, N., Aleshin, K., & Burkhardt, T. (2020). Global climate change and greenhouse effect. *Entrepreneurship and Sustainability Issues*, *7*(4), 2897.

Mishra, A. R., Rani, P., & Pandey, K. (2022). Fermatean fuzzy CRITIC-EDAS approach for the selection of sustainable third-party reverse logistics providers using improved generalized score function. *Journal of Ambient Intelligence and Humanized Computing*, *13*(1), 295–311. https://doi.org/10.1007/s12652-021-02902-w

Mohandas, S. (2022). Weather and Climate Modeling. In *Social and Economic Impact of Earth Sciences* (pp. 121–141). Springer.

Mondal, S. K., Huang, J., Wang, Y., Su, B., Zhai, J., Tao, H., Wang, G., Fischer, T., Wen, S., & Jiang, T. (2021). Doubling of the population exposed to drought

over South Asia: CMIP6 multi-model-based analysis. *Science of The Total Environment*, *771*, 145186. https://doi.org/10.1016/j.scitotenv.2021.145186

Moore, C., & Doherty, J. (2005). Role of the calibration process in reducing model predictive error. *Water Resources Research*, *41*(5), 2004WR003501. https://doi.org/10.1029/2004WR003501

Mpelasoka, F. S., & Chiew, F. H. (2009). Influence of rainfall scenario construction methods on runoff projections. *Journal of Hydrometeorology*, *10*(5), 1168–1183.

Mulvany, T. J. (1851). On the use of self-registering rain and flood gauges in making observations of the relations of rain fall and of flood discharges in a given catchment. *Proceedings of the Institution of Civil Engineers of Ireland*, *4*, 18–33.

Naveendrakumar, G., Vithanage, M., Kwon, H.-H., Chandrasekara, S. S. K., Iqbal, M. C. M., Pathmarajah, S., Fernando, W., & Obeysekera, J. (2019). South Asian perspective on temperature and rainfall extremes: A review. *Atmospheric Research*, *225*, 110–120.

Naveendrakumar, G., Vithanage, M., Kwon, H.-H., Iqbal, M. C. M., Pathmarajah, S., & Obeysekera, J. (2018). Five Decadal Trends in Averages and Extremes of Rainfall and Temperature in Sri Lanka. *Advances in Meteorology*, *2018*, 1–13. https://doi.org/10.1155/2018/4217917

Noor, M., Rehman, N. ur, Jalil, A., Fahad, S., Adnan, M., Wahid, F., Saud, S., & Hassan, S. (2020). Climate change and costal plant lives. *Environment, Climate, Plant and Vegetation Growth*, 93–108.

Oliver, M. A., & Webster, R. (1990). Kriging: A method of interpolation for geographical information systems. *International Journal of Geographical Information System*, *4*(3), 313–332.

Orellana, B., Pechlivanidis, I. G., McIntyre, N., Wheater, H. S., & Wagener, T. (2008). *A toolbox for the identification of parsimonious semi-distributed rainfall-runoff models: Application to the Upper Lee catchment*.

Panabokke, C. R. (1996). *Soils and Agro-ecological Environments of Sri Lanka*. Natural Resources, Energy & Science Authority. https://books.google.lk/books?id=R8FxAAAACAAJ

Pandi, D., Kothandaraman, S., & Kuppusamy, M. (2021). Hydrological models: A review. *International Journal of Hydrology Science and Technology*, *12*(3), 223. https://doi.org/10.1504/IJHST.2021.117540

Papailiou, I., Spyropoulos, F., Trichakis, I., & Karatzas, G. P. (2022). Artificial Neural Networks and Multiple Linear Regression for Filling in Missing Daily Rainfall Data. *Water*, *14*(18), 2892. https://doi.org/10.3390/w14182892

Peel, M. C., Finlayson, B. L., & McMahon, T. A. (2007). Updated world map of the Köppen-Geiger climate classification. *Hydrology and Earth System Sciences*, *11*(5), 1633–1644.

Perez, R., Lorenz, E., Pelland, S., Beauharnois, M., Van Knowe, G., Hemker Jr, K., Heinemann, D., Remund, J., Müller, S. C., & Traunmüller, W. (2013). Comparison of numerical weather prediction solar irradiance forecasts in the US, Canada and Europe. *Solar Energy*, *94*, 305–326.

Phan, P. T., & Nguyen, P. T. (2022). Evaluation Based on the Distance from the Average Solution Approach: A Derivative Model for Evaluating and Selecting a Construction Manager. *Technologies*, *10*(5), 107. https://doi.org/10.3390/technologies10050107

Prudhomme, C., Reynard, N., & Crooks, S. (2002). Downscaling of global climate models for flood frequency analysis: Where are we now? *Hydrological Processes*, *16*(6), 1137–1150.

Raihan, A. (2023). A review of the global climate change impacts, adaptation strategies, and mitigation options in the socio-economic and environmental sectors. *Journal of Environmental Science and Economics*, *2*(3), 36–58.

Roshan, G., Moghbel, M., & Taleghani, M. (2022). Spatial analysis of bioclimatic patterns over Iranian cities as an important step in sustainable development. *Sustainable Cities and Society*, *83*, 103939.

RStudio Team. (2020). *RStudio: Integrated Development Environment for R*. RStudio, PBC. http://www.rstudio.com/

Rubin, D. B. (1996). Multiple imputation after 18+ years. *Journal of the American Statistical Association*, *91*(434), 473–489.

Rupp, D. E., Abatzoglou, J. T., Hegewisch, K. C., & Mote, P. W. (2013). Evaluation of CMIP5 20 th century climate simulations for the Pacific Northwest USA: CMIP5 20TH CENTURY CLIMATE OF THE PNW. *Journal of Geophysical Research: Atmospheres*, *118*(19), 10,884-10,906. https://doi.org/10.1002/jgrd.50843

Sadoff, C., & Muller, M. (2009). *Water management, water security and climate change adaptation: Early impacts and essential responses*. Global Water Partnership Stockholm.

Salimian, N., Nazari, S., & Ahmadi, A. (2021). Assessment of the uncertainties of global climate models in the evaluation of standardized precipitation and runoff indices: A case study. *Hydrological Sciences Journal*, *66*(9), 1419–1436. https://doi.org/10.1080/02626667.2021.1937178

Santos, J. A., Fraga, H., Malheiro, A. C., Moutinho-Pereira, J., Dinis, L.-T., Correia, C., Moriondo, M., Leolini, L., Dibari, C., & Costafreda-Aumedes, S. (2020). A review of the potential climate change impacts and adaptation options for European viticulture. *Applied Sciences*, *10*(9), 3092.

Schmidli, J., Frei, C., & Vidale, P. L. (2006). Downscaling from GCM precipitation: A benchmark for dynamical and statistical downscaling methods. *International Journal of Climatology*, *26*(5), 679–689. https://doi.org/10.1002/joc.1287

Sen, Z. (2009). *Fuzzy logic and hydrological modeling*. CRC Press.

Siddha, S., & Sahu, P. (2022). Impact of climate change on the river ecosystem. In *Ecological Significance of River Ecosystems* (pp. 79–104). Elsevier.

Singh, V. P. (Ed.). (1995). *Computer models of watershed hydrology* (Rev. ed). Water Resources Publications.

Singh, V. P. (2018). Hydrologic modeling: Progress and future directions. *Geoscience Letters*, *5*(1), 15. https://doi.org/10.1186/s40562-018-0113-z

Stringer, L. C., Mirzabaev, A., Benjaminsen, T. A., Harris, R. M., Jafari, M., Lissner, T. K., Stevens, N., & Tirado-von Der Pahlen, C. (2021). Climate change impacts on water security in global drylands. *One Earth*, *4*(6), 851–864.

Tabari, H. (2020). Climate change impact on flood and extreme precipitation increases with water availability. *Scientific Reports*, *10*(1), 13768. https://doi.org/10.1038/s41598-020-70816-2

Tayfur, G. (2014). *Soft computing in water resources engineering: Artificial neural networks, fuzzy logic and genetic algorithms*. WIT Press.

Taylor, K. E. (2001). Summarizing multiple aspects of model performance in a single diagram. *Journal of Geophysical Research: Atmospheres*, *106*(D7), 7183–7192. https://doi.org/10.1029/2000JD900719

Thornthwaite, C. W. (1948). An approach toward a rational classification of climate. *Geographical Review*, *38*(1), 55–94.

Thrasher, B., Maurer, E. P., McKellar, C., & Duffy, P. B. (2012). Bias correcting climate model simulated daily temperature extremes with quantile mapping. *Hydrology and Earth System Sciences*, *16*(9), 3309–3314.

Turrado, C., López, M., Lasheras, F., Gómez, B., Rollé, J., & Juez, F. (2014). Missing Data Imputation of Solar Radiation Data under Different Atmospheric Conditions. *Sensors*, *14*(11), 20382–20399. https://doi.org/10.3390/s141120382

Upadhyay, R. K. (2020). Markers for global climate change and its impact on social, biological and ecological systems: A review. *American Journal of Climate Change*, *9*(03), 159.

Visweshwaran, R., Ramsankaran, R., Eldho, T. I., & Jha, M. K. (2022). Hydrological Impact Assessment of Future Climate Change on a Complex River Basin of Western Ghats, India. *Water*, *14*(21), 3571. https://doi.org/10.3390/w14213571

Wagener, T., Wheater, H., & Gupta, H. V. (2004). *Rainfall-runoff modelling in gauged and ungauged catchments*. Imperial College Press ; Distributed by World Scientific.

Wang, H.-M., Chen, J., Xu, C.-Y., Zhang, J., & Chen, H. (2020). A framework to quantify the uncertainty contribution of GCMs over multiple sources in hydrological impacts of climate change. *Earth's Future*, *8*(8), e2020EF001602.

Wesonga, R. (2015). On multivariate imputation and forecasting of decadal wind speed missing data. *SpringerPlus*, *4*(1), 12. https://doi.org/10.1186/s40064-014-0774-9

Wheater, H. S. (2002). Progress in and prospects for fluvial flood modelling. *Philosophical Transactions of the Royal Society of London. Series A: Mathematical, Physical and Engineering Sciences*, *360*(1796), 1409–1431.

Wilcock, A. A. (1968). Köppen after fifty years. *Annals of the Association of American Geographers*, *58*(1), 12–28.

Wood, A. W., Leung, L. R., Sridhar, V., & Lettenmaier, D. P. (2004). Hydrologic implications of dynamical and statistical approaches to downscaling climate model outputs. *Climatic Change*, *62*(1–3), 189–216.

Worku, G., Teferi, E., Bantider, A., & Dile, Y. T. (2019). Observed changes in extremes of daily rainfall and temperature in Jemma Sub-Basin, Upper Blue Nile Basin, Ethiopia. *Theoretical and Applied Climatology*, *135*, 839–854.

Worku, G., Teferi, E., Bantider, A., & Dile, Y. T. (2020). Statistical bias correction of regional climate model simulations for climate change projection in the Jemma sub-basin, upper Blue Nile Basin of Ethiopia. *Theoretical and Applied Climatology*, *139*, 1569–1588.

Yang, D., Yang, Y., & Xia, J. (2021). Hydrological cycle and water resources in a changing world: A review. *Geography and Sustainability*, *2*(2), 115–122.

APPENDICES

Appendix A: Stripplots of imputed datasets with PMM and Norm method

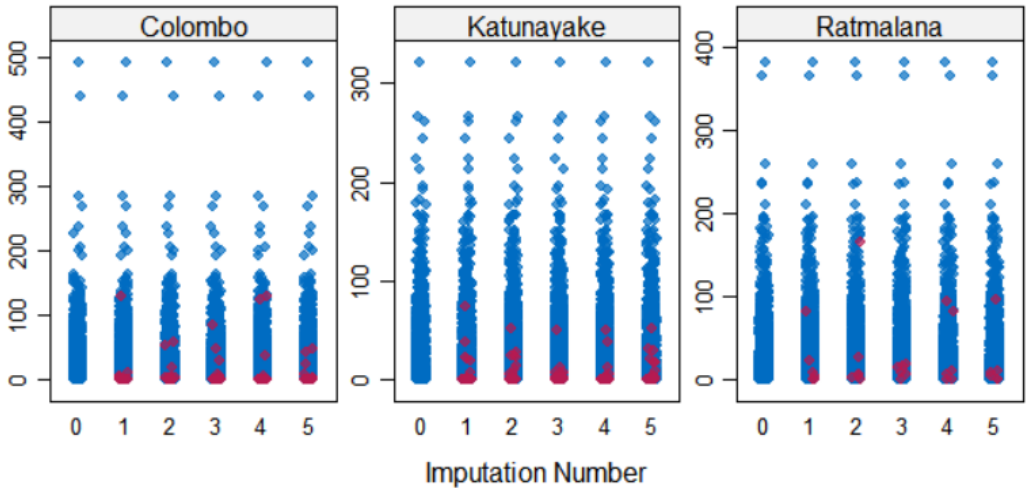

Appendix A-1 Strip plot of Wet Zone-1 in the original data and the five imputed data sets (PMM method)

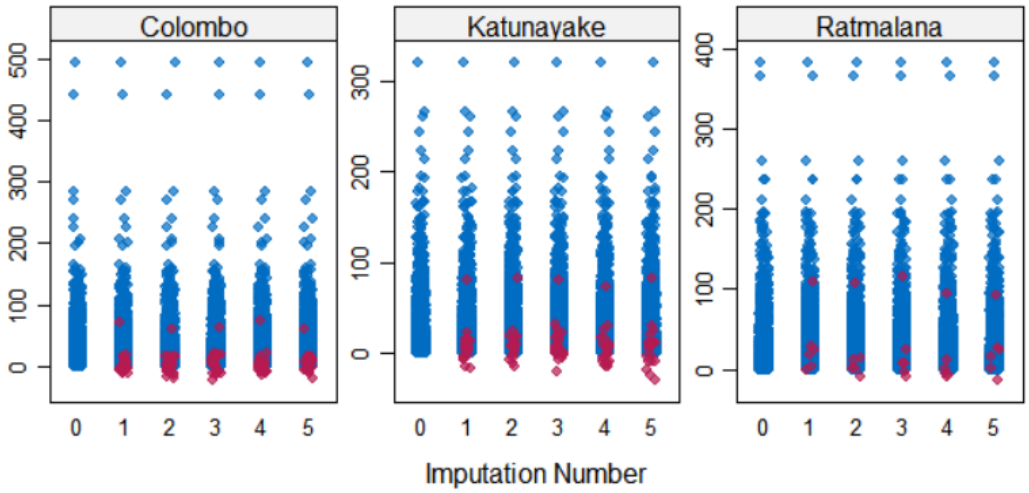

Appendix A-2 Strip plot of Wet Zone-1 in the original data and the five imputed data sets (Norm method)

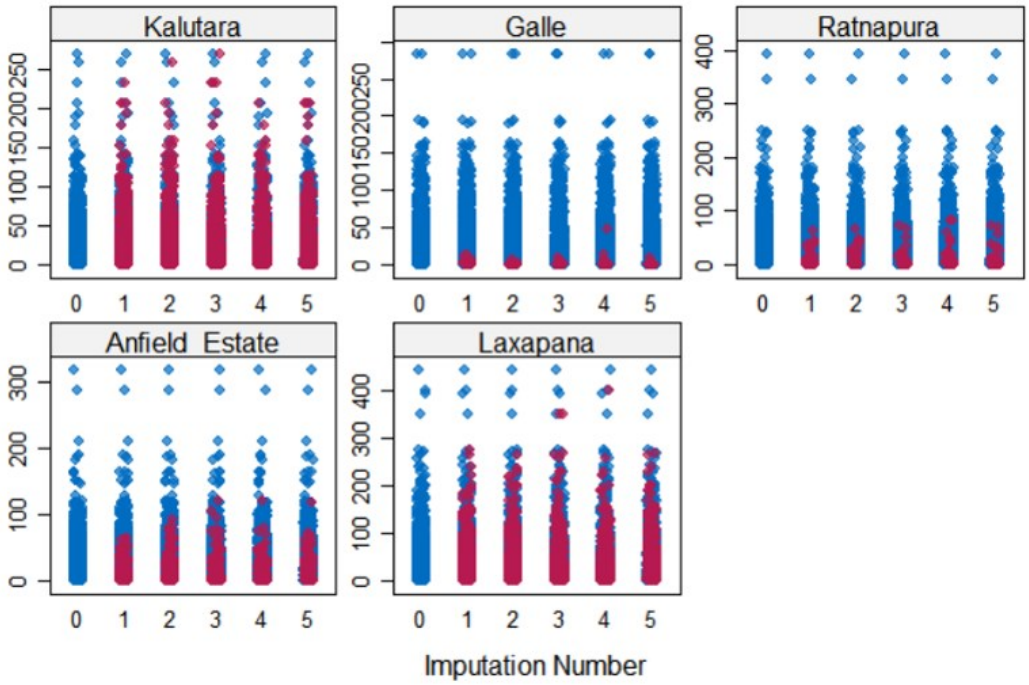

Appendix A-3 Strip plot of Wet Zone-2 in the original data and the five imputed data sets (PMM method)

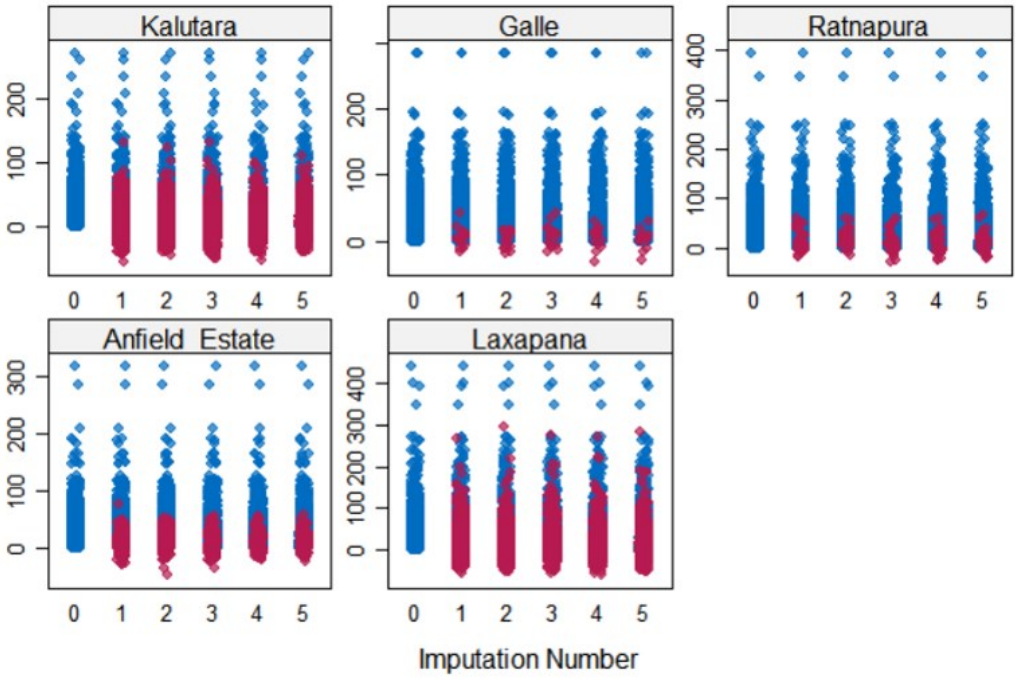

Appendix A-4 Strip plot of Wet Zone-2 in the original data and the five imputed data sets (Norm method)

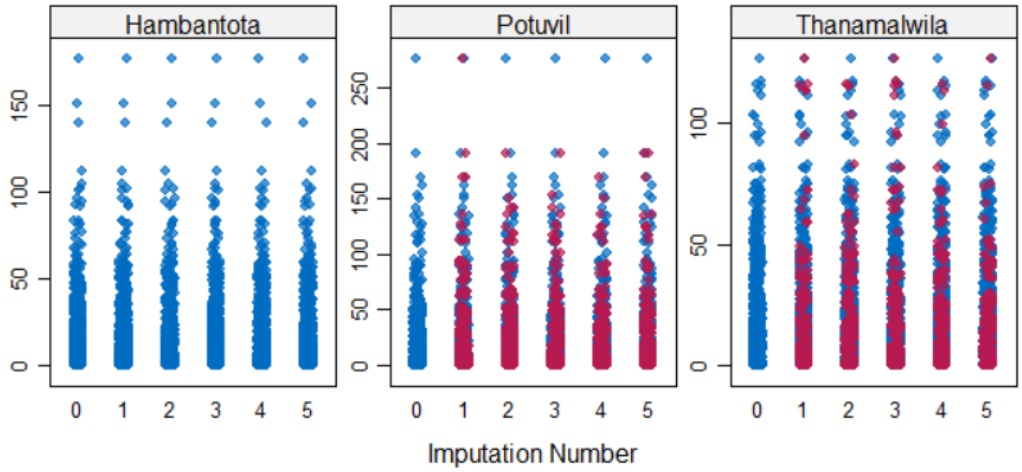

Appendix A-5 Strip plot of South in the original data and the five imputed data sets (PMM method)

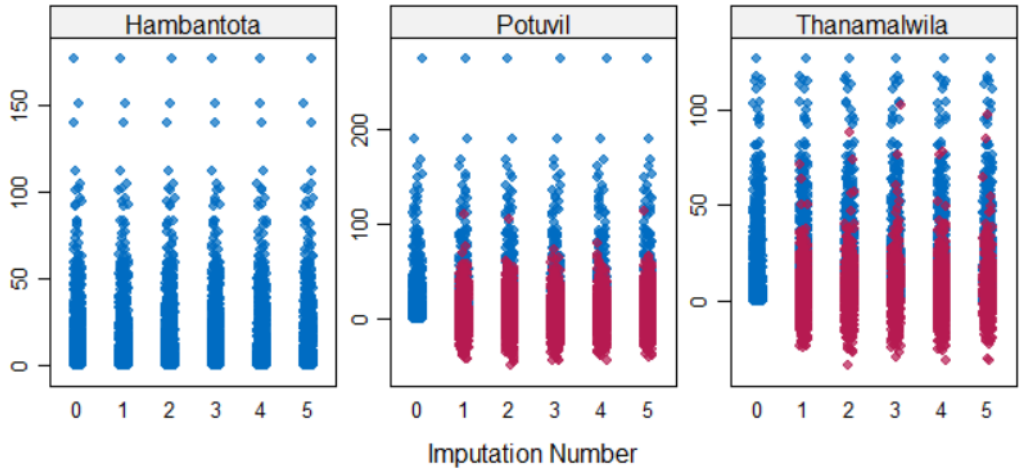

Appendix A-6 Strip plot of South in the original data and the five imputed data sets (Norm method)

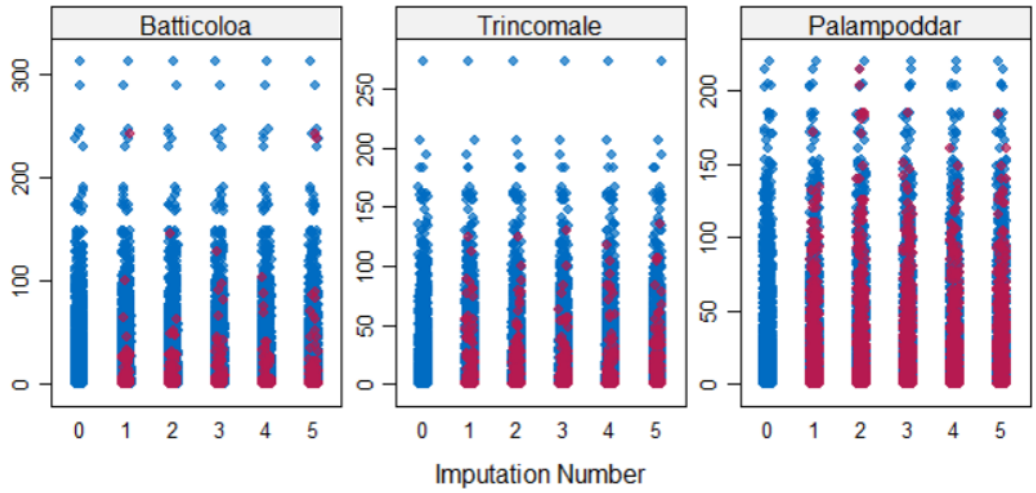

Appendix A-7 Strip plot of East in the original data and the five imputed data sets (PMM method)

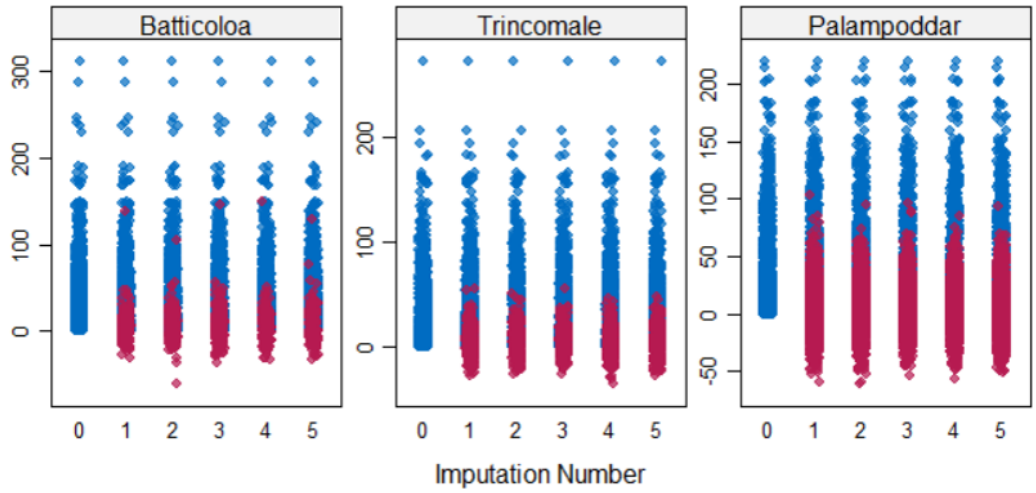

Appendix A-8 Strip plot of East in the original data and the five imputed data sets (Norm method)

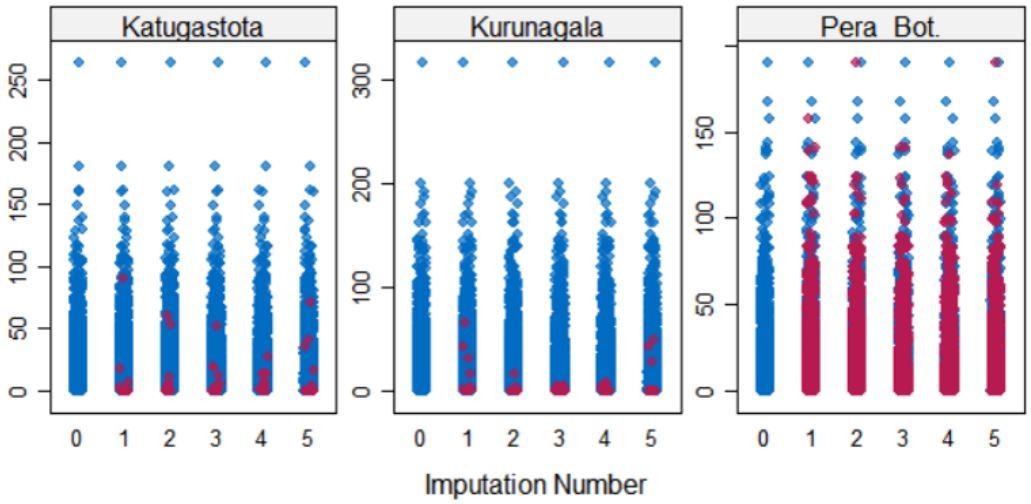

Appendix A-9 Strip plot of Central-1 in the original data and the five imputed data sets (PMM method)

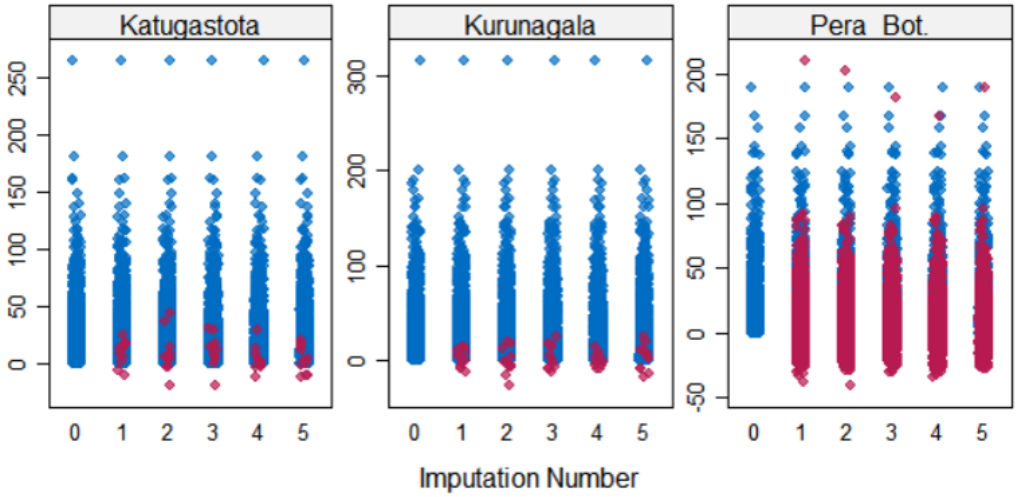

Appendix A-10 Strip plot of Central-1 in the original data and the five imputed data sets (Norm method)

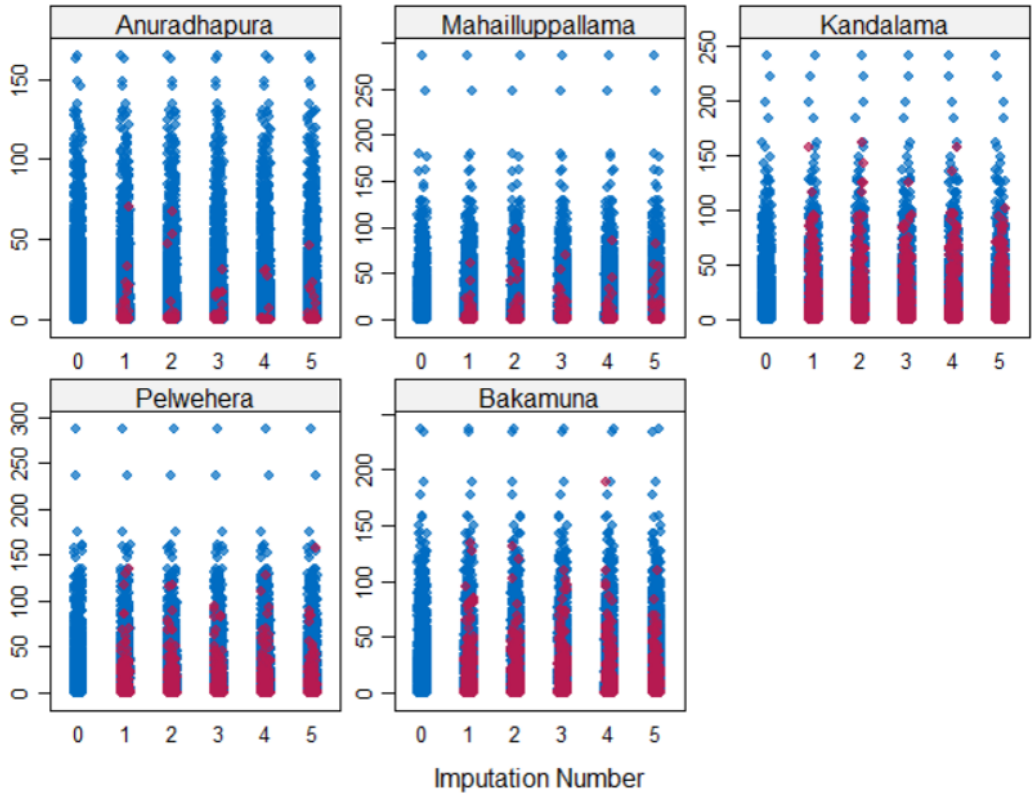

Appendix A-11 Strip plot of North Central in the original data and the five imputed data sets (PMM method)

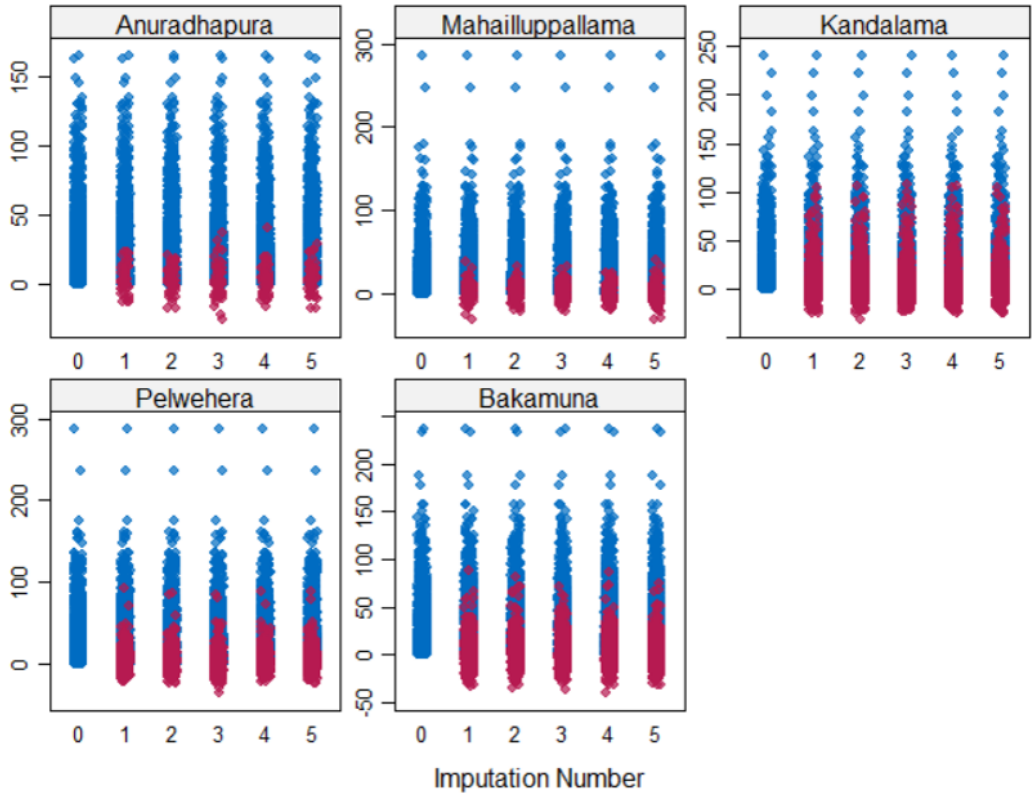

Appendix A-12 Strip plot of North Central in the original data and the five imputed data sets (Norm method)

Appendix B: Double Mass Curve for the data imputation groups

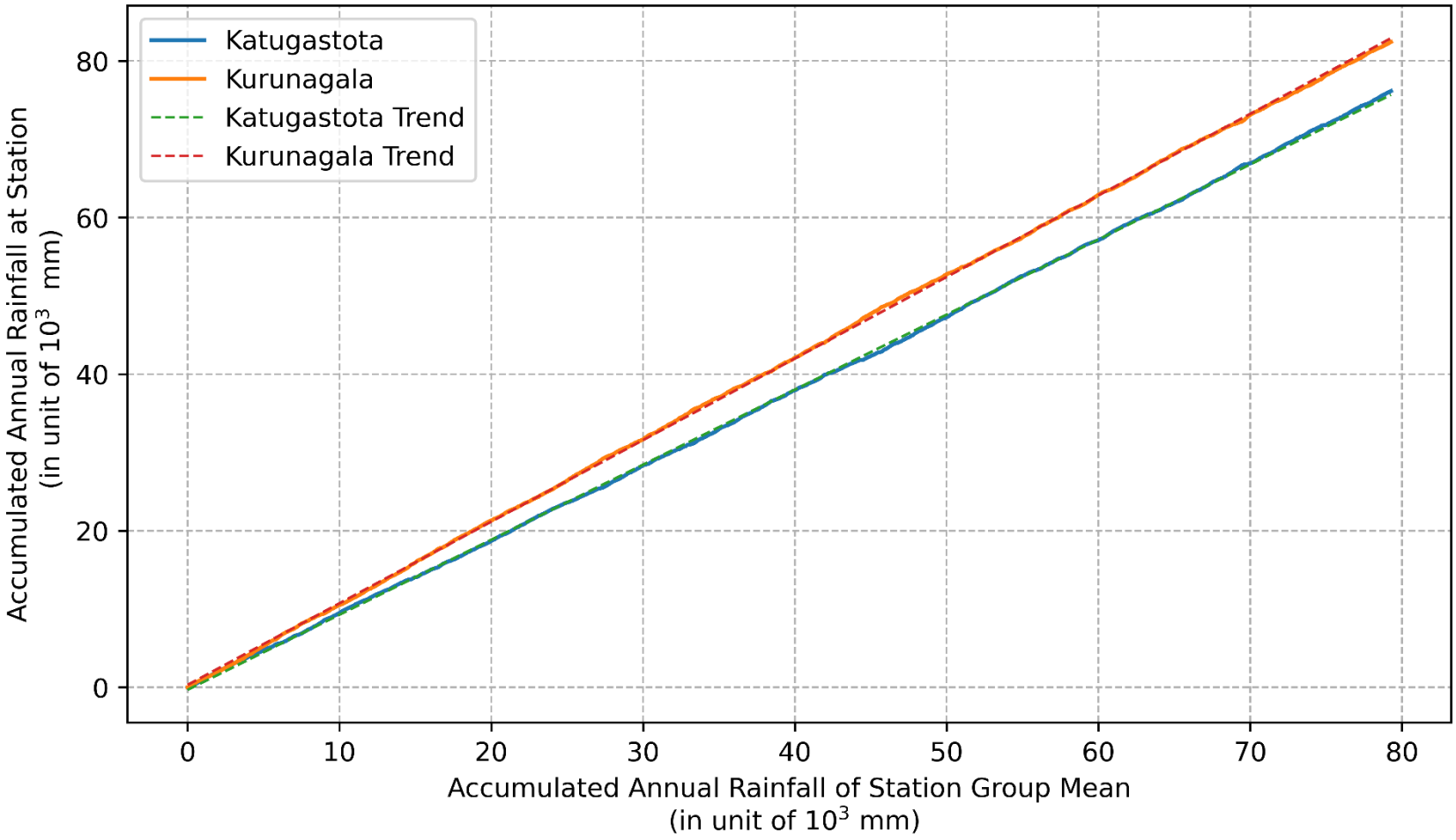
Katugastota
Kurunagala
Katugastota Trend
Kurunagala Trend
Accumulated Annual Rainfall at Station
(in unit of 10^3 mm)
0
20
40
60
80
0
10
20
30
40
50
60
70
80
Accumulated Annual Rainfall of Station Group Mean
(in unit of 10^3 mm)

3

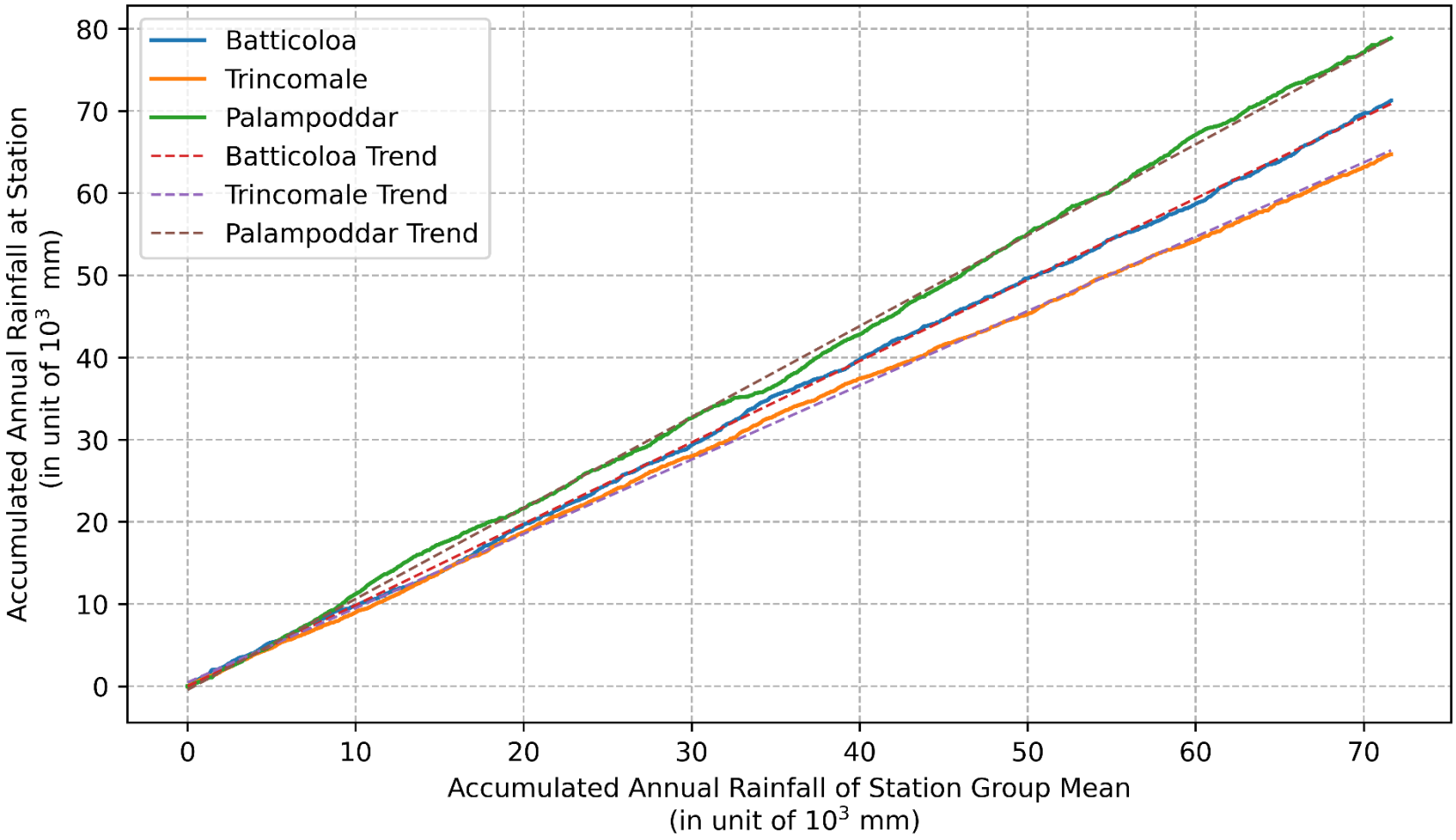
Batticoloa
Trincomale
Palampoddar
Batticoloa Trend
Trincomale Trend
Palampoddar Trend
Accumulated Annual Rainfall at Station
(in unit of 10^3 mm)
Accumulated Annual Rainfall of Station Group Mean
(in unit of 10^3 mm)
0
10
20
30
40
50
60
70
80

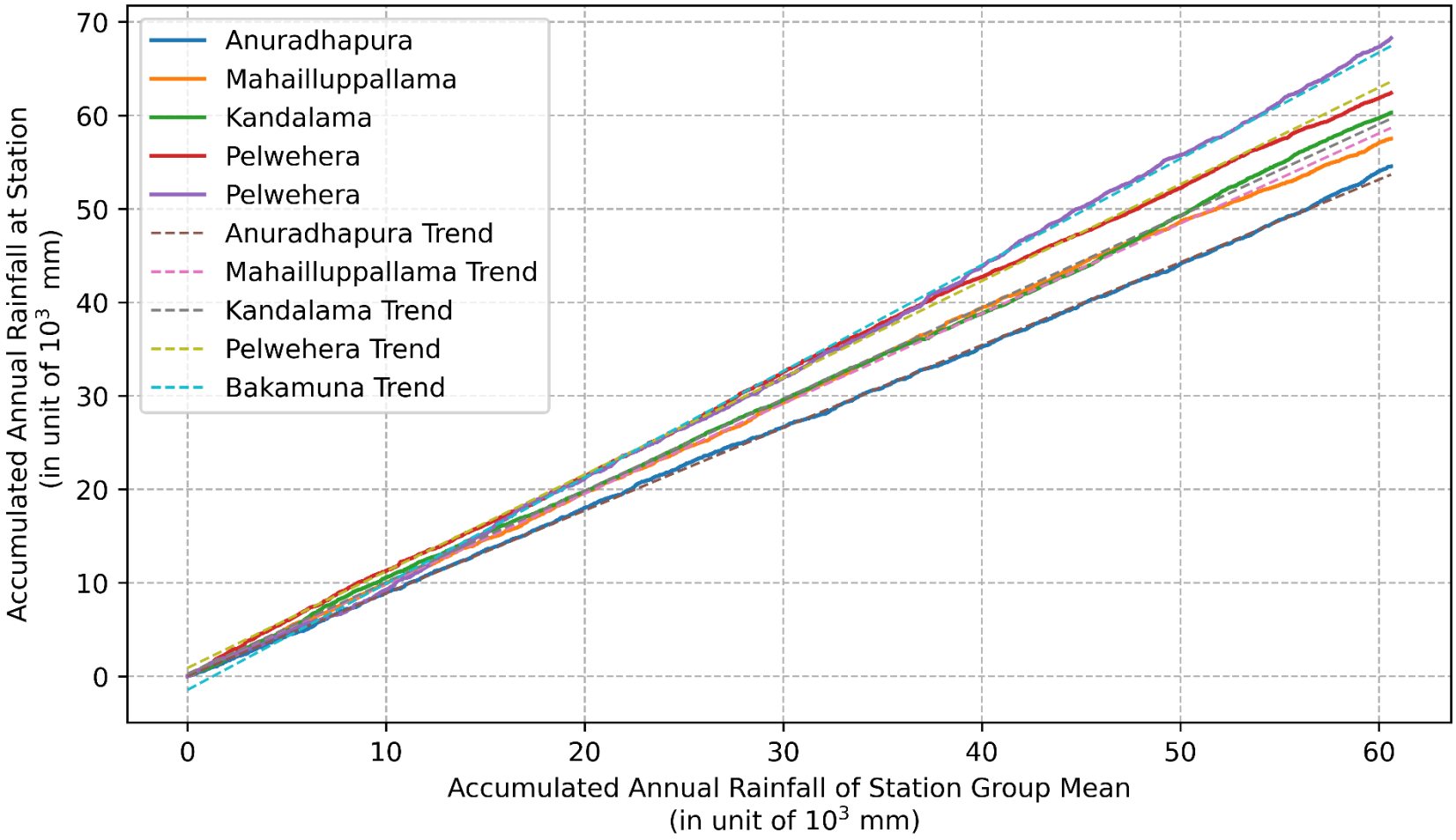
Anuradhapura
Mahailluppallama
Kandalama
Pelwehera
Pelwehera
Anuradhapura Trend
Mahailluppallama Trend
Kandalama Trend
Pelwehera Trend
Bakamuna Trend
Accumulated Annual Rainfall at Station
(in unit of 10^3 mm)
Accumulated Annual Rainfall of Station Group Mean
(in unit of 10^3 mm)
0
10
20
30
40
50
60
70

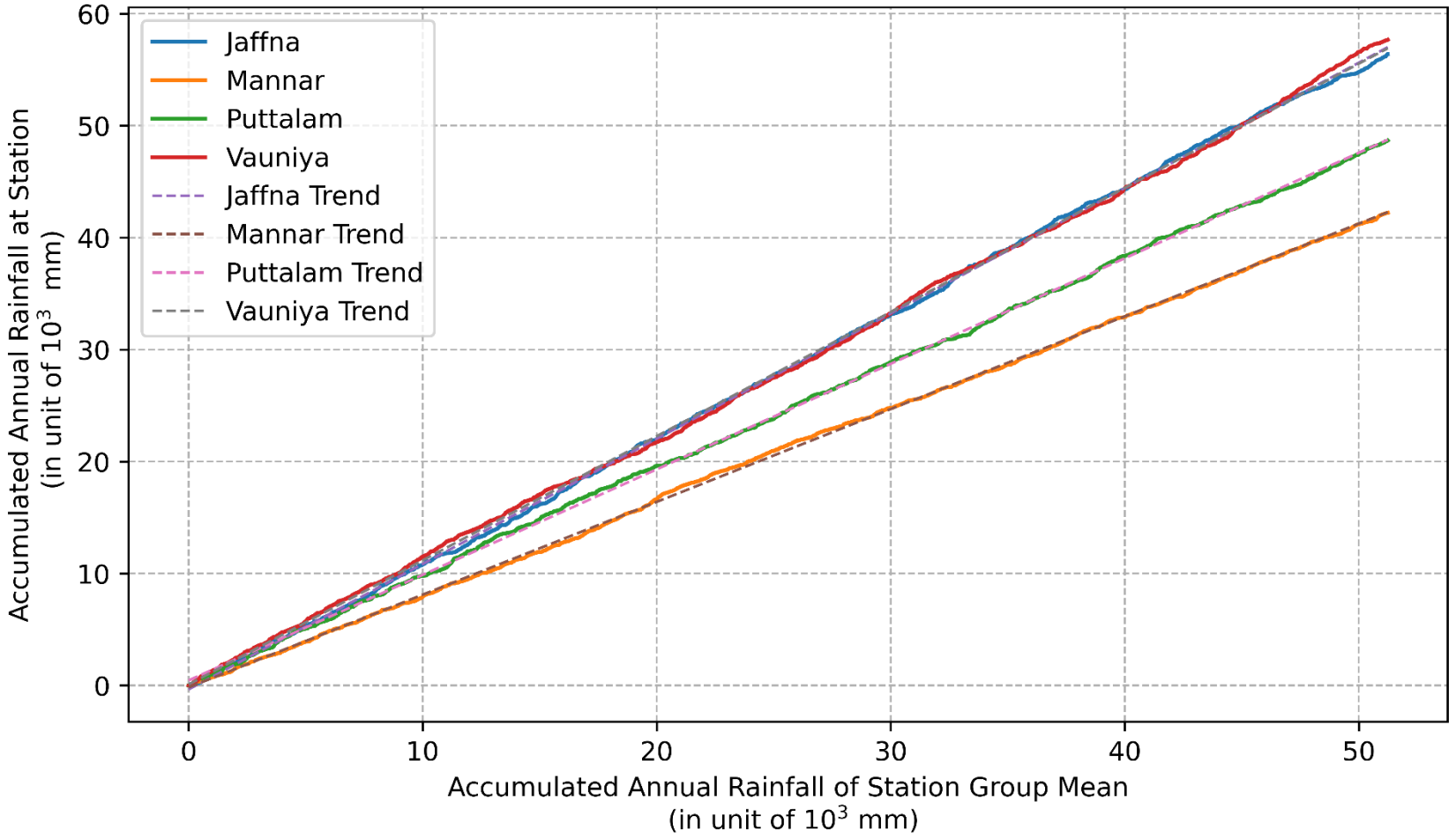
Jaffna
Mannar
Puttalam
Vauniya
Jaffna Trend
Mannar Trend
Puttalam Trend
Vauniya Trend
Accumulated Annual Rainfall at Station
(in unit of 10^3 mm)
Accumulated Annual Rainfall of Station Group Mean
(in unit of 10^3 mm)
0
10
20
30
40
50
60

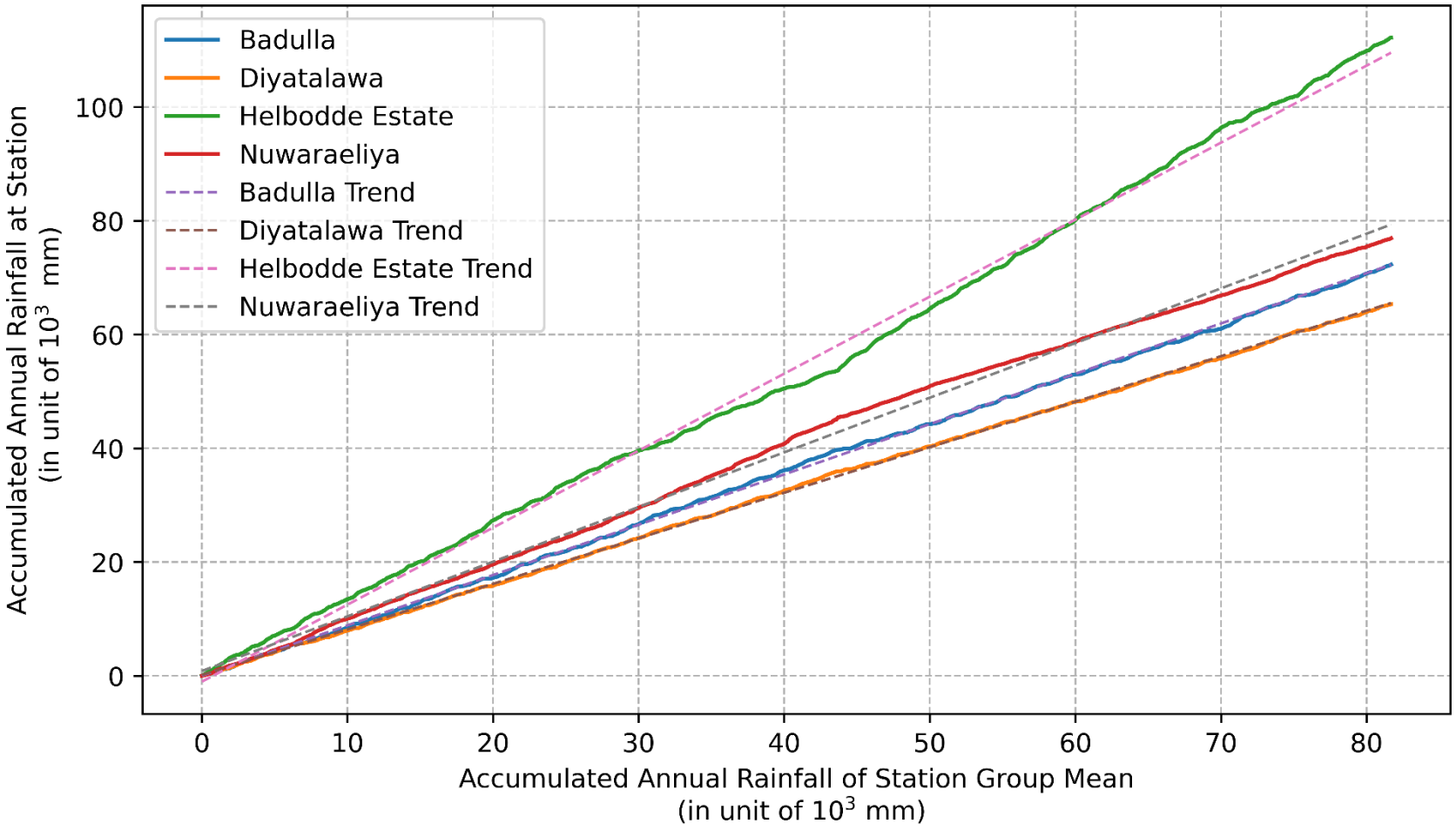
Badulla
Diyatalawa
Helbodde Estate
Nuwaraeliya
Badulla Trend
Diyatalawa Trend
Helbodde Estate Trend
Nuwaraeliya Trend
Accumulated Annual Rainfall at Station
(in unit of 10^3 mm)
Accumulated Annual Rainfall of Station Group Mean
(in unit of 10^3 mm)
0
20
40
60
80
100
0
10
20
30
40
50
60
70
80

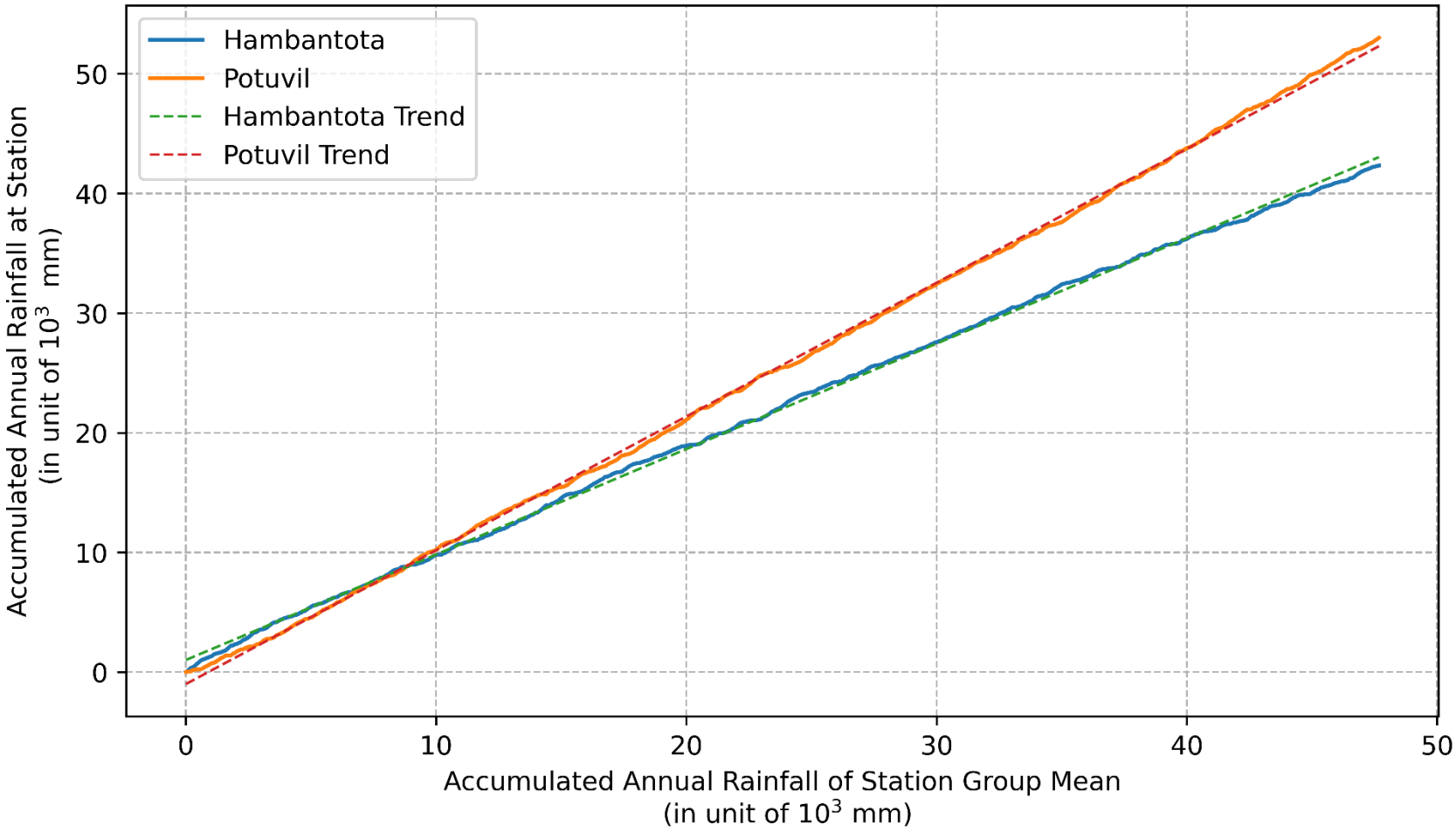
Hambantota
Potuvil
Hambantota Trend
Potuvil Trend
Accumulated Annual Rainfall at Station
(in unit of 10^3 mm)
Accumulated Annual Rainfall of Station Group Mean
(in unit of 10^3 mm)
0
10
20
30
40
50

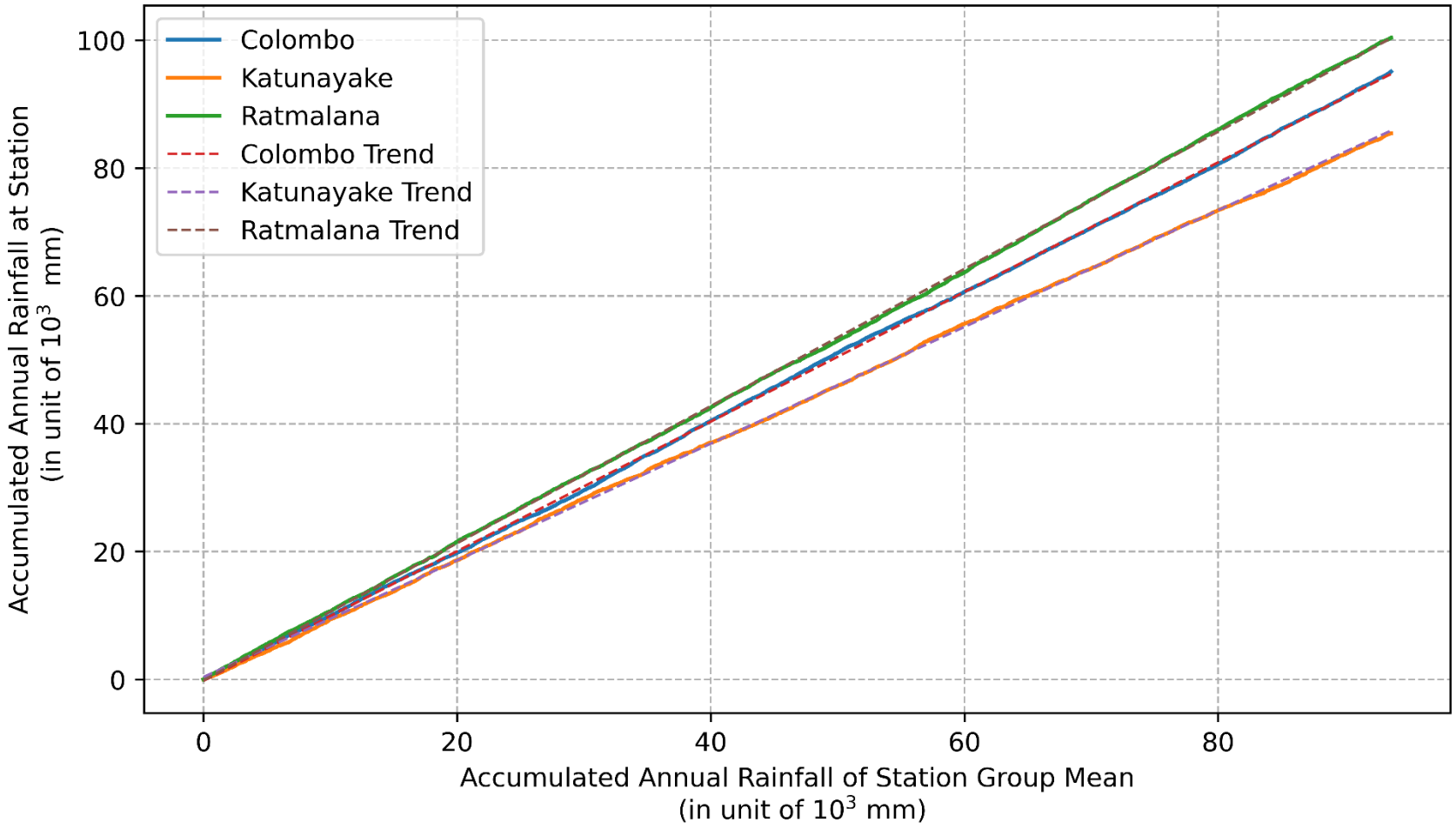
Colombo
Katunayake
Ratmalana
Colombo Trend
Katunayake Trend
Ratmalana Trend
Accumulated Annual Rainfall at Station
(in unit of 10^3 mm)
Accumulated Annual Rainfall of Station Group Mean
(in unit of 10^3 mm)
0
20
40
60
80
100

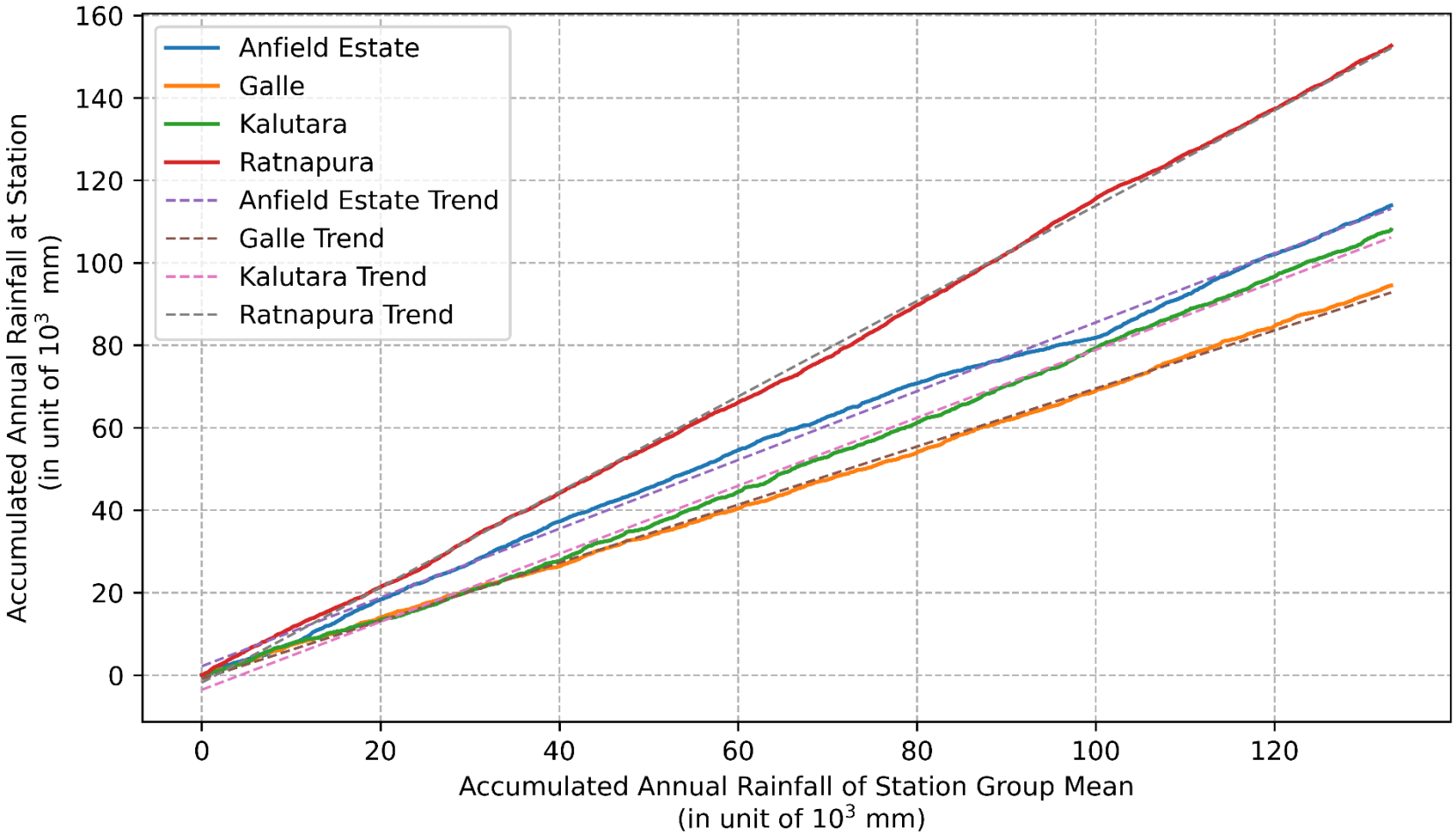
Anfield Estate
Galle
Kalutara
Ratnapura
Anfield Estate Trend
Galle Trend
Kalutara Trend
Ratnapura Trend
Accumulated Annual Rainfall at Station
(in unit of 10^3 mm)
Accumulated Annual Rainfall of Station Group Mean
(in unit of 10^3 mm)
0
20
40
60
80
100
120
140
160

Appendix C: Observed vs model monthly normalized precipitation

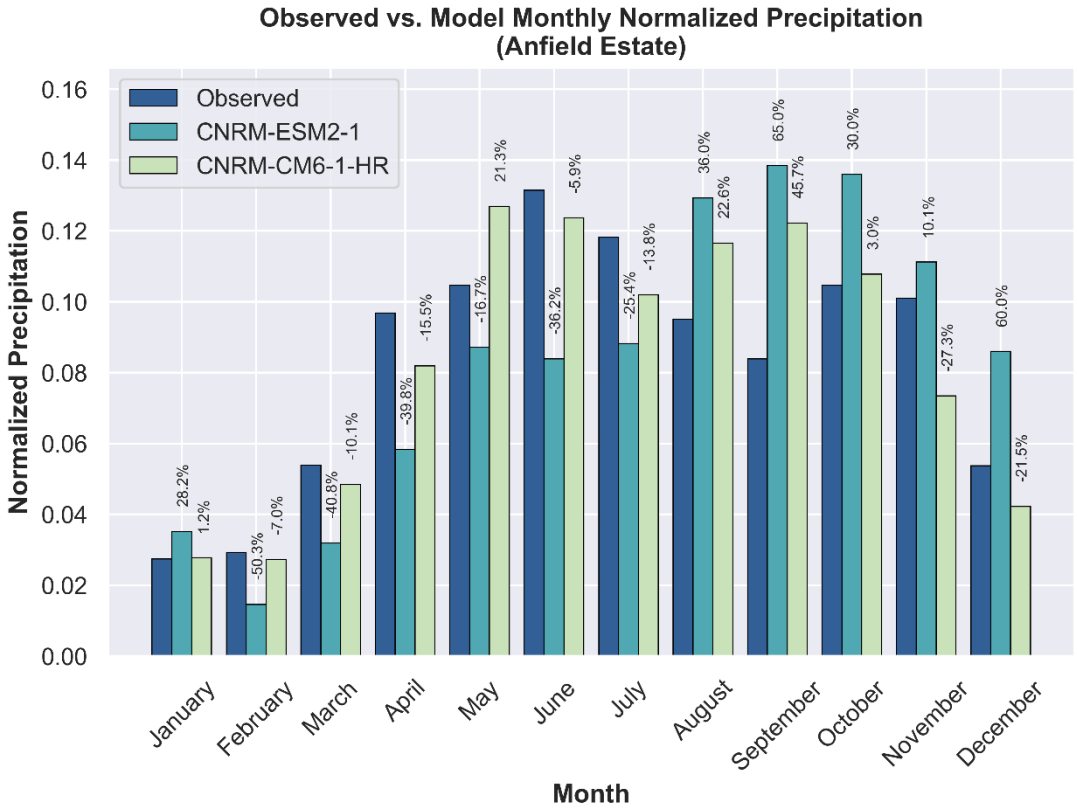
Observed vs. Model Monthly Normalized Precipitation
(Anfield Estate)
Observed
CNRM-ESM2-1
CNRM-CM6-1-HR
Normalized Precipitation
0.00
0.02
0.04
0.06
0.08
0.10
0.12
0.14
0.16
28.2%
1.2%
-50.3%
-7.0%
-40.8%
-10.1%
-39.8%
-15.5%
-16.7%
21.3%
-36.2%
-5.9%
-25.4%
-13.8%
36.0%
22.6%
65.0%
45.7%
30.0%
3.0%
10.1%
-27.3%
60.0%
-21.5%
January
February
March
April
May
June
July
August
September
October
November
December
Month

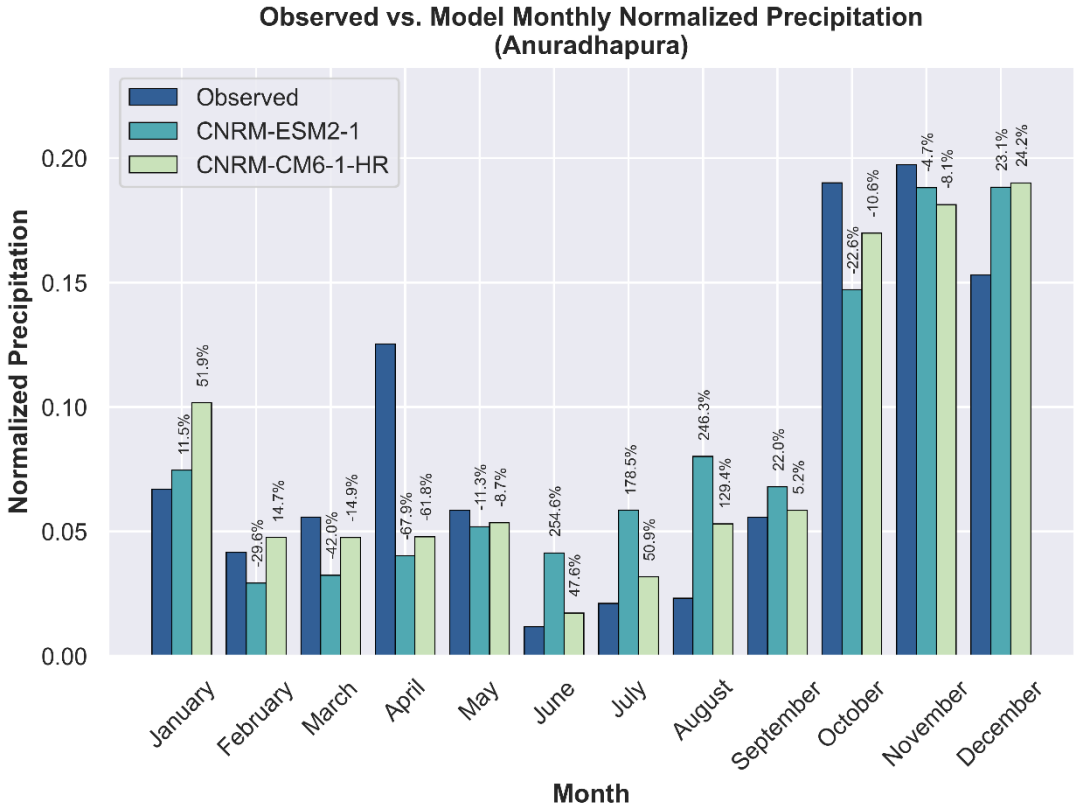
Observed vs. Model Monthly Normalized Precipitation
(Anuradhapura)
Observed
CNRM-ESM2-1
CNRM-CM6-1-HR
Normalized Precipitation
0.00
0.05
0.10
0.15
0.20
11.5%
51.9%
-29.6%
14.7%
-42.0%
-14.9%
-67.9%
-61.8%
-11.3%
-8.7%
254.6%
47.6%
178.5%
50.9%
246.3%
129.4%
22.0%
5.2%
-22.6%
-10.6%
-4.7%
-8.1%
23.1%
24.2%
January
February
March
April
May
June
July
August
September
October
November
December
Month

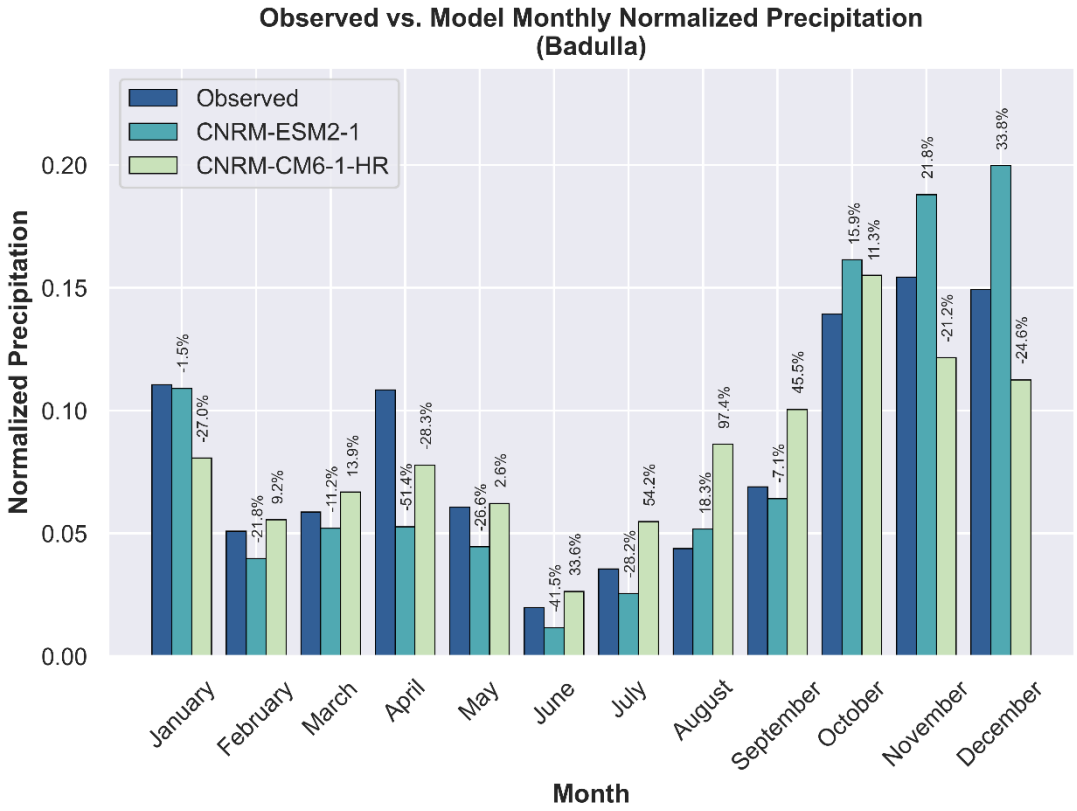
Observed vs. Model Monthly Normalized Precipitation
(Badulla)
Observed
CNRM-ESM2-1
CNRM-CM6-1-HR
Normalized Precipitation
0.00
0.05
0.10
0.15
0.20
-1.5%
-27.0%
-21.8%
9.2%
-11.2%
13.9%
-51.4%
-28.3%
-26.6%
2.6%
-41.5%
33.6%
-28.2%
54.2%
18.3%
97.4%
-7.1%
45.5%
15.9%
11.3%
21.8%
-21.2%
33.8%
-24.6%
January
February
March
April
May
June
July
August
September
October
November
December
Month

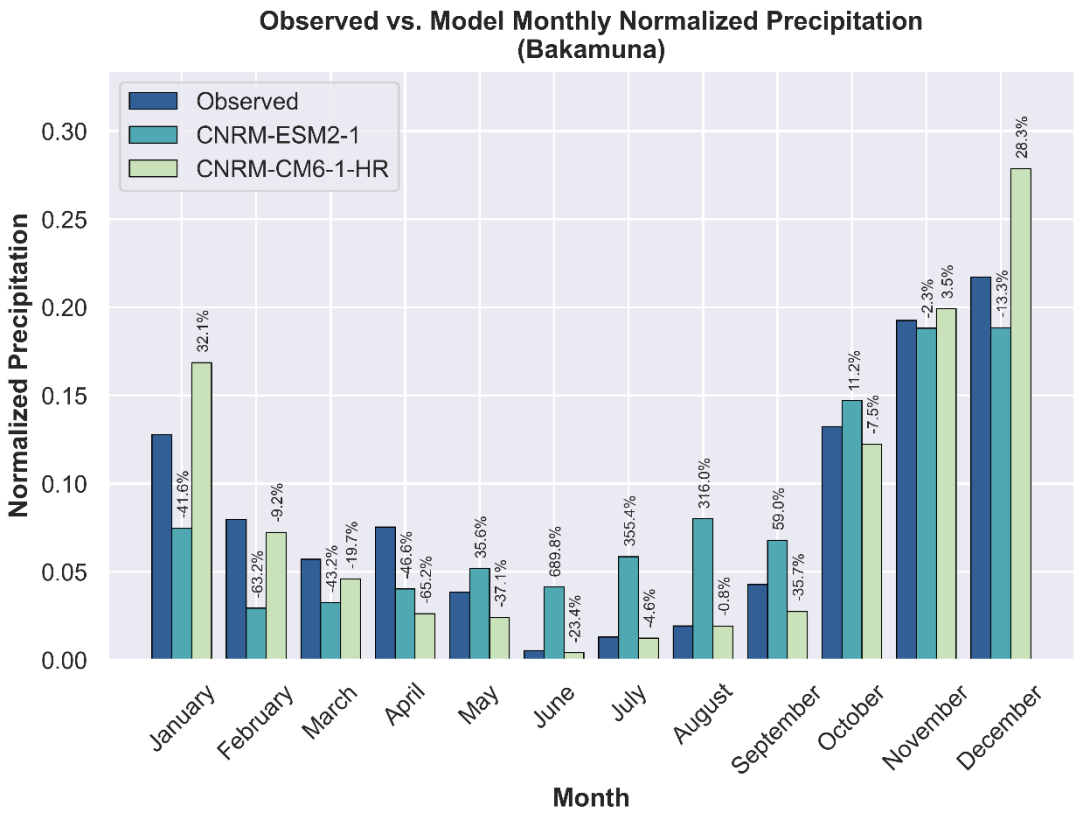
Observed vs. Model Monthly Normalized Precipitation
(Bakamuna)
Observed
CNRM-ESM2-1
CNRM-CM6-1-HR
Normalized Precipitation
0.00
0.05
0.10
0.15
0.20
0.25
0.30
-41.6%
32.1%
-63.2%
-9.2%
-43.2%
-19.7%
-46.6%
-65.2%
35.6%
-37.1%
689.8%
-23.4%
355.4%
-4.6%
316.0%
-0.8%
59.0%
-35.7%
11.2%
-7.5%
-2.3%
3.5%
-13.3%
28.3%
January
February
March
April
May
June
July
August
September
October
November
December
Month

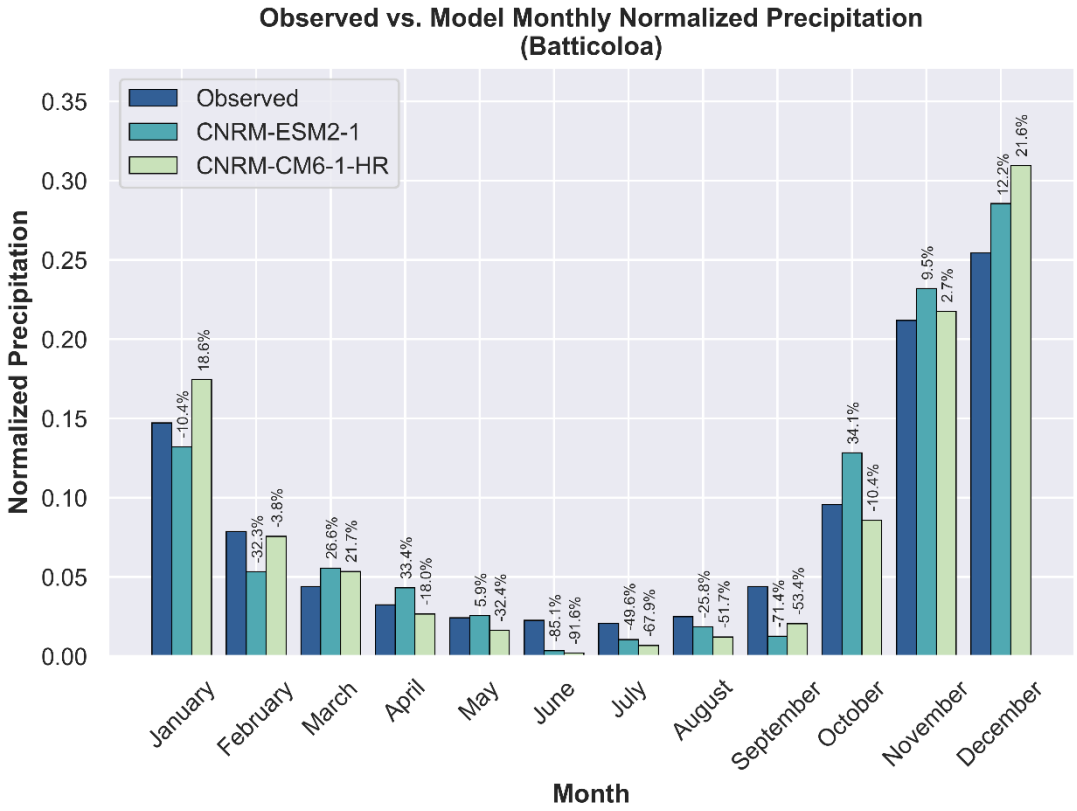
Observed vs. Model Monthly Normalized Precipitation
(Batticoloa)
Observed
CNRM-ESM2-1
CNRM-CM6-1-HR
Normalized Precipitation
0.00
0.05
0.10
0.15
0.20
0.25
0.30
0.35
-10.4%
18.6%
-32.3%
-3.8%
26.6%
21.7%
33.4%
-18.0%
5.9%
-32.4%
-85.1%
-91.6%
-49.6%
-67.9%
-25.8%
-51.7%
-71.4%
-53.4%
34.1%
-10.4%
9.5%
2.7%
12.2%
21.6%
January
February
March
April
May
June
July
August
September
October
November
December
Month

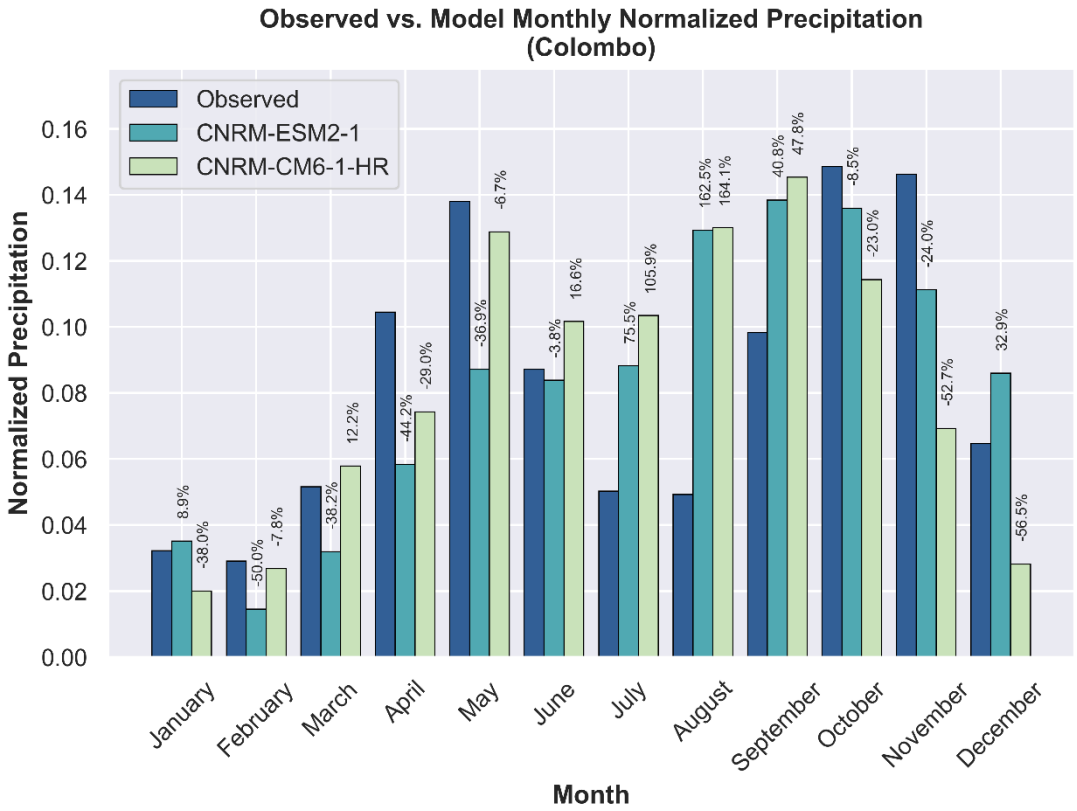
Observed vs. Model Monthly Normalized Precipitation
(Colombo)
Observed
CNRM-ESM2-1
CNRM-CM6-1-HR
Normalized Precipitation
0.00
0.02
0.04
0.06
0.08
0.10
0.12
0.14
0.16
8.9%
-38.0%
-50.0%
-7.8%
-38.2%
12.2%
-44.2%
-29.0%
-36.9%
-6.7%
-3.8%
16.6%
75.5%
105.9%
162.5%
164.1%
40.8%
47.8%
-8.5%
-23.0%
-24.0%
-52.7%
32.9%
-56.5%
January
February
March
April
May
June
July
August
September
October
November
December
Month

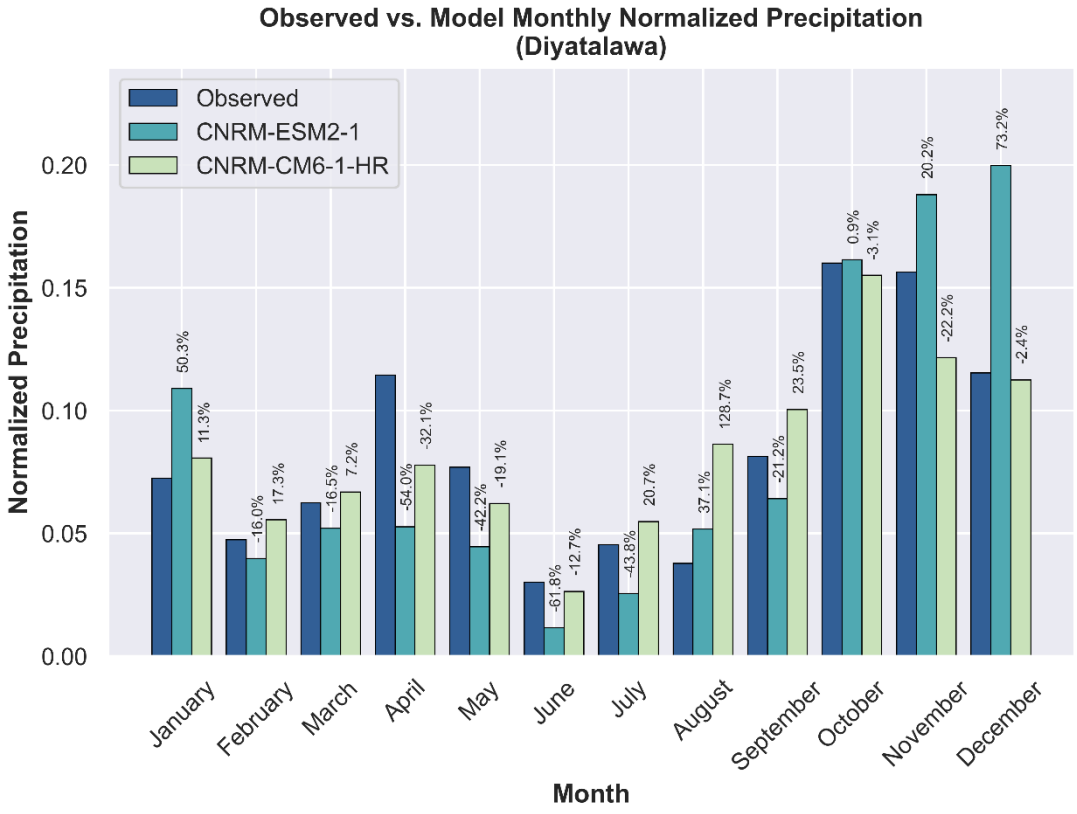
Observed vs. Model Monthly Normalized Precipitation
(Diyatalawa)
Observed
CNRM-ESM2-1
CNRM-CM6-1-HR
Normalized Precipitation
0.00
0.05
0.10
0.15
0.20
50.3%
11.3%
-16.0%
17.3%
-16.5%
7.2%
-54.0%
-32.1%
-42.2%
-19.1%
-61.8%
-12.7%
-43.8%
20.7%
37.1%
128.7%
-21.2%
23.5%
0.9%
-3.1%
20.2%
-22.2%
73.2%
-2.4%
January
February
March
April
May
June
July
August
September
October
November
December
Month

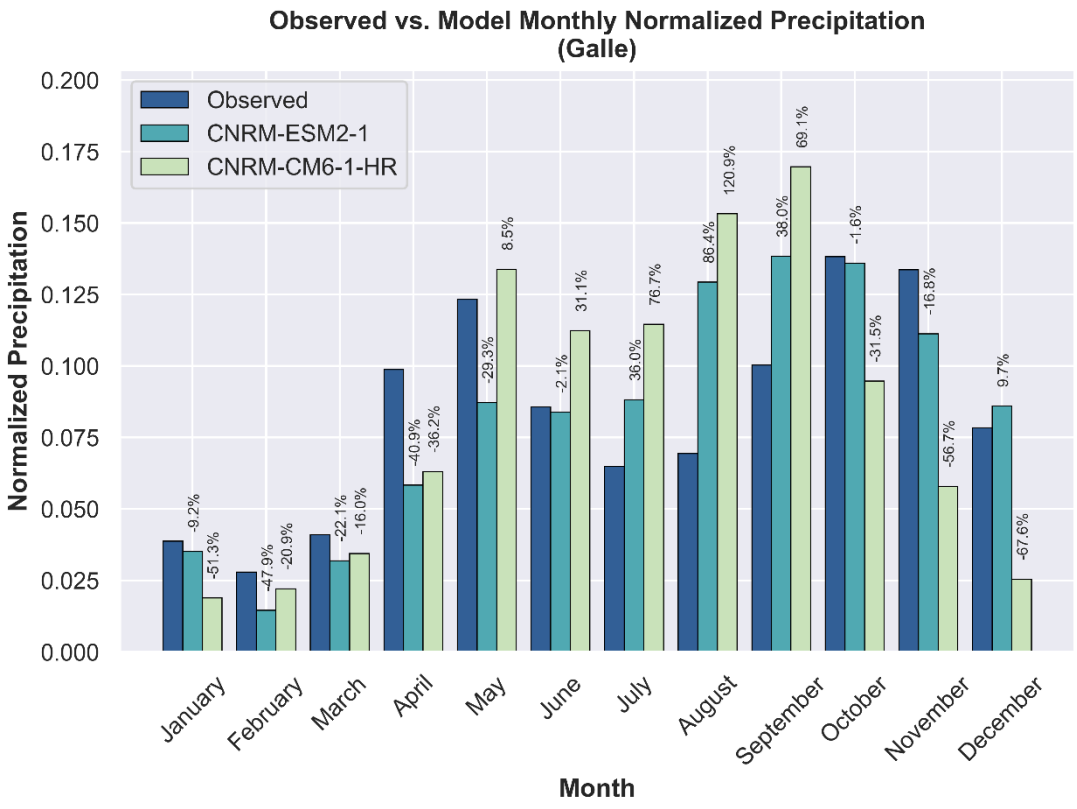
Observed vs. Model Monthly Normalized Precipitation
(Galle)
Observed
CNRM-ESM2-1
CNRM-CM6-1-HR
Normalized Precipitation
0.000
0.025
0.050
0.075
0.100
0.125
0.150
0.175
0.200
-9.2%
-51.3%
-47.9%
-20.9%
-22.1%
-16.0%
-40.9%
-36.2%
-29.3%
8.5%
-2.1%
31.1%
36.0%
76.7%
86.4%
120.9%
38.0%
69.1%
-1.6%
-31.5%
-16.8%
-56.7%
9.7%
-67.6%
January
February
March
April
May
June
July
August
September
October
November
December
Month

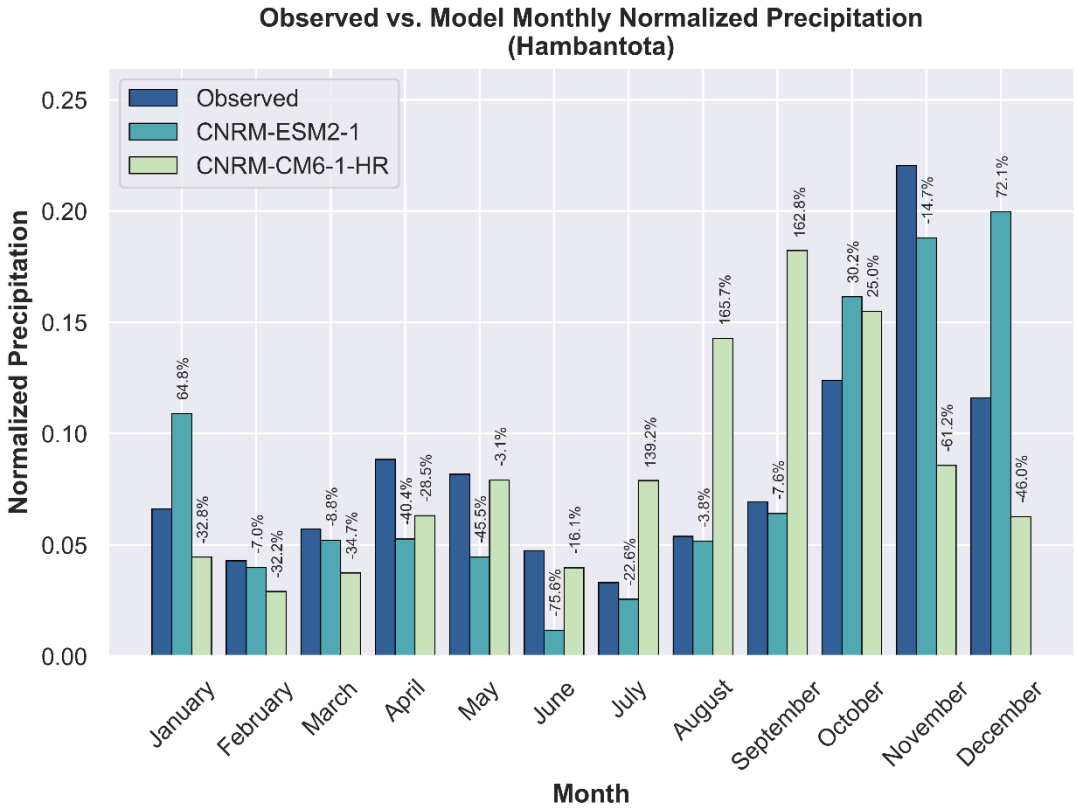
Observed vs. Model Monthly Normalized Precipitation
(Hambantota)
Observed
CNRM-ESM2-1
CNRM-CM6-1-HR
Normalized Precipitation
0.00
0.05
0.10
0.15
0.20
0.25
64.8%
-32.8%
-7.0%
-32.2%
-8.8%
-34.7%
-40.4%
-28.5%
-45.5%
-3.1%
-75.6%
-16.1%
-22.6%
139.2%
-3.8%
165.7%
-7.6%
162.8%
30.2%
25.0%
-14.7%
-61.2%
72.1%
-46.0%
January
February
March
April
May
June
July
August
September
October
November
December
Month

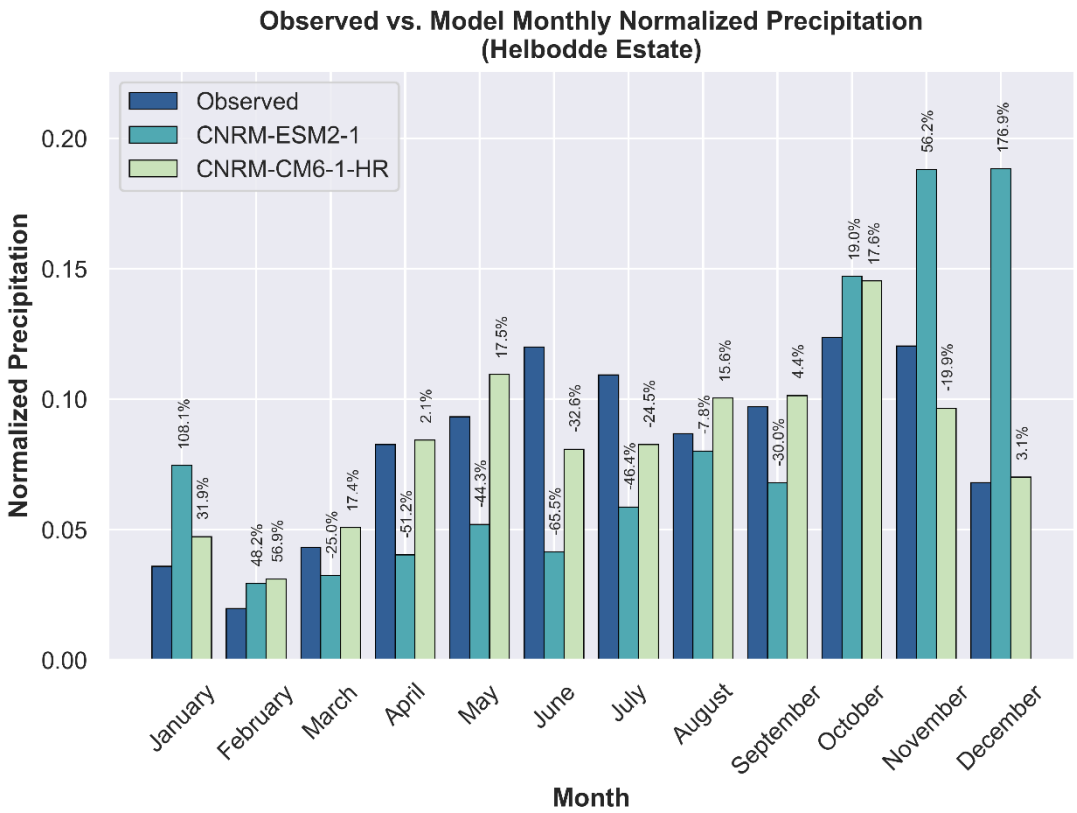
Observed vs. Model Monthly Normalized Precipitation
(Helbodde Estate)
Observed
CNRM-ESM2-1
CNRM-CM6-1-HR
Normalized Precipitation
0.00
0.05
0.10
0.15
0.20
108.1%
31.9%
48.2%
56.9%
-25.0%
17.4%
-51.2%
2.1%
-44.3%
17.5%
-65.5%
-32.6%
-46.4%
-24.5%
-7.8%
15.6%
-30.0%
4.4%
19.0%
17.6%
56.2%
-19.9%
176.9%
3.1%
January
February
March
April
May
June
July
August
September
October
November
December
Month

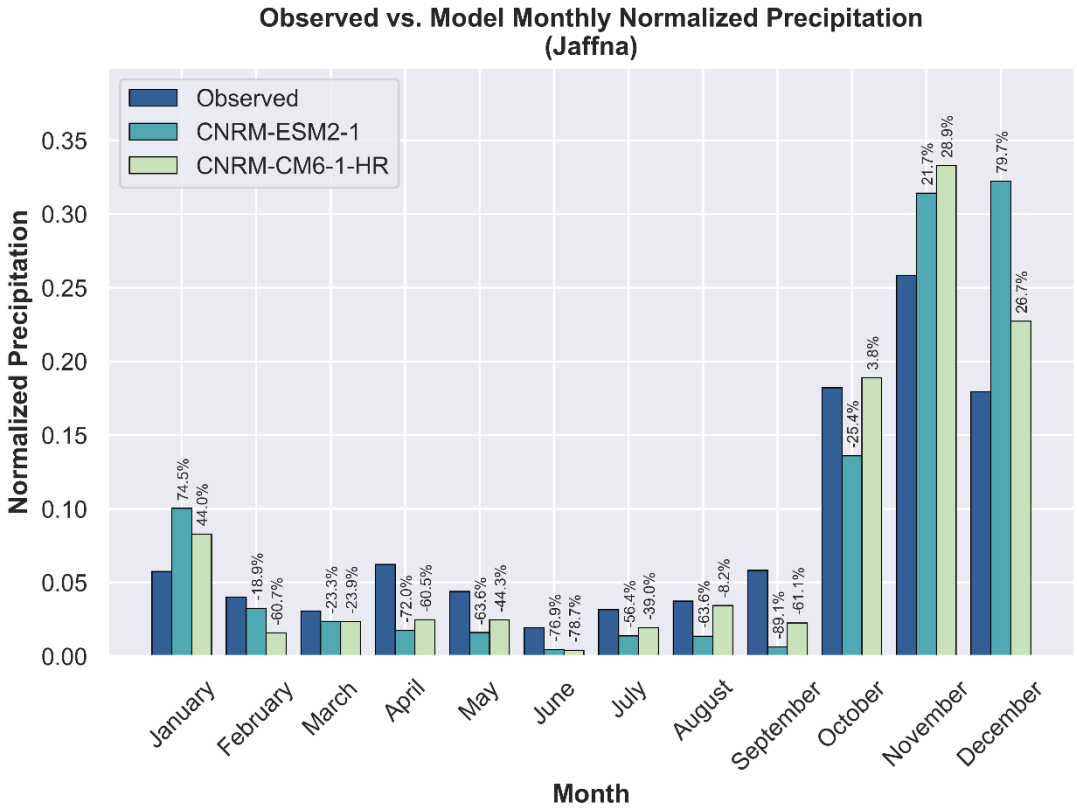
Observed vs. Model Monthly Normalized Precipitation
(Jaffna)
Observed
CNRM-ESM2-1
CNRM-CM6-1-HR
Normalized Precipitation
0.00
0.05
0.10
0.15
0.20
0.25
0.30
0.35
74.5%
44.0%
-18.9%
-60.7%
-23.3%
-23.9%
-72.0%
-60.5%
-63.6%
-44.3%
-76.9%
-78.7%
-56.4%
-39.0%
-63.6%
-8.2%
-89.1%
-61.1%
-25.4%
3.8%
21.7%
28.9%
79.7%
26.7%
January
February
March
April
May
June
July
August
September
October
November
December
Month

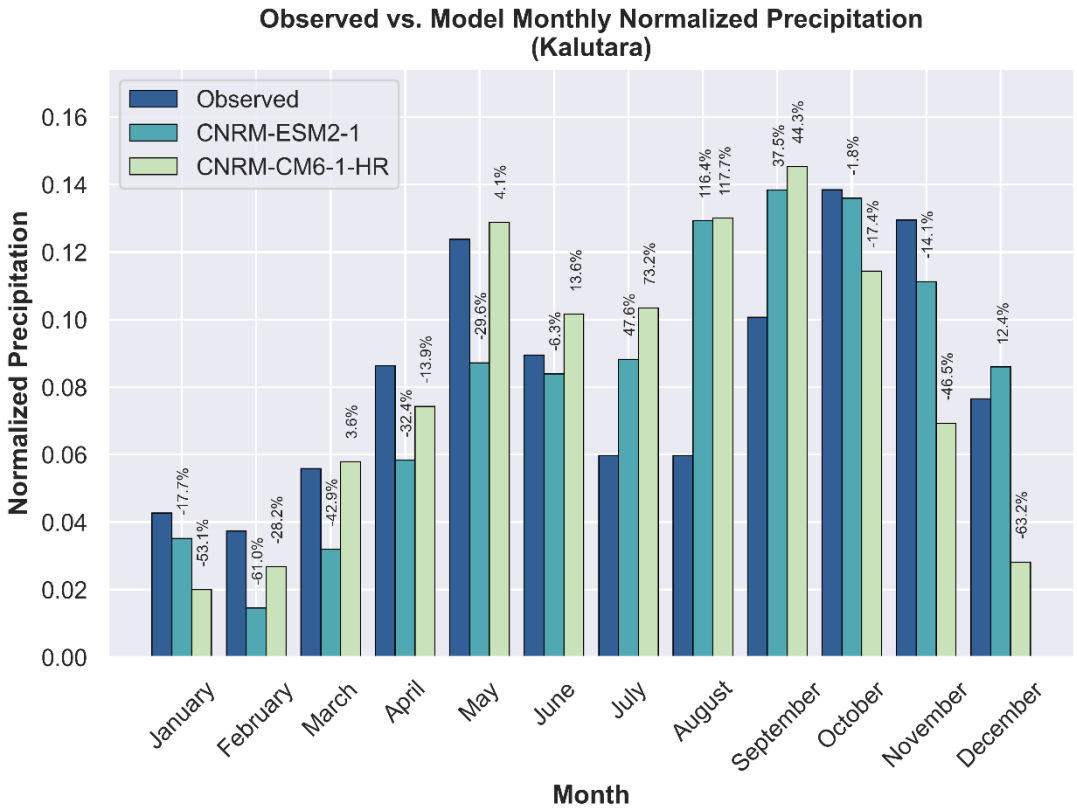
Observed vs. Model Monthly Normalized Precipitation
(Kalutara)
Observed
CNRM-ESM2-1
CNRM-CM6-1-HR
Normalized Precipitation
0.00
0.02
0.04
0.06
0.08
0.10
0.12
0.14
0.16
-17.7%
-53.1%
-61.0%
-28.2%
-42.9%
3.6%
-32.4%
-13.9%
-29.6%
4.1%
-6.3%
13.6%
47.6%
73.2%
116.4%
117.7%
37.5%
44.3%
-1.8%
-17.4%
-14.1%
-46.5%
12.4%
-63.2%
January
February
March
April
May
June
July
August
September
October
November
December
Month

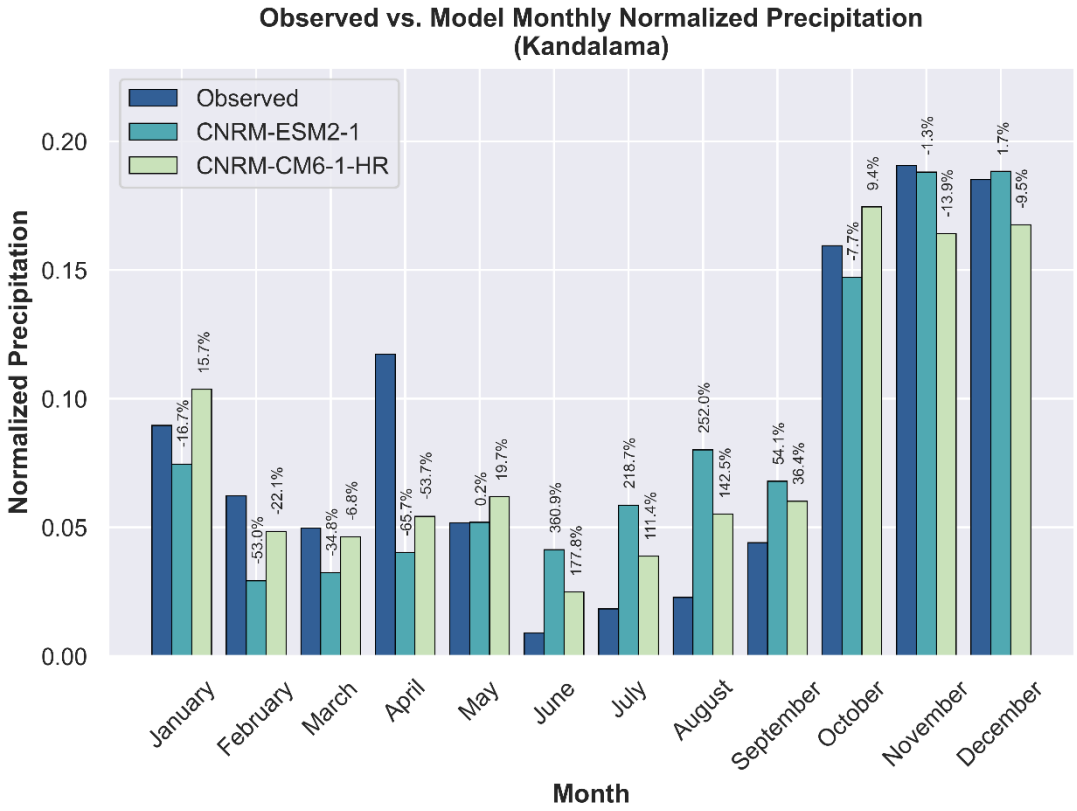
Observed vs. Model Monthly Normalized Precipitation
(Kandalama)
Observed
CNRM-ESM2-1
CNRM-CM6-1-HR
Normalized Precipitation
0.00
0.05
0.10
0.15
0.20
-16.7%
15.7%
-53.0%
-22.1%
-34.8%
-6.8%
-65.7%
-53.7%
0.2%
19.7%
360.9%
177.8%
218.7%
111.4%
252.0%
142.5%
54.1%
36.4%
-7.7%
9.4%
-1.3%
-13.9%
1.7%
-9.5%
January
February
March
April
May
June
July
August
September
October
November
December
Month

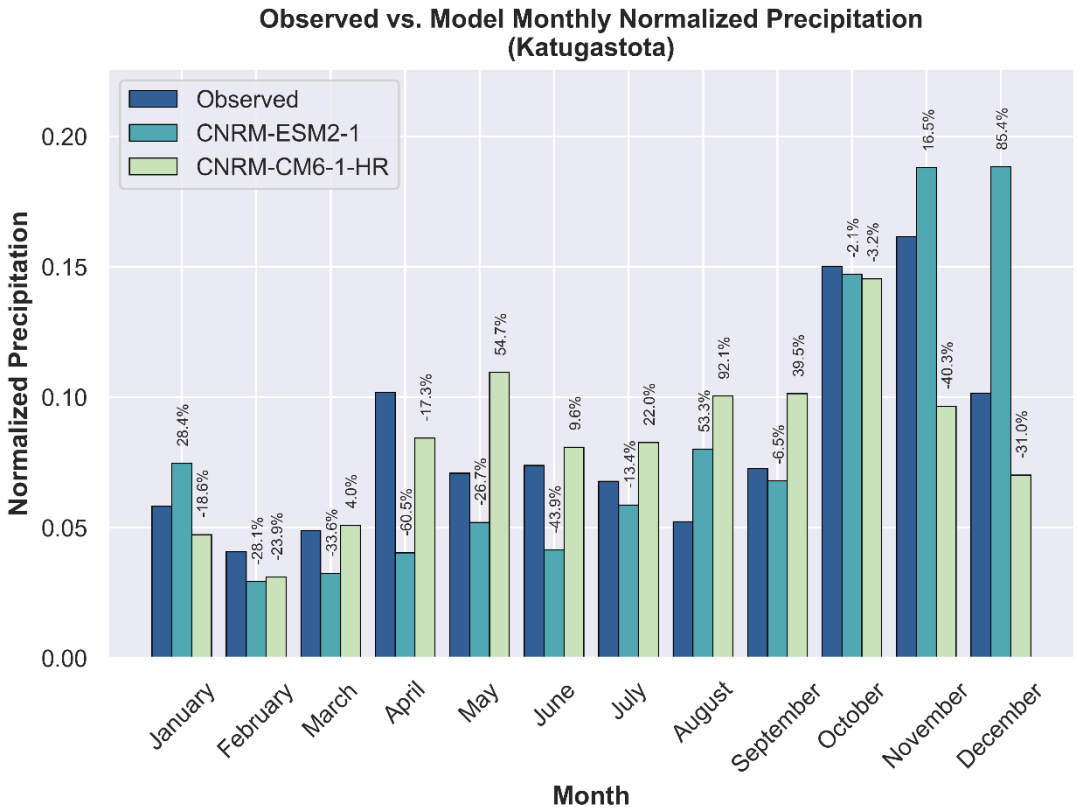
Observed vs. Model Monthly Normalized Precipitation
(Katugastota)
Observed
CNRM-ESM2-1
CNRM-CM6-1-HR
Normalized Precipitation
0.00
0.05
0.10
0.15
0.20
28.4%
-18.6%
-28.1%
-23.9%
-33.6%
4.0%
-60.5%
-17.3%
-26.7%
54.7%
-43.9%
9.6%
-13.4%
22.0%
53.3%
92.1%
-6.5%
39.5%
-2.1%
-3.2%
16.5%
-40.3%
85.4%
-31.0%
January
February
March
April
May
June
July
August
September
October
November
December
Month

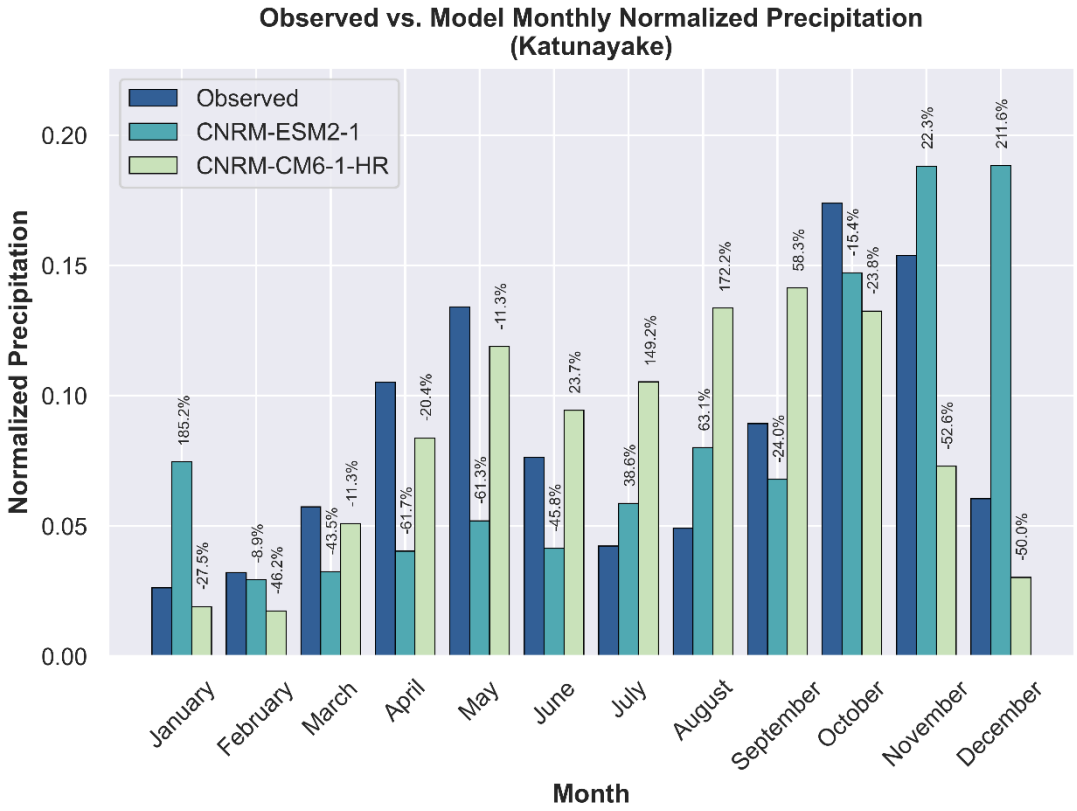
Observed vs. Model Monthly Normalized Precipitation
(Katunayake)
Observed
CNRM-ESM2-1
CNRM-CM6-1-HR
Normalized Precipitation
0.00
0.05
0.10
0.15
0.20
185.2%
-27.5%
-8.9%
-46.2%
-43.5%
-11.3%
-61.7%
-20.4%
-61.3%
-11.3%
-45.8%
23.7%
38.6%
149.2%
63.1%
172.2%
-24.0%
58.3%
-15.4%
-23.8%
22.3%
-52.6%
211.6%
-50.0%
January
February
March
April
May
June
July
August
September
October
November
December
Month

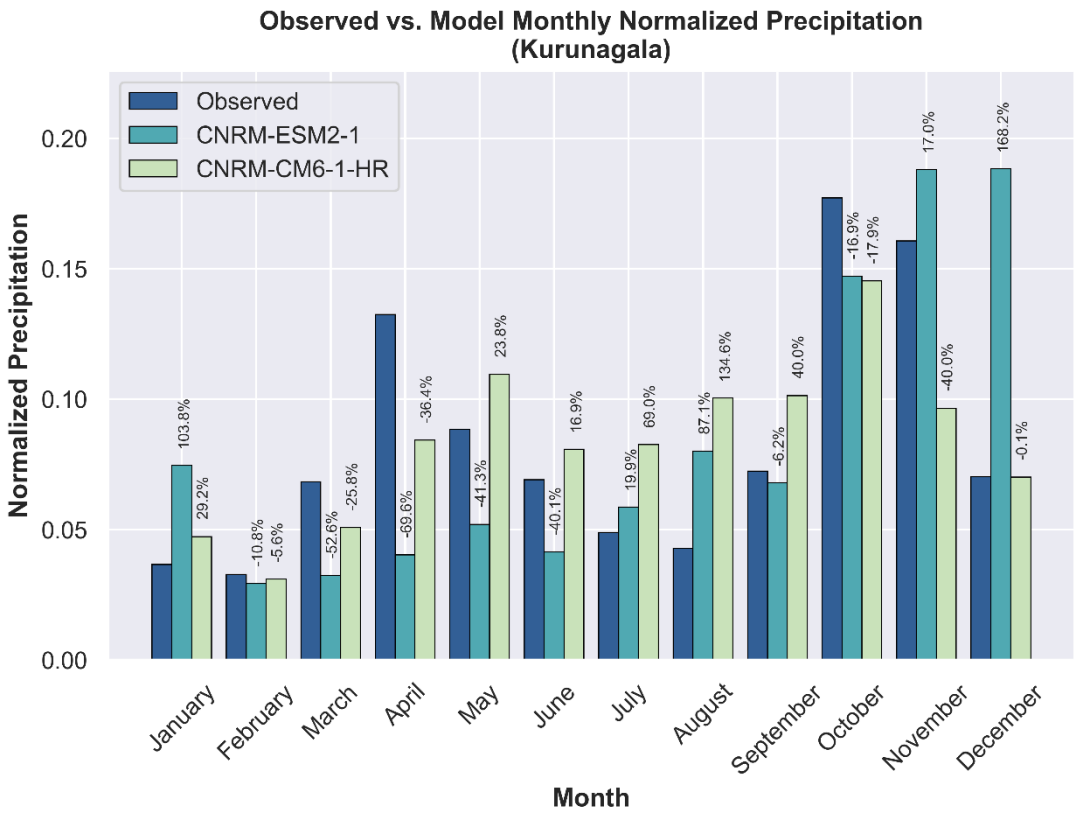
Observed vs. Model Monthly Normalized Precipitation
(Kurunagala)
Observed
CNRM-ESM2-1
CNRM-CM6-1-HR
Normalized Precipitation
0.00
0.05
0.10
0.15
0.20
103.8%
29.2%
-10.8%
-5.6%
-52.6%
-25.8%
-69.6%
-36.4%
-41.3%
23.8%
-40.1%
16.9%
19.9%
69.0%
87.1%
134.6%
-6.2%
40.0%
-16.9%
-17.9%
17.0%
-40.0%
168.2%
-0.1%
January
February
March
April
May
June
July
August
September
October
November
December
Month

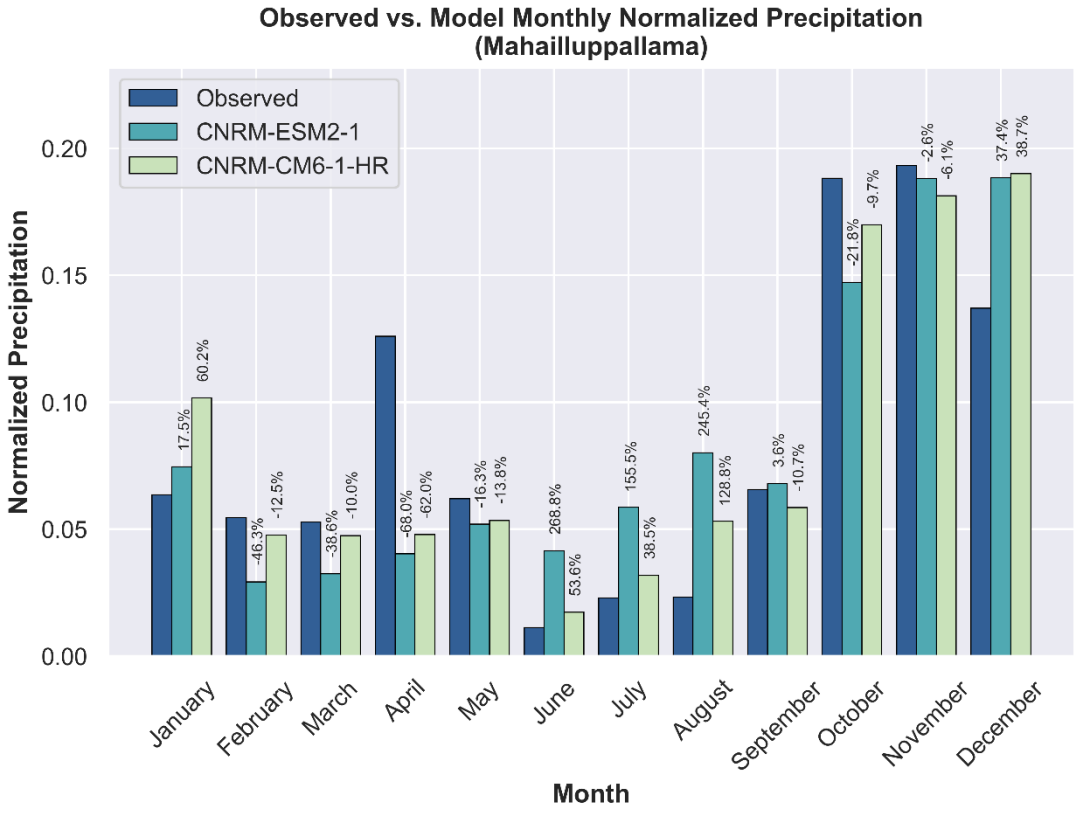
Observed vs. Model Monthly Normalized Precipitation
(Mahailluppallama)
Observed
CNRM-ESM2-1
CNRM-CM6-1-HR
Normalized Precipitation
0.00
0.05
0.10
0.15
0.20
17.5%
60.2%
-46.3%
-12.5%
-38.6%
-10.0%
-68.0%
-62.0%
-16.3%
-13.8%
268.8%
53.6%
155.5%
38.5%
245.4%
128.8%
3.6%
-10.7%
-21.8%
-9.7%
-2.6%
-6.1%
37.4%
38.7%
January
February
March
April
May
June
July
August
September
October
November
December
Month

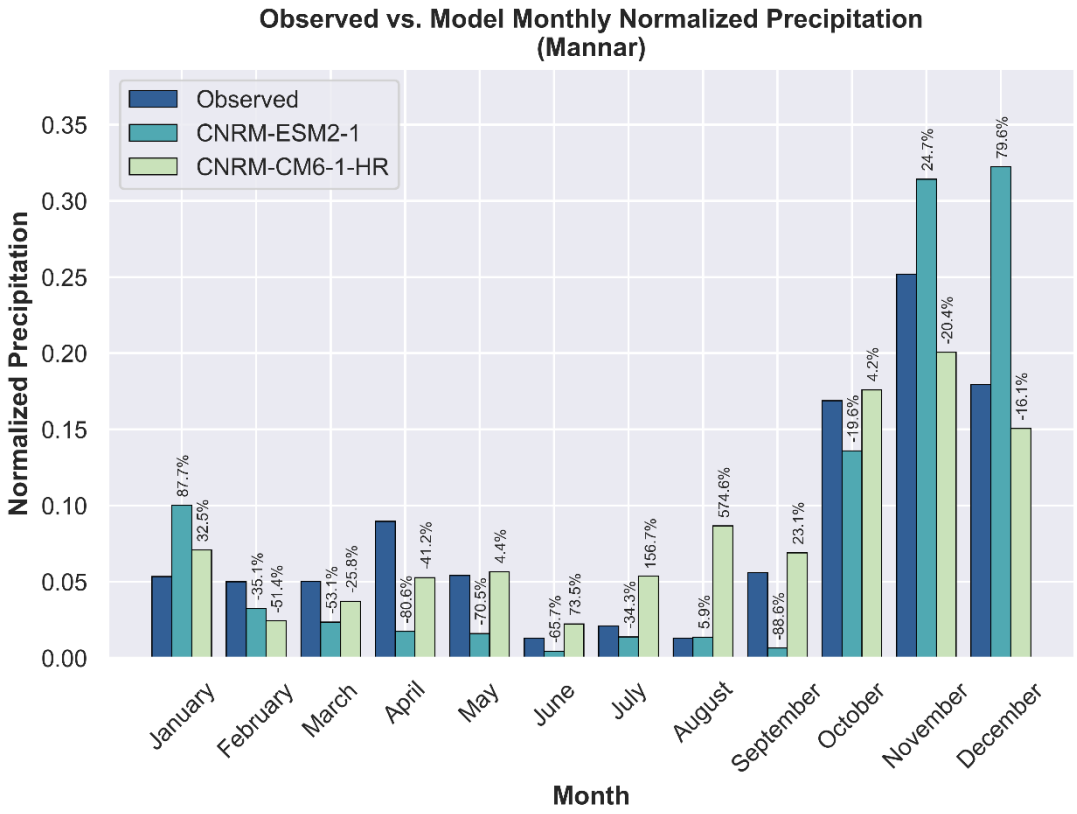
Observed vs. Model Monthly Normalized Precipitation
(Mannar)
Observed
CNRM-ESM2-1
CNRM-CM6-1-HR
Normalized Precipitation
0.00
0.05
0.10
0.15
0.20
0.25
0.30
0.35
87.7%
32.5%
-35.1%
-51.4%
-53.1%
-25.8%
-80.6%
-41.2%
-70.5%
4.4%
-65.7%
73.5%
-34.3%
156.7%
5.9%
574.6%
-88.6%
23.1%
-19.6%
4.2%
24.7%
-20.4%
79.6%
-16.1%
January
February
March
April
May
June
July
August
September
October
November
December
Month

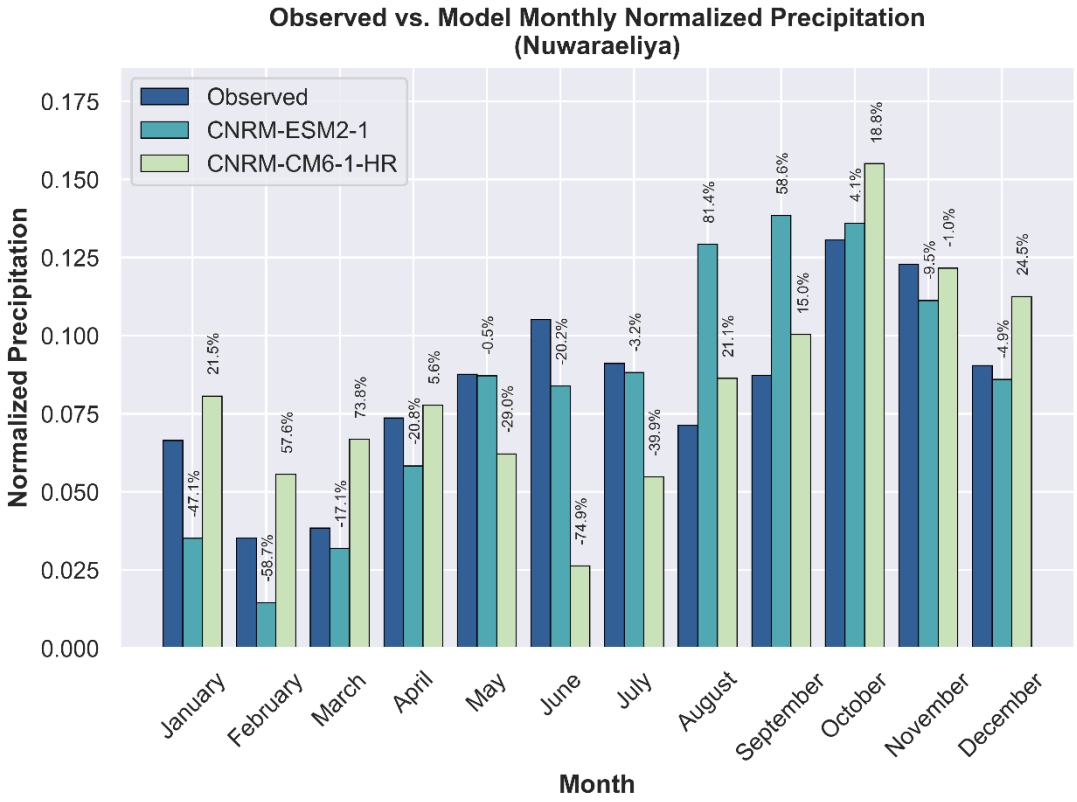
Observed vs. Model Monthly Normalized Precipitation
(Nuwaraeliya)
Observed
CNRM-ESM2-1
CNRM-CM6-1-HR
Normalized Precipitation
0.175
0.150
0.125
0.100
0.075
0.050
0.025
0.000
-47.1%
21.5%
-58.7%
57.6%
-17.1%
73.8%
-20.8%
5.6%
-0.5%
-29.0%
-20.2%
-74.9%
-3.2%
-39.9%
81.4%
21.1%
58.6%
15.0%
4.1%
18.8%
-9.5%
-1.0%
-4.9%
24.5%
January
February
March
April
May
June
July
August
September
October
November
December
Month

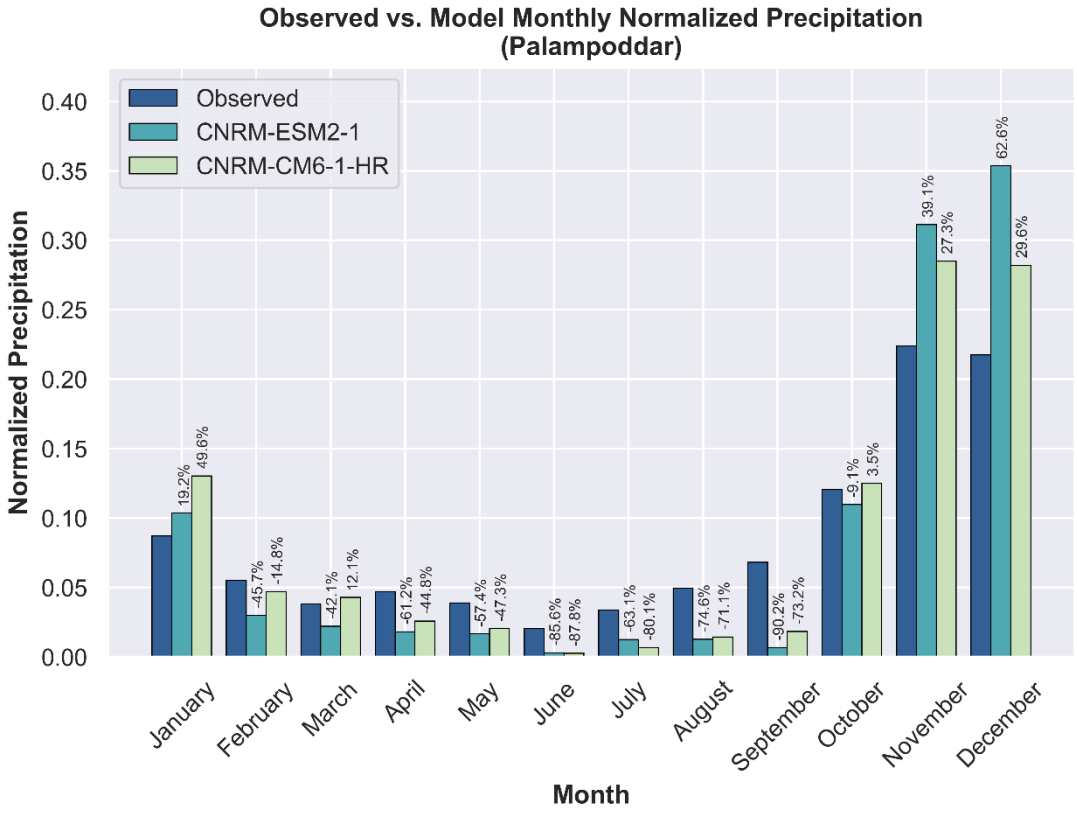
Observed vs. Model Monthly Normalized Precipitation
(Palampoddar)
Observed
CNRM-ESM2-1
CNRM-CM6-1-HR
Normalized Precipitation
0.40
0.35
0.30
0.25
0.20
0.15
0.10
0.05
0.00
19.2%
49.6%
-45.7%
-14.8%
-42.1%
12.1%
-61.2%
-44.8%
-57.4%
-47.3%
-85.6%
-87.8%
-63.1%
-80.1%
-74.6%
-71.1%
-90.2%
-73.2%
-9.1%
3.5%
39.1%
27.3%
62.6%
29.6%
January
February
March
April
May
June
July
August
September
October
November
December
Month

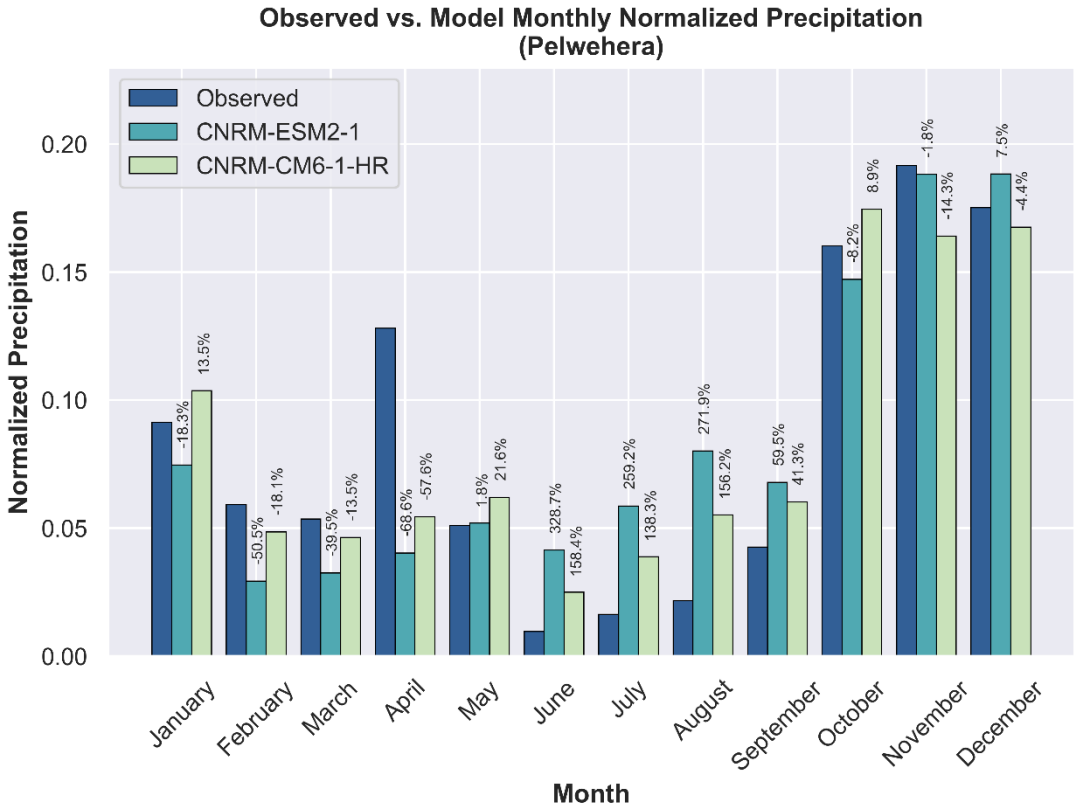
Observed vs. Model Monthly Normalized Precipitation
(Pelwehera)
Observed
CNRM-ESM2-1
CNRM-CM6-1-HR
Normalized Precipitation
0.00
0.05
0.10
0.15
0.20
-18.3%
13.5%
-50.5%
-18.1%
-39.5%
-13.5%
-68.6%
-57.6%
1.8%
21.6%
328.7%
158.4%
259.2%
138.3%
271.9%
156.2%
59.5%
41.3%
-8.2%
8.9%
-1.8%
-14.3%
7.5%
-4.4%
January
February
March
April
May
June
July
August
September
October
November
December
Month

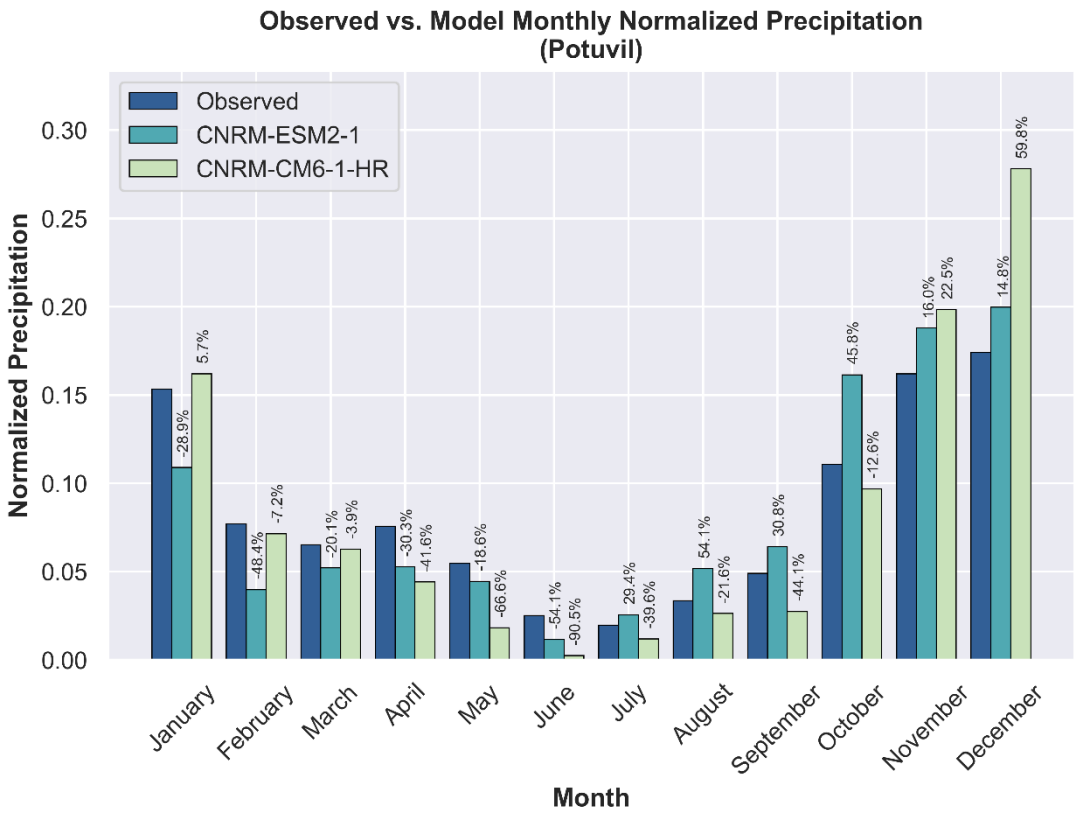
Observed vs. Model Monthly Normalized Precipitation
(Potuvil)
Observed
CNRM-ESM2-1
CNRM-CM6-1-HR
Normalized Precipitation
0.00
0.05
0.10
0.15
0.20
0.25
0.30
-28.9%
5.7%
-48.4%
-7.2%
-20.1%
-3.9%
-30.3%
-41.6%
-18.6%
-66.6%
-54.1%
-90.5%
29.4%
-39.6%
54.1%
-21.6%
30.8%
-44.1%
45.8%
-12.6%
16.0%
22.5%
14.8%
59.8%
January
February
March
April
May
June
July
August
September
October
November
December
Month

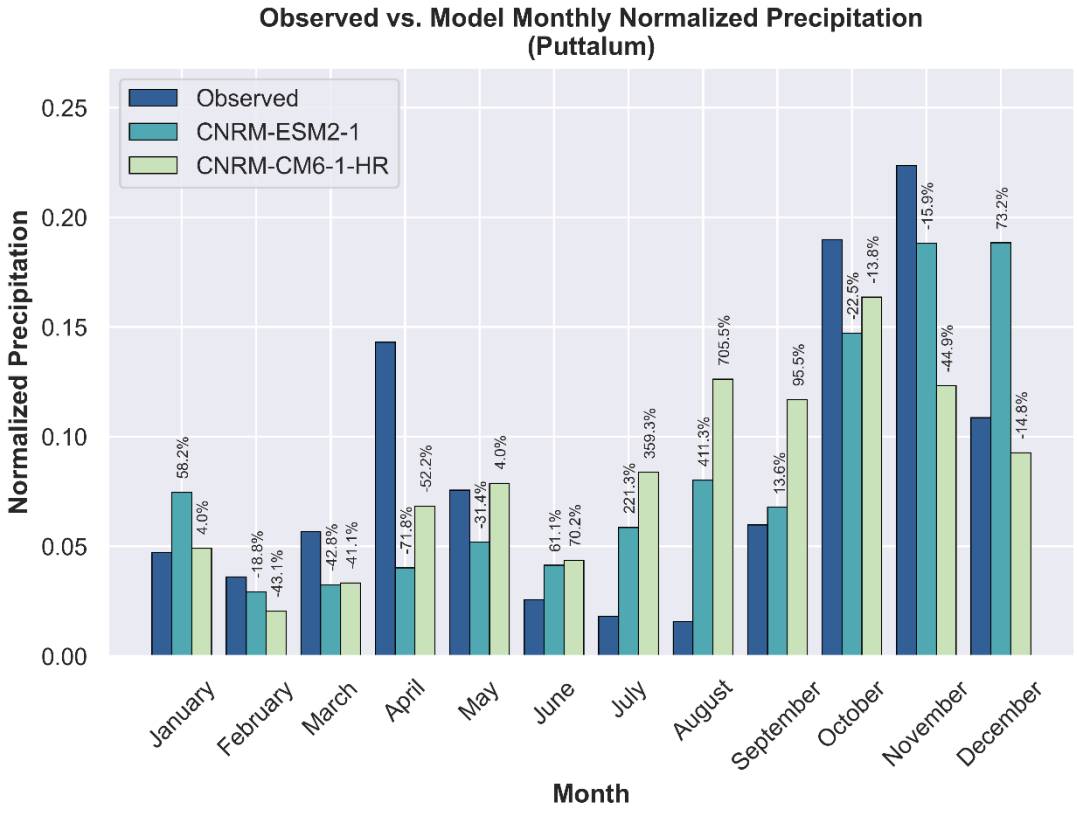
Observed vs. Model Monthly Normalized Precipitation
(Puttalum)
Observed
CNRM-ESM2-1
CNRM-CM6-1-HR
Normalized Precipitation
0.25
0.20
0.15
0.10
0.05
0.00
58.2%
4.0%
-18.8%
-43.1%
-42.8%
-41.1%
-71.8%
-52.2%
-31.4%
4.0%
61.1%
70.2%
221.3%
359.3%
411.3%
705.5%
13.6%
95.5%
-22.5%
-13.8%
-15.9%
-44.9%
73.2%
-14.8%
January
February
March
April
May
June
July
August
September
October
November
December
Month

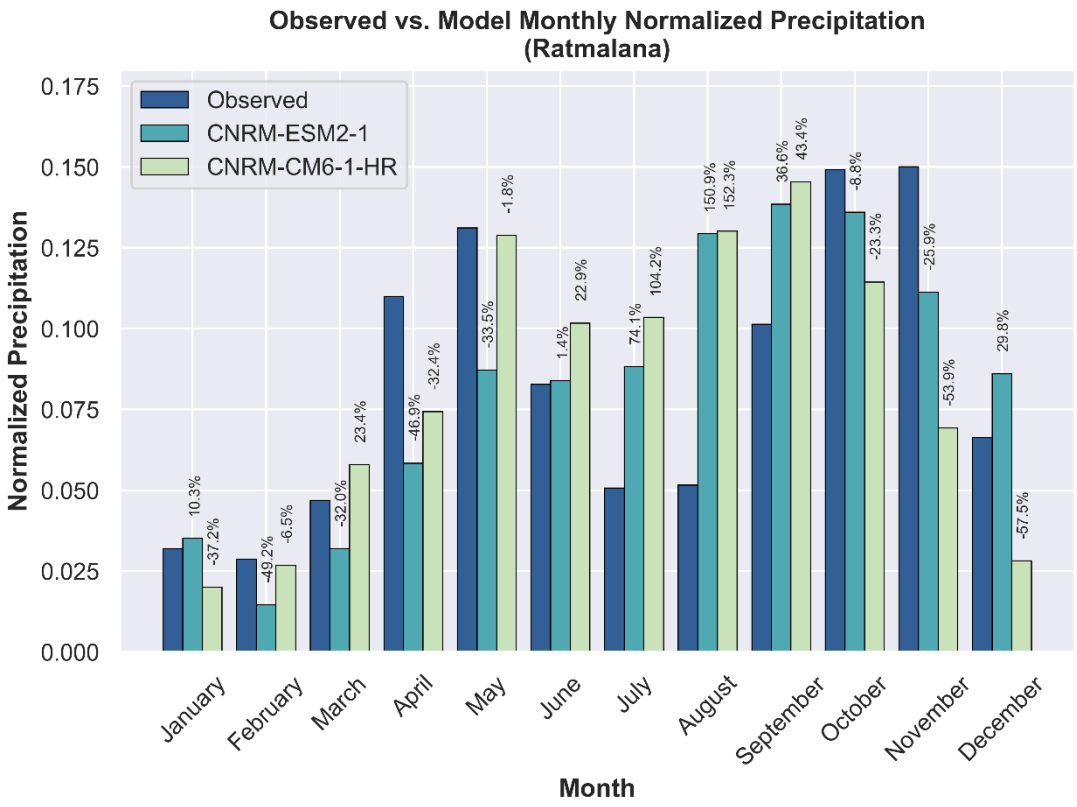
Observed vs. Model Monthly Normalized Precipitation
(Ratmalana)
Observed
CNRM-ESM2-1
CNRM-CM6-1-HR
Normalized Precipitation
0.175
0.150
0.125
0.100
0.075
0.050
0.025
0.000
10.3%
-37.2%
-49.2%
-6.5%
-32.0%
23.4%
-46.9%
-32.4%
-33.5%
-1.8%
1.4%
22.9%
74.1%
104.2%
150.9%
152.3%
36.6%
43.4%
-8.8%
-23.3%
-25.9%
-53.9%
29.8%
-57.5%
January
February
March
April
May
June
July
August
September
October
November
December
Month

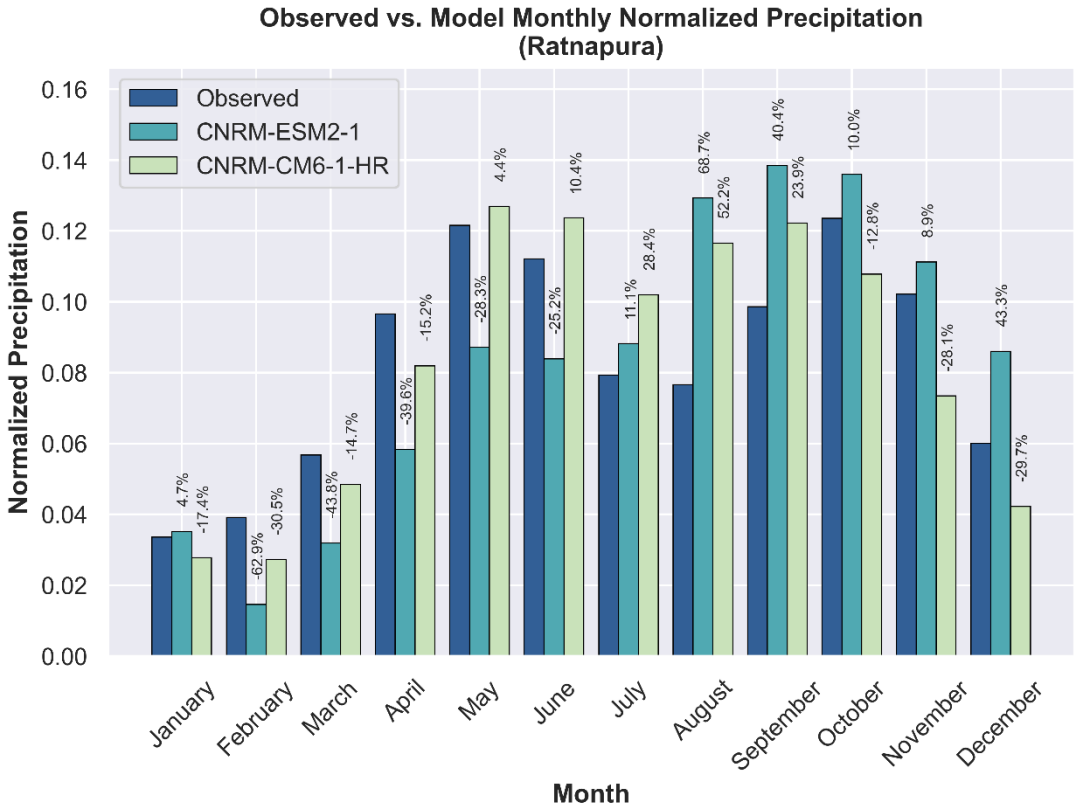
Observed vs. Model Monthly Normalized Precipitation
(Ratnapura)
Observed
CNRM-ESM2-1
CNRM-CM6-1-HR
Normalized Precipitation
0.00
0.02
0.04
0.06
0.08
0.10
0.12
0.14
0.16
4.7%
-17.4%
-62.9%
-30.5%
-43.8%
-14.7%
-39.6%
-15.2%
-28.3%
4.4%
-25.2%
10.4%
11.1%
28.4%
68.7%
52.2%
40.4%
23.9%
10.0%
-12.8%
8.9%
-28.1%
43.3%
-29.7%
January
February
March
April
May
June
July
August
September
October
November
December
Month

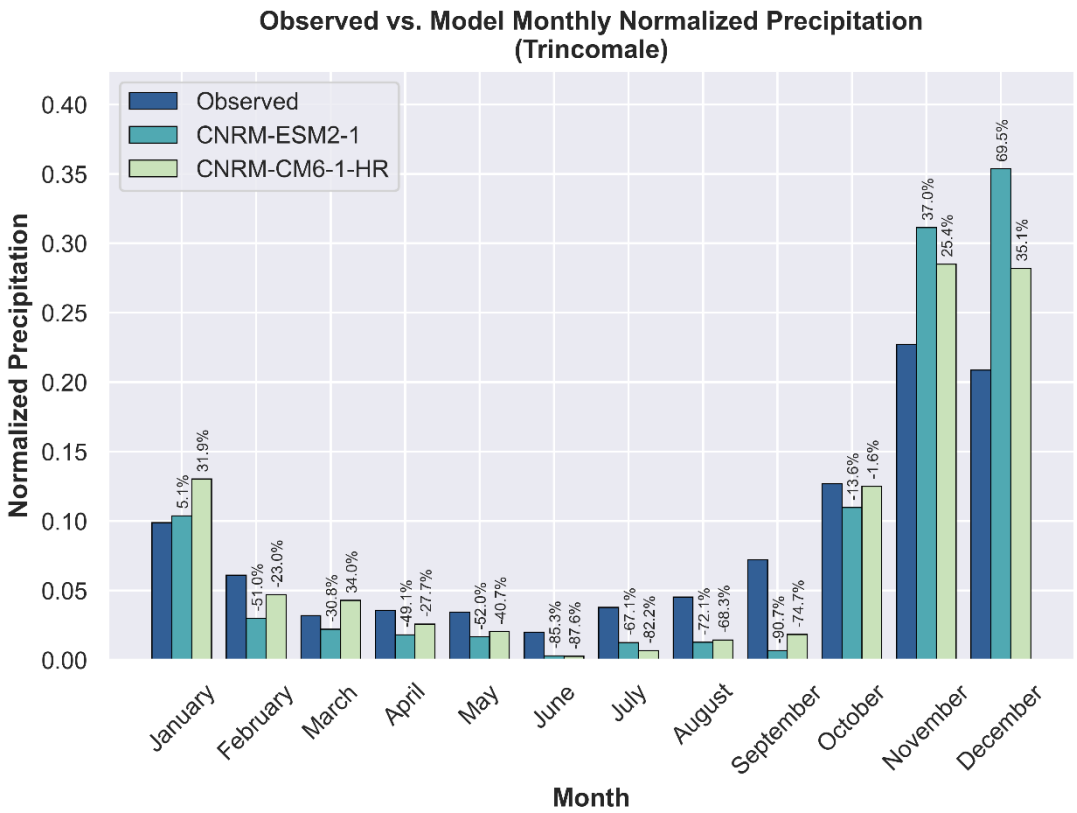
Observed vs. Model Monthly Normalized Precipitation
(Trincomale)
Observed
CNRM-ESM2-1
CNRM-CM6-1-HR
Normalized Precipitation
0.00
0.05
0.10
0.15
0.20
0.25
0.30
0.35
0.40
5.1%
31.9%
-51.0%
-23.0%
-30.8%
34.0%
-49.1%
-27.7%
-52.0%
-40.7%
-85.3%
-87.6%
-67.1%
-82.2%
-72.1%
-68.3%
-90.7%
-74.7%
-13.6%
-1.6%
37.0%
25.4%
69.5%
35.1%
January
February
March
April
May
June
July
August
September
October
November
December
Month

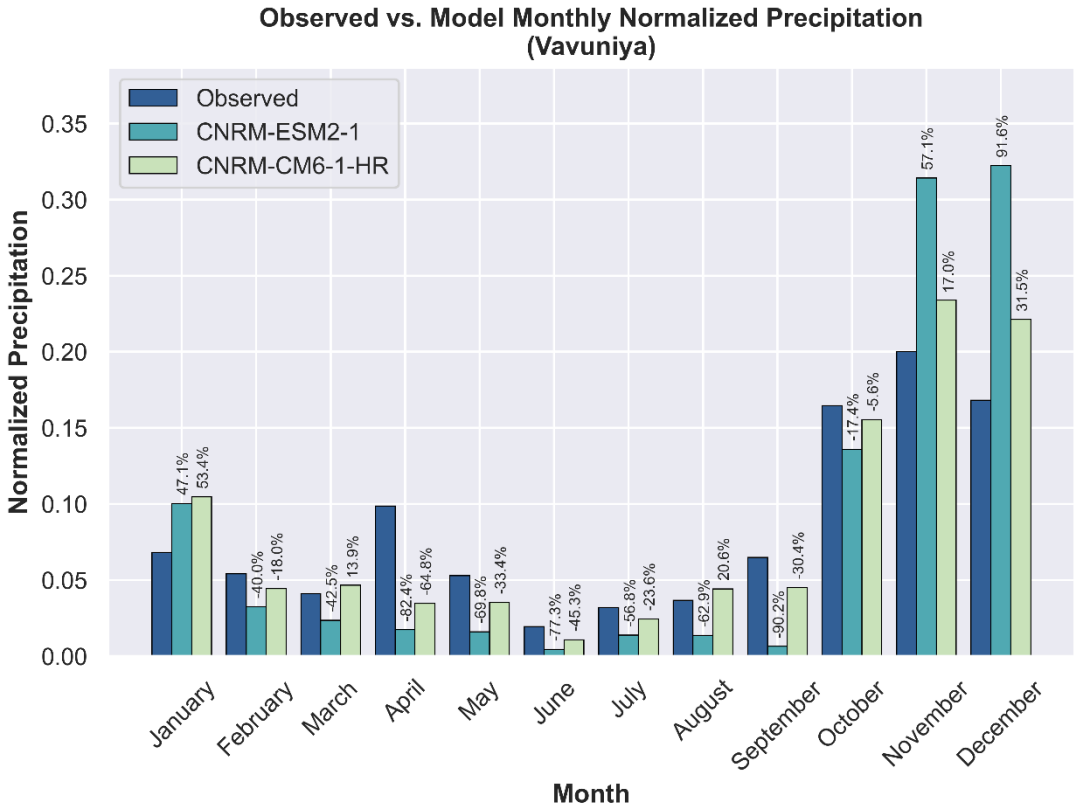
Observed vs. Model Monthly Normalized Precipitation
(Vavuniya)
Observed
CNRM-ESM2-1
CNRM-CM6-1-HR
Normalized Precipitation
0.00
0.05
0.10
0.15
0.20
0.25
0.30
0.35
47.1%
53.4%
-40.0%
-18.0%
-42.5%
13.9%
-82.4%
-64.8%
-69.8%
-33.4%
-77.3%
-45.3%
-56.8%
-23.6%
-62.9%
20.6%
-90.2%
-30.4%
-17.4%
-5.6%
57.1%
17.0%
91.6%
31.5%
January
February
March
April
May
June
July
August
September
October
November
December
Month

Appendix D: Selected models comparison for monsoon seasonal variation

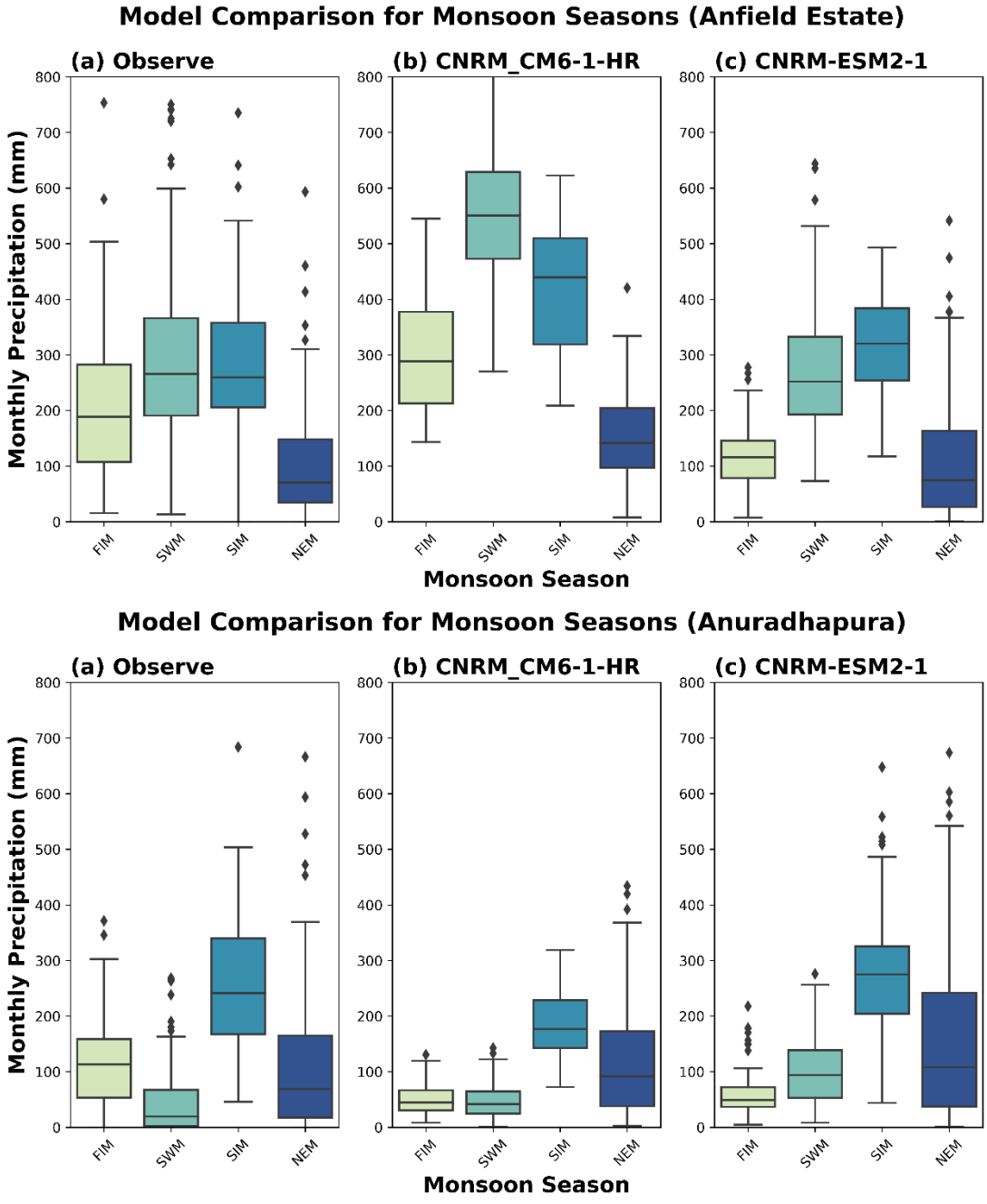
Model Comparison for Monsoon Seasons (Anfield Estate)
(a) Observe
(b) CNRM_CM6-1-HR
(c) CNRM-ESM2-1
Monthly Precipitation (mm)
0
100
200
300
400
500
600
700
800
FIM
SWM
SIM
NEM
Monsoon Season
Model Comparison for Monsoon Seasons (Anuradhapura)
(a) Observe
(b) CNRM_CM6-1-HR
(c) CNRM-ESM2-1
Monthly Precipitation (mm)
Monsoon Season

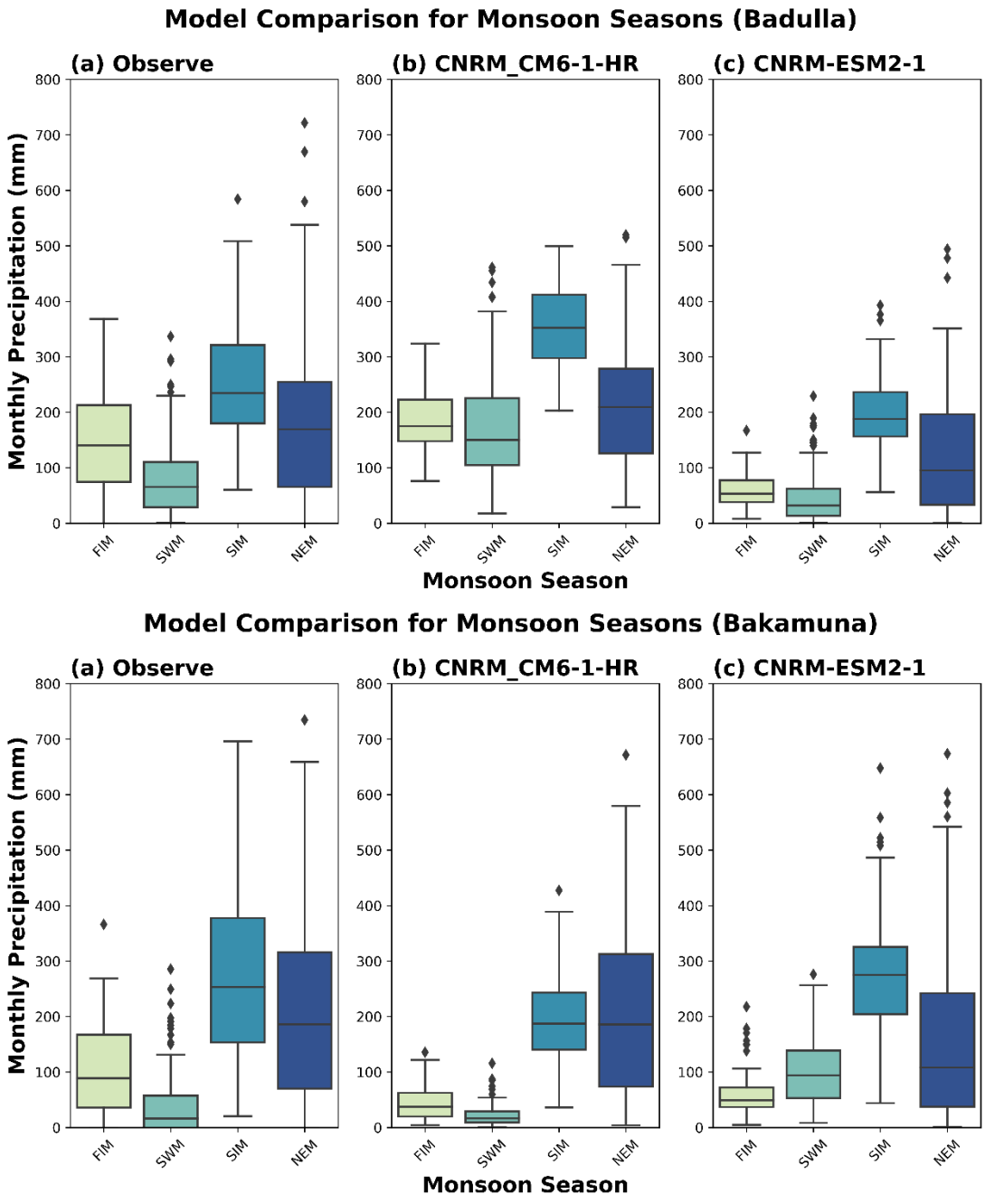
Model Comparison for Monsoon Seasons (Badulla)
(a) Observe
(b) CNRM_CM6-1-HR
(c) CNRM-ESM2-1
Monthly Precipitation (mm)
0
100
200
300
400
500
600
700
800
FIM
SWM
SIM
NEM
Monsoon Season
Model Comparison for Monsoon Seasons (Bakamuna)
(a) Observe
(b) CNRM_CM6-1-HR
(c) CNRM-ESM2-1
Monthly Precipitation (mm)
Monsoon Season

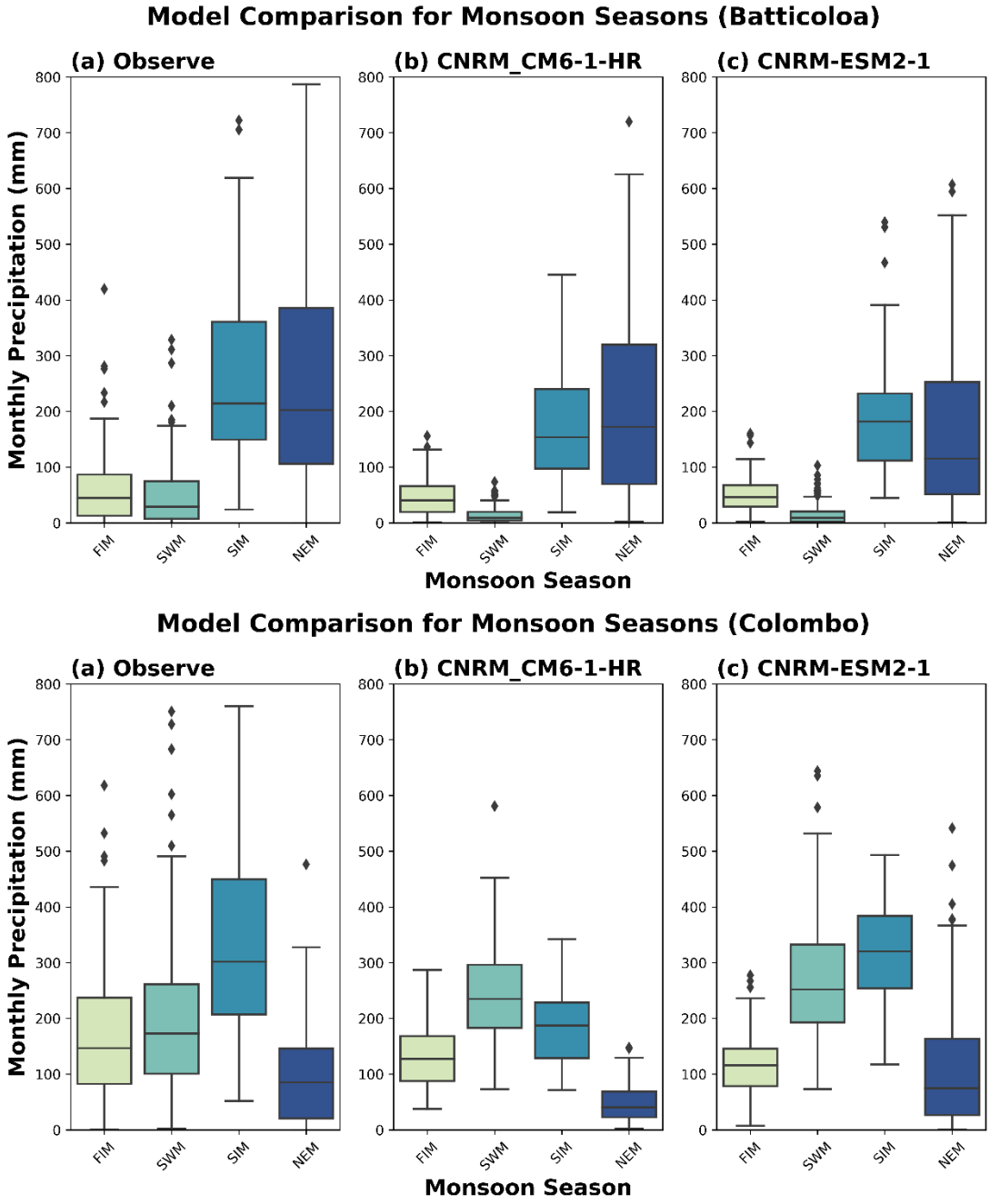
Model Comparison for Monsoon Seasons (Batticoloa)
(a) Observe
(b) CNRM_CM6-1-HR
(c) CNRM-ESM2-1
Monthly Precipitation (mm)
0
100
200
300
400
500
600
700
800
FIM
SWM
SIM
NEM
Monsoon Season
Model Comparison for Monsoon Seasons (Colombo)
(a) Observe
(b) CNRM_CM6-1-HR
(c) CNRM-ESM2-1
Monthly Precipitation (mm)
Monsoon Season

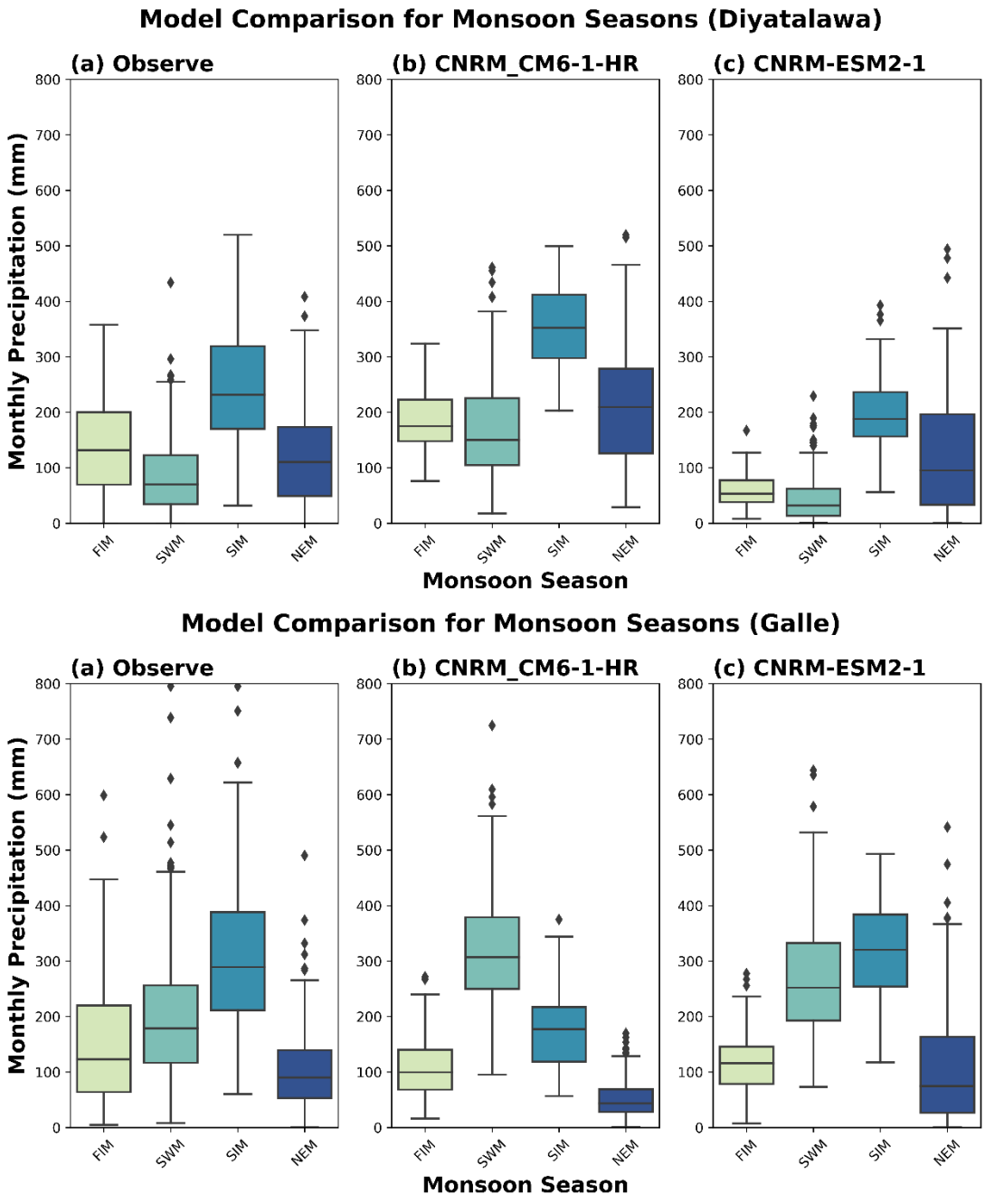
Model Comparison for Monsoon Seasons (Diyatalawa)
(a) Observe
(b) CNRM_CM6-1-HR
(c) CNRM-ESM2-1
Monthly Precipitation (mm)
0
100
200
300
400
500
600
700
800
FIM
SWM
SIM
NEM
Monsoon Season
Model Comparison for Monsoon Seasons (Galle)
(a) Observe
(b) CNRM_CM6-1-HR
(c) CNRM-ESM2-1
Monthly Precipitation (mm)
Monsoon Season

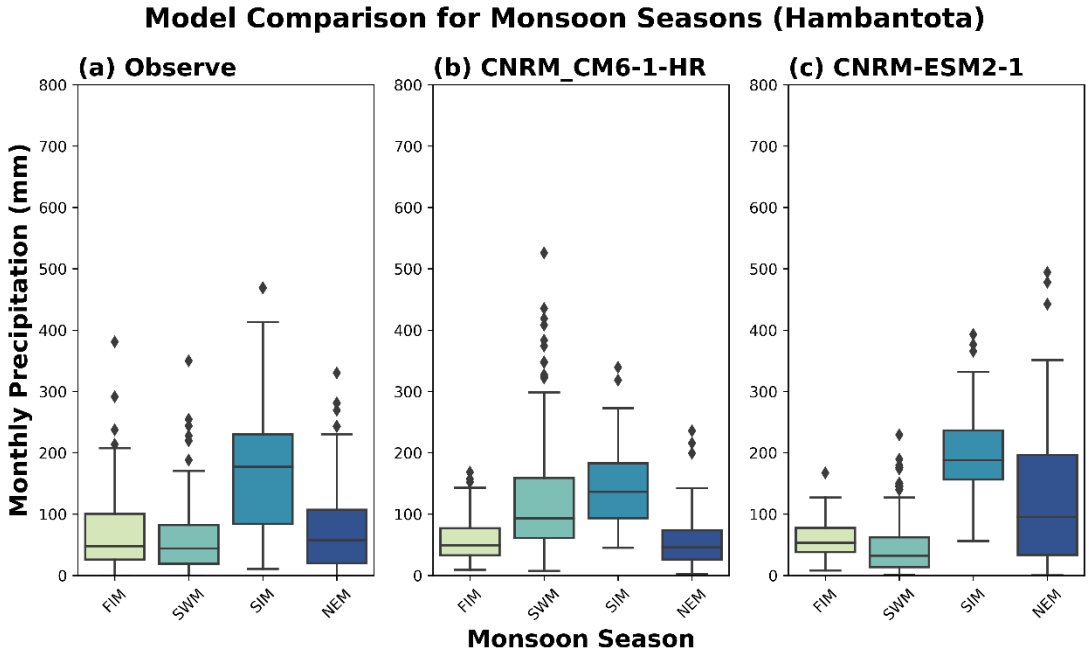
Model Comparison for Monsoon Seasons (Hambantota)
(a) Observe
(b) CNRM_CM6-1-HR
(c) CNRM-ESM2-1
Monthly Precipitation (mm)
0
100
200
300
400
500
600
700
800
FIM
SWM
SIM
NEM
Monsoon Season

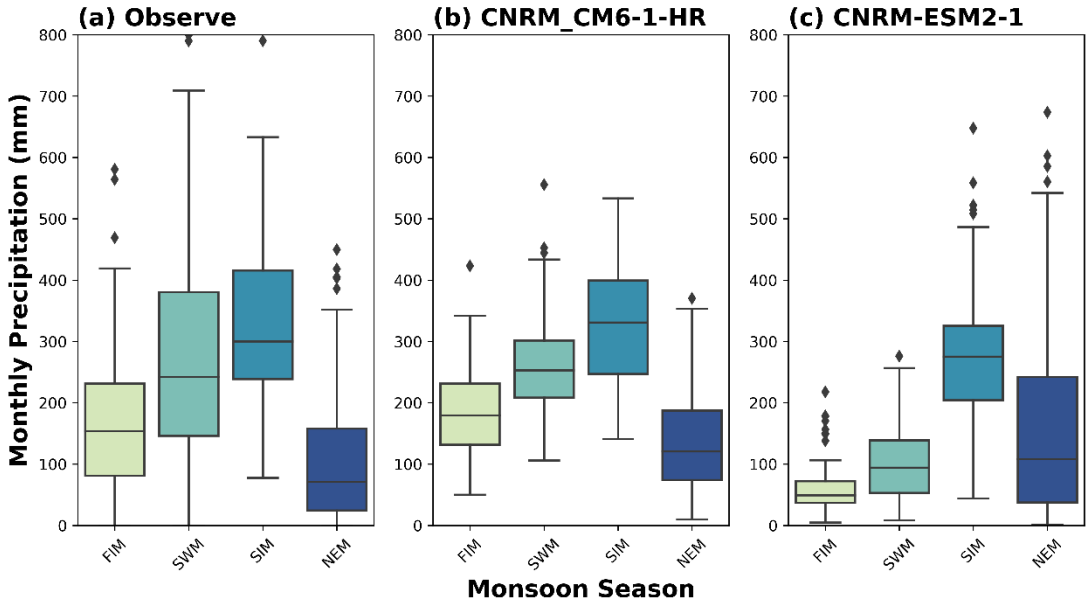
Model Comparison for Monsoon Seasons (Helbodde Estate)
(a) Observe
(b) CNRM_CM6-1-HR
(c) CNRM-ESM2-1
Monthly Precipitation (mm)
0
100
200
300
400
500
600
700
800
FIM
SWM
SIM
NEM
Monsoon Season

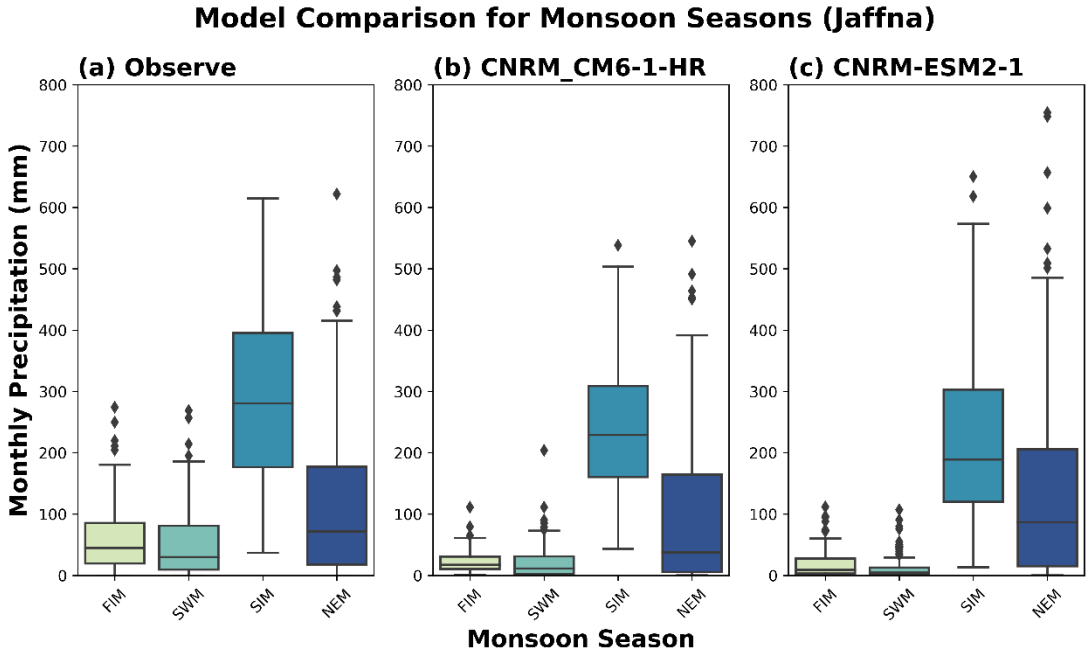
Model Comparison for Monsoon Seasons (Jaffna)
(a) Observe
(b) CNRM_CM6-1-HR
(c) CNRM-ESM2-1
Monthly Precipitation (mm)
0
100
200
300
400
500
600
700
800
FIM
SWM
SIM
NEM
Monsoon Season

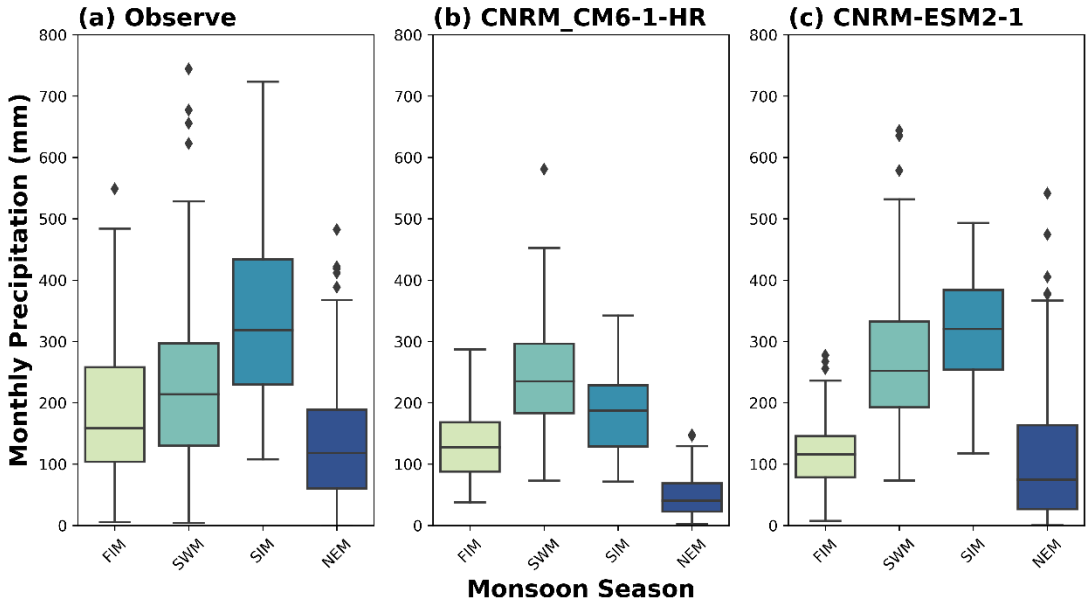
Model Comparison for Monsoon Seasons (Kalutara)
(a) Observe
(b) CNRM_CM6-1-HR
(c) CNRM-ESM2-1
Monthly Precipitation (mm)
0
100
200
300
400
500
600
700
800
FIM
SWM
SIM
NEM
Monsoon Season

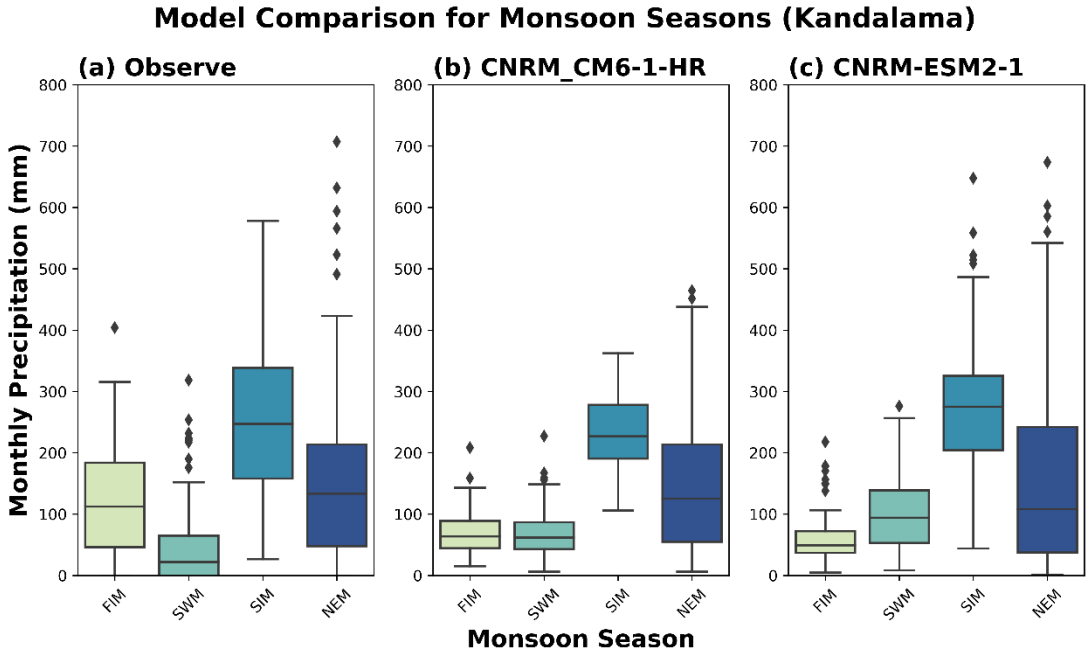
Model Comparison for Monsoon Seasons (Kandalama)
(a) Observe
(b) CNRM_CM6-1-HR
(c) CNRM-ESM2-1
Monthly Precipitation (mm)
0
100
200
300
400
500
600
700
800
FIM
SWM
SIM
NEM
Monsoon Season

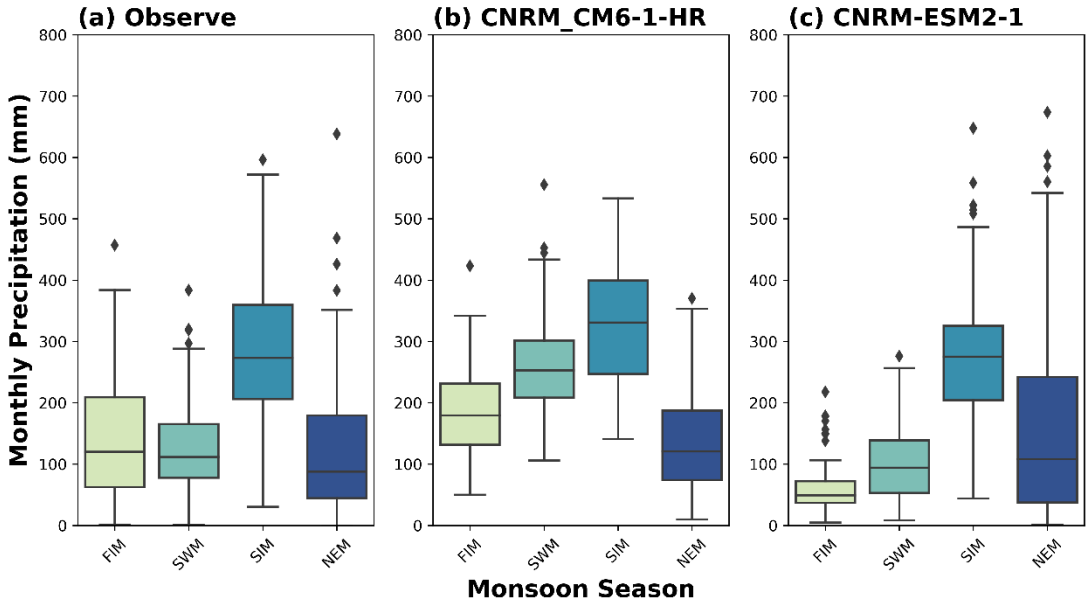
Model Comparison for Monsoon Seasons (Katugastota)
(a) Observe
(b) CNRM_CM6-1-HR
(c) CNRM-ESM2-1
Monthly Precipitation (mm)
0
100
200
300
400
500
600
700
800
FIM
SWM
SIM
NEM
Monsoon Season

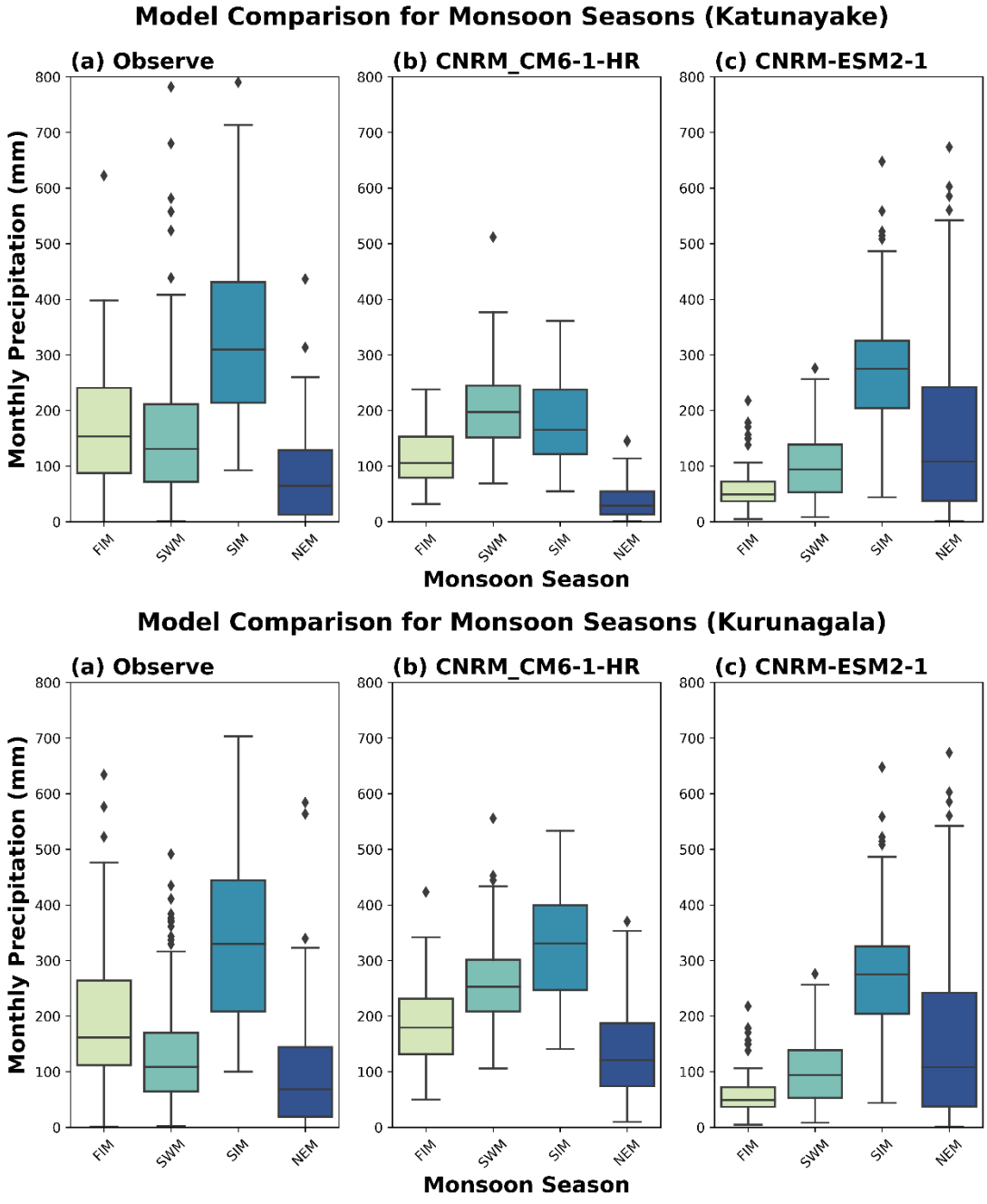
Model Comparison for Monsoon Seasons (Katunayake)
(a) Observe
(b) CNRM_CM6-1-HR
(c) CNRM-ESM2-1
Monthly Precipitation (mm)
Monsoon Season
FIM
SWM
SIM
NEM
Model Comparison for Monsoon Seasons (Kurunagala)
(a) Observe
(b) CNRM_CM6-1-HR
(c) CNRM-ESM2-1
Monthly Precipitation (mm)
Monsoon Season
FIM
SWM
SIM
NEM

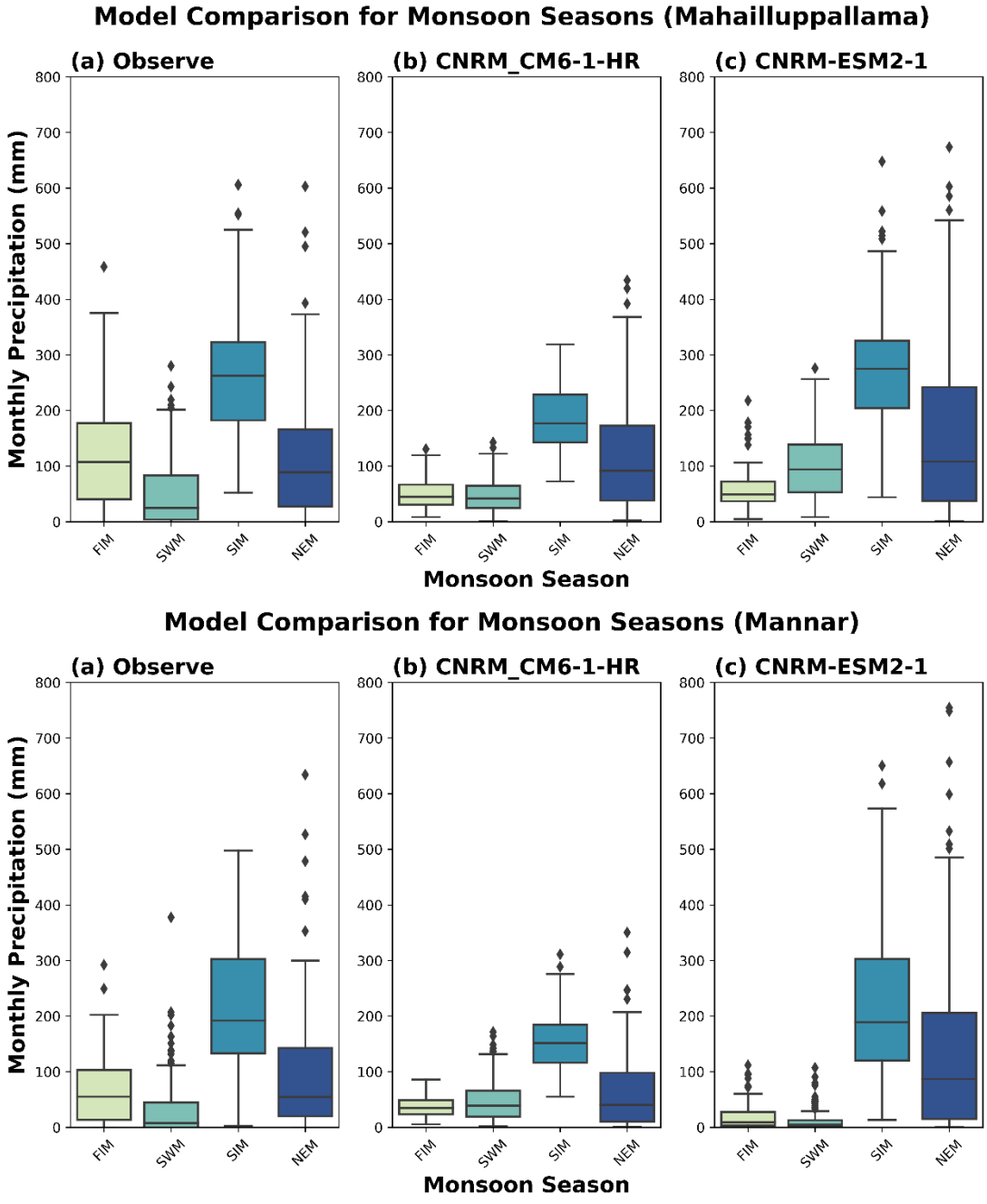
Model Comparison for Monsoon Seasons (Mahailluppallama)
(a) Observe
(b) CNRM_CM6-1-HR
(c) CNRM-ESM2-1
Monthly Precipitation (mm)
0
100
200
300
400
500
600
700
800
FIM
SWM
SIM
NEM
Monsoon Season
Model Comparison for Monsoon Seasons (Mannar)
(a) Observe
(b) CNRM_CM6-1-HR
(c) CNRM-ESM2-1
Monthly Precipitation (mm)
Monsoon Season

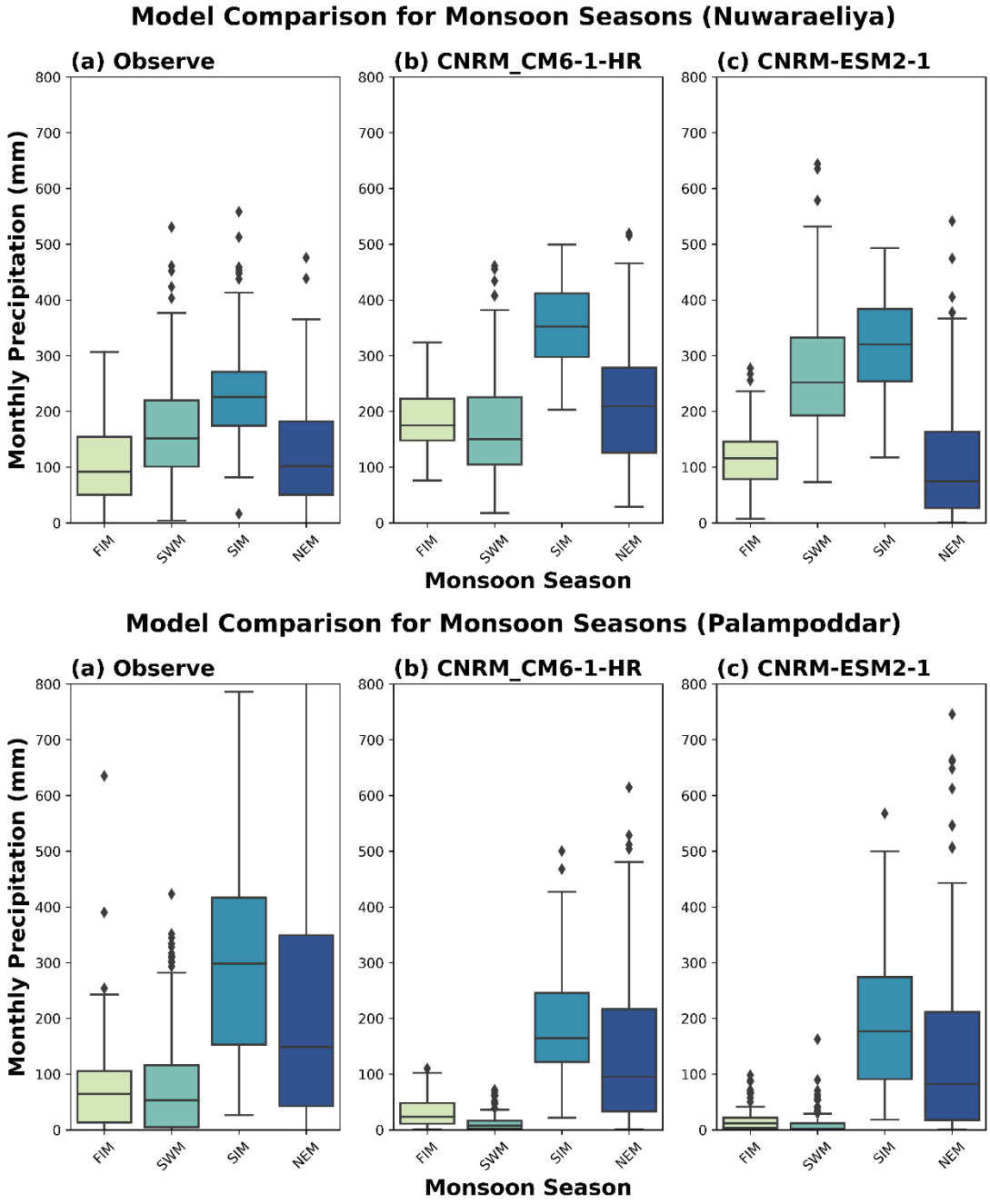
Model Comparison for Monsoon Seasons (Nuwaraeliya)
(a) Observe
(b) CNRM_CM6-1-HR
(c) CNRM-ESM2-1
Monthly Precipitation (mm)
0
100
200
300
400
500
600
700
800
FIM
SWM
SIM
NEM
Monsoon Season
Model Comparison for Monsoon Seasons (Palampoddar)
(a) Observe
(b) CNRM_CM6-1-HR
(c) CNRM-ESM2-1
Monthly Precipitation (mm)
Monsoon Season

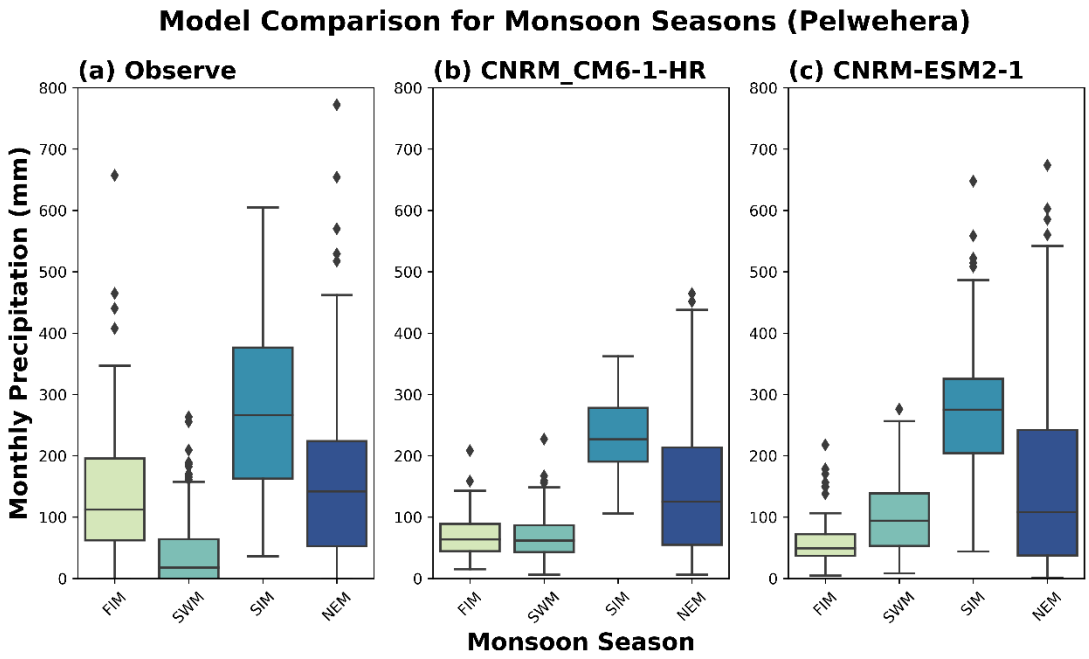
Model Comparison for Monsoon Seasons (Pelwehera)
(a) Observe
(b) CNRM_CM6-1-HR
(c) CNRM-ESM2-1
Monthly Precipitation (mm)
0
100
200
300
400
500
600
700
800
FIM
SWM
SIM
NEM
Monsoon Season

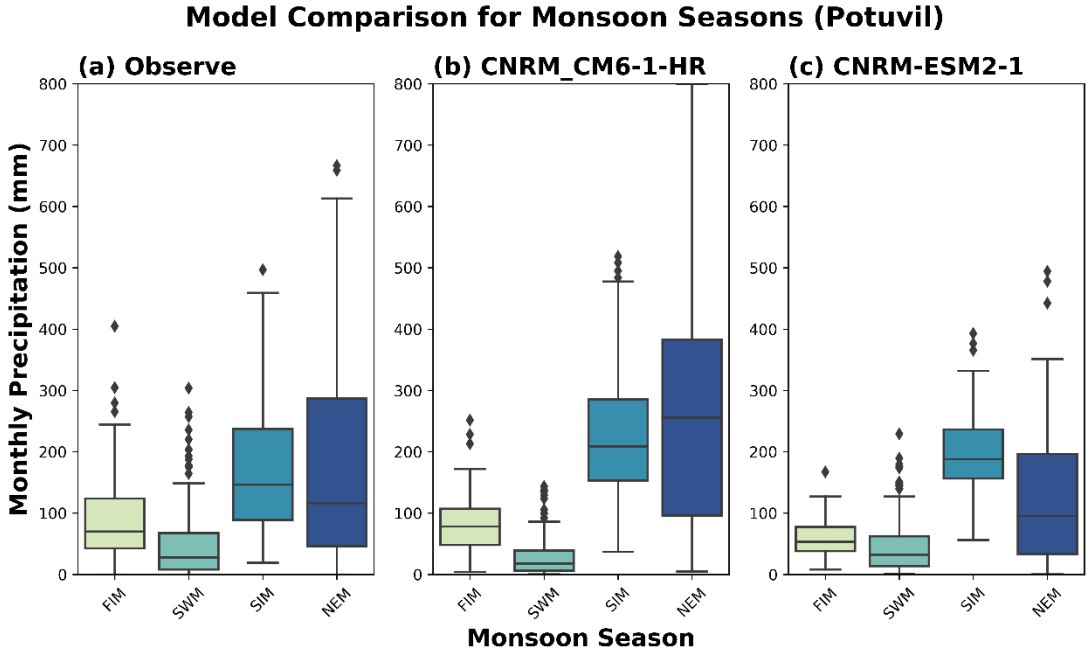
Model Comparison for Monsoon Seasons (Potuvil)
(a) Observe
(b) CNRM_CM6-1-HR
(c) CNRM-ESM2-1
Monthly Precipitation (mm)
0
100
200
300
400
500
600
700
800
FIM
SWM
SIM
NEM
Monsoon Season

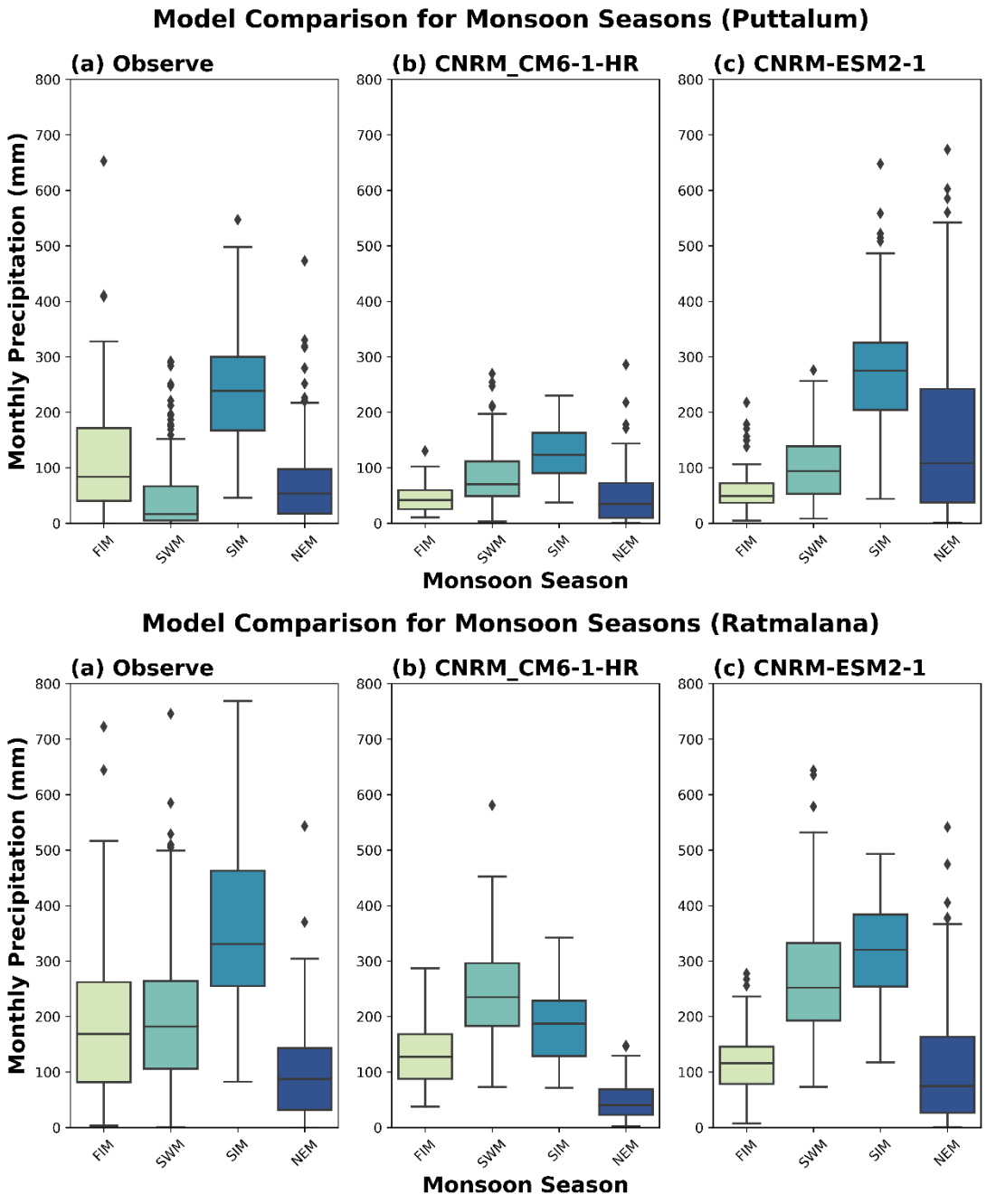
Model Comparison for Monsoon Seasons (Puttalum)
(a) Observe
(b) CNRM_CM6-1-HR
(c) CNRM-ESM2-1
Monthly Precipitation (mm)
0
100
200
300
400
500
600
700
800
FIM
SWM
SIM
NEM
Monsoon Season
Model Comparison for Monsoon Seasons (Ratmalana)
(a) Observe
(b) CNRM_CM6-1-HR
(c) CNRM-ESM2-1
Monthly Precipitation (mm)
Monsoon Season

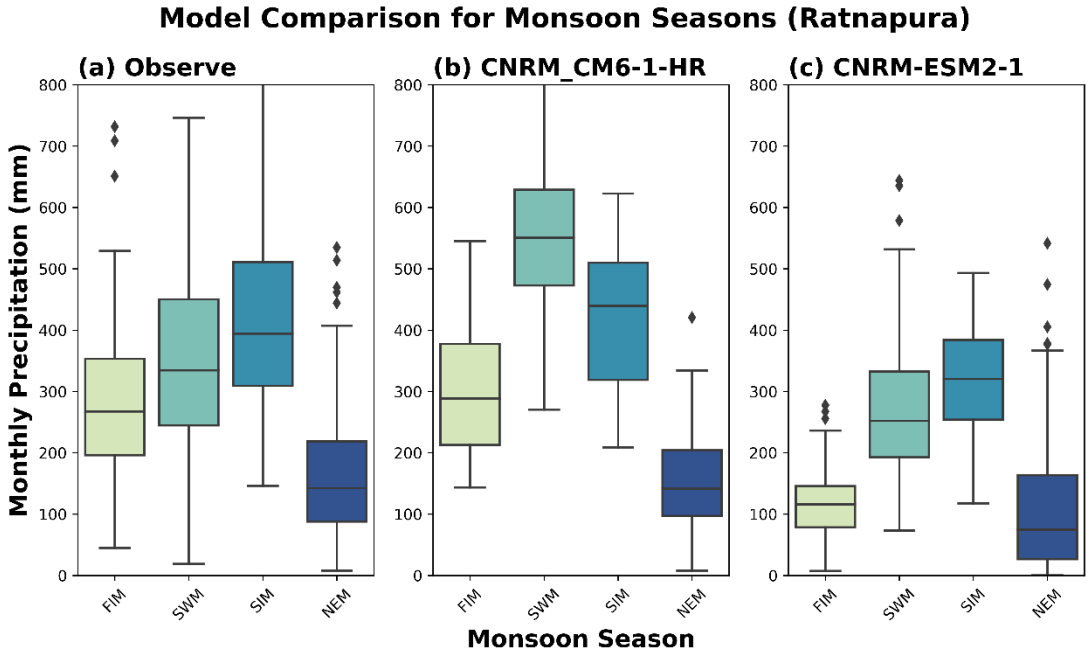
Model Comparison for Monsoon Seasons (Ratnapura)
(a) Observe
(b) CNRM_CM6-1-HR
(c) CNRM-ESM2-1
Monthly Precipitation (mm)
0
100
200
300
400
500
600
700
800
FIM
SWM
SIM
NEM
Monsoon Season

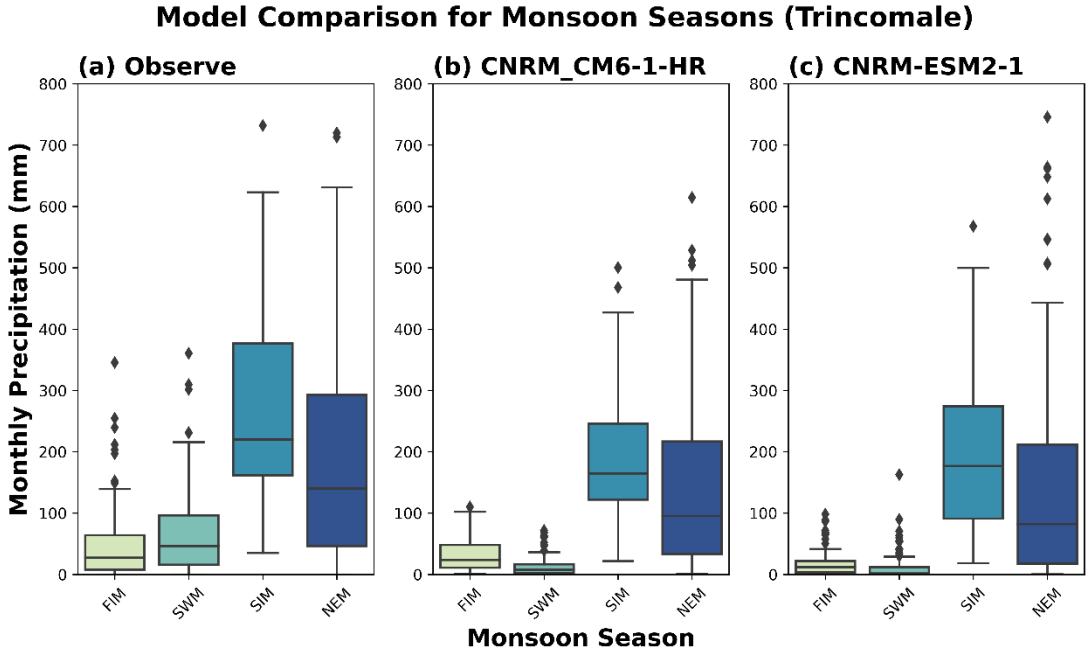
Model Comparison for Monsoon Seasons (Trincomale)
(a) Observe
(b) CNRM_CM6-1-HR
(c) CNRM-ESM2-1
Monthly Precipitation (mm)
0
100
200
300
400
500
600
700
800
FIM
SWM
SIM
NEM
Monsoon Season

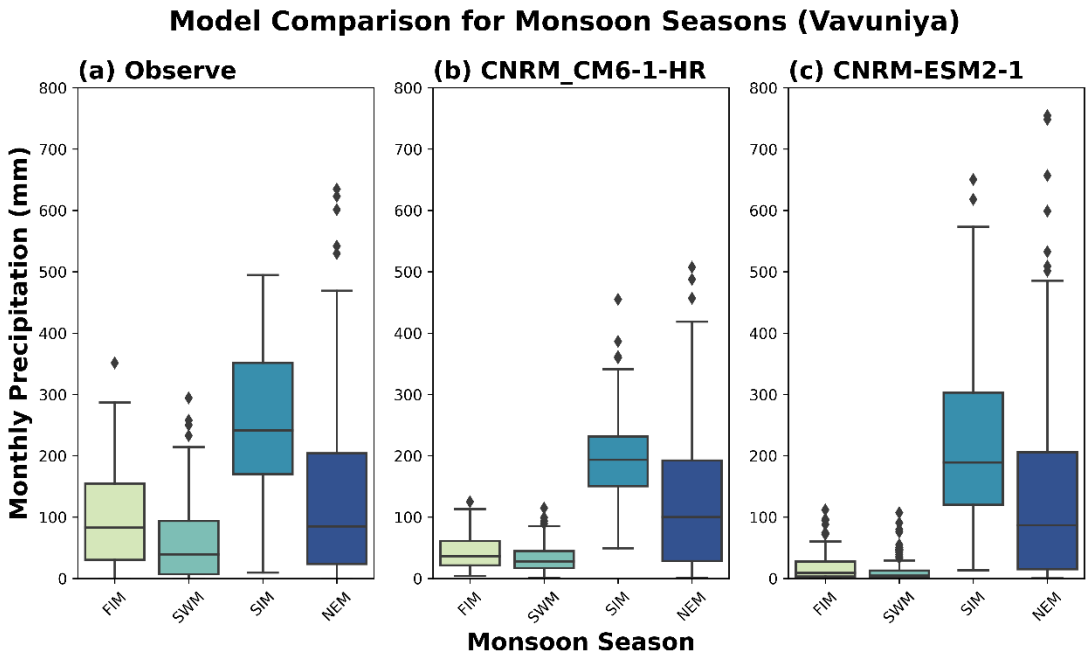
Model Comparison for Monsoon Seasons (Vavuniya)
(a) Observe
(b) CNRM_CM6-1-HR
(c) CNRM-ESM2-1
Monthly Precipitation (mm)
0
100
200
300
400
500
600
700
800
FIM
SWM
SIM
NEM
Monsoon Season

Appendix E: CDF curves between observed vs mean-based corrected model precipitation data

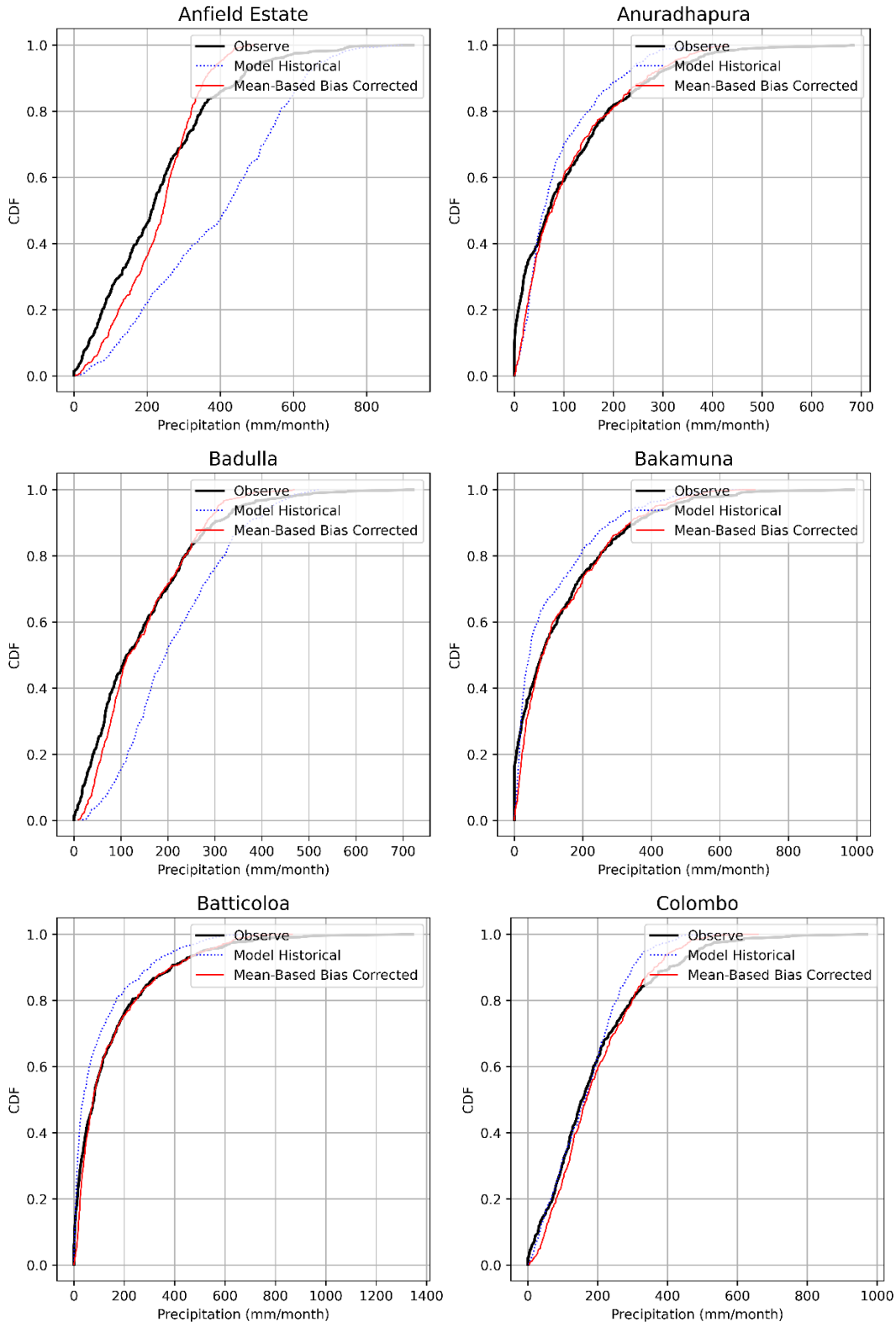
Anfield Estate
Anuradhapura
Badulla
Bakamuna
Batticoloa
Colombo
Observe
Model Historical
Mean-Based Bias Corrected
CDF
Precipitation (mm/month)

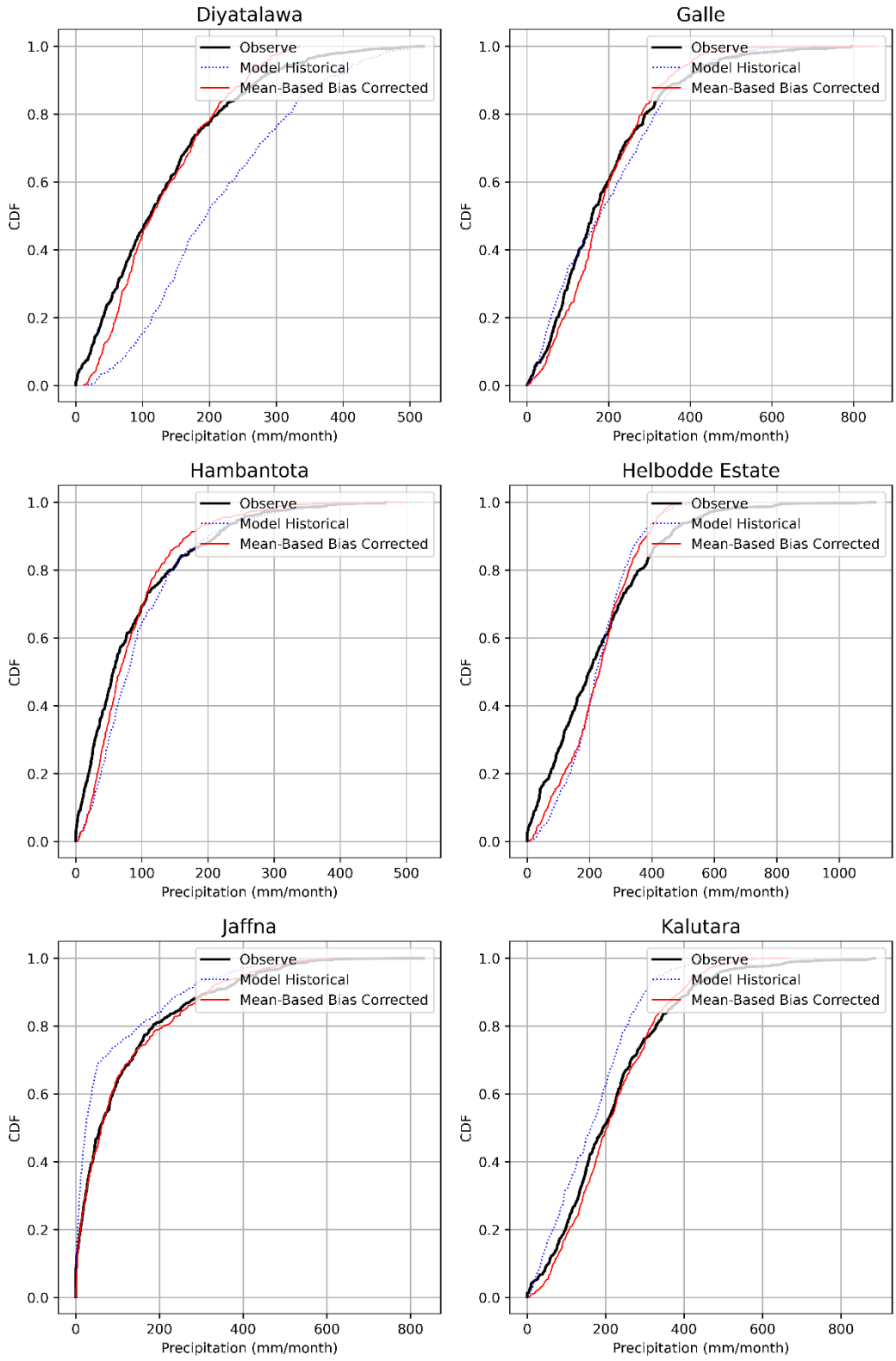
Diyatalawa
Galle
Hambantota
Helbodde Estate
Jaffna
Kalutara
Observe
Model Historical
Mean-Based Bias Corrected
CDF
Precipitation (mm/month)

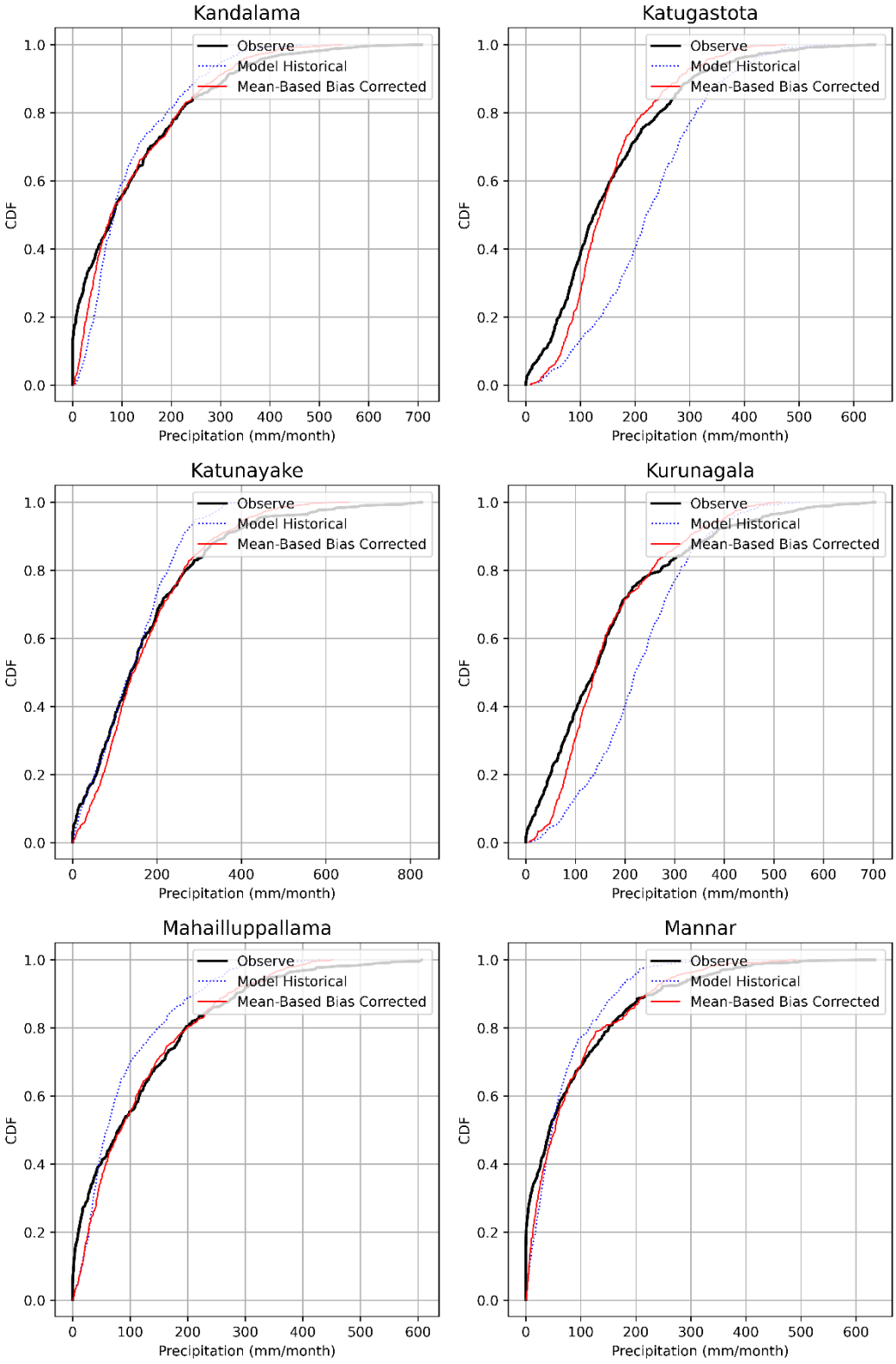
Kandalama
Katugastota
Katunayake
Kurunagala
Mahailluppallama
Mannar
Observe
Model Historical
Mean-Based Bias Corrected
CDF
Precipitation (mm/month)

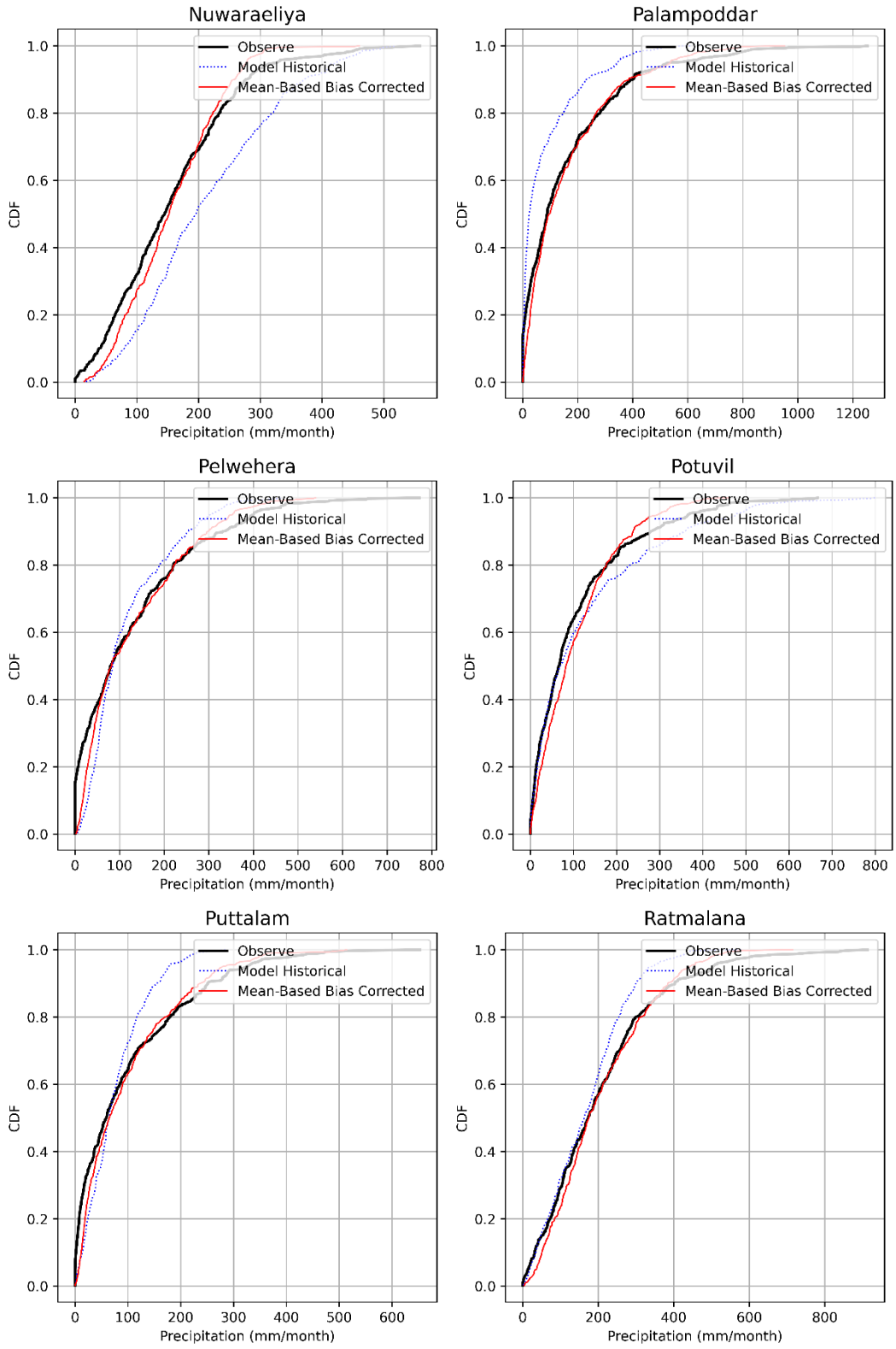
Nuwaraeliya
Palampoddar
Pelwehera
Potuvil
Puttalam
Ratmalana
Observe
Model Historical
Mean-Based Bias Corrected
CDF
Precipitation (mm/month)

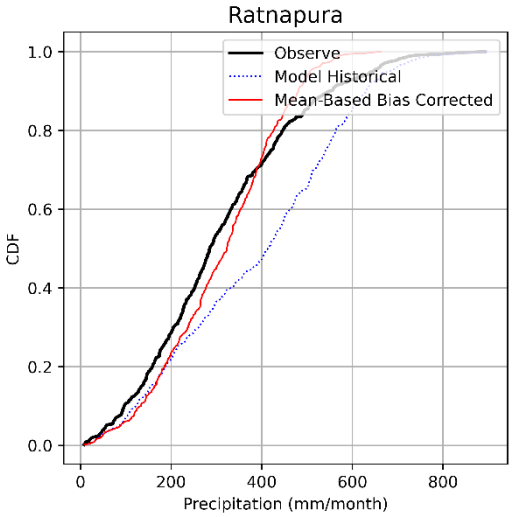
Ratnapura
Observe
Model Historical
Mean-Based Bias Corrected
CDF
Precipitation (mm/month)

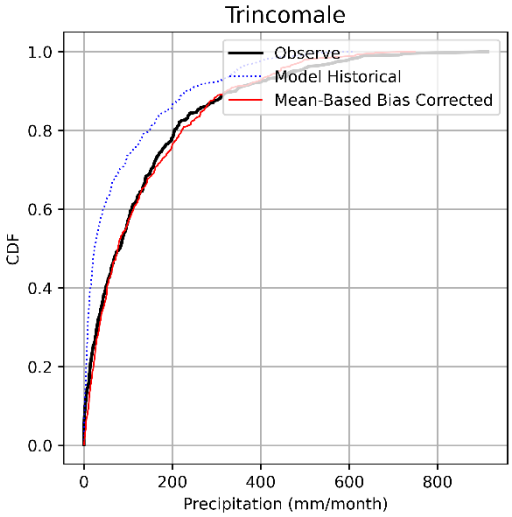
Trincomale
Observe
Model Historical
Mean-Based Bias Corrected
CDF
Precipitation (mm/month)

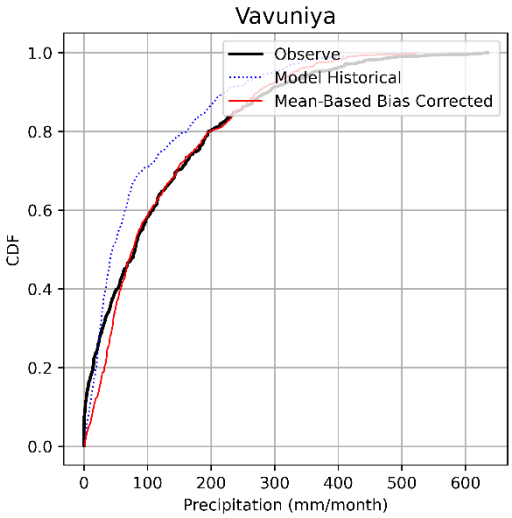
Vavuniya
Observe
Model Historical
Mean-Based Bias Corrected
CDF
Precipitation (mm/month)

Appendix F: CDF curves between observed vs bias corrected precipitation data using the quantile mapping method

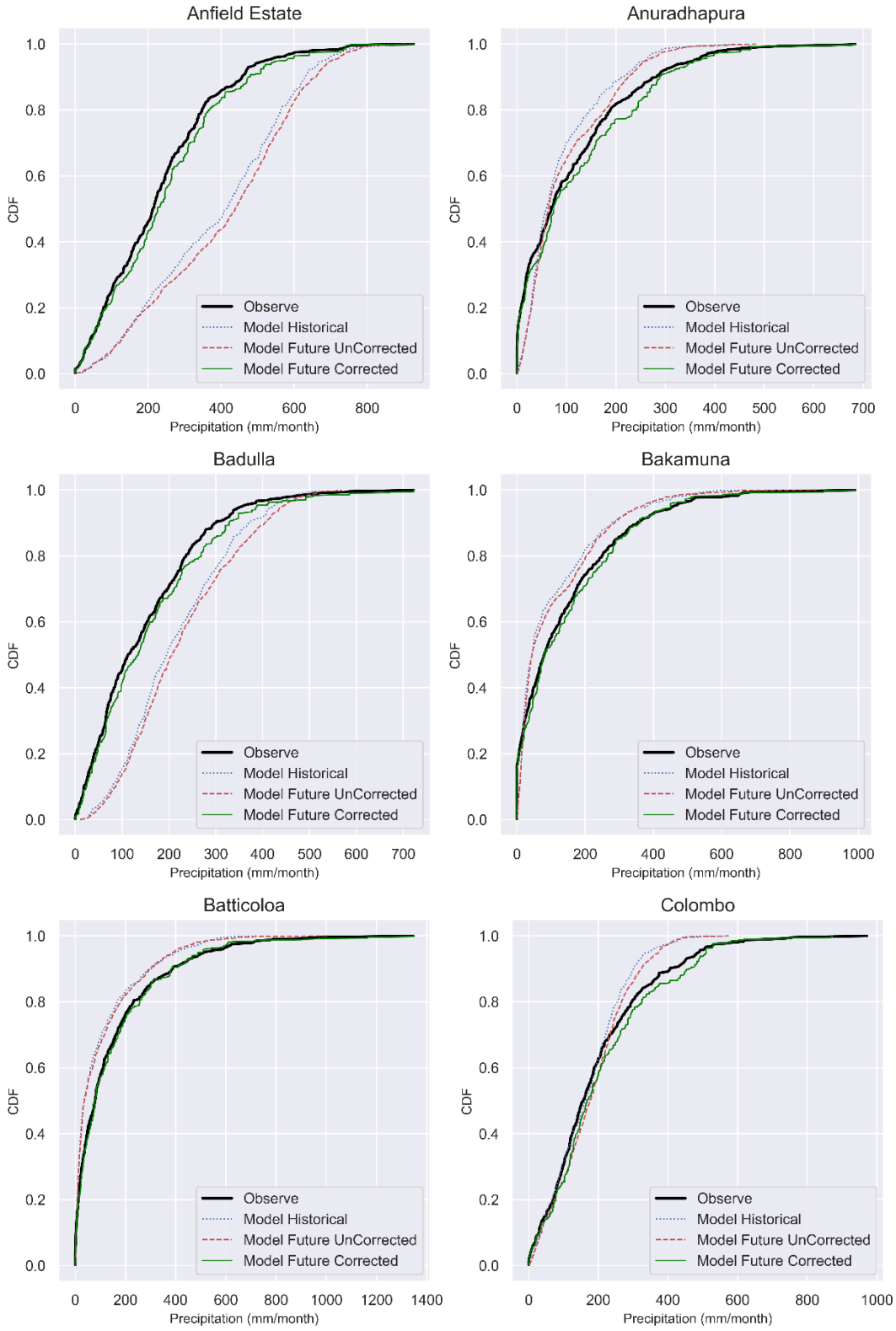
Anfield Estate
Anuradhapura
Badulla
Bakamuna
Batticoloa
Colombo
CDF
Precipitation (mm/month)
Observe
Model Historical
Model Future UnCorrected
Model Future Corrected

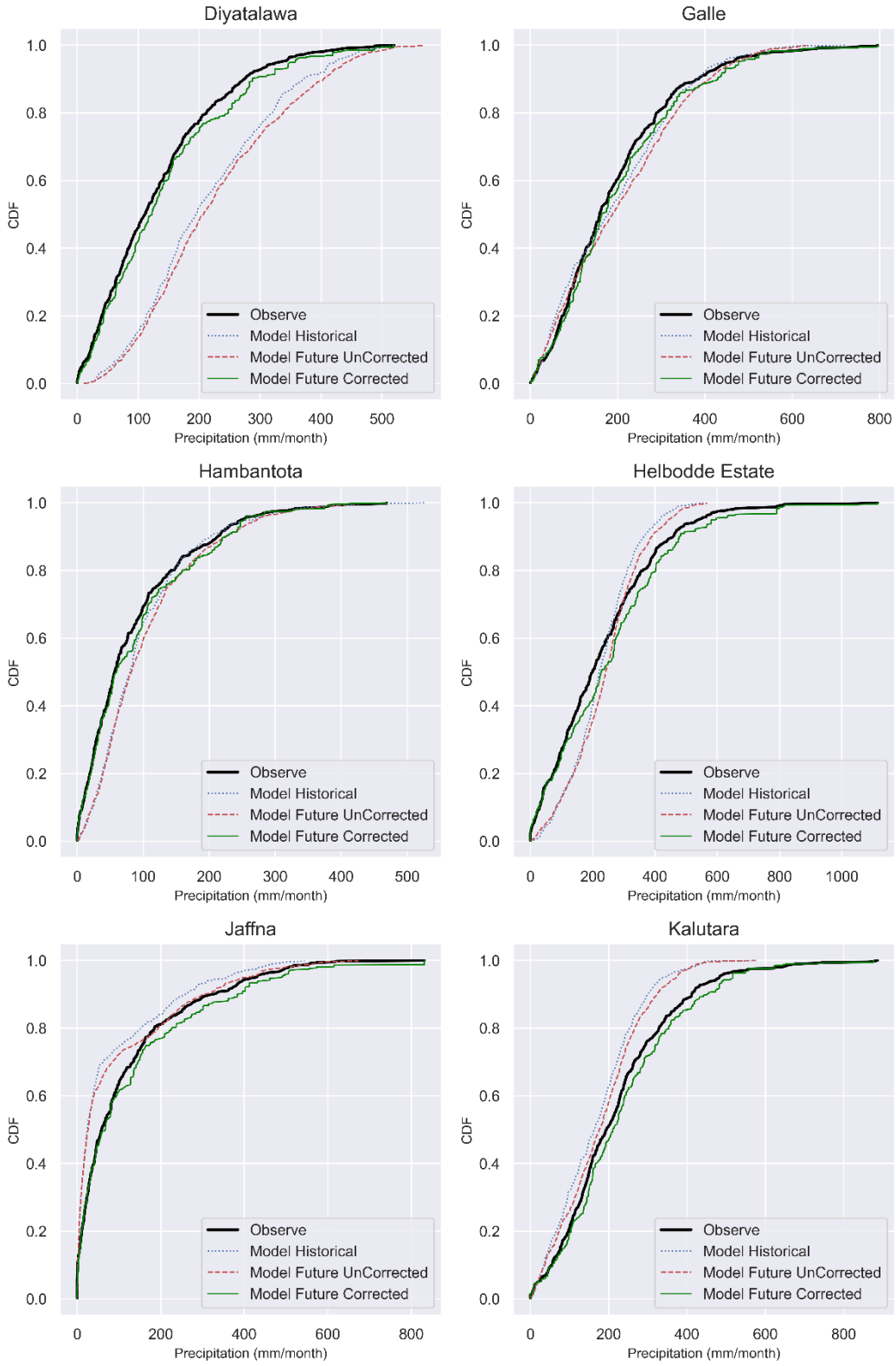
Diyatalawa
Galle
Hambantota
Helbodde Estate
Jaffna
Kalutara
CDF
Precipitation (mm/month)
Observe
Model Historical
Model Future UnCorrected
Model Future Corrected

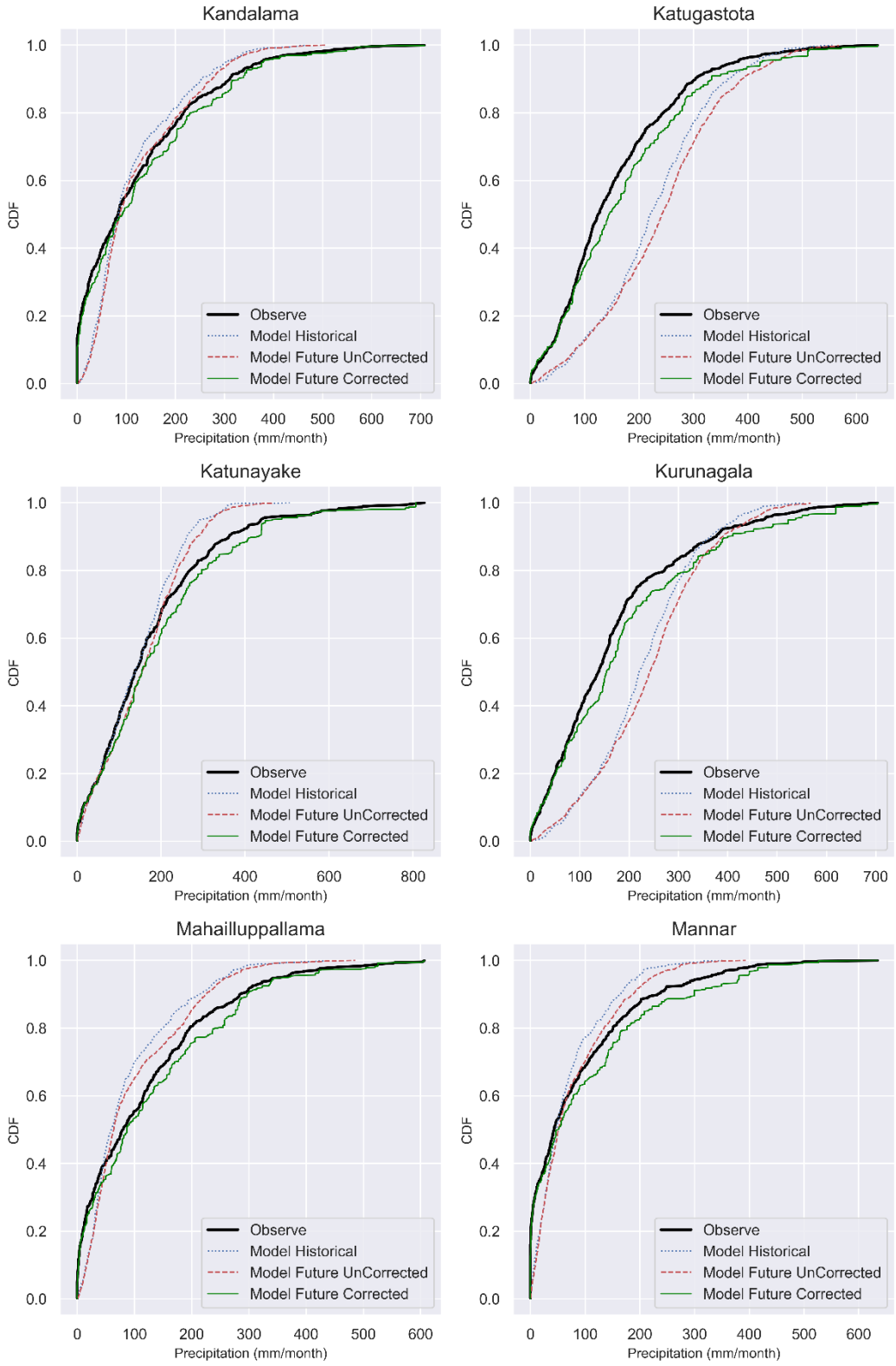
Kandalama
Katugastota
Katunayake
Kurunagala
Mahailluppallama
Mannar
CDF
Precipitation (mm/month)
Observe
Model Historical
Model Future UnCorrected
Model Future Corrected

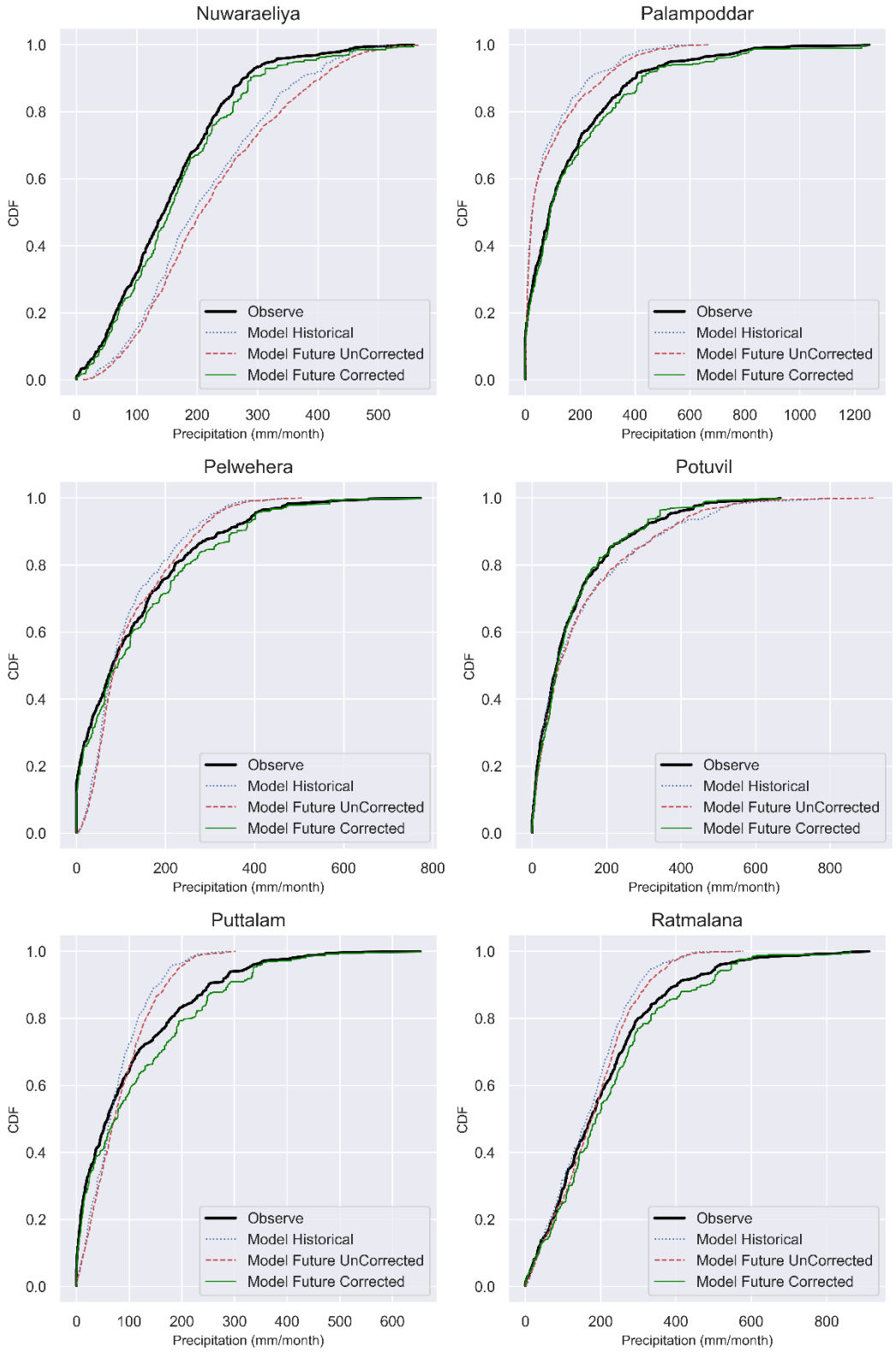
Nuwaraeliya
Palampoddar
Pelwehera
Potuvil
Puttalam
Ratmalana
CDF
Precipitation (mm/month)
Observe
Model Historical
Model Future UnCorrected
Model Future Corrected

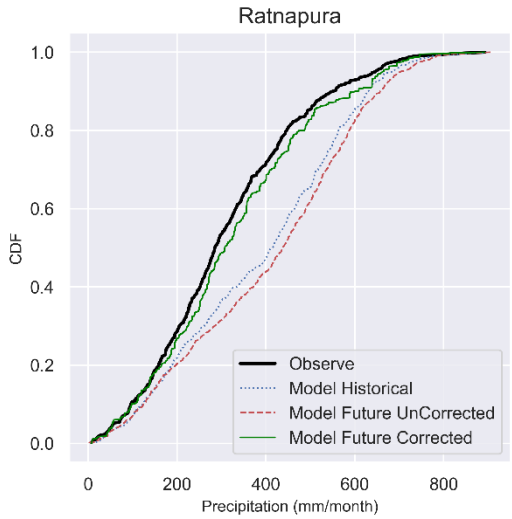
Ratnapura
CDF
Precipitation (mm/month)
Observe
Model Historical
Model Future UnCorrected
Model Future Corrected

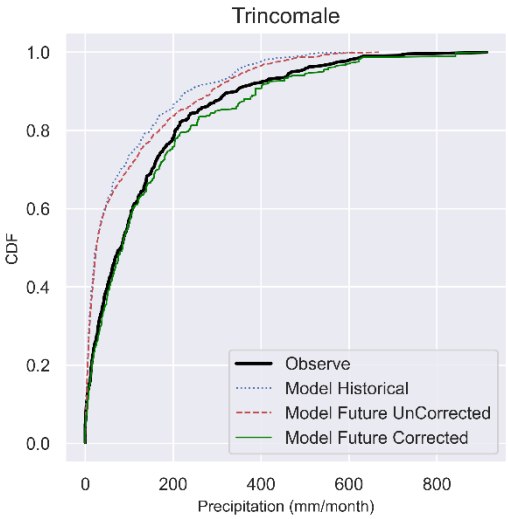
Trincomale
CDF
Precipitation (mm/month)
Observe
Model Historical
Model Future UnCorrected
Model Future Corrected

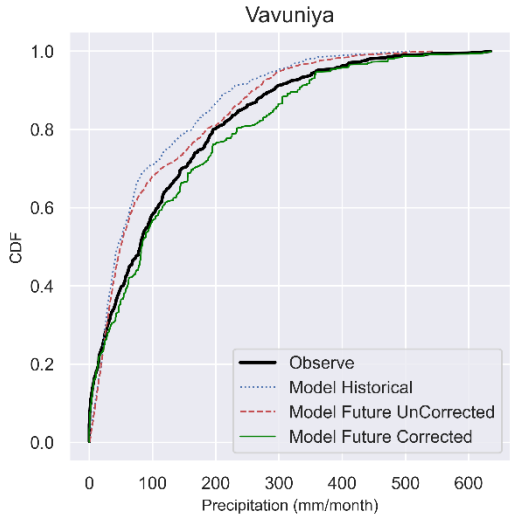
Vavuniya
CDF
Precipitation (mm/month)
Observe
Model Historical
Model Future UnCorrected
Model Future Corrected

Appendix G: CDF curves between observed vs bias corrected temperature data using the quantile mapping method

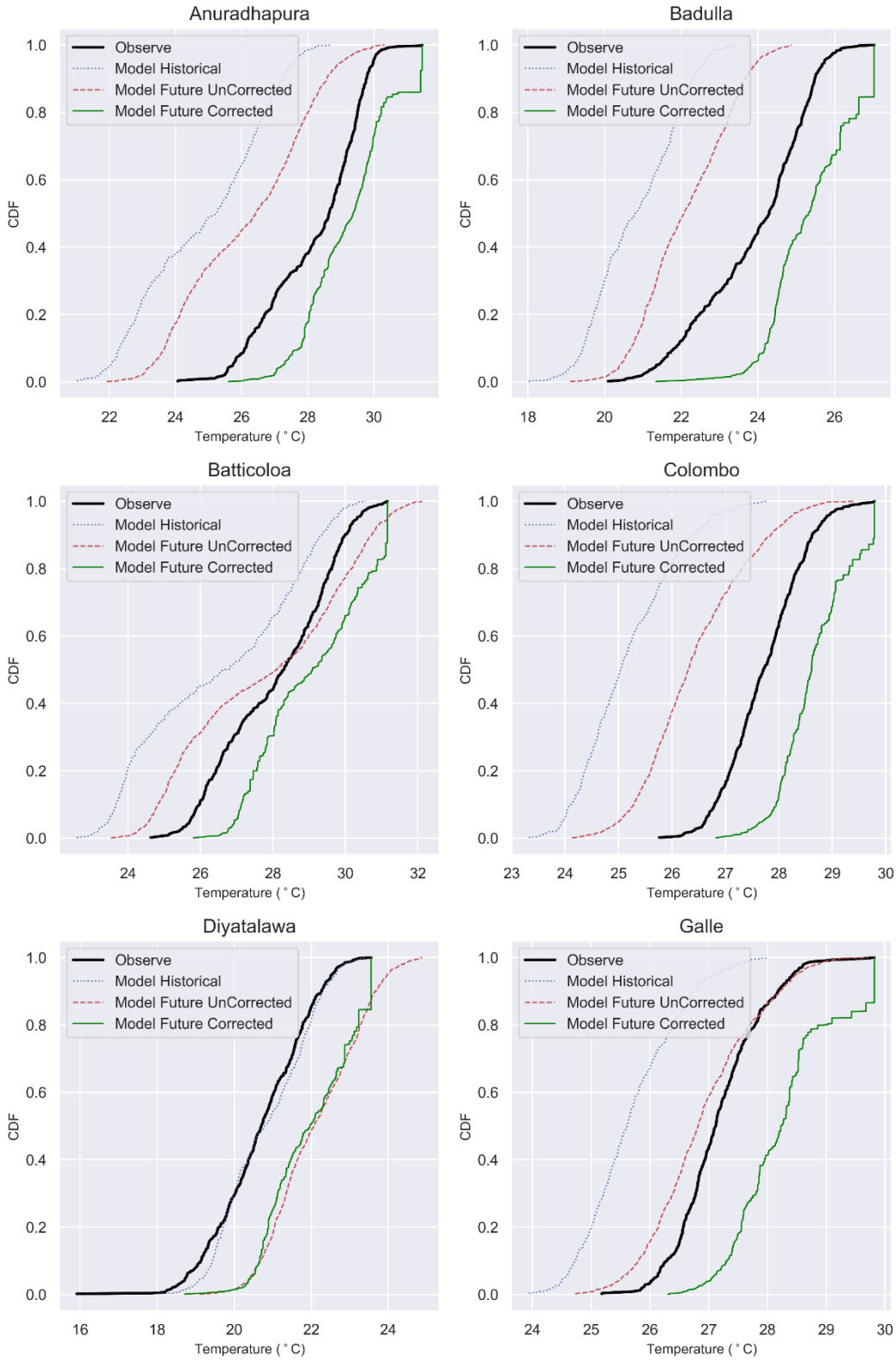
Anuradhapura
Badulla
Batticoloa
Colombo
Diyatalawa
Galle
Observe
Model Historical
Model Future UnCorrected
Model Future Corrected
CDF
Temperature (° C)

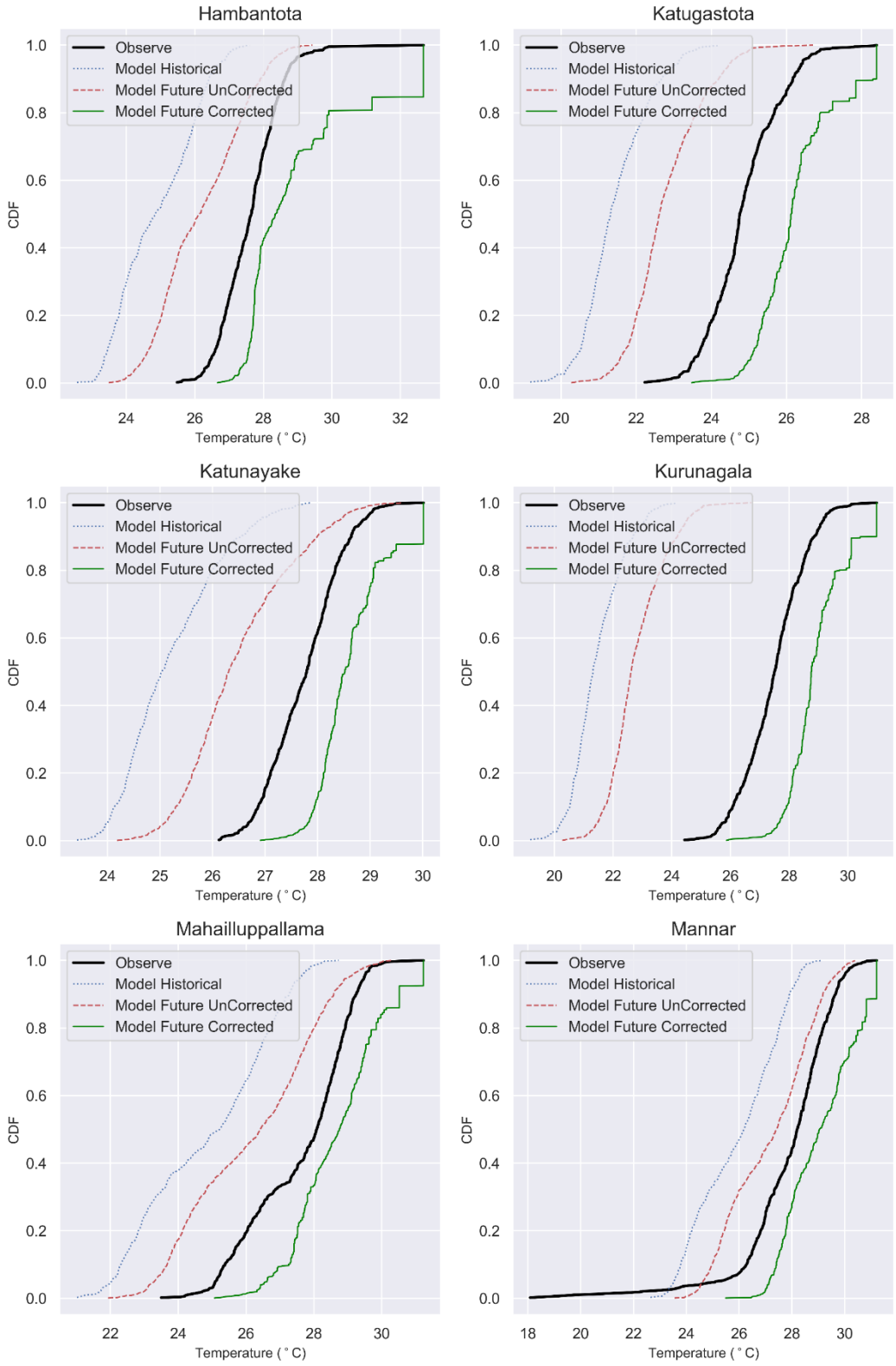
Hambantota
Katugastota
Katunayake
Kurunagala
Mahailluppallama
Mannar
Observe
Model Historical
Model Future UnCorrected
Model Future Corrected
CDF
Temperature (° C)

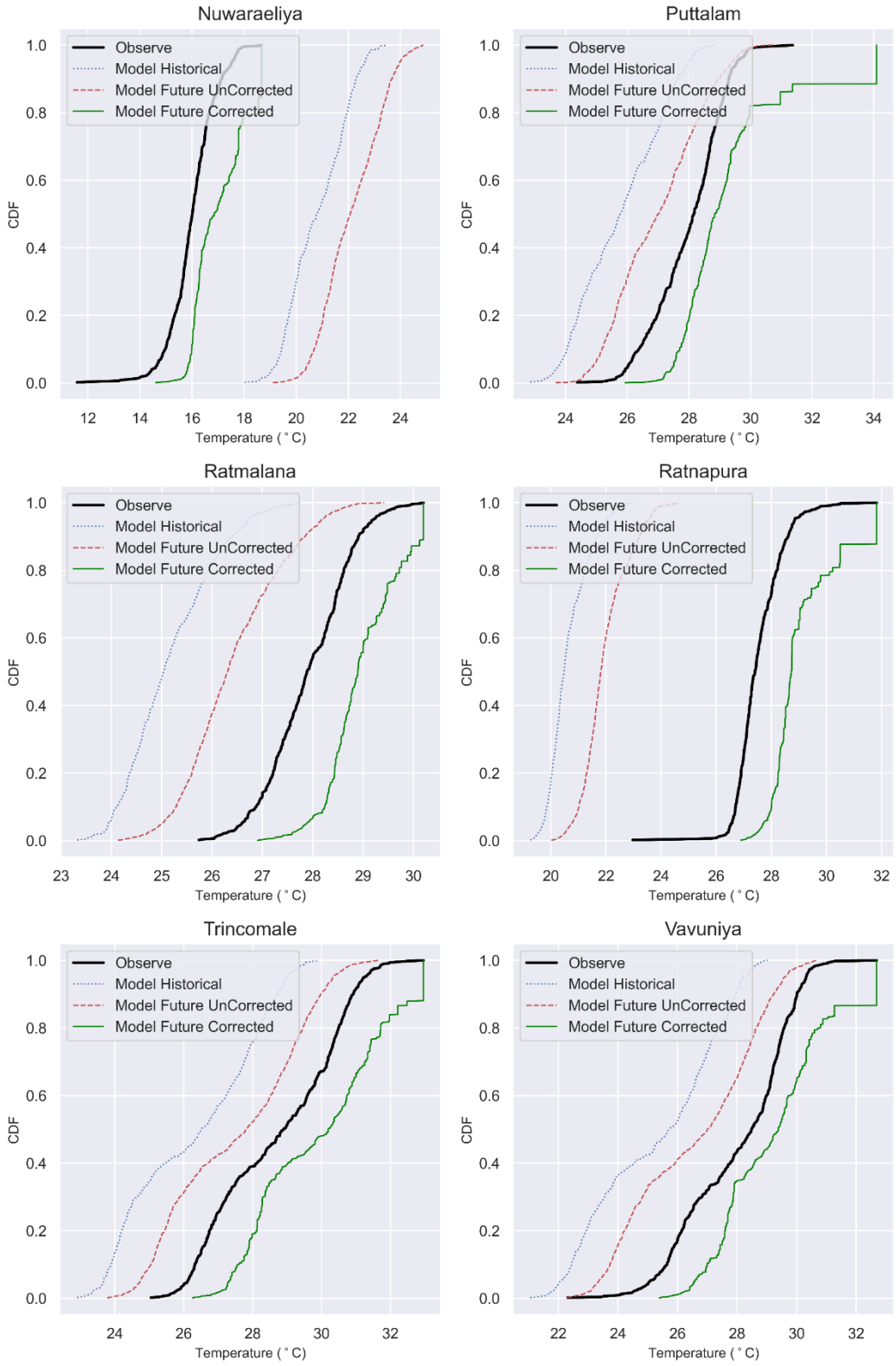
Nuwaraeliya
Puttalam
Ratmalana
Ratnapura
Trincomale
Vavuniya
Observe
Model Historical
Model Future UnCorrected
Model Future Corrected
CDF
Temperature (° C)

The findings, interpretations and conclusions expressed in this thesis/dissertation are entirely based on the results of the individual research study and should not be attributed in any manner to or do neither necessarily reflect the views of UNESCO Madanjeet Singh Centre for South Asia Water Management (UMCSAWM), nor of the individual members of the MSc panel, nor of their respective organizations.